**Bacterial-Nanoparticle Interactions**

Submitted by Jonathan McQuillan to the University of Exeter

as a thesis for the degree of

Doctor of Philosophy in Biological Sciences

In December 2010



I certify that all material in this thesis which is not my own work has been identified and that no material has previously been submitted and approved for the award of a degree by this or any other University.

Signature: ……..

Make up your mind to act decidedly and take the consequences. No good is ever done in this world by hesitation.

- Thomas H. Huxley

**Acknowledgements**

I would like to thank the many people who have helped and supported me throughout this Ph.D. Firstly I would like thank my supervisor Andrew Shaw for his dedication to this project, continuous support, patience and understanding of the various difficulties faced over the course of the Ph.D. I would like to thank Hilary Lappin-Scott and Sara Burton for the opportunity to do a Ph.D and for their contribution to the initial stages of the project. I would like to thank the BBSRC and Exeter Nano-bacteria Ltd (ENBL) for funding, and the University of Exeter for academic support. I would like to thank Paul Reip for providing me with silver nanoparticles, and for help and advice. I would also like to thank Heidi Groenaga-Infante and Volker Nischwitz at the LGC for guiding me through the process of ICP-MS, and Peter Splatt for help and support with Electron Microscopy. Thank you to Chrystala Constantinidou and Mala Patel for their assistance with microarray experiments, and thank you to all of my friends in the School of Biosciences for sharing the pain. None of this would have been possible without the support of my family; special thanks to my parents who have always done anything and everything to support my education. I would like to add additional special thanks to Emma for all her support throughout the last few years.

**Abstract**

Bionanotechnology is an intersection between biology and nanotechnology, a field in which novel applications for very small materials are being realised at an alarming rate. Nanoparticles have 3 dimensions that can be measured in nanometers, their small size conferring upon them different properties from individual atoms or the bulk material. The interactions between these unique materials and microorganisms are often toxic, thus have been exploited for antimicrobial applications. However, there is a considerable paucity of data for the underlying molecular mechanisms. This study has been carried out to investigate the interactions that occur between nanoparticles and bacteria with the objective of identifying these toxicological mechanisms and novel nanoparticle effects, using the model Gram negative organism *Escherichia coli* K12. This study has identified metal nanoparticles that are a superior vehicle for the delivery of toxic metal ions to *E. coli*. The nanoparticles associate with the bacterial surface, but do not cross the cell wall. They then dissolve, releasing a concentration of metal ions that accumulate at the bacterial-nanoparticle interface, enhancing the antibacterial efficacy compared to the concentration of metal ions in the bulk solution phase. Measurement of the whole transcriptome response to silver nanoparticles in comparison to the silver ion indicates that the different modes of ion delivery may induce a differential stress response. Moreover, this data identifies molecular mechanisms that are involved in the toxicity of this metal that is now becoming increasingly prevalent in society. The dissolution based toxic effects of zinc oxide nanoparticles are augmented by an interaction with ultra-violet light, offering an alternative mode for nanoparticle toxicity.

# List of Contents

# List of Figures

# List of Tables

# Chapter 1: Bacterial-Nanoparticle Interactions

## 1.1. General Introduction

The potential of nanotechnology in society was realised by physicist Richard Feynman in his ‘there’s plenty of room at the bottom’ lecture to the American Physical Society in 1959. Feynman introduced the idea of manipulating the very small, even down to the level of individual atoms for technological purposes. Half a century later and the nanotechnology industry has an estimated industrial market value of $147 billion (US), predicted to rise to between $750 Bn and $3,000 Bn by 2015 [1]. Although nanotechnology was originally a field within the physical sciences, the intersection of nanotechnology and biology, ‘bionanotechnology’, was realised from the potential application of nanomaterials to biological problems. Perhaps the most striking example is in the control of infection. Various nanomaterials have antimicrobial properties that may be used to control microbial populations including those that have evolved resistance to antibiotics [2-4]. Some of the most common and lethal infections of man are caused by bacteria. However, perhaps paradoxically, bacteria are the foremost contributors to the biodiversity on earth and mediate environmental processes that sustain life [5]. Therefore, there is a duality to bionanotechnology research. One aspect is to develop nanotechnology for anti-bacterial applications, which is the focus of this thesis. Another is to understand and limit the impact of nanomaterials on bacterial ecology. This is an area in which there is a considerable paucity of data [6-10].

The medicinal benefits and environmental shortcomings of nanotechnology will only be realised after extensive investigation. This is an issue that has been dealt with by the UK government through the generation of a UK Nanotechnologies Strategy, and indirectly by academic funding for ‘nanoscience’ from research councils including the BBSRC,

EPSRC and MRC. In line with these national strategic objectives, this study has been carried out to investigate how nanoparticles interact with bacteria with the overall aim of understanding the interactions that occur on the microscopic level. This will assist in understanding both the environmental impacts of nanotechnology and potential applications, for example in infection control. The regulation of the bionanotechnology industry should be tailored according to the findings of the scientific community, but with the forecast growth in this sector [1] the data must be acquired sooner rather than later.

## 1.2 Definitions and Terms

The International Organisation for Standardisation (ISO) defines a nano-structure as ‘an object that has at least one dimension within the nano-scale’; approximately 1-100 nanometers (nm)(1 nm = $10^{-9}$ m)[11]. Although nano-sized objects are typically smaller than 100 nm, the term is applied liberally because objects larger than 100 nm may display similar properties. At the other end of the scale objects approach the size of small groups of atoms, a point at which nanomaterial properties begin to diminish. This is the overriding principle in bionanotechnology; that objects within the nano-scale have properties that are distinct from either the bulk material or individual atoms. Nano-objects may have a greater catalytic activity, higher toxicity and different electrical and optical characteristics. By extension, nanomaterials can be exploited for novel applications where the properties of the atomic or bulk material are unsuitable. For example, bulk gold has a shiny surface. In contrast spherical gold nanoparticles efficiently absorb visible wavelengths with a size- and shape-dependent excitation of the particle plasmons, and may appear dark red to purple. Thus, as a material becomes nano-sized, the physical properties can become strikingly different.

Nanomaterials can be nanoparticles, nanofibres or nanoplates respectively, having 3, 2 or 1 dimensions within the nano-scale. For nanofibres the objects may be referred to as nanorods or nanotubes, depending upon whether the structure is hollow or solid. Electrically conductive nanofibres are defined as nanowires. Nanoparticles, which are investigated in this study, have all 3 dimensions within the nano-scale, but the dimensions do not differ by more than 3-fold, where the object may have properties more akin to a nanorod. For approximately-spherical nanoparticles, the size may be given as equivalent spherical diameter where the diameter of the equivalent sphere is the greatest dimension of the nanoparticle. However, the size-dependent properties of nanomaterials depend upon the level of coalescence. Thus two terms are important; ‘agglomerate’ and ‘aggregate’, which are often used interchangeably but have different meanings. Agglomerate refers to a group of nanoparticles that are associated by weak electrostatic forces but where the object has a surface area that is similar to the sum of the individual nanoparticles. An agglomerate may be dispersed within a system by a small amount of mechanical work to overcome the low energy of interaction, for example, by sonication [12]. Conversely, ‘aggregate’ refers to an association of nanoparticles with strong bonding, for example, covalent or ionic lattice bonds, where the surface area may be considerably smaller than that of the sum of the individual nanoparticles. Aggregations are therefore termed ‘secondary nanoparticles’, which have distinct properties from their constituent, smaller particles; termed ‘primary nanoparticles’ [13]. A quantum dot is a crystalline nanoparticle that has size dependant properties due to quantum confinement of excitons; with a characteristic wavelength and intensity of emitted fluorescence [14].

The terms nanocube and nanoprism have been used to describe various polyhedral nanoparticles [15, 16]. A nanosphere is a general term used to describe a quasi-spherical nanoparticle but in practise perfect spheres are not achieved; instead many near-spherical

nanoparticles have a multi-faceted topology [17, 18]. Finally, various terms have been used to describe nanomaterials according to their chemical composition; carbon related nanomaterials, dendrimers, semi-conductor nanocrystals, zero-valent metal nanoparticles and metal containing nanoparticles [9]. However, these definitions require further standardisation as many nanoparticles may fall within more than one category; for example ZnO nanoparticles can be classified as both semi-conductor nanocrystals and metal containing nanoparticles. Some authors use the term engineered nanoparticles to distinguish between the synthesised materials and the nano-sized debris that occurs naturally from weathering and attrition of sediment [19]. For clarity, the term 'nanoparticle' will be used to describe the materials used in this study, despite the mean particle size of some being beyond the 1-100 nm scale set out by the ISO.

### 1.3 Bacterial-Nanoparticle Interactions

Bacteria may be exposed to nanometre sized particles of sediment in their natural environment without adverse effects. However, the objective of this thesis is to study how synthetic nanoparticles interact with bacteria and to understand their impact on the physiology and metabolism of the organism. This could be achieved by two strategies. First, *in vivo* measurements of bacterial communities can be made where they are susceptible to nanomaterial exposure. For example, the normal flora of the skin may be exposed to large quantities of nanomaterials that are incorporated into topical preparations including sun-screen and cosmetics [8, 20-24]. However, measuring whole communities of bacteria is problematic. Most environmental bacteria are not easily cultured in the laboratory [25, 26] and culture-independent techniques, including DNA sequence-based identification, are semi-quantitative [27]. Accurate *in vivo* measurements are difficult to achieve and the great diversity of bacterial communities, both spatially and temporally,

may make data misrepresentative in small scale studies. The second approach is to study nanoparticle interactions with a well-characterised model system that is easily manipulated in the laboratory and has an international standard that can be made consistent between research groups. For this the model organism *Escherichia coli*, strain K12 was chosen.

### 1.3.1. *Escherichia coli* as a Model Organism for Studying Bacterial-Nanoparticle Interactions

*E. coli* is a member of the family *Enterobacteriaceae* within the phylum *Proteobacteria*. Other genera within this family are familiar pathogens including *Salmonella* spp., *Klebsiella* spp., *Shigella* spp. and *Yersinia* spp [28]. Thus, information gained from *E. coli* can be relevant in understanding serious and complicated bacterial infections of man. *E. coli* itself is a notorious enterohaemorrhragic pathogen and contaminant of drinking water and food [29]. The original K12 strain was isolated in 1922 from the colon of a diphtheria patient. Subsequently it was cured of a lysogenic bacteriophage, phage λ, and the $F^+$ extra-chromosomal fertility factor for conjugative transfer of plasmid DNA [30, 31]. The first whole genome sequence was determined for strain MG1655 in 1997 [32] and later for strain W3110; differing at only 8 intragenic loci [30]. The MG1655 genome contains approximately 4.64 million base pairs encoding 4,289 genes, almost half of which have been assigned a functional annotation [33].

The wealth of information available on this organism is available to the scientific community through initiatives including the EcoCyc database [34] and Coli Genetic Stock Centre [35]. These greatly benefit research with this organism, which is further reasoning for taking the model organism approach for the study of bacterial-nanoparticle interactions. Many aspects of this field have not been investigated and the details of how nanoparticles are toxic to bacteria are unclear. However publications pertaining to areas of

bionanotechnology research appear frequently in the literature, most of which have been published within the last decade.

### 1.3.2. Anti-Bacterial Nanoparticles

Anti-bacterial (against *E. coli*) nanoparticles have been synthesised from silver [36], copper [37], iron [38], cerium oxide [39], zinc oxide [40], titanium dioxide [41] and silicon dioxide [42]. Moreover, relatively inert gold nanoparticles are toxic when their surfaces are modified with ligands such as ionic surfactants or antibiotics [43, 44]. The toxicity of these nanomaterials has been determined for disperse preparations in liquid or solid bacteriological media at optimal temperature and pH for the test organism. Thus, the environmental efficacy of these nanoparticles may be significantly greater where bacteria must also respond to challenging nutrient limitation and sub-optimal conditions. Some studies have assessed the efficacy of potential nanoparticle based products directly. For example Ag and $TiO_2$ nanoparticles in surgical masks have been shown to be toxic to bacteria [41] and Ag nanoparticles are effective decontaminants in water purification filters [45]. The latter were prepared using a simple low-cost protocol whereby the filter material was immersed in a colloidal suspension of silver nanoparticles, which had an intrinsic affinity for the material fibres. This conferred the anti-bacterial properties of the nanoparticles to the filter.

Commonly used anti-bacterial nanoparticles are made from silver, Table 1.1. Experiments with GFP-labelled *E. coli* have shown that silver nanoparticles can cause cell lysis and the cells appear to shrink [46], consistent with an inhibition of cell growth. Further, silver nanoparticles denature bacterial signalling proteins [47] and the bacteria accumulate membrane protein precursors [48], indicating that protein damage and turnover may be important factors for toxicity. A recent hypothesis for silver nanoparticle

toxicity is the release of $Ag^+$, an antimicrobial cation that has been used since antiquity, and states that the toxicity of silver nanoparticles is proportional to the rate of $Ag^+$ release [36]. However, other modes of activity have been identified. For example, electron spin resonance spectroscopy experiments indicate that silver nanoparticles may generate free radicals [49], although the authors do not specify which radicals are produced. Further, the activity of these silver nanoparticles diminished in the presence of N-acetyl cysteine (NAC), a potent anti-oxidant. This leads to the hypothesis that redox stress may be an additional mechanism of toxicity, however NAC also sequesters $Ag^+$, and the matter requires further clarification.

**Table 1.1. Silver Nanoparticles in Anti-Bacterial Medical Products.**

| Brand Name | Manufacturer | Purpose |
|---|---|---|
| SilvaSorb® | AcryMed Inc. | Antimicrobial dressing for wound management |
| Silvalon® | Argentum Medical LLC | |
| Modern Medical Antimicrobial Wound Dressing | Modern Medical Equipment Manufacturing Ltd. | |
| Acticoat™ | Smith and Nephew plc | |
| Agento™ IC | C.R. Bard Inc. | Antimicrobial endotracheal tubing |
| Bardex™ IC | C.R. Bard Inc. | |
| XpressO Silver™ | Spire Corp. | Antimicrobial catheter coatings |
| RetroO Silver™ | Spire Corp. | |
| ON-Q™ SilverSoaker™ Antimicrobial Catheter | I-Flow Corp. | |
| Super G8 Nano Silver Mask | Greenhealthy Australia Pty Ltd. | Antimicrobial surgical mask |

Elsewhere, redox-active nanoparticles of iron or composite nanoparticles containing ferrous iron ($Fe^{2+}$) inhibit *E. coli* growth on solid medium [38]. Moreover, a superoxide dismutase deficient *E. coli* mutant was more sensitive to iron nanoparticles than the parent strain, indicating a potential mechanism of nanoparticle toxicity through redox stress [38]. The oxidative stress-based toxic mechanism may be reciprocated by $TiO_2$, $SiO_2$ and ZnO nanoparticles, where the effect on *E. coli* viability is more pronounced in light compared to dark, a result of the free electron by-product from photo-activation of the nanoparticle surfaces [42].

The majority of bionanotechnology studies have focused on the medical applications of nanoparticles, specifically where nanoparticles could be used as anti-bacterials, either independently or in combination with other treatments. For example, there is a synergistic toxic effect between silver nanoparticles and antibiotics when tested against *E. coli*. Originally this was reported for amoxicillin [50], and later the observation was extended to include enhancement of the effects of penicillin, erythromycin, clindamycin and vancomycin [51]. The latter study also reported a similar effect with *S. aureus*; both organisms are frequently isolated with antibiotic resistance [52]. Thus, there is potential to breathe new life into failing anti-bacterial strategies through synergistic effects with nanoparticles. The effect is not restricted to silver. Zinc oxide nanoparticles increase the sensitivity of laboratory *E. coli* to ciprofloxacin in disc diffusion assays [40]. However, this observation was specific for ciprofloxacin and none of 13 additional antibiotics showed any synergistic effects. In references [50] and [51] the silver nanoparticles and antibiotics were applied separately. In other work vancomycin was conjugated directly to the surface of gold nanoparticles and had a greater activity compared to adding vancomycin alone. In this case, the observed synergistic effects may occur because of an enhanced reactivity of molecules presented at a nanoparticle surface.

Nanoparticles are frequently observed in close association with *E. coli* [17, 39, 47, 53-55], thus the efficacy of anti-bacterial conjugates may be increased where they are concentrated directly at the cell envelope.

### 1.3.3. Other Applications of Bionanotechnology

In addition to antimicrobial effects, *E. coli* has been the subject of study in nanoparticle based bio-detection applications. A challenge in medical diagnostics is the rapid and accurate detection of specific bacteria. This is achieved clinically using culture based techniques or by amplification and sequencing of nucleic acids by Polymerase Chain Reaction (PCR), a process that is slow (hours or days) and labour intensive. The application of bionanotechnology for microbial detection strategies has been investigated using nanoparticles with an affinity for a bacterial surface. For example, immunoglobulin-functionalised quantum dots allow for fluorescence-based detection of a specific microbial antigen. Furthermore, photo-stable fluorescent dyes have been doped into a nano-scale silicon matrix and targeted towards pathogenic *E. coli* using specific monoclonal antibodies [56]. The detection method reported in that study allowed specific identification of *E. coli* within 20 minutes. Additionally magnetic iron-platinum composite nanoparticles conjugated to vancomycin can remove small numbers of *E. coli* from suspension [57, 58]. The vancomycin-*E. coli* interaction stabilises the nanoparticles on the bacterial surface, and the bacteria can be sedimented in an electromagnetic field according to the magnetic properties of the nanoparticles. Although purely prototypical, these methods clearly have potential for clinical use.

Another prototypical application for bionanotechnology is in bacterial transformation, a routine practice in the molecular biology laboratory for introducing nucleic acids into *E. coli* and other bacteria. A drawback of traditional electro-permeabilisation or chemical

transformation methods is that large numbers of bacteria must be used to compensate for the high percentage loss in cell viability. Using carbon nanotubes, Chapana and co-workers demonstrate that plasmid DNA (in this case the ~2.7 Kbp plasmid pUC19) can be transformed into viable *E. coli* K12 using a relatively low starting cell number [59]. The transient permeabilisation of the *E. coli* envelope also facilitated the internalisation of gold nanoparticles. However, a mechanistic understanding of this phenomenon has so far eluded researchers in the field, but must involve some disruption of the membrane integrity. Nanoparticle-based disruption of bacterial membranes is a recurring theme in this field [17, 43, 46, 53-55], and probably depends upon the nanoparticle surface charge. Gold nanoparticles with an uncharged polyethylene glycol (PEG) surface molecule did not inhibit the growth of *E. coli* in liquid culture [60]. Contrarily, gold nanoparticles with a cationic surface, but not an anionic surface, were toxic [43]. Additionally polyvinylpropylene (PVP)-coated silver nanoparticles were toxic to *E. coli* but anionic surfactant coated nanoparticles were not [61]. In reference [43] the electrostatic binding of nanoparticles to lipid vesicles resulted in release of contents. Perhaps this is reciprocated with viable *E. coli* where the nanoparticle binding destabilises the cell membrane.

Nanoparticles that may not disrupt bacterial membranes have also been exploited for potential applications. Gold nanoparticles have been used to coat *Bacillus cereus,* thus making the bacterium electrically conductive with potential applications in microelectronics [62]. The same nanoparticle-membrane interaction has been used to exploit the photo-thermal properties of various gold nanoparticles for therapeutic purposes. Anti-body coated gold nanospheres have been targeted to the surface of *Staphylococcus aureus*, followed by excitation of surface plasmons with a high-intensity pulse LASER [63]. The photo-thermal interaction on the nanoparticle surface led to thermal ablation of the

bacteria, the same principle being utilised in other biological disciplines for the destruction of various biological tissues including the disruption of tumours [64-68].

The various applications described here may have considerable potential but the most common large scale use of bionanotechnology is currently for antimicrobial applications. However, very little is known about the mechanism of nanomaterial toxicity including how an organism may defend itself. Perhaps the most important physical interaction is with the cell envelope [17, 53, 54], the interface between the bacterium and the nanomaterial in the environment.

### 1.3.4. The *E. coli* Cell Envelope

*E. coli* is an archetypical Gram negative organism and it is distinguished from Gram positive organisms as it does not retain crystal violet during the Gram staining procedure according to differences in the thickness of peptidoglycan in the cell wall [69]. The cell wall and underlying cell membrane are collectively referred to as the cell envelope, Figure 1.1

The *E. coli* surface is dominated by polysaccharide moieties, covalently attached to lipids within the external leaflet of the outer membrane. Perhaps $10^6$ lipopolysaccharides (LPS) [70] are interspersed by the exposed domains of integral outer membrane proteins. These molecules may determine the initial, physical interaction with a nanostructure. In immunology the LPS and exposed surface proteins constitute the pathogen associated molecular patterns (PAMPs), which are utilised by the innate immune system to differentiate between pathogen and host [71]. For example, the LPS of *E. coli* is recognised directly by Tol-Like Receptor 4 (TLR-4) on polymorphonuclear leukocytes and macrophages, cells which phagocytose and kill *E. coli* [72]. Accordingly, purified LPS can be conjugated to nanoparticles and subsequently phagocytosed by immune cells, specifically dendritic cells *in vitro* [73].

(A) The *E.coli* cell envelope

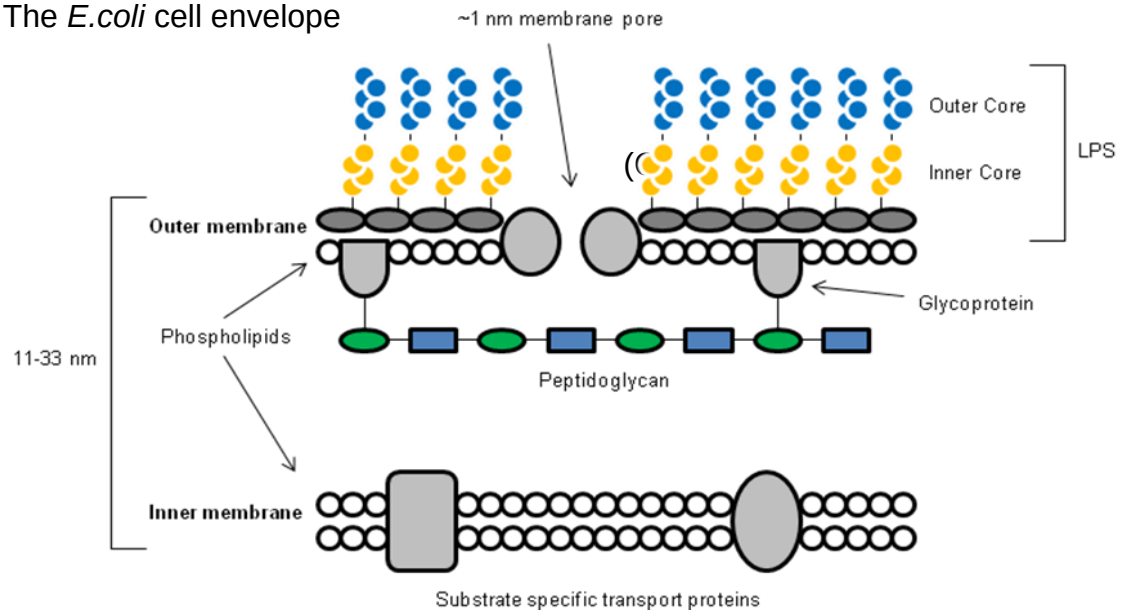


(B) Lipid A

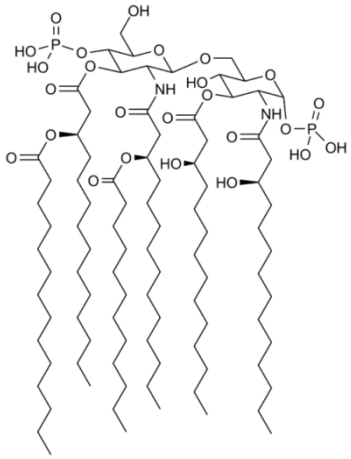

(C) Peptidoglycan

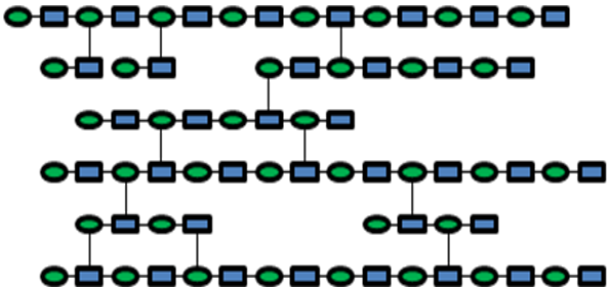

**Figure 1.1. (A) A cartoon of the *E. coli* cell envelope. The inner membrane is a 'fluid mosaic' of phospholipids and integral transport proteins with substrate specificity. The external membrane is made permeable by water filled channels allowing passage of small solutes into the periplasm. The inner membrane has a variable potential, but has been measured at -220 mV [74, 75] and is a source of electrochemical energy for integral membrane proteins. The outer leaflet of the exterior membrane is formed from Lipid A (shown in B), which is covalently modified with oligosaccharides on which phosphate groups confer an overall negative charge to the cell surface. The thickness of the cell wall has been estimated to be between 11 and 33 nm [76, 77]. The peptidoglycan has a mesh structure (shown in C) formed from repeating units of β-(1, 4) linked N-acetylglucosamine (blue squares) and N-acetylmuramic acid (green ovals), which are cross linked by short peptide bridges (4-5 amino acids) and attached to the outer membrane by glycoprotein anchors.**

The LPS is anchored to the cell surface by the hydrophobic acyl chains of lipid A, a glucosamine based saccharolipid [78]. Lipid A is synthesised by at least 9 enzymes and then covalently modified with a short polysaccharide 'core' from nucleotide sugars in a coordinated catalysis by membrane-associated transferase enzymes [79, 80]. The core polysaccharide contains two structurally different regions, the inner core and outer core. Whilst lipid A may be structurally conserved, the polysaccharide structures are highly variable between bacterial species and between different strains of *E. coli*. This may account for any differences in nanoparticle binding affinities where the LPS serve as the attachment site. Further, an extension to the core polysaccharides – the O-antigen – displays greater variability than the core sequences, a property that may favour evasion of immune-recognition. The MG1655 strain does not possess the extended O-antigen due to a mutation within the *rfb* gene cluster [81]. This may partly explain why the strain is less virulent than other *E. coli*; therefore MG1655 LPS may be structurally atypical of the wild-type but it does not cause disease in immunocompetent hosts and is suitable for manipulation in a Class I (Advisory Committee on Dangerous Pathogens, ACDP) microbiology facility. Phosphate residues on the inner and outer core domains of the LPS contribute to the overall surface charge of *E. coli*. The cell surface carries a net negative charge, a property that is important for bacterial adhesion to host tissues [82] or inorganic sub-strata during the initial stages of biofilm formation.

The cell envelope acts as a circumferential barrier that resists the turgor pressure of solutes within the cell cytosol [83]. The barrier allows passage of small solutes but not high molecular weight molecules such as nm-sized particles under normal conditions. This is evident in differential live-dead staining techniques where bacteria take up different fluorescent molecules according to molecular weight. Only live bacteria with a functional cell wall are able to exclude propidium iodide (molecular weight = 668) [84]. The outer

membrane is semi-permeable because it contains at least two types of water filled protein channels that are approximately 1 nm across [85] and small molecular weight molecules may pass according to an electrochemical gradient. In contrast the inner membrane is largely impassable, but does contain a plethora of integral protein transporters that control the movement of hydrophilic molecules.

The inter-membrane space is referred to as the periplasm and contains the sacculus (peptidoglycan), a mesh structure formed from repeating units of β-(1, 4) linked N-acetlyglucosamine (NAG) and N-acetylmuramic acid (NAM), which are cross linked by short peptide bridges (4-5 amino acids) and attached to the outer membrane by glycoprotein anchors [86]. The thickness of the peptidoglycan layer is what differentiates between Gram negative and Gram positive organisms during Grams staining procedure and maintains cell shape [87, 88]. Yet despite observation of the sacculus over 50 years ago, and its importance as a target for the β-lactam antibiotics including penicillin, the precise structural details remain controversial. A predicted topographical view of the peptidoglycan structure in *E. coli* is shown in Figure 1.1 (B). The length of the glycan strands is variable between strains and at different growth rates, growth phases and temperature, as is the degree of peptide cross-linking [89-92]. Typically the architecture is that of parallel strands of 20-40 NAG-NAM units (approximately 21-42 nm long) running with the longitudinal axis of the cell, which are cross linked [92]. Experiments on the permeability of purified sacculi to fluorescent dextran molecules indicate that the peptidoglycan may act as a molecular sieve, excluding molecules above 25 Kilodaltons (KDa) [93]. Thus, the sacculus may not present an effective barrier to smaller nanoparticles if one assumes that a 25 KDa globular protein may be less than 6 nm within the greatest dimension (determined by observation of general protein size and molecular weight on the Protein Data Bank [94]). It is still unknown whether the peptidoglycan in *E.*

*coli* is composed of a single layer or multiple layers [95] and it is difficult to comment on the potential for a molecule to be excluded through entanglement. As a covalent polymer, the sacculus is an important physical barrier within the cell wall, but is clearly dynamic being synthesised rapidly to facilitate cell growth and division, and flexing according to the turgor of the cytosol or deformation by physical stress. These surface features dominate the initial bacterial-nanoparticle interactions depending critically on the size of the nanoparticle and its surface chemistry.

## 1.4 Strategies for Nanoparticle Synthesis

Historically the greatest contributors to the global supply of nanomaterials were natural processes. Nanomaterials are formed through weathering and attrition of mineral deposits, during volcanic eruptions and in smoke from forest fires [96, 97]. After the industrial revolution, nanomaterials began to accumulate as by-products from metal working, combustion and mining. Subsequently, in the 20$^{th}$ century and today nanomaterials are produced in high tonnage for industrial purposes. They will ultimately end up in the environment once they have served their purpose to mankind.

Although several nano-enabled products are already available there is still a discrepancy between the nanoparticles that are frequently reported in the academic literature and those produced in bulk for industrial and commercial applications. Many academic publications that report research on noble metal nanoparticles use a wet-chemical synthesis approach. This is often referred to as the bottom-up approach in the literature [98]. For example, noble metal nanoparticles can be prepared by reducing metal cations in solution, a technique that was used by Michael Faraday in 1851. In recent times, a simple method for preparing colloidal gold nanoparticles was pioneered by John Turkevich and is one of the most widely used processes for preparing stable, mono-

disperse nanoparticles in solution [99-101]. Typically the metal ion ($Au^{3+}$) is reduced in solution, beginning an elementary growth reaction with metal atoms adding to the surface of a growing nanoparticle [102, 103]. The suspensions of nanoparticles may be stabilised by ionic ligands or surface-associated large, long chain molecules. These prevent agglomeration of the primary nanoparticles by electrostatic repulsion or steric hindrance respectively [43, 60]. The advantage to this approach for synthesis is that a stable suspension of nanoparticles can be prepared using standard laboratory apparatus with chemically controlled surfaces and shapes.

Wet chemical synthesised nanoparticle suspensions are usually referred to as ‘colloids’, where small particles are dispersed evenly through a medium, usually a fluid. In contrast, many industrial processes for nanoparticle synthesis are top-down, beginning with the bulk material and dispersing it into nano-sized particles. One of the most common industrial processes for the formation of nanoparticles is vapour phase synthesis in which the bulk material is vaporised and condensed. During this process the nanoparticles form from nucleation and growth processes [104, 105]. Volatilisation of noble metals followed by oxidisation prior to condensation has also been developed for the generation of metal oxide nanoparticles with distinct properties to their noble metal counterparts. The underlying principle encompassing all vapour phase synthesis techniques is that the gaseous phase becomes super-saturated to a point where it is thermodynamically favourable for the system to undergo spontaneous nucleation of sub-nanometre particles, followed by condensation of the remaining vapour. The advantage of this process is that large (gram) quantities of material can be produced, but typically having a poorly defined size and shape in comparison to wet-chemical techniques.

Many researchers favour the development of biological synthesis routes for nanoparticle production based upon their ‘green’ credentials. Species of microorganism

(Bacteria and Fungi) and plants possess the metabolic apparatus for the synthesis of noble metal nanoparticles from metal ion precursors by both intra- and extra-cellular catalysis (bottom-up synthesis) [106, 107]. To date, almost 50 species of bacteria have been identified as nanoparticle producers including the model organisms *Bacillus subtilis* [108], *Escherichia coli* [109, 110] and *Pseudomonas aeruginosa* [111]. Although the molecular mechanism is poorly understood the evolution of these processes may have been driven by the toxicity of metal ions in solution. Complexation of metal ions into elementary metal nanoparticles could, thus, constitute an effective defence.

## 1.5 Nanoparticle Characterisation

With the numerous methods available for nanoparticle synthesis, and the diversity of possible sizes, shapes and chemical compositions, it is important to characterise nanoparticles with accuracy to relate their physical and chemical properties to their observed behaviour in biological systems. Simple characteristic information (shape and size) is typically achieved by direct imaging and measurement, by electron microscopy, or by measuring the interaction between nanomaterials and electromagnetic radiation, by UV-Visible Spectroscopy and dynamic light scattering. Moreover, the rate of nanomaterial dissolution in various environments can be measured using mass spectrometry and atomic absorption or optical emission spectroscopy. These methods are considered here, with focus on those that were used for study.

### 1.5.1. Electron Microscopy

The first biological ‘cells’ were described by Robert Hooke in 1665 [112], only after invention of the compound microscope in the 16$^{th}$ century. In the last century optical microscopes became sufficiently sophisticated to allow microbiologists to observe viable

microorganisms with cellular detail. However, they do not provide sufficient resolving power to image nano-structures directly, which may have dimensions that are typically an order of magnitude smaller than a bacterium, and smaller than the smallest known virus. Optical microscopes are limited because the minimum wavelength of visible light ($\lambda$) is approximately 400 nm. Accordingly, the minimum resolvable distance between objects ($v$) is restricted, according to equation (1).

$$v = \frac{0.61\lambda}{N.A.}$$

*Equation (1)*

Where *N.A.* refers to the numerical aperture of the microscope system, which is related to the half angle of the greatest cone of light that may enter the objective. In practice this is always greater than 1.4 [113]. Therefore $v$ is equivalent to approximately 0.2 microns using the most sophisticated optical systems.

In contrast, the electron microscope utilises the electro-magnetic wave properties of electrons, which may have a wavelength several orders of magnitude smaller than that of visible light. Electrons are accelerated within a vacuum by a potential difference between the filament electron source and a detector, with the specimen in between. The wavelength of an electron is related to its velocity, and therefore the operating potential of the electron microscope. In the Transmission Electron Microscope (TEM) a typical operating potential is 100 keV where the wavelength of an electron ($\lambda_e$) is approximately 3.5 picometers (pm), providing sufficient resolution to image nm-sized objects and microorganisms with sub-cellular detail.

The TEM is acknowledged by the ISO as a standard characterisation tool for nanomaterials. As such, TEM is often used to determine nanoparticle size, shape and the

configuration of surface facets [17, 37, 40, 47, 49, 53, 54]. However, TEM may be limited by a 2-dimensional field of view. For example, the standard bright field mode TEM produces an image from the electron shadow that is formed as electrons pass through the specimen, with no resolution in the *z*-axis. In contrast, the Scanning Electron Microscope (SEM) is capable of generating 3-D images of nano-structure topography at sub-nm resolution. The technique is based upon a raster scan of the specimen with an electron beam, usually at a lower potential than in the TEM (typically 10-30 keV) and so a lower resolution may be achieved. Electrons are scattered backwards efficiently by high molecular weight regions of the specimen, thus generating the contrast required to produce an image. Additionally an SEM can be fitted with an X-Ray detector for elemental mapping and composition analysis. X-ray fluorescence is characteristic of the nuclei of atoms and allows identification of elements and their relative proportions in the specimen. This is utilised to determine the purity and composition of a specimen, which may be necessary where nanomaterials are produced through processes that are susceptible to contamination, for example by milling. All externally synthesised nanomaterials that were used in this study were characterised by TEM and Energy Dispersive Analysis of X-rays (EDAX) in combination with SEM prior to experimentation.

### 1.5.2. UV-Visible Spectroscopy

Information pertaining to the composition and structure of nanomaterials can be acquired using optical spectroscopy. This is most commonly applied to wet-chemical synthesised noble metal nanoparticles, where the extinction (absorbance and scattering) spectra of mono-disperse nanoparticles in suspension are dominated by a particle plasmon resonance (PPR). The plasmon is a wave within the conduction electrons of a metal surface and is a characteristic of all metals with freely-moving electrons in the

conduction band. The observed PPRs provide characteristic information about the nanoparticles, for example the wavelength of maximum extinction ($\lambda_{max}$) is characteristic for different materials and nanoparticle sizes [114, 115]. Moreover, the spectral trend (the number of peaks in the absorption spectra and their relative $\lambda_{max}$) is characteristic of different nanoparticle shapes [17]. The surface plasmons propagate around the interface between the surface of a metal nanoparticle and the medium. Therefore they are sensitive to changes at this interface and can be used as a characteristic tool to observe the interaction of surface adsorbed species. This property has been exploited for bio-sensing applications where the association or dissociation of biomaterial at the particle surface changes the wave propagation and therefore the position and intensity of $\lambda_{max}$ [116-118].

Although a detailed understanding of PPR is usually beyond the scope of microbiological studies, a spectrum of optical extinction is usually reported where metal nanoparticles are used in a colloidal suspension, and to indicate association with molecules such as protein ligands [17, 47, 49, 53, 54, 119]. PPR gives colloidal suspensions of spherical, disperse metal nanoparticles characteristic colours. This is a property that has been known since at least the 16$^{th}$ century, where colloidal gold was used for staining glass and ceramics.

### 1.5.3. Nanoparticle Dissolution

In addition to the characterisation of nanoparticle physical properties, the rate of dissolution in aqueous suspension is of particular interest. For example, dissolution kinetics are important for understanding the pharmacokinetic parameters of nano-sized drug particles, ‘nano-drugs’ [120]. Moreover, dissolution may determine the effective lifetimes of nanoparticles in medical products where they may release toxic constituents. The dissolution phenomenon is a dynamic and complicated process that has been

reviewed extensively [121], and has been linked with the toxic effects of metal and metal oxide nanoparticles to bacteria. For example, in Chapter 4 of this work there is evidence that the dissolution of silver nanoparticles releases silver cations into solution, which may be responsible for the anti-bacterial effects. Moreover, in Chapter 6 the dissolution of zinc oxide nanoparticles is considered, wherein dissolution may only account for partial toxic effects, which may be augmented with whole nanoparticle effects.

For dissolution, the atoms at the nanoparticle surface migrate into the bulk solution through a diffusion layer, a fluid layer that is proximal to the nanoparticle surface and that contains a high concentration of the solute, Figure 1.2. Dissolution is moderated by several factors including the proportion of atoms that are at the surface (surface area), thus is favoured for nanoparticles where a 30 nm particle may have 10% of total atoms at the surface, increasing to 20% for a 10 nm particle and 50% for a 3 nm particle [10, 122]. Tang and co-workers found that dissolution rate is dependent on particle size and shape, even if surface area and starting solute concentration are the same [123]. This may reflect protrusion or recession of surface morphologies with respect to the diffusion layer; effectively increasing or decreasing its thickness. For example, rough (high energy) surfaces will dissolve faster than smooth surfaces and an irregular nanoparticle topology may favour an initial high rate of dissolution with gradual smoothing followed by a slower and uniform rate. In nature, nanoparticles rarely exist as individual entities, but come together to form larger secondary particles, sometimes visible to the naked eye. If the energy of interaction is low the nanoparticles form an ‘agglomerate’ with a surface area that is similar to that of the sum of the individual nanoparticles and therefore may dissolve at a similar rate. An ‘aggregate’ has a high energy of interaction and a surface area that is significantly lower than the sum of the individual nanoparticles. Moreover, aggregations form negative curvatures that may increase the thickness of the diffusion layer and reduce

the rate of dissolution further. The rate of agglomeration and aggregation of nanoparticles is controlled by many factors.

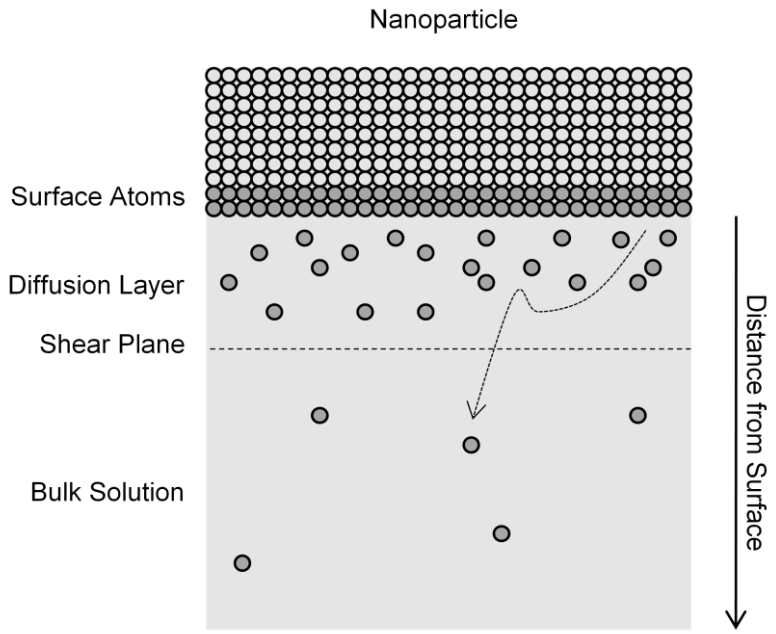


**Figure 1.2. A model for the dissolution of a nanoparticle adapted from reference [121]. Surface atoms dissociate from the nanoparticle and pass through a concentrated diffusion layer, demarcated from the bulk solution by a shear plane. The diffusion layer moves with the nanoparticle in suspension. In contrast, the bulk solution is turbulent and solutes are quickly dispersed. Dissolution kinetics are dependent on the surface area, the concentration of the solute within the diffusion layer and the bulk solution, the thickness of the diffusion layer, the diffusion coefficient, the redox potential of the medium and temperature. Other factors that may affect dissolution at the nano-scale are the nanoparticle size and shape.**

In the natural environment nanoparticle surfaces become coated with a dynamic protein 'corona' [124, 125] and nucleic acids [126]. The adsorbed molecules can act as a dispersant, preventing the nanoparticle surfaces from interacting by steric factors. This association may either promote or inhibit dissolution. If the surface molecules sequester the dissolved material then they can enhance the rate at which it is moved into the bulk solution, depending on the rate at which the molecule associates and dissociates with the

nanoparticle surface. Conversely, if the association is relatively unchanging, then the molecule may perturb the dissolution by obstructing the path of the solute into the bulk solution phase [121]. The fluid dynamics of a system may also impact nanoparticle dissolution where a turbulent system may favour a slower rate of aggregation. Further, the redox potential of the solution will be an important factor, where metal ions may dissolve from nanoparticles at a rate that is dependent upon the rate of oxidation of the surface [127]. The effects of these parameters have not been studied with biological systems in detail but a theoretical rate of dissolution can be calculated using the Noyes-Whitney model, equation (2).

$$\frac{dV}{dt} = \frac{DA(C_s - C_t)}{L}$$

*Equation (2)*

Where *D* is the diffusion coefficient, *V* is the particle volume, *A* is the surface area, $C_s$ is the concentration of the material within the diffusion layer, $C_t$ is the concentration of the material within the bulk solution and *L* is the thickness of the diffusion layer. The application of a dissolution model to nanoparticle research is clearly important and needs to be measured directly for well defined standardised systems [19, 121, 128-130]. For example, in Chapter 4 of this study the rate of dissolution for silver nanoparticles is measured in a bacteriological culture medium.

Previously, nanoparticle dissolution has been measured by atomic absorption (AA) [19], optical emission (OE) [128], and mass spectrometry (MS) [129, 131]. The latter, when coupled to sample ionisation in an inductively coupled plasma (ICP), is a quantitative technique for measuring total species concentrations with parts per trillion (PPT) sensitivity. A schematic of the ICP-MS principle is shown in Figure 1.3. ICP-MS is sensitive

to total species concentration regardless of the phase, and therefore, to measure the rate of nanoparticle dissolution, the solution phase must be extracted with minimum contamination with non-dissolved nanoparticles. This has been carried out using ultra-filtration [19] and equilibrium dialysis [132] techniques. Dialysis is clearly limited by the time required to allow each sample to reach equilibrium across the dialysis membrane, and then one cannot be sure that complete equilibrium has been reached. Filtration of nanoparticles of more than 100 nm may be possible using modern filter membranes. However, there is potential for solution phase material to interact with the filter, thus reducing the measured concentration in the sample. Ultracentrifugation using modern apparatus can produce gravitational forces suitable for sedimentation of very small molecules including proteins. Thus it may be suitable for measurement of dissolution in biological systems where only the free ion concentration may be important. Ions that are sequestered by proteins and other bio-molecules may not be relevant in a toxicological study.

(A) Sample injection and ionisation

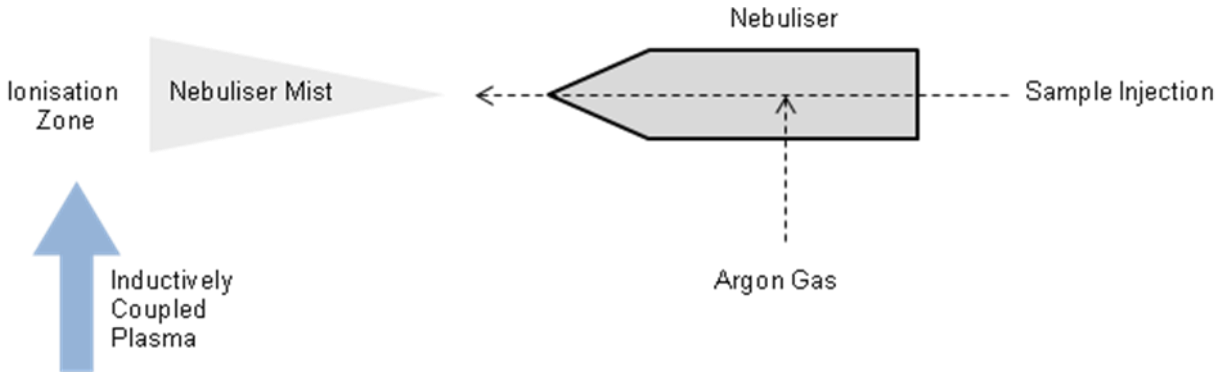


(B) Mass Spectrometry

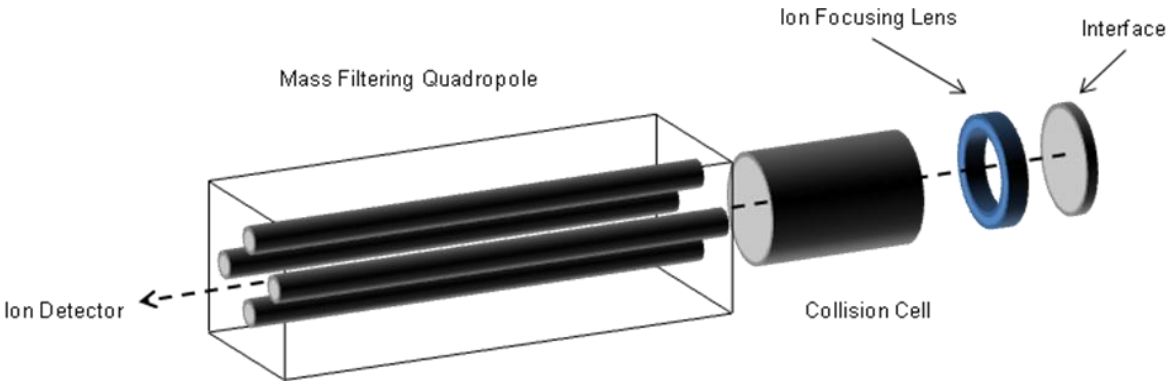


**Figure 1.3. Inductively Coupled Plasma Mass Spectrometry. (A) A sample for measurement is injected into a nebuliser, generating a fine mist in argon gas. In the inductively coupled plasma the sample is dried, vaporised and ionised at approximately 6,000$^{o}$C. (B) The sample passes through the interface, which isolates the hot, pressurised ionisation chamber from the cool vacuum of the mass spectrometer. The ion beam is electrostatically focused and passes through a collision cell, which removes interfering ions, and then a mass filtering quadrupole. Finally the ions are detected and the information is passed to a processing system.**

## 1.6. Conclusions

Nanoparticles may exist with properties that are different to the bulk material or individual atoms. Therefore they represent a potentially un-tapped resource from which their physical and chemical characteristics could be used for novel applications. In the life sciences bionanotechnology has already realised a number of prototypical applications for nanoparticle properties such as new bio-detection and sensing strategies, and potential antimicrobial activities. Moreover, some of these applications have already entered the commercial sector, wherein nanoparticle based antimicrobial products are now available in a variety of formulations. However, the precise mechanism of how these materials are toxic to microbes is unclear.

## 1.7. Objectives

This study has been carried out to investigate the interactions that occur between nanoparticles and bacteria. For this, the model Gram negative bacterium *Escherichia coli* K12 has been chosen. Its physiology, metabolism, genome and proteome are comparatively well characterised, and the organism has already featured highly in published literature in this field. Several theoretical *E. coli*-nanoparticle interactions are considered, Figure 1.4, and this thesis aims to address each of them, utilising the model-organism approach.

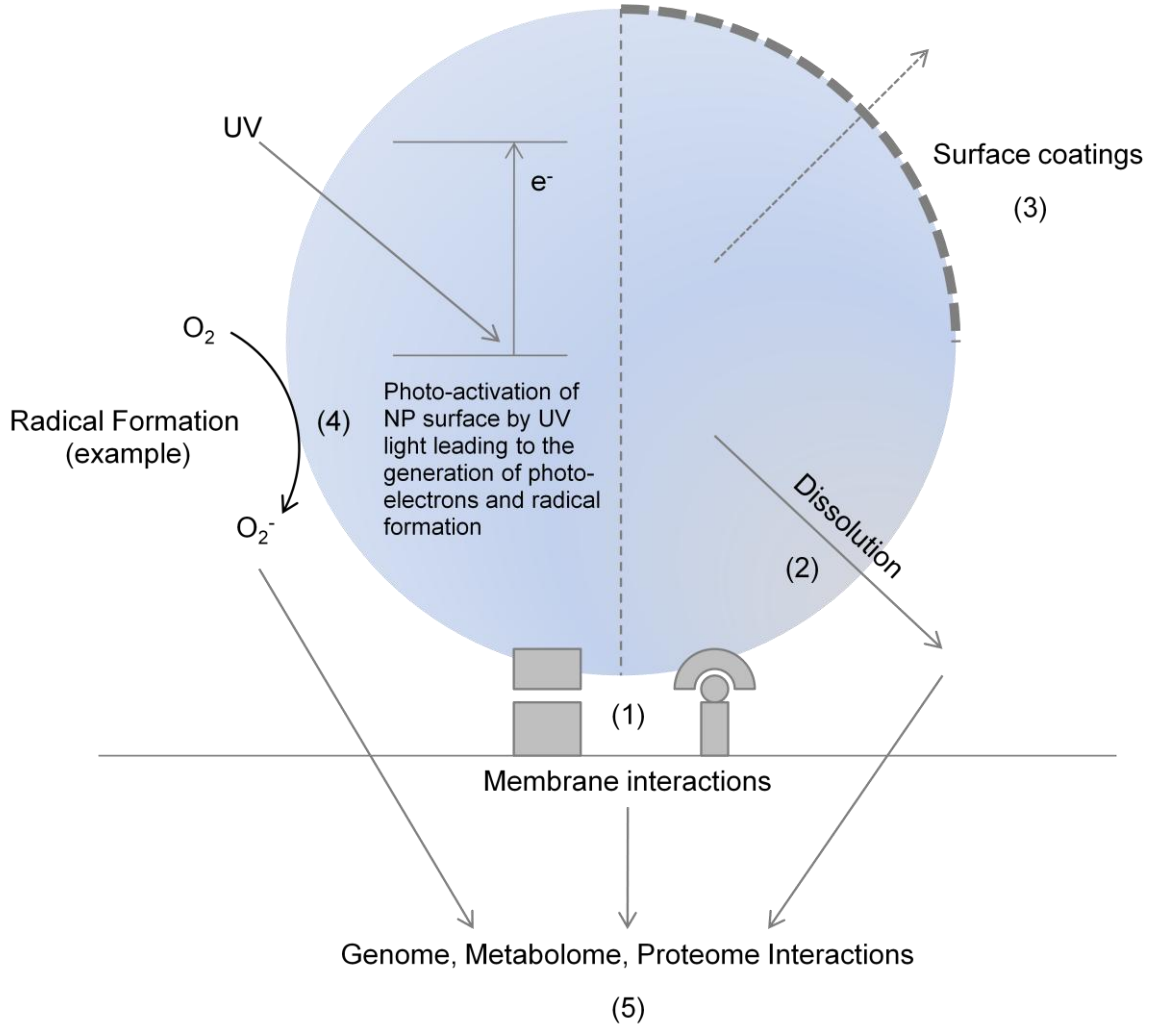


**Figure 1.4. Bacterial-nanoparticle interactions for investigation in this study. (1) A nanoparticle may associate with a bacterial membrane. (2) A nanoparticle may dissolve, releasing anti-bacterial constituents into the surrounding medium. (3) Surface coatings may influence a membrane interaction and the rate of dissolution. (4) photo-active nanoparticles may interact with UV light, leading to the formation of photo-radicals. (5) The aforementioned interactions influence the bacterial genome, metabolome and proteome.**

## 1.8. Thesis Overview

In **Chapter 3** the interaction between *E. coli* and chemically synthesised gold and silver nanoparticles is investigated using transmission electron micrographs. The aim of the chapter is to establish the nature of the physical membrane-nanoparticle interaction, including the effect of the nanoparticle surface coating, and to clarify the issue of nanoparticle uptake into viable bacteria. The limitations of TEM as a technique for assessing the bacterial-nanoparticle interactions are considered.

In **Chapter 4** the anti-bacterial effects of an industrial grade silver nanoparticle preparation are investigated using culture-based techniques and by measuring a transcriptional stress response. A hypothesis for nanoparticle dissolution is addressed by directly measuring the rate at which silver nanoparticles may release ions into the bulk solution phase. Moreover, an observed nanoparticle-membrane interaction leads to the generation of a novel hypothesis for a differential nanoparticle and ion anti-bacterial effect.

In **Chapter 5** the interaction between silver nanoparticles and the *E. coli* transcriptome is investigated using gene expression microarrays. The transcriptional response for silver ions, and differentially for silver ions from nanoparticles that dissolve at the membrane is measured in independent experiments.

In **Chapter 6** an investigation is undertaken into the anti-bacterial effects of an industrial grade zinc oxide nanoparticle formulation. Anti-bacterial activity is identified from dissolution and also from whole nanoparticle effects, based upon photo-electron generation from the interaction of the nanoparticle surfaces with ultra-violet light. The photo-redox stress response is also discussed as a new mechanism of nanoparticle toxicity.

## 1.9 References


1. Thornton, M., Young, R., Park, B., *Nanotechnology: A UK Industry View*. 2010.
2. Li, Q., et al., *Antimicrobial nanomaterials for water disinfection and microbial control: potential applications and implications.* Water Res, 2008. **42**(18): p. 4591-602.
3. Rai, M., A. Yadav, and A. Gade, *Silver nanoparticles as a new generation of antimicrobials.* Biotechnol Adv, 2009. **27**(1): p. 76-83.
4. Levy, S., B., *The Antiobiotic Paradox: How the Misuse of Antibiotics Destroys Their Curative Powers*. 1st Edition ed. 2002: Da Capo Press.
5. Horner-Devine, C., K. Carney, and B. Bohannan, *An ecological perspective on bacterial biodiversity.* Proceedings of the Royal Society of London. Series B: Biological Sciences, 2004. **271**(1535): p. 113-122.
6. OberdÃrster, G., E. OberdÃrster, and J. OberdÃrster, *Nanotoxicology: an emerging discipline evolving from studies of ultrafine particles.* Environmental health perspectives, 2005. **113**(7): p. 823-839.
7. Oberdorster, G., et al., *Principles for characterizing the potential human health effects from exposure to nanomaterials: elements of a screening strategy.* Particle and Fibre Toxicology, 2005. **2**(1): p. 8.
8. Tsuji, J.S., et al., *Research strategies for safety evaluation of nanomaterials, part IV: risk assessment of nanoparticles.* Toxicol Sci, 2006. **89**(1): p. 42-50.
9. Klaine, S.J., et al., *Nanomaterials in the environment: behavior, fate, bioavailability, and effects.* Environ Toxicol Chem, 2008. **27**(9): p. 1825-51.
10. Nel, A., et al., *Toxic Potential of Materials at the Nanolevel.* Science, 2006. **311**(5761): p. 622-627.
11. *ISO/TS 27687 Nanotechnologies - Terminology and Definitions for Nano-Objects - Nanoparticle, Nanofibre and Nanoplate*. 2008.
12. Bihari, P., et al., *Optimized dispersion of nanoparticles for biological in vitro and in vivo studies.* Particle and Fibre Toxicology, 2008. **5**(1): p. 14.
13. Müller, F., et al., *Dispersing nanoparticles in liquids.* International Journal of Mineral Processing, 2004. **74**(Supplement 1): p. S31-S41.
14. Bukowski, T.J. and J.H. Simmons, *Quantum Dot Research: Current State and Future Prospects.* Critical Reviews in Solid State and Materials Sciences, 2002. **27**(3): p. 119 - 142.

15. Gou, L. and C.J. Murphy, *Solution-Phase Synthesis of Cu2O Nanocubes.* Nano Letters, 2002. **3**(2): p. 231-234.

16. Jin, R., et al., *Photoinduced Conversion of Silver Nanospheres to Nanoprisms.* Science, 2001. **294**(5548): p. 1901-1903.

17. Pal, S., Y.K. Tak, and J.M. Song, *Does the Antibacterial Activity of Silver Nanoparticles Depend on the Shape of the Nanoparticle? A Study of the Gram-Negative Bacterium Escherichia coli.* Appl. Environ. Microbiol., 2007. **73**(6): p. 1712-1720.

18. Wang, Z.L. and X. Feng, *Polyhedral Shapes of CeO2 Nanoparticles.* The Journal of Physical Chemistry B, 2003. **107**(49): p. 13563-13566.

19. Miao, A.J., et al., *Zinc oxide engineered nanoparticles: Dissolution and toxicity to marine phytoplankton.* Environmental Toxicology and Chemistry, 2010. **29**(12): p. 2814-2822.

20. Hoet, P., I. Bruske-Hohlfeld, and O. Salata, *Nanoparticles - known and unknown health risks.* Journal of Nanobiotechnology, 2004. **2**(1): p. 12.

21. Kreilgaard, M., *Influence of microemulsions on cutaneous drug delivery.* Advanced Drug Delivery Reviews, 2002. **54**(Supplement 1): p. S77-S98.

22. Cross, S.E., et al., *Human skin penetration of sunscreen nanoparticles: in-vitro assessment of a novel micronized zinc oxide formulation.* Skin Pharmacol Physiol, 2007. **20**(3): p. 148-54.

23. Zhang, L.W., et al., *Biological interactions of quantum dot nanoparticles in skin and in human epidermal keratinocytes.* Toxicology and Applied Pharmacology, 2008. **228**(2): p. 200-211.

24. Zvyagin, A.V., et al., *Imaging of zinc oxide nanoparticle penetration in human skin in vitro and in vivo.* Journal of Biomedical Optics, 2008. **13**(6): p. 064031-9.

25. Barer, M.R., *Viable but non-culturable and dormant bacteria: time to resolve an oxymoron and a misnomer?* J Med Microbiol, 1997. **46**(8): p. 629-631.

26. Oliver, J.D., *The viable but nonculturable state in bacteria.* J Microbiol, 2005. **43 Spec No**: p. 93-100.

27. Weng, L., E.M. Rubin, and J. Bristow, *Application of sequence-based methods in human microbial ecology.* Genome Research, 2006. **16**(3): p. 316-322.

28. Madigan, M., T., Martinko, J., M., Dunlap, P., D., Clark, D., P, *Brock Biology of Microorganisms*. 2008, Benjamin Cummings. p. 1168.

29. Doyle, M.P., *Escherichia coli O157:H7 and its significance in foods.* Int J Food Microbiol, 1991. **12**(4): p. 289-301.

30. Hayashi, K., et al., *Highly accurate genome sequences of Escherichia coli K-12 strains MG1655 and W3110.* Mol Syst Biol, 2006. **2**.

31. Guyer, M.S., et al., *Identification of a sex-factor-affinity site in E. coli as gamma delta.* Cold Spring Harb Symp Quant Biol, 1981. **45 Pt 1**: p. 135-40.

32. Blattner, F.R., et al., *The Complete Genome Sequence of Escherichia coli K-12.* Science, 1997. **277**(5331): p. 1453-1462.

33. Riley, M., et al., *Escherichia coli K-12: a cooperatively developed annotation snapshot.* Nucleic Acids Research, 2005. **34**(1): p. 1-9.

34. Keseler, I.M., et al., *EcoCyc: A comprehensive view of Escherichia coli biology.* Nucleic Acids Research, 2009. **37**(suppl 1): p. D464-D470.

35. Maloy, S.R., et al., *Strain Collections and Genetic Nomenclature*, in *Methods in Enzymology*. 2007, Academic Press. p. 3-8.

36. Wijnhoven, S.W.P., et al., *Nano-silver: a review of available data and knowledge gaps in human and environmental risk assessment.* Nanotoxicology, 2009. **3**(2): p. 109 - 138.

37. Yoon, K.-Y., et al., *Susceptibility constants of Escherichia coli and Bacillus subtilis to silver and copper nanoparticles.* Science of The Total Environment, 2007. **373**(2-3): p. 572-575.

38. Auffan, M.l., et al., *Relation between the Redox State of Iron-Based Nanoparticles and Their Cytotoxicity toward Escherichia coli.* Environmental Science & Technology, 2008. **42**(17): p. 6730-6735.

39. Thill, A., et al., *Cytotoxicity of CeO2 Nanoparticles for Escherichia coli. Physico-Chemical Insight of the Cytotoxicity Mechanism.* Environmental Science & Technology, 2006. **40**(19): p. 6151-6156.

40. Banoee, M., et al., *ZnO nanoparticles enhanced antibacterial activity of ciprofloxacin against Staphylococcus aureus and Escherichia coli.* Journal of Biomedical Materials Research Part B: Applied Biomaterials, 2010. **93B**(2): p. 557-561.

41. Li, Y., et al., *Antimicrobial effect of surgical masks coated with nanoparticles.* Journal of Hospital Infection, 2006. **62**(1): p. 58-63.

42. Adams, L.K., D.Y. Lyon, and P.J.J. Alvarez, *Comparative eco-toxicity of nanoscale TiO2, SiO2, and ZnO water suspensions.* Water Research, 2006. **40**(19): p. 3527-3532.

43. Goodman, C.M., et al., *Toxicity of Gold Nanoparticles Functionalized with Cationic and Anionic Side Chains.* Bioconjugate Chemistry, 2004. **15**(4): p. 897-900.

44. Gu, H., et al., *Presenting Vancomycin on Nanoparticles to Enhance Antimicrobial Activities.* Nano Letters, 2003. **3**(9): p. 1261-1263.

45. Jain, P. and T. Pradeep, *Potential of silver nanoparticle-coated polyurethane foam as an antibacterial water filter.* Biotechnology and Bioengineering, 2005. **90**(1): p. 59-63.

46. Gogoi, S.K., et al., *Green Fluorescent Protein-Expressing Escherichia coli as a Model System for Investigating the Antimicrobial Activities of Silver Nanoparticles.* Langmuir, 2006. **22**(22): p. 9322-9328.

47. Siddhartha, S. and et al., *Characterization of enhanced antibacterial effects of novel silver nanoparticles.* Nanotechnology, 2007. **18**(22): p. 225103.

48. Lok, C.-N., et al., *Proteomic Analysis of the Mode of Antibacterial Action of Silver Nanoparticles.* Journal of Proteome Research, 2006. **5**(4): p. 916-924.

49. Kim, J.S., et al., *Antimicrobial effects of silver nanoparticles.* Nanomedicine, 2007. **3**(1): p. 95-101.

50. Ping, L. and et al., *Synergistic antibacterial effects of Î²-lactam antibiotic combined with silver nanoparticles.* Nanotechnology, 2005. **16**(9): p. 1912.

51. Shahverdi, A.R., et al., *Synthesis and effect of silver nanoparticles on the antibacterial activity of different antibiotics against Staphylococcus aureus and Escherichia coli.* Nanomedicine, 2007. **3**(2): p. 168-71.

52. Kronvall, G., *Antimicrobial resistance 1979-2009 at Karolinska hospital, Sweden: normalized resistance interpretation during a 30-year follow-up on Staphylococcus aureus and Escherichia coli resistance development.* APMIS, 2010. **118**(9): p. 621-39.

53. Jose Ruben, M. and et al., *The bactericidal effect of silver nanoparticles.* Nanotechnology, 2005. **16**(10): p. 2346.

54. Sondi, I. and B. Salopek-Sondi, *Silver nanoparticles as antimicrobial agent: a case study on E. coli as a model for Gram-negative bacteria.* Journal of Colloid and Interface Science, 2004. **275**(1): p. 177-182.

55. Stoimenov, P.K., et al., *Metal Oxide Nanoparticles as Bactericidal Agents.* Langmuir, 2002. **18**(17): p. 6679-6686.

56. Zhao, X., et al., *A rapid bioassay for single bacterial cell quantitation using bioconjugated nanoparticles.* Proceedings of the National Academy of Sciences of the United States of America, 2004. **101**(42): p. 15027-15032.

57. Gu, H., et al., *Using biofunctional magnetic nanoparticles to capture Gram-negative bacteria at an ultra-low concentration.* Chemical Communications, 2003(15): p. 1966-1967.

58. Lin, Y.-S., et al., *Affinity Capture Using Vancomycin-Bound Magnetic Nanoparticles for the MALDI-MS Analysis of Bacteria.* Analytical Chemistry, 2005. **77**(6): p. 1753-1760.

59. Rojas-Chapana, J., et al., *Multi-walled carbon nanotubes for plasmid delivery into Escherichia coli cells.* Lab on a Chip, 2005. **5**(5): p. 536-539.

60. Williams, D., S. Ehrman, and T. Pulliam Holoman, *Evaluation of the microbial growth response to inorganic nanoparticles.* Journal of Nanobiotechnology, 2006. **4**(1): p. 3.

61. Cho, K.-H., et al., *The study of antimicrobial activity and preservative effects of nanosilver ingredient.* Electrochimica Acta, 2005. **51**(5): p. 956-960.

62. Berry, V. and R.F. Saraf, *Self-Assembly of Nanoparticles on Live Bacterium: An Avenue to Fabricate Electronic Devices.* Angewandte Chemie, 2005. **117**(41): p. 6826-6831.

63. Zharov, V.P., et al., *Photothermal Nanotherapeutics and Nanodiagnostics for Selective Killing of Bacteria Targeted with Gold Nanoparticles.* Biophysical journal, 2006. **90**(2): p. 619-627.

64. Huang, X., et al., *Plasmonic photothermal therapy (PPTT) using gold nanoparticles.* Lasers in Medical Science, 2008. **23**(3): p. 217-228.

65. Huang, X., et al., *Comparative study of photothermolysis of cancer cells with nuclear-targeted or cytoplasm-targeted gold nanospheres: continuous wave or pulsed lasers.* Journal of Biomedical Optics, 2008. **15**(5): p. 58002-7.

66. Wang, S., et al., *Photothermal Effects of Supramolecularly Assembled Gold Nanoparticles for the Targeted Treatment of Cancer Cells.* Angewandte Chemie International Edition, 2010. **49**(22): p. 3777-3781.

67. Chen, J., et al., *Gold Nanocages as Photothermal Transducers for Cancer Treatment.* Small, 2010. **6**(7): p. 811-817.

68. Cobley, C.M., et al., *Targeting gold nanocages to cancer cells for photothermal destruction and drug delivery.* Expert Opinion on Drug Delivery, 2010. **7**(5): p. 577-587.

69. Biswas, B.B., P.S. Basu, and M.K. Pal, *Gram staining and its molcecular mechanism.* Int Rev Cytol, 1970. **29**: p. 1-27.

70. Guan, Z., S.D. Breazeale, and C.R.H. Raetz, *Extraction and identification by mass spectrometry of undecaprenyl diphosphate-MurNAc-pentapeptide-GlcNAc from Escherichia coli.* Analytical Biochemistry, 2005. **345**(2): p. 336-339.

71. Janeway, C., Travers, P., Walport, M., Schlomchik, M., *Immunobiology*. 6th ed. 2004: Garland Science. 800.

72. Miller, S.I., R.K. Ernst, and M.W. Bader, *LPS, TLR4 and infectious disease diversity.* Nat Rev Micro, 2005. **3**(1): p. 36-46.

73. Demento, S.L., et al., *Inflammasome-activating nanoparticles as modular systems for optimizing vaccine efficacy.* Vaccine, 2009. **27**(23): p. 3013-3021.

74. Bot, C.T. and C. Prodan, *Quantifying the membrane potential during E. coli growth stages.* Biophysical Chemistry. **146**(2-3): p. 133-137.

75. Felle, H., et al., *Quantitative measurements of membrane potential in Escherichia coli.* Biochemistry, 1980. **19**(15): p. 3585-3590.

76. de Petris, S., *Ultrastructure of the cell wall of Escherichia coli and chemical nature of its constituent layers.* Journal of Ultrastructure Research, 1967. **19**(1-2): p. 45-83.

77. Matias, V.R.F., et al., *Cryo-Transmission Electron Microscopy of Frozen-Hydrated Sections of Escherichia coli and Pseudomonas aeruginosa.* J. Bacteriol., 2003. **185**(20): p. 6112-6118.

78. Fahy, E., et al., *A comprehensive classification system for lipids.* Journal of Lipid Research, 2005. **46**(5): p. 839-862.

79. Raetz, C.R.H., et al., *Lipid A Modification Systems in Gram-Negative Bacteria.* Annual Review of Biochemistry, 2007. **76**(1): p. 295-329.

80. Wang, X. and P.J. Quinn, *Lipopolysaccharide: Biosynthetic pathway and structure modification.* Progress in Lipid Research, 2010. **49**(2): p. 97-107.

81. Stevenson, G., et al., *Structure of the O antigen of Escherichia coli K-12 and the sequence of its rfb gene cluster.* J. Bacteriol., 1994. **176**(13): p. 4144-4156.

82. Li, J. and L.A. McLandsborough, *The effects of the surface charge and hydrophobicity of Escherichia coli on its adhesion to beef muscle.* International Journal of Food Microbiology, 1999. **53**(2-3): p. 185-193.

83. Scheie, P., *Osmotic Pressure in Escherichia coli as Rendered Detectable by Lysozyme Attack.* J. Bacteriol., 1973. **114**(2): p. 549-555.

84. Stocks, S.M., *Mechanism and use of the commercially available viability stain, BacLight.* Cytometry Part A, 2004. **61A**(2): p. 189-195.

85. Nikaido, H., *Microdermatology: cell surface in the interaction of microbes with the external world.* J Bacteriol, 1999. **181**(1): p. 4-8.

86. Gan, L., S. Chen, and G.J. Jensen, *Molecular organization of Gram-negative peptidoglycan.* Proc Natl Acad Sci U S A, 2008. **105**(48): p. 18953-7.

87. Huang, K.C., et al., *Cell shape and cell-wall organization in Gram-negative bacteria.* Proceedings of the National Academy of Sciences, 2008. **105**(49): p. 19282-19287.

88. Gram, C., *Ueber dieisolirte Farbung der Schizomyceten in Schnitt-und Trockenpraparaten.* Fortschritte der Medicin, 1884. **2**: p. 185-189.

89. Driehuis, F. and J.T. Wouters, *Effect of growth rate and cell shape on the peptidoglycan composition in Escherichia coli.* J. Bacteriol., 1987. **169**(1): p. 97-101.

90. Glauner, B., J.V. HÃ¶ltje, and U. Schwarz, *The composition of the murein of Escherichia coli.* Journal of Biological Chemistry, 1988. **263**(21): p. 10088-10095.

91. Schindler, M., D. Mirelman, and U. Schwarz, *Quantitative Determination of N-Acetylglucosamine Residues at the Non-reducing Ends of Peptidoglycan Chains by Enzymic Attachment of [14C]-d-Galactose.* European Journal of Biochemistry, 1976. **71**(1): p. 131-134.

92. Vollmer, W. and S.J. Seligman, *Architecture of peptidoglycan: more data and more models.* Trends in Microbiology, 2010. **18**(2): p. 59-66.

93. Demchick, P. and A.L. Koch, *The permeability of the wall fabric of Escherichia coli and Bacillus subtilis.* J. Bacteriol., 1996. **178**(3): p. 768-773.

94. Berman, H., K. Henrick, and H. Nakamura, *Announcing the worldwide Protein Data Bank.* Nat Struct Mol Biol, 2003. **10**(12): p. 980-980.

95. Gan, L., S. Chen, and G.J. Jensen, *Molecular organization of Gram-negative peptidoglycan.* Proceedings of the National Academy of Sciences, 2008. **105**(48): p. 18953-18957.

96. Hough, R.M., et al., *Naturally occurring gold nanoparticles and nanoplates.* Geology, 2008. **36**(7): p. 571-574.

97. Goldman, L., Coussens, C. *Implications of Nanotechnology for Environmental Health Research*. in *Institute of Medicine (US) Roundtable on Environmental Health Sciences, Research, and Medicine*. 2005: National Academies Press

98. Wang, Y. and Y. Xia, *Bottom-Up and Top-Down Approaches to the Synthesis of Monodispersed Spherical Colloids of Low Melting-Point Metals.* Nano Letters, 2004. **4**(10): p. 2047-2050.

99. Frens, G., *Particle size and sol stability in metal colloids.* Colloid & Polymer Science, 1972. **250**(7): p. 736-741.

100. Kimling, J., et al., *Turkevich Method for Gold Nanoparticle Synthesis Revisited.* The Journal of Physical Chemistry B, 2006. **110**(32): p. 15700-15707.

101. Turkevich, J., P. Stevenson, and J. Hillier, *A study of the nucleation and growth processes in the synthesis of colloidal gold.* Discuss. Faraday Soc., 1951. **11**: p. 55-75.

102. Schmid, G., *Nanoparticles: From Theory to Application*. 1st Edition ed. 2004: Wiley-VCH.

103. Polte, J.r., et al., *Mechanism of Gold Nanoparticle Formation in the Classical Citrate Synthesis Method Derived from Coupled In Situ XANES and SAXS Evaluation.* Journal of the American Chemical Society, 2010. **132**(4): p. 1296-1301.

104. Granqvist, C., G., Kish, L., B., Marlow, W., H., *Gas Phase Nanoparticle Synthesis*. 2004: Springer.

105. Schoonman, J., *Vapour-phase Synthesis and Processing of Nanoparticle Materials (ESF/NANO): Four Years of European Collaboration.* Journal of Nanoparticle Research, 1999. **1**(3): p. 325-328.

106. Narayanan, K.B. and N. Sakthivel, *Biological synthesis of metal nanoparticles by microbes.* Advances in Colloid and Interface Science, 2010. **156**(1-2): p. 1-13.

107. Rai, M., A. Yadav, and A. Gade, *CRC 675â€"Current Trends in Phytosynthesis of Metal Nanoparticles.* Critical Reviews in Biotechnology, 2008. **28**(4): p. 277-284.

108. Beveridge, T.J. and R.G. Murray, *Sites of metal deposition in the cell wall of Bacillus subtilis.* J. Bacteriol., 1980. **141**(2): p. 876-887.

109. Du, L., et al., *Biosynthesis of gold nanoparticles assisted by Escherichia coli DH5[alpha] and its application on direct electrochemistry of hemoglobin.* Electrochemistry Communications, 2007. **9**(5): p. 1165-1170.

110. Sweeney, R.Y., et al., *Bacterial biosynthesis of cadmium sulfide nanocrystals.* Chem Biol, 2004. **11**(11): p. 1553-9.

111. Husseiny, M.I., et al., *Biosynthesis of gold nanoparticles using Pseudomonas aeruginosa.* Spectrochimica Acta Part A: Molecular and Biomolecular Spectroscopy, 2007. **67**(3-4): p. 1003-1006.

112. Hooke, R., *Micrographia*. 1665.

113. Mertz, C., J., *Introduction to Optical Microscopy*. 1st Edition ed. 2009: Roberts and Company Publishers.

114. Otto, A., *Excitation of nonradiative surface plasma waves in silver by the method of frustrated total reflection.* Zeitschrift für Physik A Hadrons and Nuclei, 1968. **216**(4): p. 398-410.

115. Wood, R., W., *Remarkable Spectrum from a Diffraction Grating.* Philosophical Magazine, 1902. **4**: p. 396-402.

116. Haes, A.J., et al., *A Localized Surface Plasmon Resonance Biosensor:â€‰ First Steps toward an Assay for Alzheimer's Disease.* Nano Letters, 2004. **4**(6): p. 1029-1034.

117. He, L., et al., *Colloidal Au-Enhanced Surface Plasmon Resonance for Ultrasensitive Detection of DNA Hybridization.* Journal of the American Chemical Society, 2000. **122**(38): p. 9071-9077.

118. Willets, K.A. and R.P. Van Duyne, *Localized Surface Plasmon Resonance Spectroscopy and Sensing.* Annual Review of Physical Chemistry, 2007. **58**(1): p. 267-297.

119. Pissuwan, D., et al., *Gold Nanosphere-Antibody Conjugates for Hyperthermal Therapeutic Applications.* Gold Bulletin, 2007. **40**: p. 121-129.

120. Heng, D., et al., *What is a Suitable Dissolution Method for Drug Nanoparticles?* Pharmaceutical Research, 2008. **25**(7): p. 1696-1701.

121. Borm, P., et al., *Research Strategies for Safety Evaluation of Nanomaterials, Part V: Role of Dissolution in Biological Fate and Effects of Nanoscale Particles.* Toxicological Sciences, 2006. **90**(1): p. 23-32.

122. Reddy, K.M., et al., *Selective toxicity of zinc oxide nanoparticles to prokaryotic and eukaryotic systems.* Appl Phys Lett, 2007. **90**(213902): p. 2139021-2139023.

123. Tang, R., C.A. Orme, and G.H. Nancollas, *Dissolution of crystallites: surface energetic control and size effects.* Chemphyschem, 2004. **5**(5): p. 688-96.

124. Casals, E., et al., *Time Evolution of the Nanoparticle Protein Corona.* ACS Nano, 2010. **4**(7): p. 3623-3632.

125. Cedervall, T., et al., *Understanding the nanoparticle protein corona using methods to quantify exchange rates and affinities of proteins for nanoparticles.* Proceedings of the National Academy of Sciences, 2007. **104**(7): p. 2050-2055.

126. Goodman, C.M., et al., *DNA-binding by Functionalized Gold Nanoparticles: Mechanism and Structural Requirements.* Chemical Biology & Drug Design, 2006. **67**(4): p. 297-304.

127. Lok, C.-N., et al., *Silver nanoparticles: partial oxidation and antibacterial activities.* Journal of Biological Inorganic Chemistry, 2007. **12**(4): p. 527-534.

128. Elzey, S. and V.H. Grassian, *Nanoparticle Dissolution from the Particle Perspective: Insights from Particle Sizing Measurements.* Langmuir, 2010. **26**(15): p. 12505-12508.

129. Navarro, E., et al., *Toxicity of Silver Nanoparticles to Chlamydomonas reinhardtii.* Environmental Science & Technology, 2008. **42**(23): p. 8959-8964.

130. Rimer, J.D., et al., *Kinetic and Thermodynamic Studies of Silica Nanoparticle Dissolution.* Chemistry of Materials, 2007. **19**(17): p. 4189-4197.

131. Schmidt, J. and W. Vogelsberger, *Dissolution Kinetics of Titanium Dioxide Nanoparticles: The Observation of an Unusual Kinetic Size Effect.* The Journal of Physical Chemistry B, 2006. **110**(9): p. 3955-3963.

132. Franklin, N.M., et al., *Comparative Toxicity of Nanoparticulate ZnO, Bulk ZnO, and ZnCl2 to a Freshwater Microalga (Pseudokirchneriella subcapitata): The Importance of Particle Solubility.* Environmental Science & Technology, 2007. **41**(24): p. 8484-8490.

# Chapter 2: Materials and Methods

## 2.1. General Materials

All reagents were purchased from Sigma unless otherwise stated, and used without further purification. Tryptone, yeast extract and standard microbiological agar were purchased from Oxoid. All solutions were prepared in ultrapure water (18 mΩ/cm$^3$ at 25$^o$C, MilliQ, Millipore).

*Escherichia coli* K12 MG1655 (CGSC #7740) was purchased from the Coli Genetic Stock Centre (CGSC, Yale University, USA). *Pseudomonas aeruginosa* (PAO1) and *Staphylococcus aureus* (ATCC #10390) were available in the University of Exeter EMERGE culture collection. All bacterial strains were stored as frozen stocks at -80$^o$C (Protect Bacterial Preservation System, Technical Service Consultants), and maintained on Luria Agar (LA) medium at 37$^o$C.

Silver nanoparticles were manufactured by QinetiQ Nanomaterials Ltd (Farnborough, UK). These were synthesised in a gas plasma (vapour phase) without a surface ligand. They were characterised by Scanning Electron Microscopy (SEM) (S3200N, HITACHI) with Energy Dispersive X-Ray Analysis (EDAX) (INCA, Oxford Instruments) and Transmission Electron Microscopy (TEM) (TEM 1400, JEOL). The nanoparticles had a mean diameter of 142 nm and a surface area determined by BET isotherm of 3-5 m$^2$/g.

The Z-COTE® zinc oxide nanopowder was purchased from BASF and had been characterised by the manufacturer using the same techniques as for the silver nanoparticles. These nanoparticles had a mean diameter of less than 200 nm and had a surface area determined by BET isotherm of 12-14 m$^2$/g.

The microarrays were the Agilent Model Organism Gene Expression Microarrays for *E. coli* K12 (MG1655, Product Number G4813A-020097) in 15K x 8 array format.

## 2.2. Bacterial Culture

Bacterial culture was carried out in Luria Broth (LB), or LB lacking sodium chloride (modified-LB) or Neidhardts Minimal Salts Medium with 0.1 % (w/v) glucose. LB was 10 g/L Tryptone, 5 g/L yeast extract, 10 g/L NaCl and pH 7.5. The solid medium, Luria Agar (LA), contained 1.5 % (w/v) standard microbiological agar. LB, modified-LB and LA were sterilised by autoclaving at 121$^{o}$C for 15 minutes. Neidhardts' Minimal Salts Medium was prepared according to the recipe provided in appendix A and sterilised by 0.2 µm filtration. All liquid cultures were incubated at 37$^{o}$C, aerobically on a rotary shaker at 200 rpm.

Optical density (OD) was preferentially used to monitor bacterial growth and replication unless in a medium containing nanoparticles, wherein optical density measurements were not possible due to the large scattering cross sections of the nanoparticles. The OD of bacterial cultures at 600 nm ($OD_{600}$) was measured in 1 cm optical path length cuvettes with a UV-Visible Spectrophotometer (Jenway). Alternatively, bacterial viable cell numbers were measured as Colony Forming Units (CFU). For this, a sample of culture was 10-fold serially diluted in ¼ strength Ringers' solution (7.2 g/L NaCl, 170 mg/L CaCl2 and 370 mg/L KCl in ultrapure water, pH 7.2) and a known volume of each dilution was spread onto LA medium. Colonies were counted after an overnight incubation at 37$^{o}$C.

## 2.3. Chapter 3 Methods

### 2.3.1. Gold and Silver Nanoparticle Synthesis

All nanoparticle synthesis reactions were performed in glass beakers cleaned with Aqua Regia (1 volume of $HNO_3$ and 3 volumes of HCl) and thoroughly rinsed with de-ionised water.

Citrate coated gold nanoparticles were synthesised using the method of Turkevich [1, 2]. In a glass beaker, 90 mL of chloroauric acid was heated to 95$^{o}$C. The solution was stirred vigorously with a Teflon® coated magnetic bar as 10 mL of sodium citrate was added rapidly from a plastic syringe. The reaction was allowed to cool to room temperature and then stored in the dark until needed.

Citrate coated silver nanoparticles were synthesised in a 2 step reaction, consistent with the method of Pal [3]. First, silver seeds were synthesised by mixing 20 mL of 1 mM sodium citrate with 0.5 mL of 10 mM silver nitrate and 0.5 mL of 10 mM potassium borohydride. The reaction was stirred vigorously for 5 minutes and then kept in the dark for 2 hours. Subsequently, 100 mL of 1 mM silver nitrate solution was heated until boiling. Then, 3 mL of the silver seed solution and 1 mL of 100 mM sodium citrate were added simultaneously. The reaction was stirred and allowed to cool to room temperature and then stored in the dark until needed.

To prepare protein coated nanoparticles a sample of each colloid was mixed with Bovine Serum Albumin (BSA) at different concentrations (1-100 µg/mL). The mixtures were stirred for 30 minutes at room temperature and then a few drops of 10 % (w/v) NaCl were added to each mixture. The optimum concentration of BSA for coating the nanoparticles was the lowest concentration at which the colloid was stable, and did not undergo a colour change upon addition of NaCl. The appropriate amount of BSA was mixed with a fresh batch of citrate-coated nanoparticles for use in experiments.

### 2.3.2. Bacterial-Nanoparticle Exposure

*E. coli* K12 were cultured in LB medium until mid-exponential phase ($OD_{600}$=0.5) and then washed by sequential centrifugation (8000 x *g*, 2 minutes) and suspension in phosphate buffered saline (8 g/L NaCl, 200 mg/L KCl, 1.44 g/L $Na_2HPO_4$, 240 mg/L $KH_2PO_4$, pH 7.0). Approximately $10^9$ viable bacteria were added to 10 mL of the synthesised gold or silver nanoparticles in a colloidal suspension. The nanoparticles had either a negatively charged citrate surface ligand or were coated with BSA. For controls, bacteria were added to the supernatants after the nanoparticle colloids had been de-stabilised (by sonicating) and sedimented by ultracentrifugation (20,000 x *g*, 30 minutes). To determine whether the nanoparticles were toxic to the bacteria, Colony Forming Units per mL were determined at several time points (0, 10, 30, 60, 120 and 180 minutes) during the exposures.

### 2.3.3. Transmission Electron Microscopy (TEM)

#### 2.3.3.1. Nanoparticle Size Analysis

A 2-4 µL drop of nanoparticle colloid was placed directly onto a copper/palladium mesh grid with a formvar/carbon support film. After drying under a hot lamp the nanoparticles were viewed at 80,000 x magnification in a JEOL 1400 TEM and image capture was carried out using Digital Micrograph software (Gatan). Nanoparticle sizes were measured using the particle size analysis function of the software. This method is based on a high contrast between the image background and the nanoparticles. The software detects dark pixels, which are assigned as nanoparticles based on their large scattering cross section from their metallic composition, their shape and the measured diameter. The nanoparticle diameter is equivalent to the greatest dimension of each patch

of dark pixels, thus, nanoparticle sizes determined in this way are given as ‘equivalent spherical diameter’.

#### 2.3.3.2. TEM of Bacterial-Nanoparticle Interactions

The bacteria were exposed to the nanoparticles for 30 minutes. Then the cells were washed by sequential centrifugation (8000 x *g*, 2 minutes) and suspension in phosphate buffered saline. Subsequently, the cells were fixed and stained by sequential suspension in 1% (v/v) glutaraldehyde, 1% (w/v) osmium tetroxide and 1% (v/v) uranyl acetate for 1 hour each, washing 3 times between each step. Then the cells were dehydrated by suspending in ethanol solutions (30, 50, 75, 90 and 100%, 10 minutes in each) and propylene oxide (twice for 10 minutes). The bacteria were embedded in a low viscosity, medium grade epoxy resin (Taab, Agar Scentific), mixed (1:1) with propylene oxide for 24 hours. Then the bacteria were transferred into pure resin for a further 24 hours. Finally the samples were placed in gelatin capsules and cured at 60$^{o}$C for 16 hours in a dry heat oven.

Ultrathin sections of the embedded specimens were cut on a microtome using an ‘Ultra AFM’ diamond knife (Electron Microscopy Services, UK). The sections were rested on copper/palladium mesh grids (SPI, USA) and sat on droplets of lead citrate for 5 minutes. The sections were approximately 80 nm thick, where the measurement was based on the reflection colour of the resin slither compared to a reference chart. The specimens were viewed at between 50,000 x magnification and 120,000 x magnification in a JEOL 1400 TEM and image capture was carried out using Digital Micrograph software.

## 2.4. Chapter 4 Methods

### 2.4.1. Suspension of Silver Nanopowder in Modified-LB Medium

The vapour phase synthesised nanoparticles were provided as a dry powder and had to be suspended in the medium to form a colloid before experiments with bacteria. Silver nanoparticles were dispersed in the modified-LB medium by sonication (Soniprep 150, exponential probe, MSE Instruments), at a constant amplitude of 15 µm for 30 minutes, on ice.

### 2.4.2. Electron Microscopy

*E. coli* were exposed to silver nanoparticles in modified-LB medium for 30 minutes, at 37$^{o}$C, with constant agitation at 200 rpm. The cells were washed 5 times in modified-LB medium and 3 times in PBS to remove unbound or loosely associated nanoparticles. The washed bacteria, approximately $10^9$ CFU, were prepared and imaged using TEM (as described in **2.3.3.2**). Additionally, the bacteria were imaged by Scanning Electron Microscopy (SEM). These bacteria, also approximately $10^9$ CFU, were fixed in 1% glutaraldehyde in PBS and then 1% osmium tetroxide in water, for 24 hours each. The samples were transferred onto a 0.22 µm pore size polycarbonate filter (Millipore) and substituted with acetone, and subsequently with liquid $CO_2$ in a critical point drying apparatus (SPI, USA). Filter paper sections were metallised with gold, by sputter coating, and imaged with a JEOL JSM-6390LV SEM.

### 2.4.3. Exposure to Silver Nanoparticles on Solid Modified-LB medium

Solid modified-LB containing silver nanoparticles was prepared by mixing the silver nanopowder with molten modified-LB agar, at 50$^{o}$C, and sonicating for 2 minutes. The agar was poured immediately into plastic Petri dishes and solidified under a sterile laminar

flow. *E. coli*, *P. aeruginosa* and *S. aureus* bacteria were cultured overnight in modified-LB medium and diluted in ¼ strength Ringers solution. The bacteria were spread onto the nanoparticle agar using a glass spreader before incubation for 48 hours at 37$^{o}$C.

### 2.4.4. Silver Nanoparticle Dissolution Measurements and Differential Silver Nanoparticle-Silver Ion Toxicity Test

This was to compare the effects of the silver nanoparticles with the concentration of silver in the bulk solution phase. Therefore, the bulk solution phase concentration was first determined by ICP-MS.

Colloidal silver nanoparticles, at a concentration of 100 µg/mL, were prepared in 100 mL of modified-LB medium (as described in **2.4.1**). The rate of dissolution was determined from the concentration of silver in the bulk solution phase, after removing the nanoparticles by ultracentrifugation. At various time points (0, 0.5, 1, 2, 4, 6, 8, 12 and 24 hours) 5 mL of the colloid was removed to a polypropylene tube and centrifuged at 50,000 x *g* for 30 minutes (Beckmann-Coulter). Subsequently, 1 mL of the supernatant was aspirated. A 200 mg aliquot of the supernatant was measured on electronic scales, and mixed with 1 mL of nitric acid and hydrogen peroxide (50:50) in glass tubes that had been soaked in 10% (v/v) nitric acid, thoroughly rinsed in ultrapure water and air dried. The samples were microwave digested for 10 minutes at 150 W and 150$^{o}$C (Discover SP-D Pressurised Microwave Digestion System, CEM). These digests were made up to 5 g with HPLC-grade water.

The determination of Ag present in each sample was performed by ICP-MS in bulk analysis mode (7500 ICP-MS, Agilent) by measuring the isotopes $^{107}$Ag and $^{109}$Ag. Quantification was performed by external calibration using Ag standard solutions (in nitric acid) and $^{103}$Rh as an internal standard, correcting each sample for a procedural blank.

Additionally, $Ag^+$ solutions were prepared in the experimental medium, and the solutions underwent the same processing procedure for ICP-MS. This was to determine what proportion of the metal might be lost on the sides of the vessels, which was found to be 5 %. The experiments were repeated 3 times, and each sample was prepared in triplicate and measured 5 times. The ICP-MS measurements were converted from ng/g to ng/mL, measuring the density of the modified-LB (ρ = mass/volume) to be 1.014 g/mL and accounting for a measured 5 % loss of silver concentration during the ICP-MS procedure.

To compare the effects of the nanoparticles with the measured concentration of silver in the bulk solution *E. coli* growth and replication was measured in modified-LB medium with or without the nanoparticles, and with $Ag^+$ added at a pre-determined rate to mimic nanoparticle dissolution.

### 2.4.5. Real Time Polymerase Chain Reaction (real time PCR)

RNA was isolated from exponentially dividing *E. coli*, 10 minutes after exposure to silver nanoparticles or $Ag^+$, using the RNA Protect Bacterial Reagent and the RNeasy Mini Kit (Qiagen) according to the manufacturer's recommendations. The integrity of the RNA was determined by agarose electrophoresis. Residual DNA was removed from RNA samples by digesting with RNase-free DNase (RQ1, Promega). This RNA was purified using the RNeasy clean-up protocol prior to evaluating RNA concentration and purity on a Nanodrop spectrophotometer (Thermo Scientific). First strand cDNA synthesis was performed using the Thermoscript Avian RT System (Invitrogen). RT reactions were primed with either random hexamers, or gene specific primers if the transcripts were relatively low in abundance. DNA polymerisation was carried out at $55^oC$ for 50 minutes, otherwise all steps were performed as described by the manufacturer.

Real time PCR was performed to determine the relative abundance of specific mRNA sequences using the Stratagene MxPro system and the SYBR green detection chemistry. Primers were designed using Primer 3 [4], and the complete genome sequence of *E. coli* K12 (Genbank accession U00096), Table 2.1, for amplification of a 100-300 bp region of the target gene.

All RT-PCR reactions were performed in duplicate and each experiment was repeated at least 3 times. Each reaction contained 12.5 µL IQ SYBR supermix (100 mM KCl, 40 mM Tris-HCl, pH 8.4, 0.4 mM each dATP, dCTP, dGTP, dTTP, 6 mM $MgCl_2$, 50 U/mL iTaq DNA polymerase, Biorad), 7.5 µL nuclease free water, 2 µL of each primer (10 pmol/µL) and 1 µL of template cDNA; the total reaction volume was 25 µL. The thermal cycling program was 95$^{o}$C for 5 minutes followed by 40 cycles of 95$^{o}$C for 45 seconds, 55$^{o}$C for 30 seconds and 72$^{o}$C for 1 minute. At the end of the programme product specificity was checked by plotting a dissociation curve (55$^{o}$C to 95$^{o}$C, 1$^{o}$C increments, 30 seconds/step). The threshold cycle ($C_t$) values were determined using a manually specified fluorescence threshold within the exponential phase of the reaction curves. Data was analysed based on the method of Pfaffl [5], using a dilution series of pooled cDNA to determine primer efficiency, equation (1) and calculating the change in gene expression using equation (2).

$$E = 10^{-\frac{-1}{-m}}$$

*Equation (1)*

$$\Delta Gex = \frac{E_{(target\ )}{}^{\Delta C_{t(target\ )}}}{E_{(reference\ )}{}^{\Delta C_{t(reference\ )}}}$$

*Equation (2)*

Where *E* is the primer efficiency; *m* is the slope of a linear fit for $C_t$ as a function of template DNA concentration. ***ΔGex*** is the gene expression ratio; ***ΔCt*** is the difference in threshold cycle between the experimental and calibrator (control) samples. Target and reference refer to the gene of interest or the internal reference gene respectively. Two internal reference genes were *rrsB* and *gapA*.

### 2.4.6. Gene Deletion

Gene deletions were performed as described by Datsenko and Wanner [6]. Plasmid DNA was recovered from *E. coli* strains (Coli Genetic Stock Centre: CGSC7669, CGSC7629, CGSC7632 and CGSC7631) in overnight LB cultures using the QIAprep Spin Miniprep Kit (Qiagen). Linear gene deletion constructs were synthesised by PCR amplification from plasmid pKD3 using primer sequences that were designed using Primer 3 [4] and the complete genome sequence of *E. coli* K12 (Genbank accession U00096), Table 2.2. The constructs contained a chloramphenicol acetyl transferase (*cat*) selection marker flanked by Flippase Recognition Target (FRT) sites and 5' and 3' 36 bp regions of homology to the target gene. Reactions contained 25 µL of GoTaq® Green PCR master mix (Promega), 15 µL of nuclease free water, 4 µL of each primer (10 pmol/µL) and 100 ng of plasmid pKD3; the final volume was 50 µL. The thermal cycling program was 95$^{o}$C for 5 minutes, followed by 40 cycles of 95$^{o}$C for 1 minute, 55$^{o}$C for 30 seconds and 72$^{o}$C for 2 minutes, and a final extension step of 72$^{o}$C for 5 minutes. PCR products were purified using the QIAquick PCR purification kit (Qiagen) and the DNA concentration was determined spectrophotometrically using a Nanodrop (Thermo Scientific).

A background strain of *E. coli* K12 (MG1655) was prepared by $CaCl_2$-based transformation with plasmid pKD46. *E. coli* pKD46 was cultured in SOB medium (10 g/L tryptone, 5 g/L yeast extract, 2.5 g/L NaCl) containing 10 mM L-arabinose and 100 µg/mL

ampicillin, at 37$^{o}$C. The cells were recovered by centrifugation (8000 x *g*, 2 minutes) and washed 4 times in ice cold 10% glycerol (in ultrapure water). Finally the cells were suspended in 50 µL of 10 % glycerol and mixed with 500 ng of knockout construct in 0.2 cm gap Micropulser cuvettes (Biorad). The cells were transformed by electroporation (Gene Pulser, Biorad) and allowed to recover in SOB/10 mM Arabinose at 37$^{o}$C for 2 hours before selection on LB agar containing 25 µg/mL chloramphenicol.

After overnight incubation at 37$^{o}$C, colonies were screened for insertion of the construct by colony PCR using the checking primer sequences in Table 2.2. Positive colonies were purified once, non-selectively, at 43$^{o}$C to allow loss of pKD46 and then transformed ($CaCl_2$) with plasmid pCP20. After selection of pCP20 transformants, the *E. coli* were again colony purified at 43$^{o}$C and tested for loss of *cat* by colony PCR, and loss of ampicillin and chloramphenicol resistance.

### 2.4.7. Minimum Inhibitory Concentration Assay for Metal Ions

The Minimum Inhibitory Concentration (MIC) of $Ag^{+}$, $Zn^{2+}$ and $Cu^{2+}$ was determined for *E. coli* K12 MG1655 and mutant strains Δ*copA*, Δ*cueO*, Δ*cusA* and Δ*cusR*. The growth rate of each strain was measured in modified-LB by taking optical density measurements as a function of time. For MIC testing, stock solutions of $AgNO_3$, $ZnCl_2$ or $CuSO_4$ were prepared in modified-LB and the assay was set up in a 96-well micro-titer plate format (Corning). For $CuSO_4$ and $ZnCl_2$ a 2-fold dilution series was used to determine the MIC. For $AgNO_3$, where differences in sensitivity were minimal, the concentration range was 1 µg/mL increments. Overnight cultures were diluted in modified-LB to an $OD_{600}$ of 0.1, corresponding to approximately 2 x$10^{7}$ CFU/mL and mixed (1:1) with modified-LB containing $Ag^{+}$, $Cu^{2+}$ or $Zn^{2+}$ ions. The total volume in each well was 100 µL. The plates were incubated at 37$^{o}$C in the dark with agitation at 200 rpm. The MIC was determined by

visual examination, recording each concentration of metal as showing growth or no growth.

## 2.5. Chapter 5 Methods (Gene Expression Microarray Experiments)

### 2.5.1. *E. coli* Culture

Two independent gene expression microarray experiments were carried out to determine the *E. coli* K12 transcriptome response to silver nitrate or 142 nm silver nanoparticles. Each experiment was carried out in quadruplicate and each replicate experiment was carried out as follows. First, an exponentially replicating culture, 100 mL modified-LB medium, was divided equally into 2 separate flasks which had been pre-warmed to 37$^{o}$C. To one of each pair of flasks was added an equivalent volume of sterile, pre-warmed modified-LB medium. To the other was added modified-LB medium containing silver; either a solution of silver nitrate or a suspension of silver nanoparticles. The silver concentration was 4 µg/mL for $Ag^{+}$, from $AgNO_3$, or, 400 µg/mL for silver nanoparticles. This concentration was not inhibitory but caused a reduction in growth rate and was determined empirically by plotting bacterial growth in modified-LB medium containing different concentrations of silver. The *E. coli* were allowed a period of precisely 10 minutes to mount a transcriptional response. Subsequently a 2 mL sample of each flask, approximately 5 x $10^8$ CFU, was mixed (1:2) with RNAprotect® Bacterial Reagent (Qiagen) for the isolation of total RNA.

### 2.5.2. RNA Isolation

RNA was isolated (as described for real time PCR in **2.4.5**) with an additional clean-up step following elution using the RNeasy Clean-Up Protocol (Qiagen). RNA samples were stored at -80$^{o}$C and used within 48 hours.

### 2.5.3. RNA Amplification and Labeling

RNA amplification and labelling was carried out using the MessageAmp-II Bacteria Kit (Ambion). All incubation and heating steps were performed on a PTC-200 Peltier Thermocycler (MJ Research), and all steps were carried out in RNase-free microfuge tubes (Ambion), on ice. All reactions were carried out as indicated by the MessageAmp-II Bacteria Kit. Briefly, 500 ng of each RNA sample was polyadenylated in a 5 µL reaction containing RNase inhibitor, ATP and *E. coli* polyadenylate polymerase. The RNA was heated (70$^{o}$C, 10 minutes) and then polyadenylated (37$^{o}$C, 15 minutes). Subsequently the poly(A)-RNA was reverse transcribed in a 15 µL reaction volume containing ArrayScript™ recombinant reverse transcriptase, and primed with oligo(dT)-containing a T7 promoter sequence (42$^{o}$C, 2 hours). Next, cDNA was converted to dsDNA using DNA polymerase in a 95 µL reaction volume including *E. coli* RNase H to degrade the original RNA sample. The dsDNA was purified into approximately 16 µL of nuclease free water and was vacuum dried. Next the dsDNA was transcribed in a 22 µL reaction incorporating 5-(3-aminoallyl)-UTP and catalysed by T7 RNA polymerase (37$^{o}$C, 14 hours). Finally, antisense RNA (aRNA) was labelled by NHS-ester with fluorescent dye molecules, Cy3 (control samples) or Cy5 (silver-treated samples). During the procedure the Nanodrop spectrophotometer was used routinely to measure nucleic acid concentration and the purity of the samples and the ratio of dye molecules per unit mass of nucleic acid. After transcription, the antisense RNA was purified, first using aRNA filter cartridges supplied with the MessageAmp-II kit, and subsequently using the RNeasy cleanup protocol of the RNeasy Mini Kit.

### 2.5.4. Microarray Hybridisation

Hybridisation was carried out as described in the Agilent Two-Colour Microarray-Based Gene Expression Analysis manual (Agilent). Briefly, 300 ng of RNA was mixed with fragmentation and blocking buffer at 60$^{o}$C for 30 minutes. The fragmentation reaction was terminated by mixing (1:1) with Agilent Gex Hybridisation buffer. Then, 40 µL of hybridization sample was loaded onto each array using the SureHyb assembly apparatus (Agilent). The hybridization reaction was carried out in a rotisserie oven (Corning Scientific) at 65$^{o}$C for 17 hours. The array was washed with Agilent Gene Expression Wash Buffers. These steps were carried out in a 1L staining dish, previously washed with acetonitrile and ultrapure water, and in an ozone controlled environment.

### 2.5.5. Data Analysis and Biological Interpretation

The gene chip was scanned on a GenePix 4000B array scanner (Axon Scientific) and feature extraction was carried out using the Agilent Feature Extraction software (version 9.5.3). Data analysis was carried out using GeneSpring (version 3.0, Axon Scientific). Biological interpretation of the data was performed automatically using the GeneCoDis web-based bioinformatics tool [7, 8], and manually using the information available in the EcoCyC database [9, 10].

### 2.5.6. Microarray Validation

The microarray data was validated by comparing the expression ratio of 4 genes: *cusA*, *cueO*, *ompF* and *soxS*, with an expression ratio that was determined using the real-time PCR method (as described in **2.4.5**). The internal reference gene was *rrsB*. Primer sequences are shown in Table 2.1.

## 2.6 Chapter 6 Methods

### 2.6.1. Suspension of Zinc Oxide Nanopowder in Neidhardts' Minimal Salts Medium

Zinc oxide nanoparticles were suspended in the Neidhardts' minimal salts medium using a standard operating procedure that had been developed previously [11]. For this, an appropriate amount of the dry powder, depending upon the desired concentration, was divided into polypropylene universal tubes (30-40 mg per tube). The contents of each tube were mixed into a paste with a few drops of the liquid using a metal spatula. The paste was made up to 15 mL and sonicated twice at amplitude of 15 µm for 10 seconds. Finally, the contents of each tube were mixed into the final volume of liquid using a glass stirring rod.

### 2.6.2. Transmission Electron Microscopy

*E. coli* were added to a suspension of the zinc oxide nanoparticles in Neidhardts' minimal salts medium and mixed gently (50 rpm) on a rotary shaker at 37$^{o}$C for 30 minutes. A 2-4 µL volume of the suspension was placed onto a copper/palladium mesh grid with a formvar/carbon support film. The grid was dried under a hot lamp and then floated on droplets of water to wash the specimens. The bacteria were imaged by TEM, omitting the usual specimen preparation (as described in **2.3.3**).

### 2.6.3. UV-Visible Spectroscopy

UV-Visible absorbance spectra were recorded for suspensions of zinc oxide nanoparticles, at various concentrations, in the minimal salts medium. This was performed using 1 cm optical path length plastic cuvettes and a UV-Visible spectrometer with Vision 32 software (Spectronic Unicam).

### 2.6.4. Zinc Oxide Nanoparticle Dissolution Measurements and Differential Zinc Oxide Nanoparticle-Zinc Ion Toxicity Test

Dissolution measurements were made using Inductively Coupled Plasma Mass Spectrometry (ICP-MS) (as described for silver nanoparticles in **2.4.4**), and the process is described only briefly here. The zinc oxide nanoparticles were suspended in the minimal salts medium at a concentration of 100 µg/mL (as described in **2.6.1**). Subsequently, at various time points (0, 1, 2, 3 and 4 hours), zinc oxide nanoparticles were removed from suspension by ultracentrifugation (50,000 x *g*, 30 minutes, Beckmann-Coulter). A 200 mg aliquot of the supernatant was measured on electronic scales. This was added to 1 mL of a 1:1 (vol:vol) mixture of nitric acid and hydrogen peroxide, and microwave digested. The digests were made up to 5 g with ultrapure water and measured with ICP-MS in standard analysis mode (7500 ICP-MS, Agilent). Total Zn concentration in the samples was determined by measuring the isotopes $^{64}Zn$, $^{67}Zn$, $^{68}Zn$ and $^{69}Zn$. Quantification was performed by external calibration using Zn standard solutions and $^{103}Rh$ as an internal standard, correcting each sample for a procedural blank. The experiment was carried out twice, and each sample was prepared in triplicate and measured 5 times. Additionally, $Zn^{2+}$ solutions were prepared in the experimental medium, and the solutions underwent the same processing procedure for ICP-MS to determine what proportion of the metal might be lost on the sides of the vessels, which was found to be undetectable. The ICP-MS measurements were converted from ng/g to ng/mL, measuring the density of the minimal salts medium to be 1.003 g/mL.

For the differential toxicity test an exponentially growing culture, in Neidhardts' minimal salts medium, was mixed 1:1(vol:vol) with sterile medium containing zinc ions, from zinc chloride, or zinc oxide nanoparticles. The nanoparticles were at a concentration

of 100 µg/mL and the zinc ions were added at the predicted rate of nanoparticle dissolution. The experiment was repeated 3 times.

### 2.6.5. Gene Deletion

A zinc ion sensitive mutant, Δ*zntA*, was prepared by deleting the *zntA* gene from *E. coli* K12, MG1655. This was performed using the method of Datsenko and Wanner (as described in **2.4.5**). The oligonucleotide sequences were designed using Primer 3 software, shown in Table 2.2.

### 2.6.6. Real-Time PCR

To measure the expression of genes for zinc homeostasis *Escherichia coli* were exposed to zinc oxide nanoparticles or a concentration of zinc ions to represent nanoparticle dissolution. Alternatively, to measure the expression of genes for the response to oxidative stress, *E. coli* were exposed to zinc oxide nanoparticles with or without UV light. The exposures were carried out for 10 minutes in the minimal salts medium. The protocols for RNA isolation and real-time PCR are described in **2.4.4**. The primer sequences are shown in Table 2.1. These were designed using Primer 3 software and the complete genome sequence of *E. coli* K12, MG1655 [12]. Gene expression data was normalised using the *rrsB* gene, encoding the 16s ribosomal RNA subunit, whose expression does not change in response to $Zn^{2+}$ [13].

### 2.6.7. Ultra-Violet Irradiation

UV light was from a light emitting diode with a wavelength of 375 ± 5 nm (NICHIA, Japan) producing a power of 2 mW. This was mounted into the lid of a universal tube, which was covered with an aluminium foil jacket to ensure that the light was confined within the vessel.

### 2.6.8. Photo-Electron Production Assay and Toxicity Test

Photo-electron production was measured using the colour change of the redox sensitive dye, 2,6-dichlorophenolindolphenol (DCPIP), monitoring the absorbance change at 595 nm. DCPIP was stored aerobically and was added at a concentration of 1 mM to water with or without zinc oxide nanoparticles. Subsequently, the medium was irradiated with UV-light in a 5 mL foil jacketed glass vessel with the UV LED mounted in the lid. The effect of zinc oxide nanoparticles and UV light on bacterial survival in water or minimal salts medium was measured by colony forming units as a function of time.

## Table 2.1. Primers used for Real-Time PCR

| Target | Forward Sequence (5' - 3') | Reverse Sequence (5' - 3') |
|---|---|---|
| *copA* | CCAGACGATATCCCGCTTTA | GCGCTGTTAAATGAGCAACA |
| *cueO* | TACCGATCCCTGATTTGCTC | GACTTCACCCGGTACTTCCA |
| *cusA* | TGGATGGGCTTTCATCTTTC | TTCTGCTCGCTGAATGTTTG |
| *cusR* | AAATCGGCAACCTGAAACTG | GTTACGCTCCGCCAATAAAG |
| *gapA* | GCTACTACCGCTACTCAGAAAACC | GAACGGTCAGGTCAACTACAGATAC |
| *katG* | CAACCGAGATGGGTCTGATT | TTGTTCTTCAATCGGTGCAG |
| *ompC* | AATTTCAGACCTGCGAATGC | ATGTAGATGGCGACCAGACC |
| *ompF* | TGCGCAACTAACAGAACGTC | AGGCTTTGGTATCGTTGGTG |
| *rrsB* | CAGCCACACTGGAACTGAGA | GTTAGCCGGTGCTTCTTCTG |
| *sodA* | GGAAATCCACCACACCAAAC | GATAGCCGCTTTCAGGTCAC |
| *sodC* | TCTGGCCCTTCATGTTTACC | GCAGTCAATTGGTAGCGTCA |
| *soxS* | GTAATCGCCAAGCGTCTGAT | CCCATCAGAAAATTATTCAGGATCT |
| *zntA* | GGAAGAGGTGGCGATTAACA | TTCTGACAGCACTTCCAACG |
| *znuC* | GATGAAGTGCTGTGCCTGAA | GCAAAACAATTCGTCCCTGT |

## Table 2.2. Oligonucleotides used for Gene Deletions

| Target | Knockout Construct Primer Sequence (5' – 3')* | | Checking Primer Sequence (5' – 3') | |
|---|---|---|---|---|
| | **Forward** | **Reverse** | **Forward** | **Reverse** |
| *copA* | TTATTCCTTCGGTTTAAACCGCAGCAACCGGTTGGCGTGTAGGCTGGAGCTGCTTC | ATGTCACAAACTATCGACCTGACCCTGGACGGCCTGGGGAATTAGCCATGGTCCAT | AACCTGTGCCTGAACCGTAG | GACTTTTACCCGCCTGGTTT |
| *cueO* | ATGCAACGTCGTGATTTCTTAAAATATTCCGTCGCGGTGTAGGCTGGAGCTGCTTC | TTATACCGTAAACCCTAACATCATCCCCGTATCTTCGGGAATTAGCCATGGTCCAT | TAAATTGTGTCTGCGGCTTG | TGATAAGCGTAGCGCATCAG |
| *cusA* | ATGATTGAATGGATTATTCGTCGCTCGGTGGCGAACGTGTAGGCTGGAGCTGCTTC | TTATTTCCGTACCCGATGTCGGTGCAGCCACATCAGGGGAATTAGCCATGGTCCAT | GTTGCTGTTTTCCAGGCATC | ATCTTCCGATACGGTTGACG |
| *cusR* | TTAAGCGGGTAATGTGATAACAAACCTTGTCCCCCGGTGTAGGCTGGAGCTGCTTC | ATGAAACTGTTGATTGTCGAAGATGAAAAGAAAACCGGGAATTAGCCATGGTCCAT | AGCCAGTCCACACAAAAACC | GCCACACAAAATGGCAGAAG |
| *soxS* | TTACAGGCGGTGGCGATAATCGCTGGGAGTGCGATCGTGTAGGCTGGAGCTGCTTC | ATGTCCCATCAGAAAATTATTCAGGATCTTATCGCAGGGAATTAGCCATGGTCCAT | TTATGCAATGGATGGAGCAA | ATAGAAATGCAGCGCCGATA |
| *yebE* | TTATTCCGCCAAAGTGCGTTTTTGCTGTTCGAGATCGTGTAGGCTGGAGCTGCTTC | ATGGCTAACTGGTTAAATCAACTGCAATCCCTGCTTGGGAATTAGCCATGGTCCAT | GCGCGGATATCGAATGTTAT | GGCGCGAATTTCTTTGAATA |
| *ybdK* | TTAGTCACCGGCCCAGATCTCACAATGCTTTTTCACGTGTAGGCTGGAGCTGCTTC | ATGCCATTACCCGATTTTCATGTTTCTGAACCTTTTGGGAATTAGCCATGGTCCAT | AGAGGAAAGCCATCAGCAAA | AAATTGCTTCAGGCACCATC |
| *ybdZ* | ATGGCATTCAGTAATCCCTTCGATGATCCGCAGGGAGTGTAGGCTGGAGCTGCTTC | TCATTGTGCCTCCTGCAACTGGGTAAAATTCGTCGGGGGAATTAGCCATGGTCCAT | GCTAATCGACCTCTGGCAAC | CGAATCAACCTCTCCGGTTA |
| *yjjZ* | ATGTTGCAACGTACGCTGGGCAGTGGCTGGGGAGTGGTGTAGGCTGGAGCTGCTTC | TCATCCCTGATTCAAATTCATTATCATCAGCATGATGGGAATTAGCCATGGTCCAT | TTACCCGATAGCAAGGGATT | GGTAGACGCGCTAGCTTCAG |
| *yncJ* | TCAACGTTGTCCCGCTTCTGGTTTGCGCGATTTTTGGTGTAGGCTGGAGCTGCTTC | CGTTAATAAGACAACCGATAACGCCTTCGTAAACATGGGAATTAGCCATGGTCCAT | TGAGCTGCTGAAAACATTGC | TGCAATGCAAAATCAGGAAG |
| *ydiE* | ATGCGTTATACGGATAGCAGAAAACTCACGCCTGAAGTGTAGGCTGGAGCTGCTTC | CTACTTGGTCAACAGCAGCTTGCCAGCCTGAGTTTTGGGAATTAGCCATGGTCCAT | ACTCGCCTCTGCGGTAGATA | GTCCACCTGACTGGGGTAAA |
| *zntA* | ATGTCGACTCCTGACAATCACGGCAAGAAAGCCCCTGTGTAGGCTGGAGCTGCTTC | TTATCTCCTGCGCAACAATCTTAACGCATTCGCTGTGGGAATTAGCCATGGTCCAT | GCTACTTTGCCGGTCACTTC | TCGTAAAGGCGGTTGATAGG |

***underlined sequence is homologous to the target gene.**

## 2.7 References


1. Kimling, J., et al., *Turkevich Method for Gold Nanoparticle Synthesis Revisited.* The Journal of Physical Chemistry B, 2006. **110**(32): p. 15700-15707.
2. Turkevich, J., P. Stevenson, and J. Hillier, *A study of the nucleation and growth processes in the synthesis of colloidal gold.* Discuss. Faraday Soc., 1951. **11**: p. 55-75.
3. Pal, S., Y.K. Tak, and J.M. Song, *Does the Antibacterial Activity of Silver Nanoparticles Depend on the Shape of the Nanoparticle? A Study of the Gram-Negative Bacterium Escherichia coli.* Appl. Environ. Microbiol., 2007. **73**(6): p. 1712-1720.
4. Rozen, S. and H. Skaletsky, *Primer3 on the WWW for general users and for biologist programmers.* Methods Mol Biol, 2000. **132**: p. 365-86.
5. Pfaffl, M.W., *A new mathematical model for relative quantification in real-time RT-PCR.* Nucleic Acids Res, 2001. **29**(9): p. e45.
6. Datsenko, K.A. and B.L. Wanner, *One-step inactivation of chromosomal genes in Escherichia coli K-12 using PCR products.* Proc Natl Acad Sci U S A, 2000. **97**(12): p. 6640-5.
7. Carmona-Saez, P., et al., *GENECODIS: a web-based tool for finding significant concurrent annotations in gene lists.* Genome Biol, 2007. **8**(1): p. R3.
8. Nogales-Cadenas, R., et al., *GeneCodis: interpreting gene lists through enrichment analysis and integration of diverse biological information.* Nucleic Acids Res, 2009. **37**(Web Server issue): p. W317-22.
9. Keseler, I.M., et al., *EcoCyc: A comprehensive view of Escherichia coli biology.* Nucleic Acids Research, 2009. **37**(suppl 1): p. D464-D470.
10. Salgado, H., et al., *The comprehensive updated regulatory network of Escherichia coli K-12.* BMC Bioinformatics, 2006. **7**(1): p. 5.
11. Walker, N., 2009.
12. Blattner, F.R., et al., *The Complete Genome Sequence of Escherichia coli K-12.* Science, 1997. **277**(5331): p. 1453-1462.
13. Yamamoto, K. and A. Ishihama, *Transcriptional Response of Escherichia coli to External Zinc.* J. Bacteriol., 2005. **187**(18): p. 6333-6340.

# Chapter 3: Bacterial-Nanoparticle Interactions in Transmission Electron Micrographs

## 3.1. Introduction

Cell membranes have evolved for the purpose of physically and chemically defining the boundary between an organism and the environment. Although some molecules may be sufficiently lipophilic to diffuse freely across lipid bi-layers, the exchange of hydrophobic and polar solutes may be stringently regulated by specialised transport proteins. Active transporters use energy from ATP hydrolysis or the proton motive force and are typically substrate specific, only moving solutes that satisfy specific steric and electrostatic binding parameters. Passive transporters are water filled protein channels that permit the specific or non-specific movement of small solutes down an electrochemical gradient.

For a molecule to move across the *E. coli* cell envelope it must fulfil two requirements. Firstly size: the size limit for passive, non-specific transport across the *E. coli* outer membrane is 1.08-1.16 nm, corresponding to the pore diameters of the constitutive outer membrane porins, OmpC and OmpF [1, 2]. Secondly specificity: a molecule must satisfy strict substrate selection criteria. According to known mechanisms of active and passive membrane transport in prokaryotes, specifically in *E. coli*, the translocation of a metal nanoparticle of more than 1-2 nanometres across appears unlikely. The structure would neither be small enough to pass non-specifically and may not fulfil the binding pre-requisites for transport. Nonetheless, research into the interaction of bacteria with various nanostructures claim membrane translocation. For example, 12-39 nm diameter approximately spherical silver nanoparticles [3, 4], halogenated magnesium oxide nanoparticles [5] and Cd/Se Quantum Dots (QDs) [6] appear to enter the cytosol of *E. coli* in optical and electron microscopy studies.

Two hypotheses for nanoparticle uptake are considered. First, a previously unreported mechanism of bulk transport in bacteria. Some species of bacteria can internalise relatively large molecules including the ~27 kDa green fluorescent protein (GFP) through unreported mechanisms [7]. Conversely, bulk transport processes have never been reported in *E. coli*. Instead, most common laboratory strains of bacteria may only take up molecules larger than a few nm under specific environmental conditions. For example, membrane translocation of DNA is possible within a strong electric field, by electroporation [8], or, during heat shock [9], through transient formation of pores in the lipid bilayer, independent of proteins. Neither of these conditions were true when nanoparticle uptake was observed [3-6].

The second hypothesis for nanoparticle uptake considers the destructive nature of toxic nanoparticles on bacterial membranes. This may enable nanoparticles to enter a cell by diffusion at a site of membrane damage. If this damage is not observed due to restrictions in the imaging technique then the nanoparticles would appear to be within an intact bacterium causing a false interpretation of an uptake process. For example, Images from studies that depict silver nanoparticles inside *E. coli* have been obtained using Transmission Electron Microscopy (TEM); a technique that is based on electron scattering as they pass through an ultrathin (50-100 nm) section of a bacterium and offers no *z*-axis resolution. Therefore, while the cell wall may appear circumferential and intact in the bacterial section, the integrity of the entire structure cannot be determined because only a thin section is viewed. Further, the image is 2-dimensional and any materials that reside above or below the bacterial cross section will appear as if inside the cell.

One way to circumvent these problems is to investigate nanoparticle uptake using a nano-sized material that is non-toxic. Therefore, one can generate 2-D transmission electron micrographs, which depict adequate detail to resolve individual nanoparticles, but eliminate the membrane damage which could permit nanoparticle internalisation by diffusion. Gold is a suitable material for investigating this interaction because gold nanoparticles are chemically inert and not toxic to bacteria [10], unless surface-modified with surfactants or antibiotics [11, 12]. Gold nanoparticles can be prepared with defined size and shape, and with a non-toxic stabilising ligand such as the citrate anion. Moreover, the interaction of gold nanoparticles with bacteria is of particular interest in medical nanotechnology as vehicles for antimicrobial delivery [12]. Thus a detailed understanding of the nature of gold nanoparticle-bacterial interactions has potential therapeutic applications.

The aim of this work was to synthesise gold nanoparticles that were larger than the largest reported pore diameter in *E. coli*, which is the SecA subunit of the protein secretion complex, with a pore hole diameter that may be up to 6 nm [13]. Therefore, the nanoparticles may be excluded from the cell interior according to the barrier properties of the cell envelope. A series of bright field transmission electron micrographs were generated from thin sections of *E. coli* after nanoparticle exposure in order to assess the interaction of the nanoparticles with the bacteria; specifically any evidence of nanoparticle uptake. In addition, silver nanoparticles were synthesised to allow a comparison of the interactions with non-toxic and toxic materials. The gold and silver nanoparticles were synthesised with a surface that was covered in anionic citrate molecules. Additionally, these nanoparticles were coated with Bovine Serum Albumin (BSA) creating a protein coated surface to mimic how a bacterium might encounter a nanostructure under physiological conditions, where metal nanoparticles rapidly adsorb proteins [14].

## 3.2. Results

### 3.2.1. Nanoparticle Synthesis and Characterisation

Au (III) cations were reduced using sodium citrate in a reaction that was initiated thermally. The reduced Au formed into spherical nanoparticles, coated with anionic citrate molecules and following the reaction mechanism as investigated and reported by Polte *et al* [15]. The nanoparticles were stable in a colloidal suspension due to an electrostatic repulsion between the nanoparticle surfaces. In addition, 3 % of the nanoparticles had a non-spherical morphology, appearing as triangles in the 2-D transmission micrographs, translating to a 3-dimensional truncated triangular structure. The formation of a small percentage of triangles during the synthesis reaction has also been reported elsewhere [16].

The Turkevich synthesis route [16, 17] was optimised for mono-disperse, uniform nanoparticles by varying the sodium citrate concentration in the synthesis reaction. If the sodium citrate concentration was changed from 8 mM to 12 mM the mean nanoparticle diameter became smaller, Table 2.1.

| Sodium Citrate Concentration (mM) | Mean Spherical Diameter (nm) |
|---|---|
| 8 | 17 ± 6 |
| 9 | 15 ± 5 |
| 10 | 17 ± 7 |
| 11 | 15 ± 8 |
| 12 | 9 ± 9 |

**Table 3.1. The effect of sodium citrate concentration in the synthesis reaction on gold nanoparticle size.**

The nanoparticles for experiments were prepared with 9 mM sodium citrate, which were the most mono-disperse with an average diameter of 15 ± 5 nm. In addition, citrate coated silver nanoparticles were synthesised using methods consistent with recent studies [18]. The silver nanoparticles were approximately spherical, and had an average spherical diameter of 8 ± 8 nm. The size of the gold nanoparticles was consistent with other studies [19]. Conversely, the silver nanoparticles were smaller than reported in other work (a mean diameter of 8 nm in this study, 39 nm in reference [18]), reflecting differences in ambient temperature, pH and reagent purity, and perhaps a very different reaction vessel. Transmission electron micrographs of the nanoparticles are shown in Figure 3.1, and size distributions are presented as histograms in Figure 3.2.

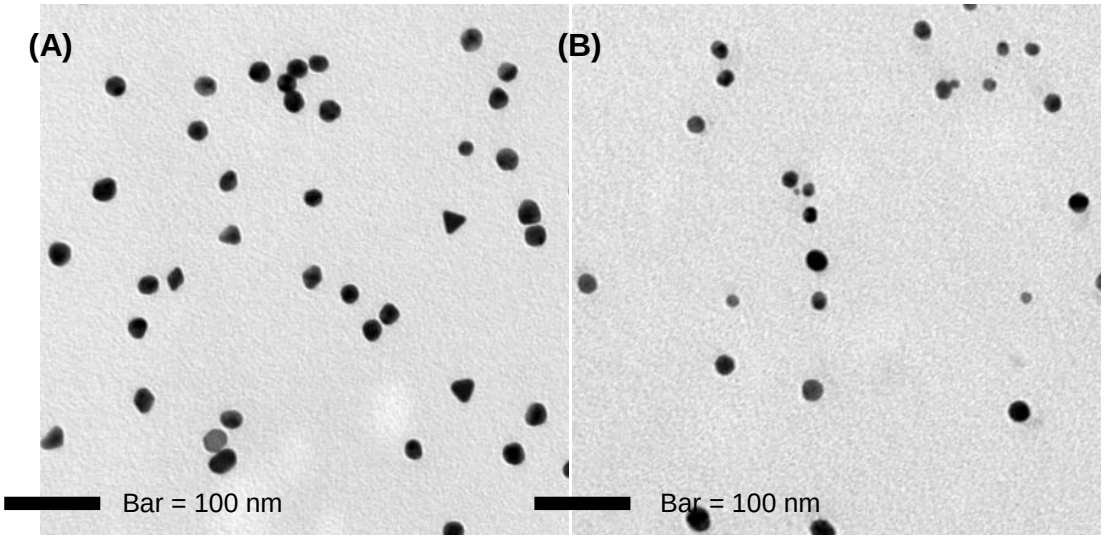


**Figure 3.1. Transmission Electron Micrographs of citrate-capped gold (A) and silver (B) nanoparticles.**

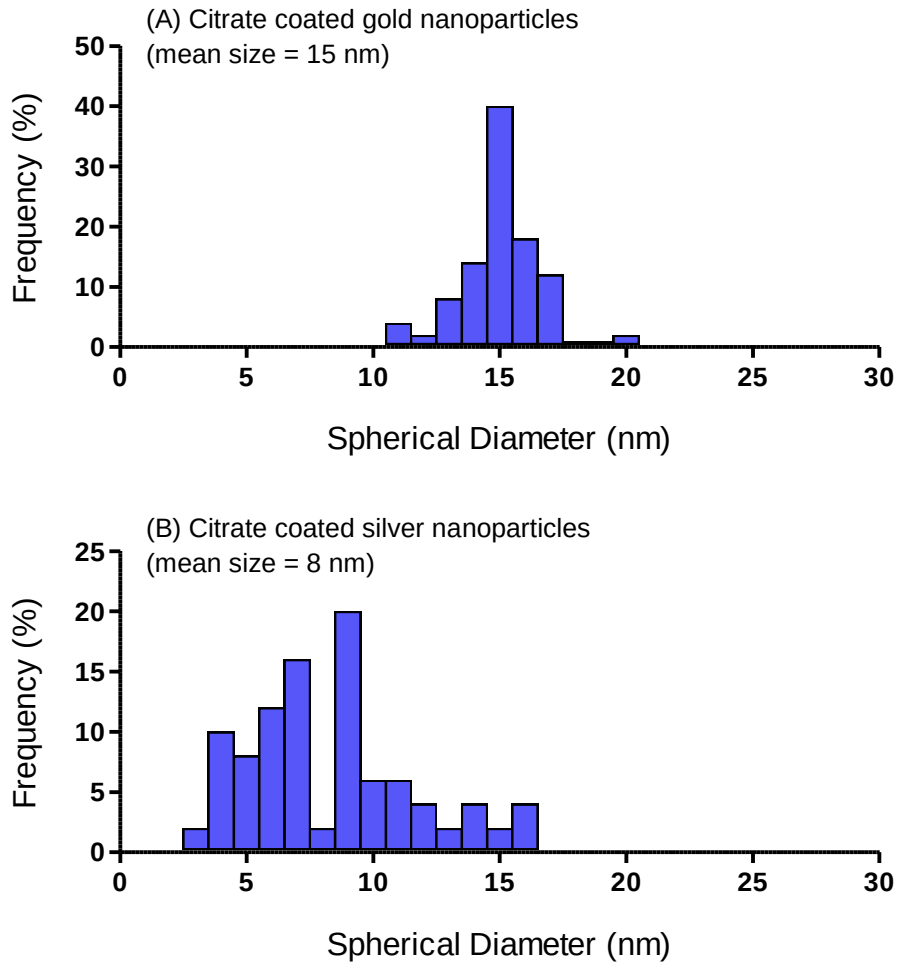


**Figure 3.2. Histograms, showing the size distribution of citrate coated gold (A) and silver (B) nanoparticles. At least a thousand nanoparticles were measured directly from transmission electron micrographs.**

The nanoparticle colloids had characteristic colours because their extinction spectra are dominated by particle plasmon resonances (PPRs). The gold nanoparticles had a $\lambda_{max}$ at 523 nm and appeared dark red. The silver nanoparticles had a $\lambda_{max}$ at 430 nm and appeared yellow-brown. The $\lambda_{max}$ is shifted towards the red end of the spectrum with increasing particle size. Thus, for the silver nanoparticles, which were synthesised in a 2 step process, the smaller silver seed particles (4 nm diameter) had a shorter $\lambda_{max}$ (386 nm) than the mature colloid (7 nm diameter, $\lambda_{max}$ = 437 nm). A single peak in the UV-Visible

absorbance spectrum is characteristic of mono-disperse spherical nanoparticles with a narrow size distribution, Figure 3.3.

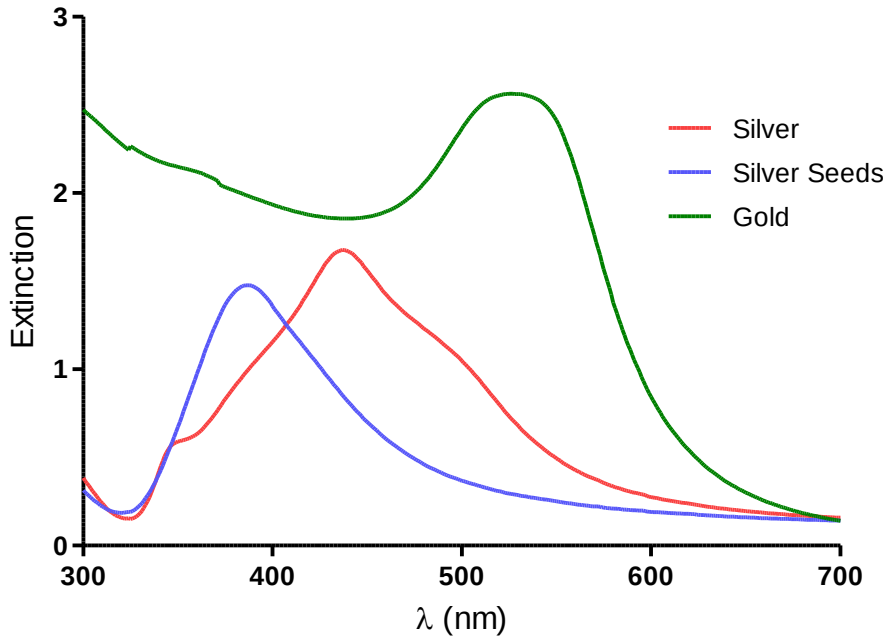


**Figure 3.3. Gold and silver nanoparticles had characteristic UV-Visible extinction spectra, which are dominated by particle plasmon resonances.**

Citrate coated gold and silver nanoparticles were mixed with Bovine Serum Albumin (BSA) to prepare protein coated nanoparticles. The optimum concentration of BSA was the minimum concentration required to prevent aggregation in the colloid after addition of 10% (w/v) NaCl, determined by performing titration experiments. This was found to be 10 µg/mL for the gold nanoparticles and 20 µg/mL for the silver nanoparticles. After addition of BSA, the colloids were not sensitive to sodium chloride, therefore the nanoparticles were stabilised by the BSA. PPR is a surface effect, so a change in $\lambda_{max}$ confirms that the BSA molecules interact with the gold or silver surfaces, Figure 3.4.

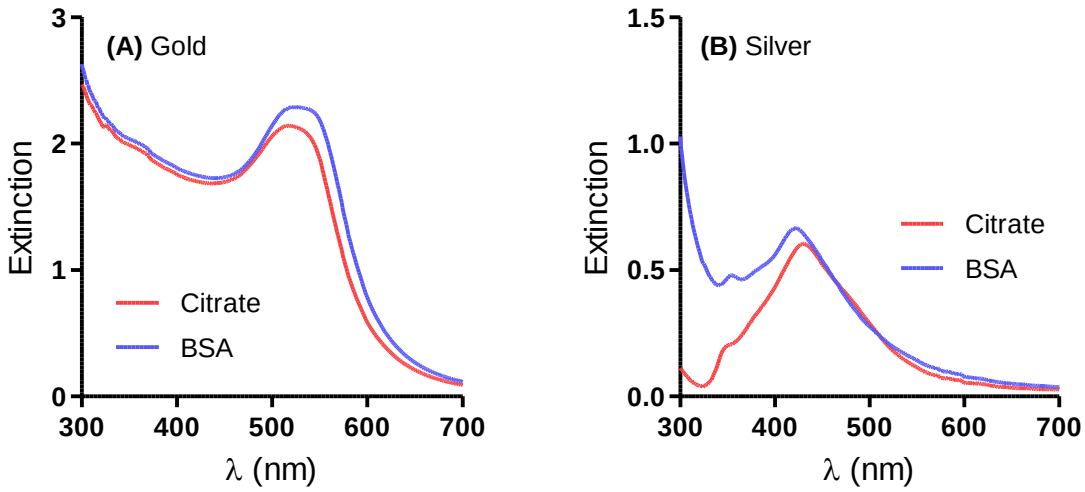


**Figure 3.4. The UV-visible extinction spectra of citrate coated and BSA coated gold (A) or silver (B) nanoparticles.**

*E. coli* were cultured in LB medium until mid-exponential phase and approximately $10^9$ colony forming units were exposed to 10 mL of the synthesised nanoparticles in water, either with a coat of citrate or BSA. The nanoparticle concentration was not determined for this study; however the experiment may be repeated by taking the gold nanoparticle colloid to have an extinction value of 2.137 at $\lambda_{max}$ (523 nm) for the citrate coat or an extinction value of 2. 289 at $\lambda_{max}$ (520 nm) for the BSA coat. The silver nanoparticle colloid had an extinction value of 0.604 at $\lambda_{max}$ (430 nm) for the citrate coat or an extinction value of 0.665 at $\lambda_{max}$ (422 nm) for the BSA coat. After exposure the bacteria were fixed, stained and sectioned for the preparation of transmission electron micrographs. Under the experimental conditions, the silver nanoparticles were toxic to the *E. coli*, but the gold nanoparticles did not inhibit bacterial survival compared to the control, Figure 3.5.

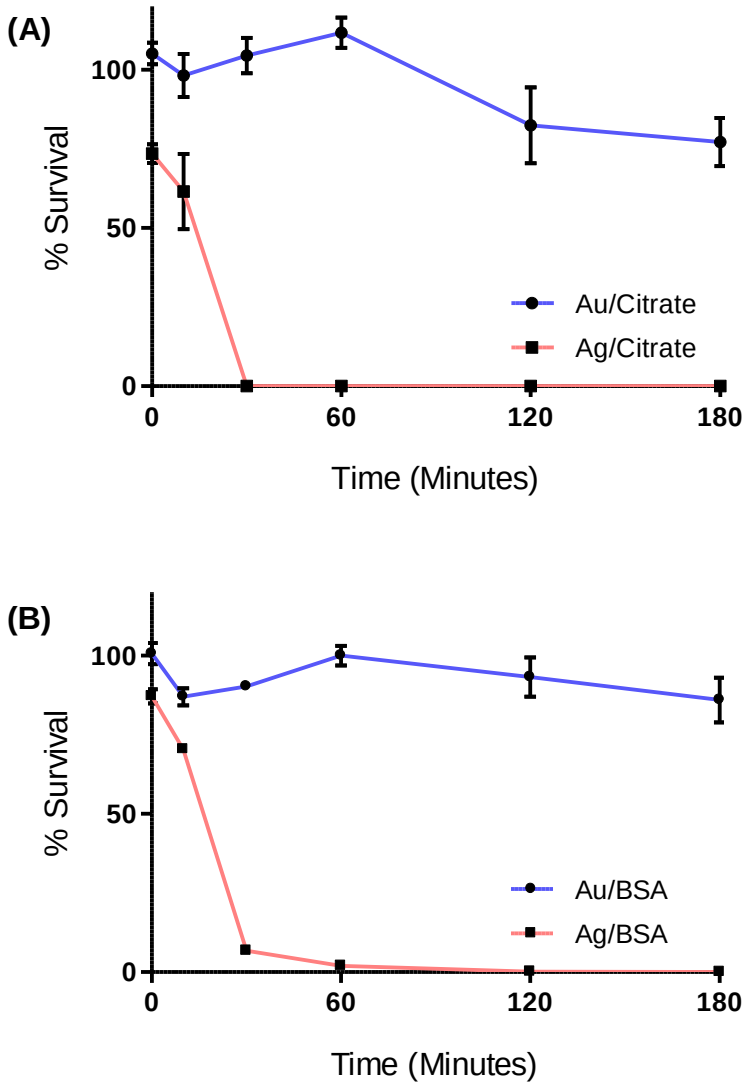


**Figure 3.5. *E. coli* were suspended in water containing colloidal nanoparticles with the anionic citrate surface ligand (A) or BSA coated surface (B). For controls, the colloids were destabilised by sonication, and agglomerated material was removed by ultracentrifugation. Then, *E. coli* were suspended in the supernatant. Bacterial survival in the presence of the nanoparticles was measured by viable cell counts, and compared to the control to determine the % survival. The error bars are the standard error of the mean (n=3).**

After suspension in gold nanoparticle colloids, *E. coli* survival was 100% after 30 minutes. Conversely, the citrate coated silver nanoparticles reduced the *E. coli* survival rate to 61% after 15 minutes, and no colony forming units were detected after 30 minutes. Capping the silver nanoparticles with BSA reduced the effect: 70% of the cells were viable after 15 minutes, 7% after 30 minutes and some colony forming units (one or two colonies) were detected after 2 hours.

### 3.2.2. Transmission Electron Microscopy of Bacterial-Nanoparticle Interactions

*E. coli* were mixed with gold or silver nanoparticles, coated with either citrate or BSA, for 30 minutes, at which time the majority of the bacteria were viable, and imaged by bright field TEM. The bacteria were embedded in an epoxy resin, which was sectioned at a thickness of approximately 80 nm. This was consistent with the interference colour of transmitted light through the resin fragments. Generally, the preparation protocol gave clear staining of the cell envelope with minimal staining artefacts. The *E. coli* sections appeared oblong or spherical, depending on whether a longitudinal section (LS) or transverse section (TS) of the bacterium was cut. The bacteria were 0.4-0.7 μm wide and 2.5-8.5 μm long (or longer where a bacterium was about to undergo cytokinesis). Each experiment was repeated at least 3 times, each replicate produced similar micrographs. Typical transmission electron micrographs for *E. coli*, without exposure to nanoparticles, are shown in Figure 3.6.

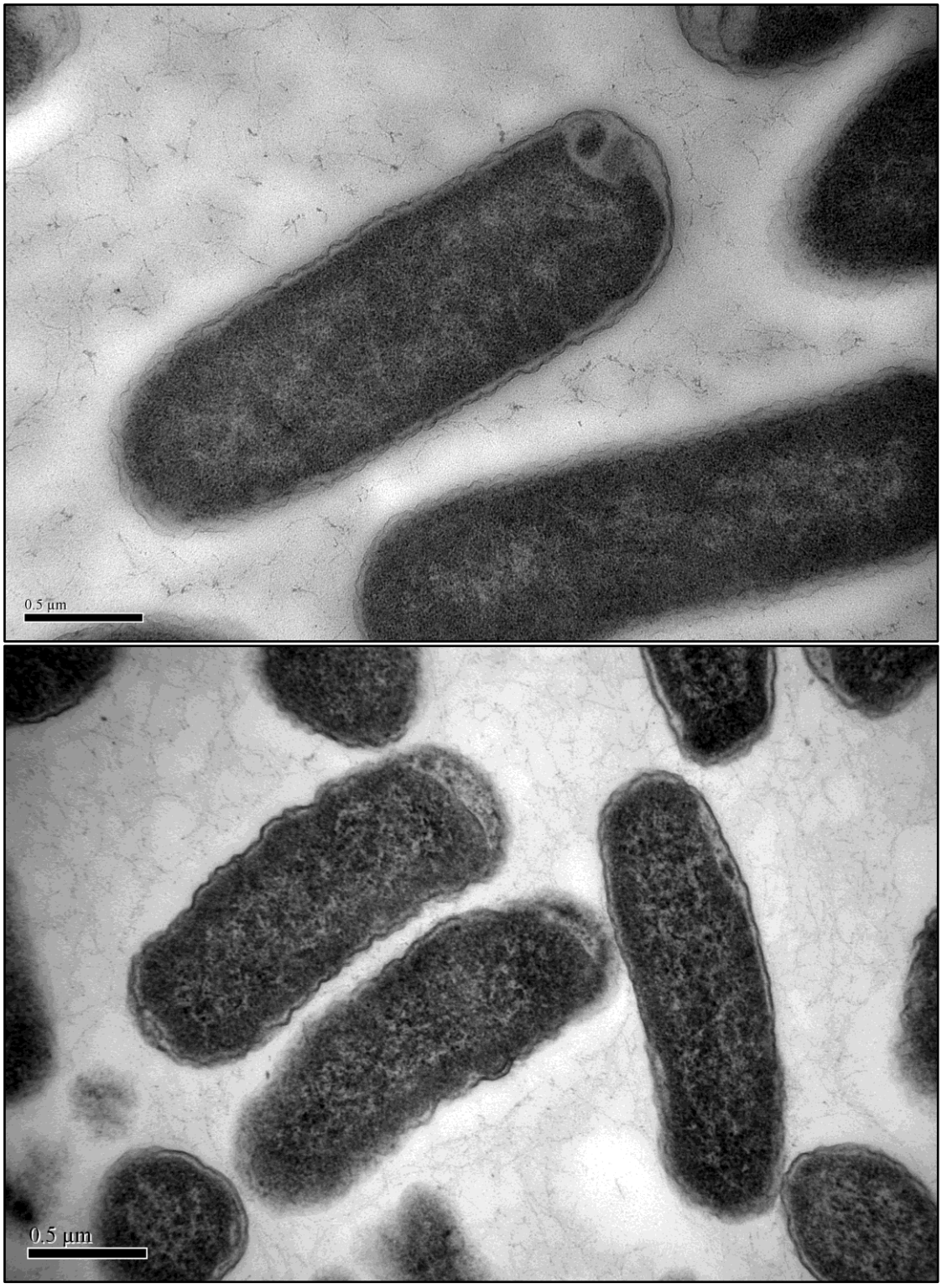


**Figure 3.6. Transmission electron micrographs of *E. coli* sections prepared from specimens, which had not been exposed to gold or silver nanoparticles. The specimens had been treated in the same way but show some minor cell-cell variation as is typical of TEM.**

After exposing the *E. coli* to gold nanoparticles, the micrographs demonstrated that some nanoparticles were associated with the cell surface. However, the bacteria had been sequentially sedimented and re-suspended throughout the procedure, removing most of the unbound nanoparticles in the accordingly coloured supernatants. The gold nanoparticles typically appeared on the extra-cellular face of the cell envelope and associated with material surrounding the cell surface, Figure 3.7, including hair-like appendages that may resemble the bacterial fimbriae, Figure 3.8. In addition, the gold nanoparticles were within the circumferential cell envelope of approximately 2% of the bacteria, appearing as if they were within the cytosol even though the specimens had been treated in the same way, Figure 3.8. The bacterial sections with nanoparticles within the cell envelope were typically cut along the longitudinal axis of the bacterium, however with exceptions as shown in Figure 3.9.

There were no qualitative differences between *E. coli* that had been exposed to citrate coated or BSA coated gold nanoparticles, both showed evidence of nanoparticles associated with the cell surface and inside the cell section. However, overall there was a quantitative difference between the numbers of nanoparticles that were associated with each bacterial section. From a sample of 200 bacteria an average of 16 ± 8 citrate coated gold nanoparticles adhered to each bacterial section, compared to an average of 27 ± 11 BSA coated gold nanoparticles. Gold nanoparticles with either coating appeared to be within the cytosol of approximately 2% of cells, having observed more than 2,000 cells from at least 3 replicate samples.

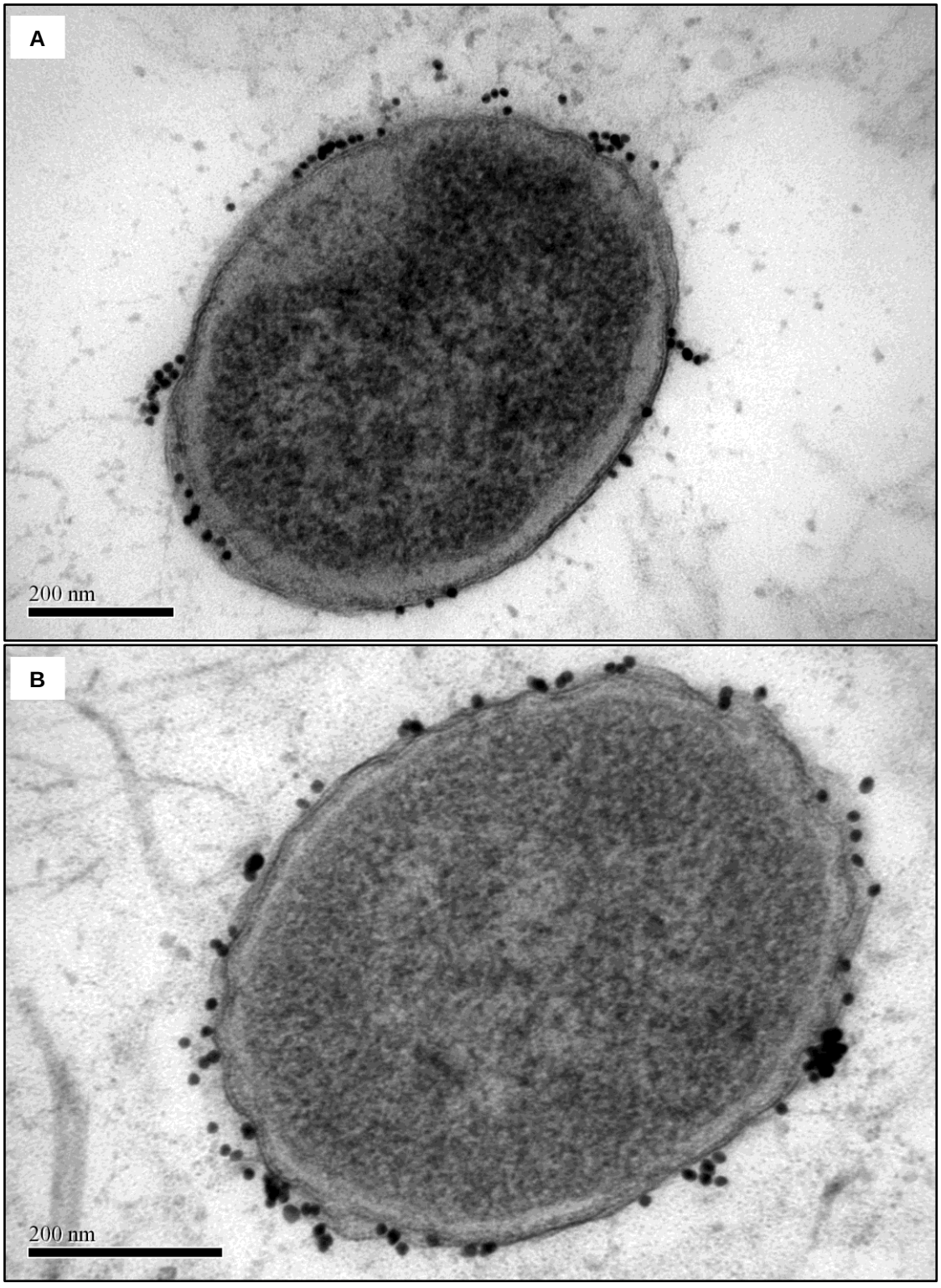


**Figure 3.7. Transmission electron micrographs of *E. coli sections* post treatment with citrate coated gold nanoparticles (A) or BSA coated gold nanoparticles (B). Transverse sections of the bacteria are shown.**

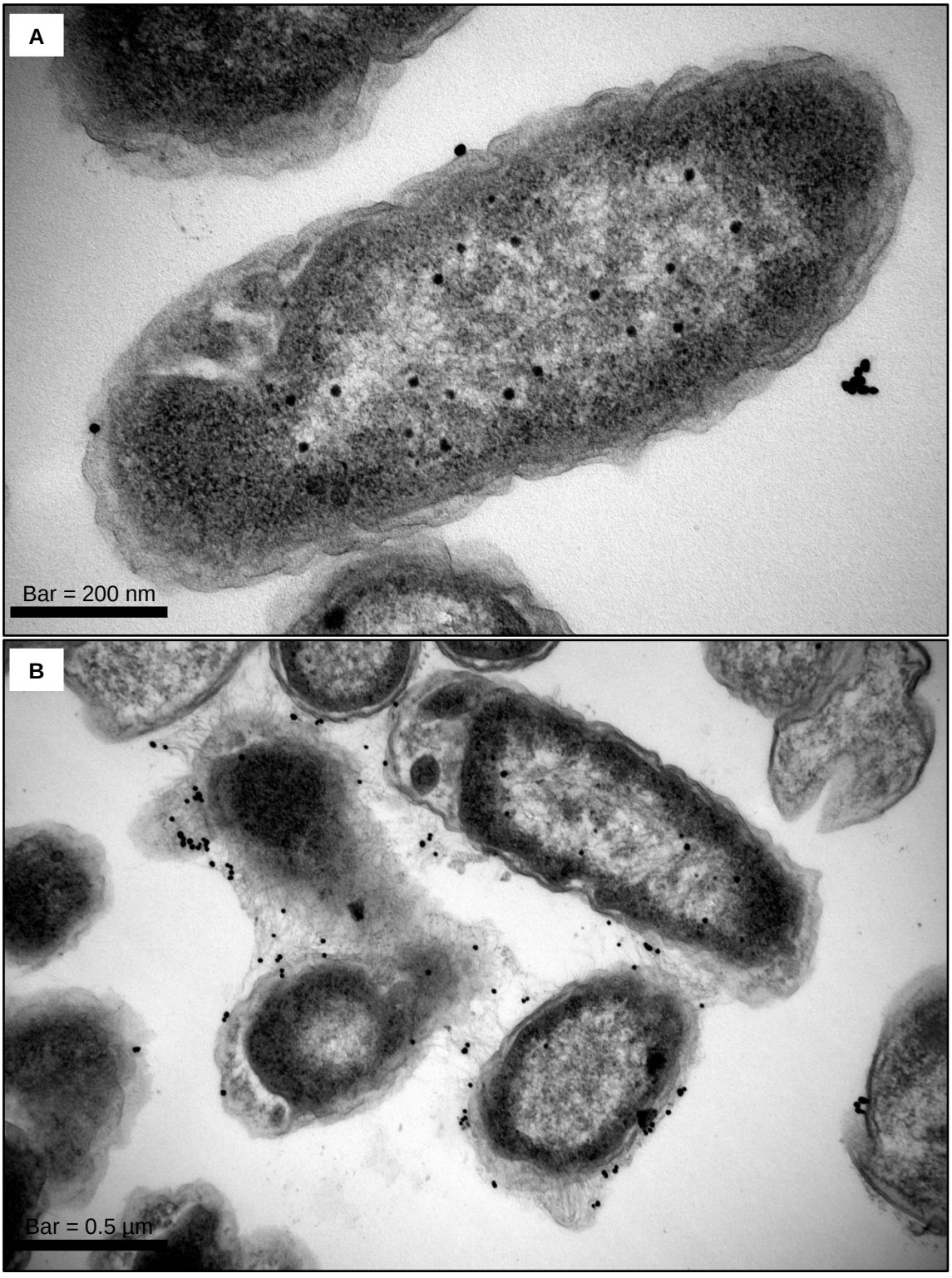


**Figure 3.8. Transmission electron micrographs of *E. coli* sections post treatment with citrate coated gold nanoparticles (A) or BSA coated gold nanoparticles (B). Longitudinal sections of the bacteria are shown.**

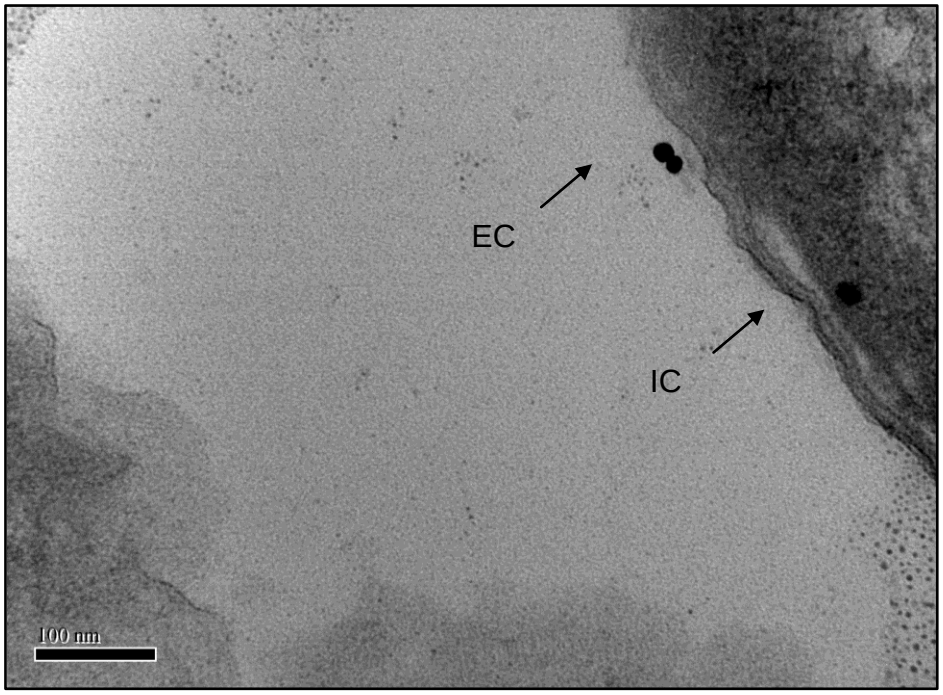


**Figure 3.9. A transverse section of an *E. coli* with gold nanoparticles on the extracellular (EC) and intracellular (IC) face of the envelope.**

The micrographs of *E. coli* after exposure to silver nanoparticles were distinct in appearance. The silver nanoparticles could not be seen in the micrographs. The bacterial sections had a similar staining pattern to the control, but with an electron-dense haze surrounding the extra-cellular face of the cell envelope, Figure 3.10.

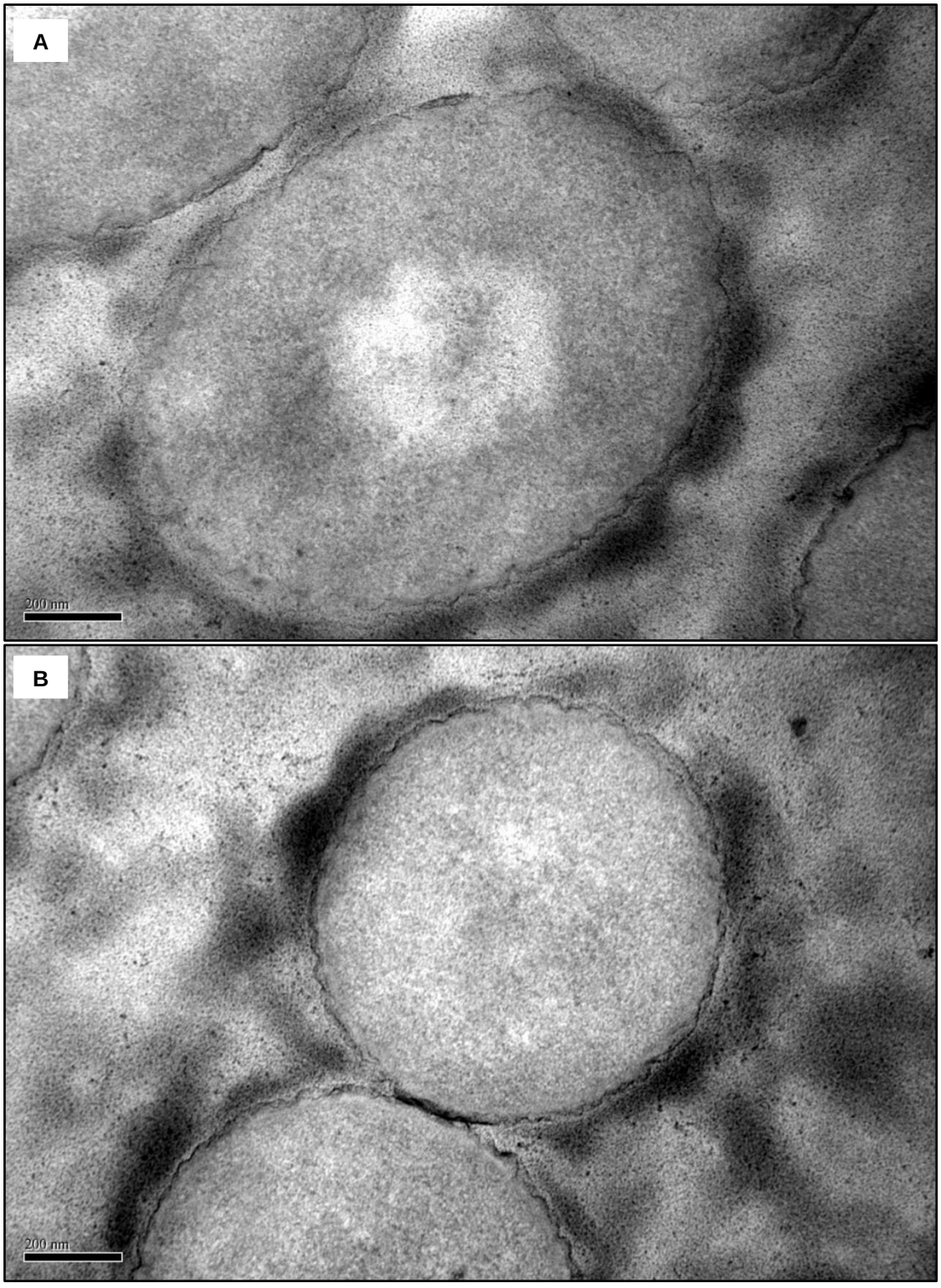


**Figure 3.10. Transmission electron micrographs of *E. coli* sections post treatment with citrate coated silver nanoparticles (A) or BSA coated silver nanoparticles (B). Note: electron dense patches at the circumference of the sections.**

## 3.3. Discussion

### 3.3.1. Nanoparticle Synthesis using 'Wet-Chemistry' Methods

Gold nanoparticles were synthesised using the method of Turkevich [16, 17, 20] where a higher concentration of sodium citrate resulted in a smaller mean nanoparticle diameter, Table 2.1. The citrate anions adsorbed to the nanoparticle surfaces, thus provided colloidal stability by preventing the nanoparticles from agglomerating according to electrostatic repulsion. Therefore, a higher concentration of citrate extends the total surface area that can be covered and favours smaller nanoparticles. The gold nanoparticles that were used experimentally were mono-disperse, typically spherical with a small (3%) proportion of truncated triangular structures, with mean diameter of 15 nm. This aided in the identification of the nanoparticles in TEM images, post exposure to bacteria, when they could be distinguished from spherical debris based upon their size. The silver nanoparticles were synthesised according to the method of Pal *et al* [18] and were also spherical, but poly-dispersed with a bi-modal size distribution, Figure 3.1 and Figure 3.2.

The synthesis reaction products were characterised using their UV-visible spectrum, with mono-disperse suspensions of spherical gold nanoparticles having single feature extinction spectra due to a Particle Plasmon Resonance (PPR), Figure 3.3. The wavelength at which maximum light is absorbed/scattered ($\lambda_{max}$) is dependent on the size and shape of the nanoparticles and also the physical properties of the material. Thus, the absorption spectra were characteristic for each type of nanoparticle in a colloidal suspension. Accordingly, the extinction spectrum for the bi-modal silver nanoparticles had multiple features, representing PPR from populations of nanoparticles that had different sizes. The silver seed nanoparticles from which the mature colloid was prepared had a single peak, indicating that the seed solution was monodisperse, and that the size

distribution of the mature colloid increased during the second phase of the two-stage synthesis reaction as the seeds were grown into larger nanoparticles.

Gold and silver nanoparticles rapidly adsorb proteins under physiological conditions [14]. Therefore, BSA coated nanoparticles were prepared to produce a surface coating that was akin to how a bacterium might encounter a nanoparticle *in vivo*. Since PPR is a surface effect, the change to the extinction maximum observed after mixing the nanoparticle colloids with BSA, Figure 3.4, is associated with the adsorption of the proteins to the nanoparticle surfaces. The BSA either displaced the native citrate anion, or covered it [21, 22]. Furthermore, the BSA-functionalised gold or silver nanoparticles were stable in the presence of sodium ions, indicating that the BSA on the surface prevented the nanoparticles from agglomerating through steric factors. In contrast, the sodium cations shield the negatively charged surface on citrate coated nanoparticles, reducing or removing the repulsive forces, leading to coalescence.

The toxicity of the nanoparticle colloids was determined by measuring *E. coli* survival after exposure to gold and silver nanoparticles, in water, and with or without the BSA on the surface, Figure 3.5. The silver nanoparticles were highly toxic, as reported previously [3, 4, 18, 23], but this effect was reduced for the nanoparticles that were coated with BSA. A hypothetical mode of silver nanoparticle toxicity is dissolution and release of the silver ion, $Ag^{+}$; a hypothesis that is tested in Chapter 3. Therefore, it is postulated that the BSA on the surface may have reduced the rate of silver ion release by blocking the path of the nanoparticle surface atoms into the bulk solution phase. The citrate coated gold nanoparticles were minimally toxic to the *E. coli* and the BSA coated gold nanoparticles were non-toxic. The low level of toxicity is consistent with other studies [10] and indicates that the gold nanoparticles may not compromise the integrity of the cell wall.

### 3.3.2. Gold Nanoparticles Associate Directly with *E. coli* Bacteria

The nanoparticles had a negative surface charge: either anionic citrate molecules or BSA proteins, which have an isoelectric point at pH 4.7, and therefore an effective negative charge in water (pH 7) [24]. Accordingly, the primary interaction of the nanoparticle with the bacterium is probably an electrostatic attraction between the nanoparticle surface and positively charged regions such as the extracellular domains of integral outer membrane proteins on the *E. coli* surface. Such interactions were evident from an instantaneous red-shift in the optical extinction trend upon addition of the bacteria to the gold and silver colloids (not shown), similar to the red-shift observed after mixing the nanoparticles with BSA protein. The observed red-shifting may reflect the formation of nanoparticle-bacterial complexes. For gold nanoparticles the complexes were observed in the electron micrographs. Therefore the change in the extinction spectrum is consistent with the TEM images, both indicating an interaction. Thus, the imaged interaction is unlikely to be an artefact from coalescence of the specimen during the sample preparation.

The surface lipopolysaccharides carry a negative charge from phosphate residues on the inner and outer core polysaccharide chains [25]. Thus, nanoparticle binding by electrostatic attraction could occur at sites where the LPS molecules are interspaced by protein ‘landing pads’. The crystal structures of some surface proteins including OmpF (8 nm across, [26, 27]) and OmpC (7 nm across, [28]), indicate that the surface domains of these proteins would be more than sufficient to accommodate binding of a 15 nm gold sphere, assuming that the contact surface is less than the radius of the sphere. This is supported by the observation of Morones *et al*, who report a size dependent interaction of silver nanoparticles with *E. coli* [3] with smaller nanoparticles binding preferentially. Larger nanoparticles may not fit onto the exposed protein domains. A variety of surface proteins are present on *E. coli* and the nanoparticle interaction will depend upon the specific charge

and topology of each molecule. In general the larger proteins may favour interaction, having a greater contact area and number of charges.

The nanoparticle surface ligand is clearly important for the bacterial-nanoparticle interaction. From a sample of 200 bacterial sections on average 16 citrate-capped gold nanoparticles adhered to each bacterial section, compared to an average of 27 BSA-capped gold nanoparticles. A BSA molecule is approximately 14 x 4 X 4 nm [29], so a uniform surface coverage will extend the average diameter of the gold-BSA nanoparticle up to 43 nm, depending on the binding orientation at the nanoparticle surface. Bacteria and nanoparticles associate on collision in suspension with an association rate that is dependent on the diameter of the nanoparticle, and hence diffusion coefficient. This can be described according to the equations of Marian Smoluchowski [30], and as interpreted by Dror-Ehre and co-workers for bacterial-nanoparticle interactions [23] (Equation (1)).

$$J_{ij} = \frac{1}{6} N_i N_j G \left(d_i + d_j\right)^3$$

*Equation (1)*

Where $J$ is the frequency of collisions between bacteria ($i$) and nanoparticles ($j$), $N_i$ and $N_j$ are their number densities and $d_i$ and $d_j$ are their diameters. According to this relationship the larger size of the gold nanoparticles with the BSA ligand would increase the rate of association. However, because the nanoparticles are so small with respect to the bacteria the influence of nanoparticle size remains minimal and the diffusion coefficient of the bacterium in solution dominates the frequency of collisions [23].

In addition to the overall nanoparticle size, the electrostatic properties of the BSA and citrate surface are different. The BSA carried a net negative charge at the experimental pH, but any positively charged sites on the protein surface, distal to the

nanoparticle, may permit some interaction with the opposite charge on the LPS. However, the coverage of BSA coated gold nanoparticles was discontinuous on the *E. coli* surface, indicating that protein-protein interactions may have been the predominant mode of association if the protein distribution in the outer membrane is similarly discontinuous. The difference in the number of citrate coated and BSA coated nanoparticles that bound to the cells indicates that *E. coli* has more possible BSA than citrate binding sites, and that the energy of interaction is more favourable. The many possible orientations of BSA on the nanoparticle surface increases the possible steric and electrostatic combinations that are available to corresponding attachment sites on the cell surface.

Some gold nanoparticles, either citrate or BSA coated, appeared proximal to the cell envelope, but did not sit directly on the cell surface. This may reflect an interaction with extracellular appendages including hair-like extensions, which resemble fimbriae (pili), Figure 3.8. Mannose-capped gold nanoparticles associate directly with type-1 pili [31]. This is an example of a receptor-ligand interaction between the FimH adhesion subunit of the pili and mannose. In contrast, the interaction observed here may be non-specific, either a protein-protein interaction between the surface BSA and the various fimbriae protein subunits, or an electrostatic interaction with the surface citrate.

### 3.3.3. Silver Nanoparticles were Absent from TEM Images

Contrary to the bacterial-gold nanoparticle interactions, silver nanoparticles were not observed either in association with the *E. coli*, or present in the surrounding medium. Changes to the extinction trend upon mixing silver nanoparticles with *E. coli* indicated that the nanoparticle surfaces initially made contact with the bacteria, and this interaction modified the propagation of the particle plasmon wave. This is as expected because the silver nanoparticle surface ligand, either citrate or BSA protein, was equivalent to that on

the gold nanoparticles, for which the interaction was clear. A resultant hypothesis is that the dissolution of the nanoparticle surfaces reduced the nanoparticle size until they were no longer visible in the TEM images. In contrast, the gold surfaces, which are not readily oxidised, dissolve at a much slower rate or not at all. The putative mechanism for silver nanoparticle toxicity is dissolution and release of silver ions, and may explain the observed toxicity to *E. coli*, Figure 3.5. Further, it is postulated that the electron dense haze that surrounded the silver nanoparticle treated bacteria may have formed where the silver ions react with, or associate with, the cell surface, or are reduced to $Ag^0$ by the outer membrane. Similar staining of bacteria after exposure to silver nanoparticles has been observed elsewhere [18].

### 3.3.4. Evidence of Gold Nanoparticle Uptake in *E. coli* from TEM Images

Previously, nanoparticles including Cd/Se quantum dots (QDs) (less than 5 nm) [6], and silver nanospheres (12-39 nm) [3, 4] have been imaged apparently within bacteria using TEM. The small QDs could in theory enter bacteria by diffusing through membrane pores. In *E. coli* the SecA protein, which is part of a multimeric protein secretion complex, may form a pore in the plasma membrane with a hole of up to 6 nm [13]. Therefore, smaller (less than 6 nm) nanoparticles could enter a bacterium by diffusion through membrane pores with similar structure to SecA. In contrast a route by which larger nanoparticles might enter a bacterium is unclear unless the integrity of the cell wall and cell membrane is compromised.

The null hypothesis for the uptake of large nanoparticles by *E. coli* is that the observation is an imaging artefact. This may occur as nanoparticles diffuse into bacteria through discontinuous and damaged cell walls, which are unseen because of the limited field of view in TEM, which has no vertical resolution. To test this null hypothesis *E. coli*

were exposed to non-toxic [10], 15 nm gold nanospheres, (Citrate coated or BSA coated), in aqueous suspensions and nanoparticle uptake was assessed using bright field mode TEM on thin (~80 nm) sections. After suspension in gold nanoparticle colloids, *E. coli* survival was 100% (BSA coated) or 90% (citrate coated) compared to an untreated control after 30 minutes, Figure 3.5. This was the time at which the cells were harvested for imaging. Therefore, even though the micrographs show only a thin, 2-dimensional section of the bacterium, there is a strong probability that the entire specimen was viable and the cell envelope was in-tact upon fixation. As expected it was found that most of the bacterial sections did not show any evidence that the gold nanoparticles were inside the cell. This is consistent with their large size, and that they are not toxic, thus, unlikely to disrupt bacterial membranes and enter the cell at a site of membrane damage. However, within each specimen preparation there were bacterial sections that contained nanoparticles within the circumferential cell envelope, and towards the centre of the cell, as in Figure 3.8. This can be explained if the *E. coli* section represented the extreme terminus of the cell wherein the nanoparticles that were bound to the underside of the section, and extracellularly, would appear to be within the cytosol because the image is based upon an electron shadow, Figure 3.11.

Consistent with this hypothesis, all of the *E. coli* that had gold nanoparticles throughout the cytosol had been sectioned along the longitudinal axis, where the likelihood of a section incorporating the cell envelope is greater than in transverse sections, according to the shape of the *E. coli*. For example, if the bacterium is approximately 0.7 µm wide, but up to 8 µm long, then out of 9 potential longitudinal sections, two of these might incorporate the cell envelope, compared to 2 out of 100 potential sections in the transverse orientation.

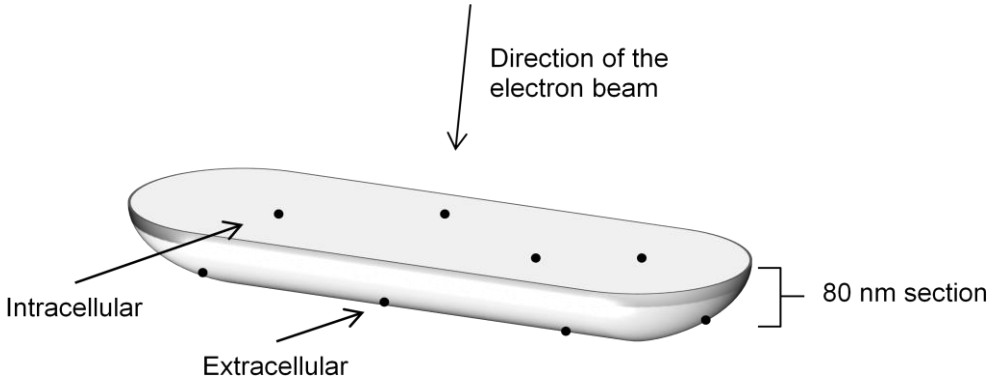


**Figure 3.11. A cartoon representation of a terminal section of an *E. coli*, with nanoparticles inside the cytosol and on the cell surface. In this case, a transmission electron micrograph, which is an electron shadow, would indicate that all of the nanoparticles, inside and outside, were within the cytosol.**

There is additional evidence that gold nanoparticles localised at the intracellular face of the cell envelope, as viewed in transverse sections, for example in Figure 3.9. In transverse sections, the intracellular position of the nanoparticles cannot be explained according to the aforementioned artefact. Had the terminus of the cell been imaged, then one would expect the nanoparticles to appear to be throughout the cytosol, corresponding to their scattered location on the underside of the cell. Conversely, the evidence of uptake from transverse sections was from individual nanoparticles that were always adjacent to the cell envelope. Further, the cell envelope appeared intact, as judged by the structural staining of the double membrane. Also, as exemplified by the image provided in Figure 3.9, if the nanoparticle had been artificially moved during the movement of the sectioning knife, then one would also expect the extracellular nanoparticles to have been moved in this direction; however they clearly remain on the extracellular face of the membrane. Although the evidence of gold nanoparticle uptake from transverse sections appears convincing, it is possible that, as for longitudinal sections, this also represents an imaging artefact due the curvature of the bacterial section, as exemplified in Figure 3.12.

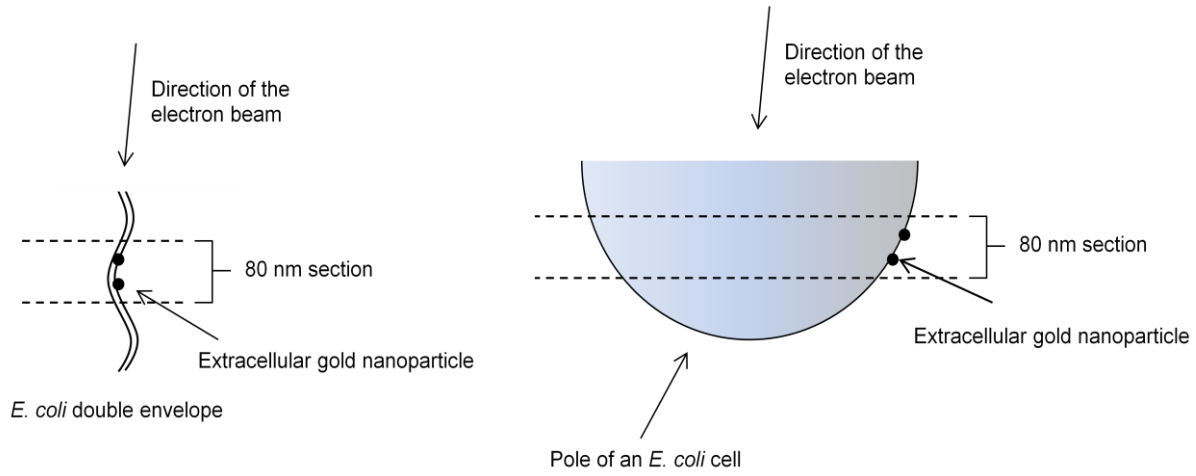


**Figure 3.12. A Cartoon representation of how extracellular nanoparticles could appear to be within the cytosol from transverse TEM sections. Left: nanoparticles reside on the extracellular face of the double envelope, but within a recess in the cell surface. Right: the section is cut near the pole of the cell, where the curvature of the cell is greatest.**

The frequency with which the putative uptake occurred was very low. Several thousand bacterial sections were viewed, from replicate experiments and only a small proportion of the bacteria, 2%, appeared to have nanoparticles within the cell. Therefore, an internalisation would be, at best, inefficient and unlikely to reflect a metabolically relevant uptake process. Instead, a hypothetical mechanism for the uptake could be that the negative charges carried by the gold nanoparticles could contribute to a threshold potential difference across the outer membrane that initiates the electroporation phenomenon [32]. However this may be restricted by the size of the gold nanoparticles used in this study. For example a 15 nm gold sphere may have a mass of ~26.17 attograms (ag, $10^{-15}$ g); assuming a 15 nm diameter gold sphere contains 80,000 gold atoms, and that the density of gold in a nanoparticle is the same as the bulk material, 19.32 g/cm$^3$. In comparison, the electroporation of plasmids over 5.14 ag (equivalent to 10 kbp, assuming 50 % G-C content) is inefficient and for plasmids over 20 Kbp it is not usually achieved [33], even when the bacteria are pre-treated and made 'electro-competent', and very large electric fields are applied. Therefore, an alternative hypothesis

for gold nanoparticle uptake is that the membrane becomes damaged, albeit transiently, and then repaired. This process has been reported, but not extensively investigated in *E. coli* [34].

### 3.3.5. Conclusions

Specific regions of the *E. coli* surface accommodate the interaction with gold nanoparticles, possibly through an attachment of the nanoparticles to the extracellular domains of integral outer membrane proteins.

The interaction is favoured if the nanoparticle surface is covered with BSA indicating that the protein-protein interactions occur more frequently than the interaction with the citrate anion-coated surfaces.

Transmission electron micrographs indicate that gold nanoparticles may enter *E. coli* bacteria, appearing to be on the cytosolic face of the double membrane. However, this was only observed in a small proportion of bacterial sections and can be explained from the specimen section and curvature.

Silver nanoparticles were not visible in association with *E. coli*, however, they could be imaged by TEM in the absence of the bacteria. A dark staining pattern proximal to the bacterial envelope was observed after exposure to the silver nanoparticles, but not visible in the gold nanoparticle treated specimens or the controls. These observations lead to the hypothesis that the nanoparticles dissolve.

The antibacterial mechanism for silver nanoparticles is unclear, however the observations made here lead to a novel hypothesis; the silver nanoparticles attached to the membrane dissolve, thus releasing toxic ions directly into the cell envelope. This hypothesis is investigated in Chapter 3.

## 3.4. References


1. Benz, R., A. Schmid, and R.E. Hancock, *Ion selectivity of gram-negative bacterial porins.* J. Bacteriol., 1985. **162**(2): p. 722-727.
2. Nikaido, H., *Microdermatology: cell surface in the interaction of microbes with the external world.* J Bacteriol, 1999. **181**(1): p. 4-8.
3. Jose Ruben, M. and et al., *The bactericidal effect of silver nanoparticles.* Nanotechnology, 2005. **16**(10): p. 2346.
4. Sondi, I. and B. Salopek-Sondi, *Silver nanoparticles as antimicrobial agent: a case study on E. coli as a model for Gram-negative bacteria.* Journal of Colloid and Interface Science, 2004. **275**(1): p. 177-182.
5. Stoimenov, P.K., et al., *Metal Oxide Nanoparticles as Bactericidal Agents.* Langmuir, 2002. **18**(17): p. 6679-6686.
6. Kloepfer, J.A., R.E. Mielke, and J.L. Nadeau, *Uptake of CdSe and CdSe/ZnS Quantum Dots into Bacteria via Purine-Dependent Mechanisms.* Appl. Environ. Microbiol., 2005. **71**(5): p. 2548-2557.
7. Lonhienne, T.G.A., et al., *Endocytosis-like protein uptake in the bacterium Gemmata obscuriglobus.* Proceedings of the National Academy of Sciences, 2010. **107**(29): p. 12883-12888.
8. Mercenier, A. and B.M. Chassy, *Strategies for the development of bacterial transformation systems.* Biochimie, 1988. **70**(4): p. 503-517.
9. Dagert, M. and S.D. Ehrlich, *Prolonged incubation in calcium chloride improves the competence of Escherichia coli cells.* Gene, 1979. **6**(1): p. 23-38.
10. Williams, D., S. Ehrman, and T. Pulliam Holoman, *Evaluation of the microbial growth response to inorganic nanoparticles.* Journal of Nanobiotechnology, 2006. **4**(1): p. 3.
11. Goodman, C.M., et al., *Toxicity of Gold Nanoparticles Functionalized with Cationic and Anionic Side Chains.* Bioconjugate Chemistry, 2004. **15**(4): p. 897-900.
12. Grace, A.N. and K. Pandian, *Quinolone Antibiotic-Capped Gold Nanoparticles and Their Antibacterial Efficacy Against Gram Positive and Gram Negative Organisms.* Journal of Bionanoscience, 2007. **1**: p. 96-105.
13. Wang, H.-W., et al., *Ring-like pore structures of SecA: Implication for bacterial protein-conducting channels.* Proceedings of the National Academy of Sciences of the United States of America, 2003. **100**(7): p. 4221-4226.

14. Lundqvist, M., et al., *Nanoparticle size and surface properties determine the protein corona with possible implications for biological impacts.* Proceedings of the National Academy of Sciences, 2008. **105**(38): p. 14265-14270.

15. Polte, J., et al., *Mechanism of gold nanoparticle formation in the classical citrate synthesis method derived from coupled in situ XANES and SAXS evaluation.* J Am Chem Soc, 2010. **132**(4): p. 1296-301.

16. Kimling, J., et al., *Turkevich Method for Gold Nanoparticle Synthesis Revisited.* The Journal of Physical Chemistry B, 2006. **110**(32): p. 15700-15707.

17. Turkevich, J., P. Stevenson, and J. Hillier, *A study of the nucleation and growth processes in the synthesis of colloidal gold.* Discuss. Faraday Soc., 1951. **11**: p. 55-75.

18. Pal, S., Y.K. Tak, and J.M. Song, *Does the Antibacterial Activity of Silver Nanoparticles Depend on the Shape of the Nanoparticle? A Study of the Gram-Negative Bacterium Escherichia coli.* Appl. Environ. Microbiol., 2007. **73**(6): p. 1712-1720.

19. Pissuwan, D., et al., *Functionalised gold nanoparticles for controlling pathogenic bacteria.* Trends in Biotechnology, 2010. **28**(4): p. 207-213.

20. Frens, G., *Particle size and sol stability in metal colloids.* Colloid & Polymer Science, 1972. **250**(7): p. 736-741.

21. Krasovskii, V., et al., *Interaction of gold nanoparticles with bovine serum albumin.* Bulletin of the Lebedev Physics Institute, 2007. **34**(11): p. 321-324-324.

22. Wangoo, N., et al., *Synthesis and capping of water-dispersed gold nanoparticles by an amino acid: Bioconjugation and binding studies.* Journal of Colloid and Interface Science, 2008. **323**(2): p. 247-254.

23. Dror-Ehre, A., et al., *Silver nanoparticle-E. coli colloidal interaction in water and effect on E. coli survival.* J Colloid Interface Sci, 2009. **339**(2): p. 521-6.

24. Böhme, U. and U. Scheler, *Effective charge of bovine serum albumin determined by electrophoresis NMR.* Chemical Physics Letters, 2007. **435**(4-6): p. 342-345.

25. Schletter, J., et al., *Molecular mechanisms of endotoxin activity.* Archives of Microbiology, 1995. **164**(6): p. 383-389.

26. *Image from the RCSB PDB (www.pdb.org) of PDB 3K19 (Kefala, G., et al., Structures of the OmpF porin crystallized in the presence of foscholine-12. Protein Sci. 19(5): p. 1117-25).*

27. Kefala, G., et al., *Structures of the OmpF porin crystallized in the presence of foscholine-12.* Protein Sci, 2010. **19**(5): p. 1117-25.

28. Lou, H., Chen, M., Beis, K., Low, A., Bayley, H., Booth, I., R., Naismith, J., H., *Molecular Insights Into Clinically Isolated OmpC Mutants and Their Role in Multi-Drug Resistance (Unpublished Work)*. 2010.

29. Wright, A.K. and M.R. Thompson, *Hydrodynamic structure of bovine serum albumin determined by transient electric birefringence.* Biophys J, 1975. **15**(2 Pt 1): p. 137-41.

30. Gregory, J., *Particles in water: properties and processes*. 2006: IWA Publications.

31. Lin, C.-C., et al., *Selective Binding of Mannose-Encapsulated Gold Nanoparticles to Type 1 Pili in Escherichia coli.* Journal of the American Chemical Society, 2002. **124**(14): p. 3508-3509.

32. Neumann, E., et al., *Gene transfer into mouse lyoma cells by electroporation in high electric fields.* EMBO J, 1982. **1**(7): p. 841-5.

33. Szostková, M. and D. Horáková, *The effect of plasmid DNA sizes and other factors on electrotransformation of Escherichia coli JM109.* Bioelectrochemistry and Bioenergetics, 1998. **47**(2): p. 319-323.

34. Gillies, N.E., et al., *Repair of membrane damage in X-irradiated E. coli.* Br J Cancer Suppl, 1984. **6**: p. 129-34.

# Chapter 4: Enhanced Silver Nanoparticle Stress Response in *Escherichia Coli* K12

## 4.1. Introduction

Silver nanoparticles have anti-viral (against HIV-1)[1], anti-fungal (against species of *Candida, Saccharomyces* and *Aspergillus*) [2-4] and anti-bacterial [5-22] properties, thus offering a broad spectrum alternative to conventional anti-microbial agents including antibiotics. The anti-bacterial efficacy of silver nanoparticles was reported in Chapter 3, wherein 8 nm diameter silver spheres, with anionic citrate or Bovine Serum Albumin (BSA) protein on the surface, hindered the survival of *E. coli* in water. However, the anti-microbial mechanism of action is unclear.

The differential efficacy of various silver-based formulations may be explained by a hypothesis described by Wijnhoven *et al*, which states that the anti-bacterial effects are proportional to the rate of release of the free silver ion, $Ag^+$ [23]. Silver ions interact with the thiol functional group on protein cysteine residues, and may react to form insoluble silver sulfide, $Ag_2S$. The functional thiol on cysteine residues is utilised for the coordination of various structural and catalytic metal ion co-factors, including $Cu^+$, $Zn^{2+}$ and $Fe^{3+}$, and also for the formation of intra-molecular di-sulfide bonds, which contribute to protein tertiary structure. In addition, $Ag^+$ has reactivity with phosphorous, nitrogen and oxygen-containing molecules [24, 25], including nucleic acids [26-29] and the amino acid, histidine via the imidazole side chain [30]. Accordingly the predicted mechanism of silver toxicity is the indiscriminate reaction of $Ag^+$ with proteins to perturb their structure and function, leading to pan-metabolism toxic effects, metabolic disintegration and cell death.

Bacteria respond to silver ions, as to other metal ions, by producing specific proteins to remove the ions from the cell: an adaptive response [31, 32]. In *E. coli*, the

concentration of free, mono-valent metal ions, $Ag^+$ and $Cu^+$, is controlled by two independent regulons. The first regulon, CusRS, is controlled by a two-component sensor/responder system. The sensor, CusS, is an integral plasma membrane histidine kinase, which interacts with metal ions in the periplasm and phosphorylates a transcriptional regulator, CusR [33, 34]. Phospho-CusR positively regulates the expression of the *cusCFBA* operon, which is encoded adjacent to the *cusRS* genes, and transcribed divergently from a common promoter region [35]. The genes encode a tripartite RND-protein driven chemiosmotic metal ion antiporter at the plasma membrane, CusCBA [33, 35-39], and a periplasmic $Ag^+/Cu^+$ binding protein. The second regulon is under the control of CueR, a cytosolic transcription factor, and a member of the MerR family of metal responding transcriptional regulators [40]. The CueR protein senses free silver and copper ions in the cytosol, and positively regulates the expression CopA, a P-Type ATPase family metal ion exporter [41], and a periplasmic cuprous oxidase, CueO, which catalyses oxidation of $Cu^+$ ions into the less toxic $Cu^{2+}$ form [42]. Presently, it is considered that these systems evolved for the purpose of maintaining optimal intracellular copper ions [37], which are metabolically important co-factors [43, 44]. However, silver and copper ions have the same $d^{10}$ electronic configuration and similar ionic radii (0.67-1.28 Å for $Ag^+$ and 0.46-0.77 Å for $Cu^+$) [45]. Thus, coordination with the associated regulatory proteins that control their expression may be similar. The $Zn^{2+}$ ion has the same $d^{10}$ electron configuration but with different valency and distinct systems exist in *E. coli* for zinc homeostasis [46, 47]. In addition to efflux the constitutive outer membrane porins, OmpF and OmpC are not produced by silver resistant strains of *E. coli* [48], which may provide a chemiosmotic defence. However, the regulation of the porin genes in response to silver ions has not previously been reported.

Nanoparticulate silver has a higher anti-bacterial activity compared to the bulk material because of the greater surface area to volume ratio. This favours a high rate of dissolution and release of $Ag^+$. In theory, the efficacy could be enhanced by a nanoparticle through interaction with the bacterial surface where local dissolution generates a high interfacial concentration of the ion. In contrast, silver ions that are released into the bulk solution phase may be quickly dispersed and contact the bacteria at a rate that is dependent upon various physical processes, including the diffusion coefficient of $Ag^+$.

This hypothesis was tested using an industrial grade silver nanopowder from an industry-leading manufacturer. The nanoparticles' physical and antibacterial properties, and the rate of dissolution in a nutrient medium, were characterised. Subsequently, the interaction between the silver nanoparticles and the model bacterium, *E. coli* K12, was determined using electron microscopy. The efficacy of the nanoparticles against the *E. coli* was compared with that of silver ions at a concentration that was determined to have been released by the nanoparticles. Additionally, a transcriptional response to silver ions was measured quantitatively using real-time PCR and similarly compared. The results demonstrate that the concentration of bulk solution phase silver ions, derived from silver nanoparticles, is disproportional to the anti-bacterial effects and strength of a transcriptional response. It is postulated that, because of the close association of the nanoparticles with the bacterial surface, the nanoparticles act as a vehicle to deliver silver ions directly to their site of action and enhance the concentration of bio-available silver.

## 4.2. Results

### 4.2.1. Nanoparticle characterisation

A dry silver nanopowder was provided by QinetiQ Nanomaterials Ltd (QNL), with physical characterisation data. The nanoparticles were produced using a novel gas plasma based approach. They had an irregular, approximately spherical morphology with an average particle size of 142 nm (± 20 nm), given as equivalent spherical diameter, and an average Brunauer–Emmett–Teller (BET) isotherm specific surface area of 4 $m^2$/g. X-ray diffraction analysis (QNL) indicated that the nanoparticles are silver, with no other elements detected. The nanoparticle size range and composition was confirmed in this work using Transmission Electron Microscopy (TEM) and Scanning Electron Microscopy (SEM), coupled with Energy Dispersive Analysis of X-rays (EDAX), Figure 4.1.

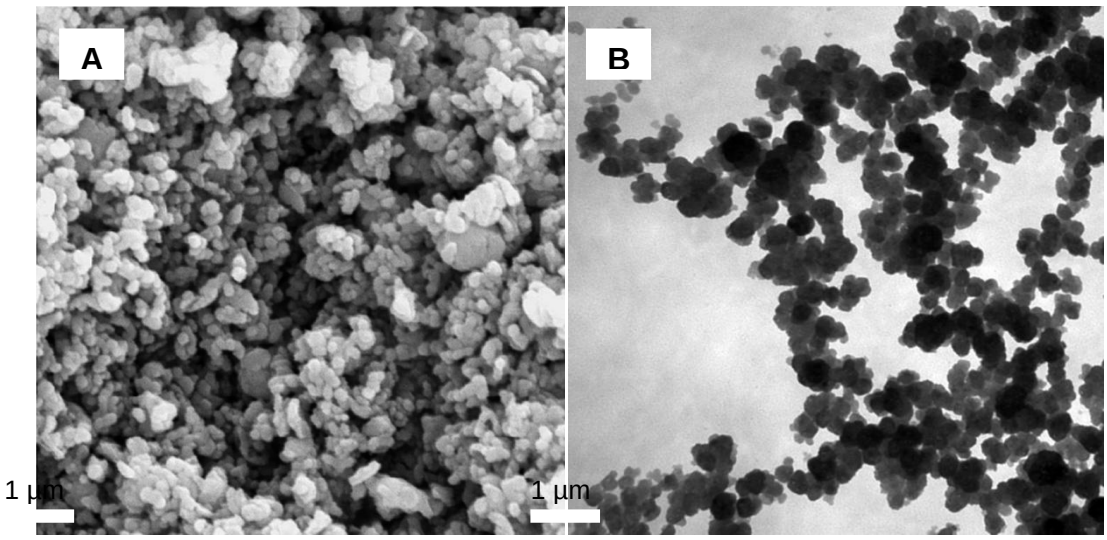


**Figure 4.1. Gas plasma-synthesised silver nanoparticles, viewed in scanning (A) and transmission (B) electron micrographs. SEM-coupled EDAX was used to confirm that the nanoparticles were silver, with no other elements present at a typical detection limit of Parts Per Million (data not shown).**

To test the anti-bacterial efficacy, first, colloidal suspensions of the nanopowder were prepared in various biological media using an ultrasonic probe to overcome the energy of interaction and to disperse the nanoparticles. In both a phosphate buffered saline (pH 7.2), and a minimal salts culture medium of equivalent pH, the nanoparticles were dispersed by the sonicator to form a homogeneous, dark grey suspension. However, immediately after sonication, the nanoparticles agglomerated into visible flocculates. This process was unaffected if the pH of the medium was 6.8 or 7.4. In contrast, in Luria broth, after dispersing the nanopowder with the ultrasonic probe, the nanoparticles remained in a homogeneous suspension for at least 8 hours (judged by eye as the nanoparticles had no detectable particle plasmon resonance). Further, by preparing the LB without 171 mM sodium chloride, which is referred to herein as modified-LB, prolonged the time until agglomeration of the nanoparticles was visible. Accordingly, modified-LB medium was used as the bacterial culture medium throughout this work to increase the colloidal stability of the nanoparticles.

Initially, the anti-bacterial activity of the nanopowder was tested on solid modified-LB medium using a simple agar plate assay, Table 4.1. Nanoparticles in the agar prevented growth of *Escherichia coli* (K12) and also *Pseudomonas aeruginosa* (PA01) and *Staphylococcus aureus* (ATCC 10390) in a dose dependent manner. *S. aureus* was the most resistant organism, demonstrating growth at a concentration of up to 200 µg/mL of the nanopowder but was completely inhibited at a concentration of 500 µg/mL. In comparison, the same inoculum size of *E. coli* or *P. aeruginosa* could only grow on plates containing 10 µg/mL but not 50 µg/mL. The results of the agar-based anti-bacterial tests are shown in Figure 4.2. The experiment was performed in triplicate with consistent results.

| | **Inoculum Size (Colony Forming Units)** | | | | | | | | |
|---|---|---|---|---|---|---|---|---|---|
| | *Escherichia coli* | | | *Pseudomonas aeruginosa* | | | *Staphylococcus aureus* | | |
| Silver nanopowder load/plate (µg/mL) | **$10^2$** | **$10^3$** | **$10^4$** | **$10^2$** | **$10^3$** | **$10^4$** | **$10^2$** | **$10^3$** | **$10^4$** |
| **Control (0)** | +++ | +++ | +++ | +++ | +++ | +++ | +++ | +++ | +++ |
| **10** | + | ++ | +++ | + | + | ++ | ++ | +++ | +++ |
| **50** | - | - | - | - | - | - | + | +++ | +++ |
| **100** | - | - | - | - | - | - | - | ++ | +++ |
| **200** | - | - | - | - | - | - | - | + | + |
| **500** | - | - | - | - | - | - | - | - | - |

**Table 4.1. The anti-bacterial efficacy of the gas plasma-synthesised silver nanoparticles was tested in solid, modified-LB medium against three species of bacteria; *E. coli*, *P. aeruginosa* and *S. aureus.* After 48 hours at 37°C the medium was observed for signs of colony formation; either showing colony numbers that were equivalent to the control (+++), less than the control (++), almost completely inhibited (one or two colonies) (+), or none (-). N=3.**

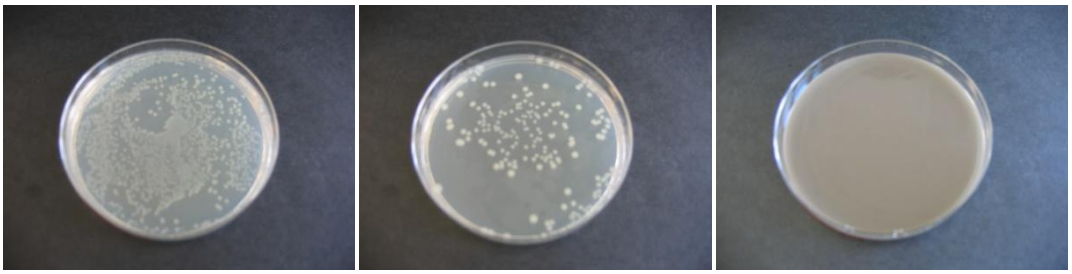

(A) *E. coli* Control, $10^3$ CFU

(B) *E. coli* 10 µg/mL, $10^3$ CFU

(C) *E. coli* 50 µg/mL, $10^3$ CFU

**Figure 4.2. An example of modified-LB agar containing silver nanoparticles. Approximately 1,000 colony forming units (CFU) of *E. coli* were spread onto plates containing no silver (A), 10 µg/mL silver nanoparticles (B) or 50 µg/mL silver nanoparticles (C). The medium was incubated at 37 °C for 48 hours.**

### 4.2.2. Silver Nanoparticle Interactions with the *E. coli* Cell Envelope

Scanning electron micrographs were prepared for *E. coli* treated with silver nanoparticles in modified-LB medium. During this procedure the bacteria were washed by sequential sedimentation and re-suspension in sterile medium, phosphate buffer, and various fixatives and staining solutions. This clearly removed unbound silver nanoparticles which remained in the supernatant, and the cell pellets which were initially coloured dark grey by the nanoparticles became a similar colour to the controls (without silver). SEM images, Figure 4.3, show agglomerates of material bound to the *E. coli*. Elemental analysis by EDAX, Table 4.2, confirmed that the agglomerates contained more than 70% silver, indicating that these were primarily formed from the silver nanoparticles.

Greater detail was achieved in transmission electron micrographs, using the same experimental conditions as for SEM. TEM images show small clusters (two or three nanoparticles) and individual silver nanoparticles attached to the *E. coli* double envelope, Figure 4.4. Some of the nanoparticles appeared within the periphery of the cell, on the left and right of the image, but proximal to the cell wall, and do not appear at the cell interior. Silver nanoparticles are also located distal from the cell. However, most of the detached nanoparticles were scattered in the same orientation with respect to the nearest bacterium, thus may have been moved by the sectioning knife.

**Figure 4.3. Scanning electron micrograph of *E. coli* (A), and *E. coli* after treatment with silver nanoparticles (B) in modified-LB.**

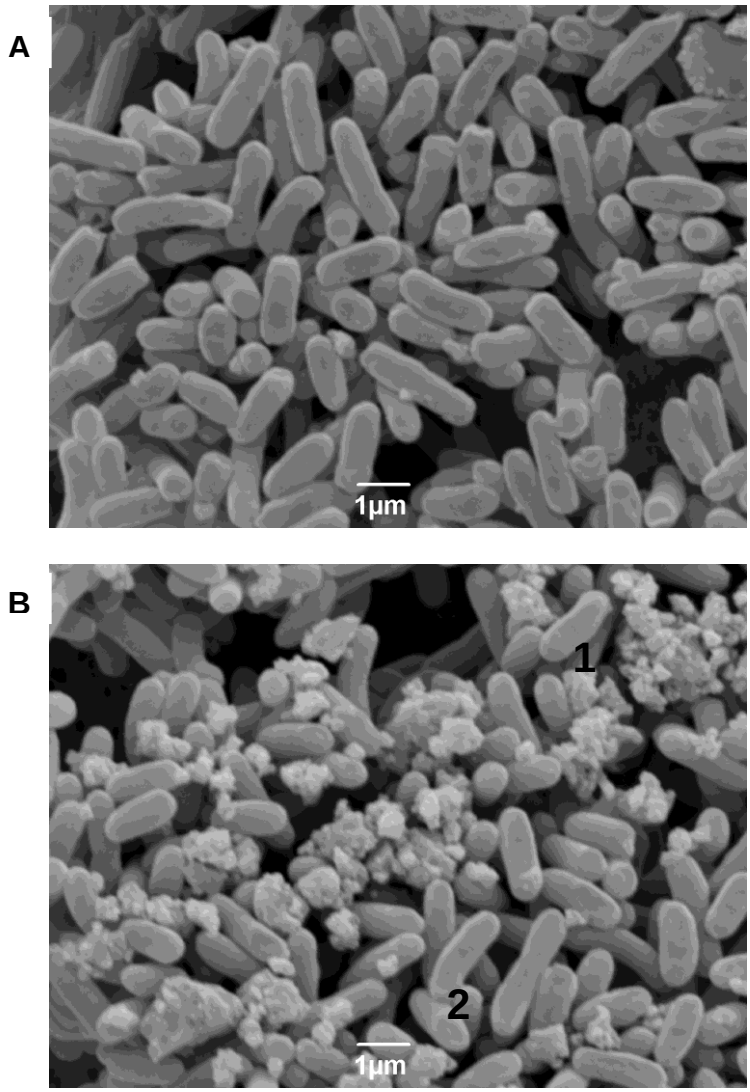


**Table 4.2. Elemental analysis by EDAX indicates that the agglomerates of material in association with the bacteria are mostly silver nanoparticles.**

| | Element (% weight) | | | | | | | | |
|---|---|---|---|---|---|---|---|---|---|
| Area | **C** | **O** | **Na** | **Si** | **Cl** | **K** | **Ag** | **Os** | **Total** |
| 1 | 9.79 | 7.92 | - | - | 2.99 | - | 70.87 | 8.43 | 100 |
| 2 | 53.23 | 25.65 | 1.58 | 1.47 | - | 0.69 | 2.39 | 14.99 | 100 |

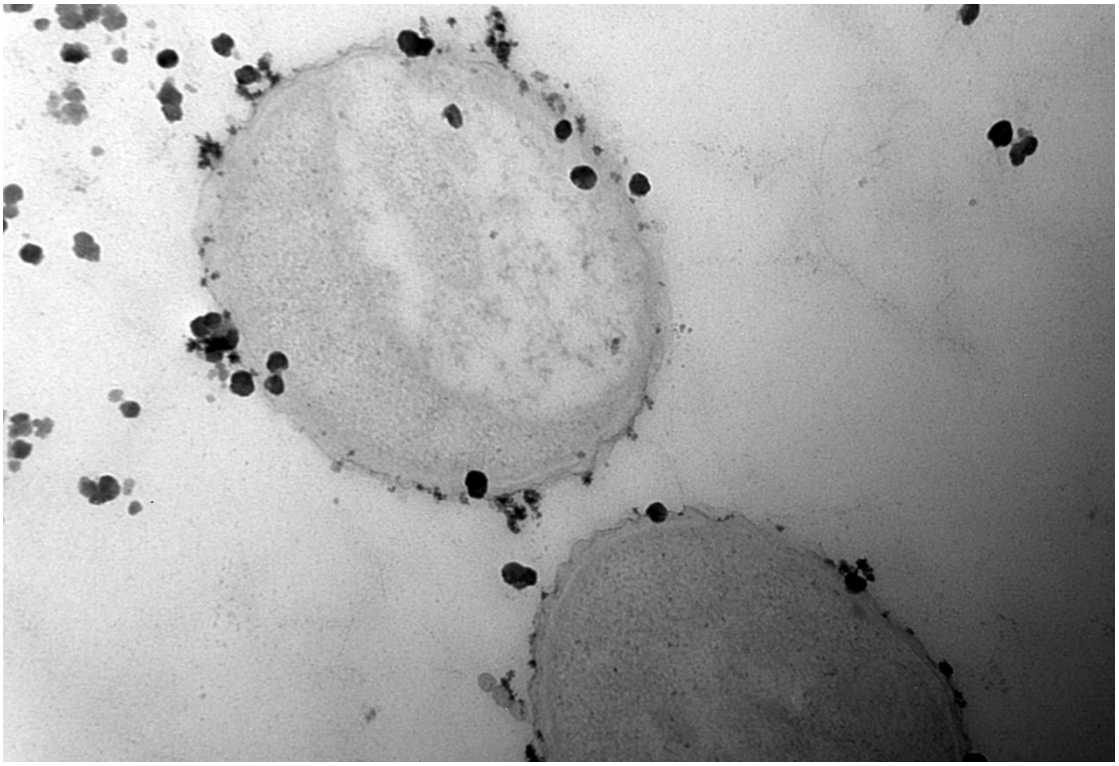

**Figure 4.4. Transmission electron micrograph of thin (~80 nm) sections of *E. coli*, which had been treated with silver nanoparticles in modified-LB medium for 30 minutes at 37$^{o}$C.**

### 4.2.3. Silver Nanoparticle Dissolution in Modified-LB Medium

The rate of dissolution of the silver nanoparticles in modified-LB medium was measured using Inductively Coupled Plasma Mass Spectrometry (ICP-MS). Measurements were made from a colloidal suspension of the silver nanoparticles at a concentration of 100 µg/mL, in 100 mL of modified-LB medium and whilst the medium was shaking at 37$^{o}$C. At time points a sample of the medium was purged of non-dissolved silver by ultracentrifugation and quantitative measurements of the bulk solution Ag were made by ICP-MS, detecting both isotopes $^{107}$Ag and $^{109}$Ag, and using $^{103}$Rh for internal calibration. The measurements made using both isotopes were consistent within experimental error and only results obtained for the most abundant isotope, $^{109}$Ag, are reported, Figure 4.5.

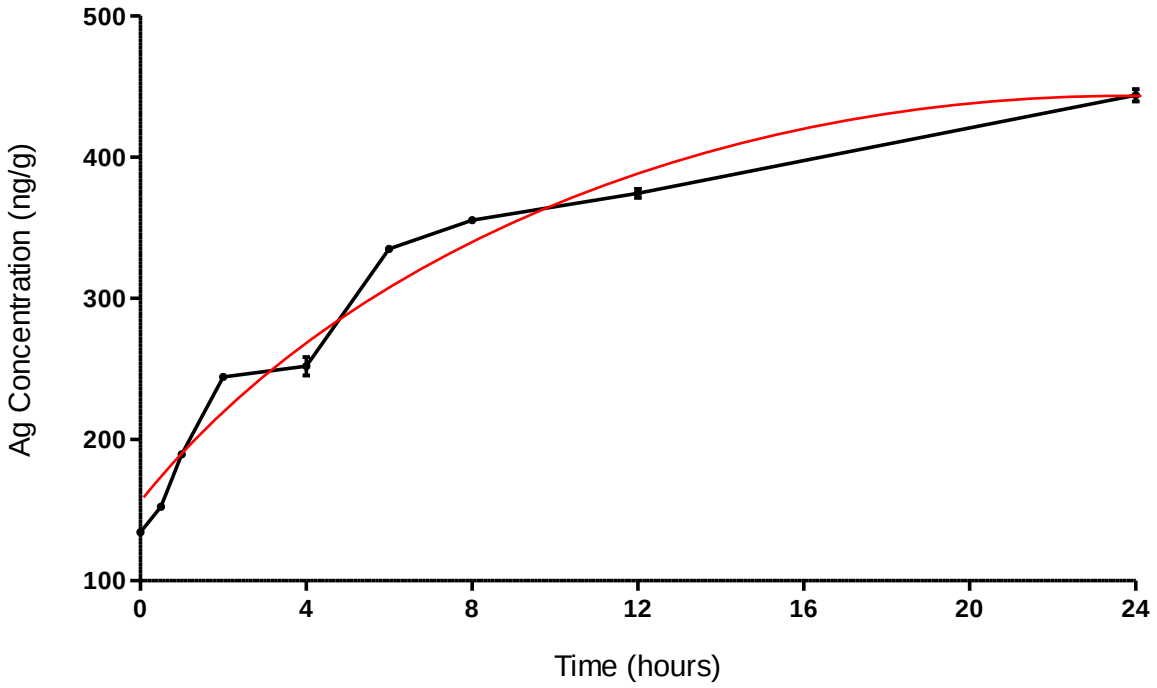


**Figure 4.5. The rate of silver nanoparticle dissolution in modified-LB medium. The fitted line is a theoretical fit of the data, assuming that the rate of nanoparticle dissolution is linearly related to nanoparticle surface area (see text). The error bars are the relative standard deviation (RSD) for 3 replicate samples, each measured at least 5 times by ICP-MS.**

The background concentration of silver in the modified-LB medium was 19.54 ± 0.07 ng/g and increased to 134.49 ± 0.46 ng/g as the nanoparticles were dispersed by sonication for 30 minutes. The concentration of silver in the supernatants – representing the bulk solution phase silver concentration in the medium - follows an asymptotic trend. This represents nanoparticle dissolution and thus release of $Ag^{+}$. Replicate suspensions of the silver nanoparticles dissolved at the same rate. The relative standard deviation (RSD) for the silver concentration in 3 suspensions of silver nanoparticles, prepared on different days, was 1.26%.

The fitted line on Figure 4.5 is a theoretical fit of the data that assumes the rate of dissolution is linearly related to particle surface area, Equation (1).

$$\frac{d[Ag^+]}{dt} = k\,4\pi r^2$$

*Equation (1)*

This simple, first-order equation was integrated analytically to give the $Ag^+$ concentration as a function of time, Equation (2).

$$[Ag^+](t) = -\frac{4}{3}\pi\rho N_p r_0^3\left[\left(1-\frac{t}{t_{diss}}\right)^3 - 1\right]$$

*Equation (2)*

where $\rho$ is the bulk density of silver, 10.5 g/cm$^{-3}$ which is assumed to be in the same in the nanoparticle, $r_0$ is the initial radius of the particle, 142 nm, $N_p$ is the particle density, and $t_{d\text{-}iss}$ is the time to complete dissolution of the particle: $t_{diss} = r_0/k$, where $k$ is the first order rate constant with units nm/s. Fitting the data gives $t_{diss}$ = 23.4 (± 3.3) hrs, $k$ = 3.0 (± 0.4) nm/hr (assuming $r_0$ = 142 nm) which corresponds to 1% of the surface atoms per second entering the bulk solution phase.

### 4.2.4. The Differential Efficacy of Silver Nanoparticles and Silver Ions

*E. coli* were cultured in modified-LB medium, at 37$^o$C, until late-exponential phase. The bacteria were diluted 1:100 in sterile medium containing either a suspension of silver nanoparticles or silver nitrate. The silver nanoparticle concentration was 100 µg/mL,

consistent with the measurements made for nanoparticle dissolution. To the silver ion-treated culture, additional silver nitrate was added every hour at a rate consistent with the measured rate of nanoparticle dissolution. The silver nanoparticles were observed to have a greater anti-bacterial efficacy in three replicate experiments, even though the measured bulk solution phase concentration of silver ions was the same, Figure 4.6.

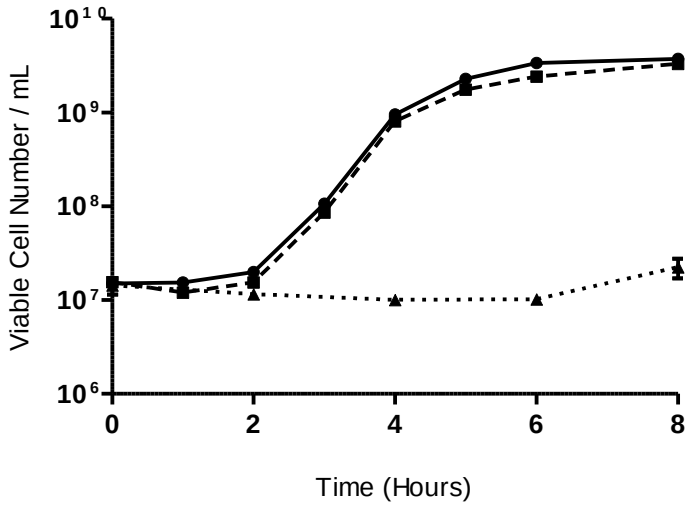


**Figure 4.6. Differential anti-bacterial efficacy of silver nanoparticles and silver ions, as a function of silver ion concentration in the bulk solution phase. An *E. coli* culture was treated with silver nanoparticles (dotted line, ▲) or silver ions (dashed line, ■), which were added to the culture at a rate to mimic the nanoparticle dissolution. Bacterial replication was measured by colony forming units, and compared to an untreated control (solid line, ●). Error bars are too small to be seen for most data points but where visible they show the standard error of the mean (n=3).**

Silver nanoparticles exhibited bacteriostatic activity in modified-LB for at least 6 hours, after which the bacterial CFU count increased. At higher concentration, 1 mg/mL, the silver nanoparticles caused cell numbers to decline, but a sub-population of the cells remained in a quiescent state for several hours and then began replicating. This was also observed in cultures that were treated with 8 µg/mL of silver ions as the nitrate, Figure 4.7.

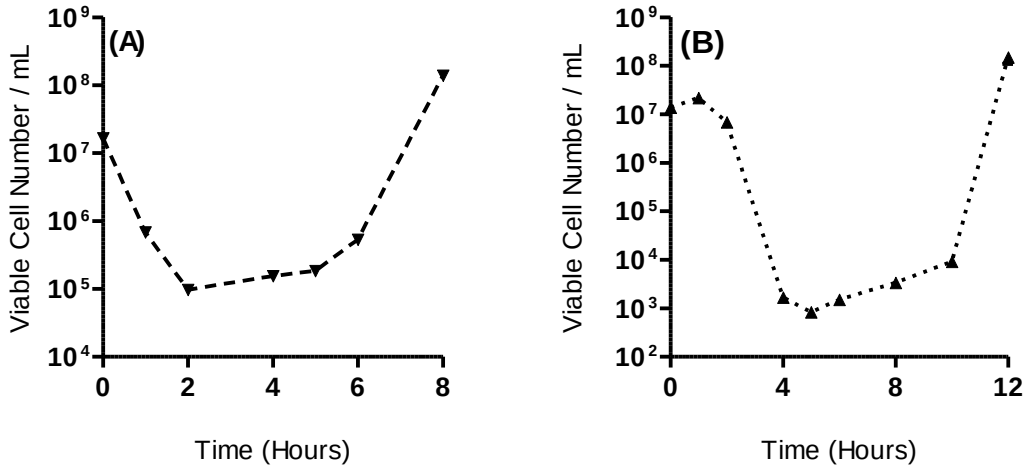


**Figure 4.7. Decline and recovery of viable cell numbers in modified-LB medium containing silver ions (A) and silver nanoparticles (B).**

### 4.2.5. The Transcriptional Response to Silver

The silver nanoparticles had a notable, enhanced activity against *E. coli* compared to silver ions as a function of bulk solution phase silver ion concentration. To explain this, the hypothesis was that the bioavailability of silver ions might be greater if delivered to the bacteria from nanoparticles dissolving adjacent to the cell surface, as supported by observations in electron micrographs (Figure 4.3 and Figure 4.4). To test this, a genetic response to the presence of silver ions was determined quantitatively in *E. coli* that had been treated with either silver nanoparticles or silver nitrate. As previously, the bulk solution phase silver ion concentration was made equivalent in silver nanoparticle and silver nitrate treated cultures. However, to avoid any changes in gene expression that might occur due to a change in growth rate the inoculum size was increased so that the silver concentration was sub-inhibitory. Therefore differences in the level of gene expression reflect the concentration of bio-available silver ions that interact with gene regulatory proteins.

To measure the genetic response, an exponentially replicating culture of *E. coli* was mixed (1:1, vol/vol) with sterile growth medium containing silver nanoparticles or silver ions (with a bulk solution phase concentration in each medium of 280 ng/mL) and after 10 minutes of exposure the total RNA was isolated. The silver nanoparticles could not be separated from the bacteria during this procedure. However, there was no evidence that their presence changed the efficiency of RNA isolation based upon final yield or the integrity of the RNA product (data not shown). The transcriptional response to silver was measured using real-time PCR and primer sequences that were specific for a panel of genes shown in Table 4.3 and Figure 4.8.

**Table 4.3. The Gene Panel.**

| Gene | Protein Function | [1]Mutant Sensitivity | Reference |
|---|---|---|---|
| *copA* | Cu+ efflux; responds to $Ag^+$ | Cu | [37, 41] |
| *cueO* | Cuprous oxidase; responds to $Ag^+$ | Cu | |
| *cusA* | Cu+/Ag+ ion efflux | Ag | [35, 36] |
| *cusR* | Regulator for *cusA* | Ag | |
| *ompC* | Outer membrane pores; associated with $Ag^+$ resistance | - | [49] |
| *ompF* | | - | |
| [2]*zntA* | P-Type ATPase; $Zn^{2+}$ efflux | Zn | [46, 47] |

**[1]Gene deletions were prepared in this study and metal ion sensitivity was measured by 2-fold, serial dilution MIC assay (see text). [2]The *zntA* gene is expressed in response to excess $Zn^{2+}$ and $Cd^{2+}$ ions, not $Ag^+$, and was used as a control.**

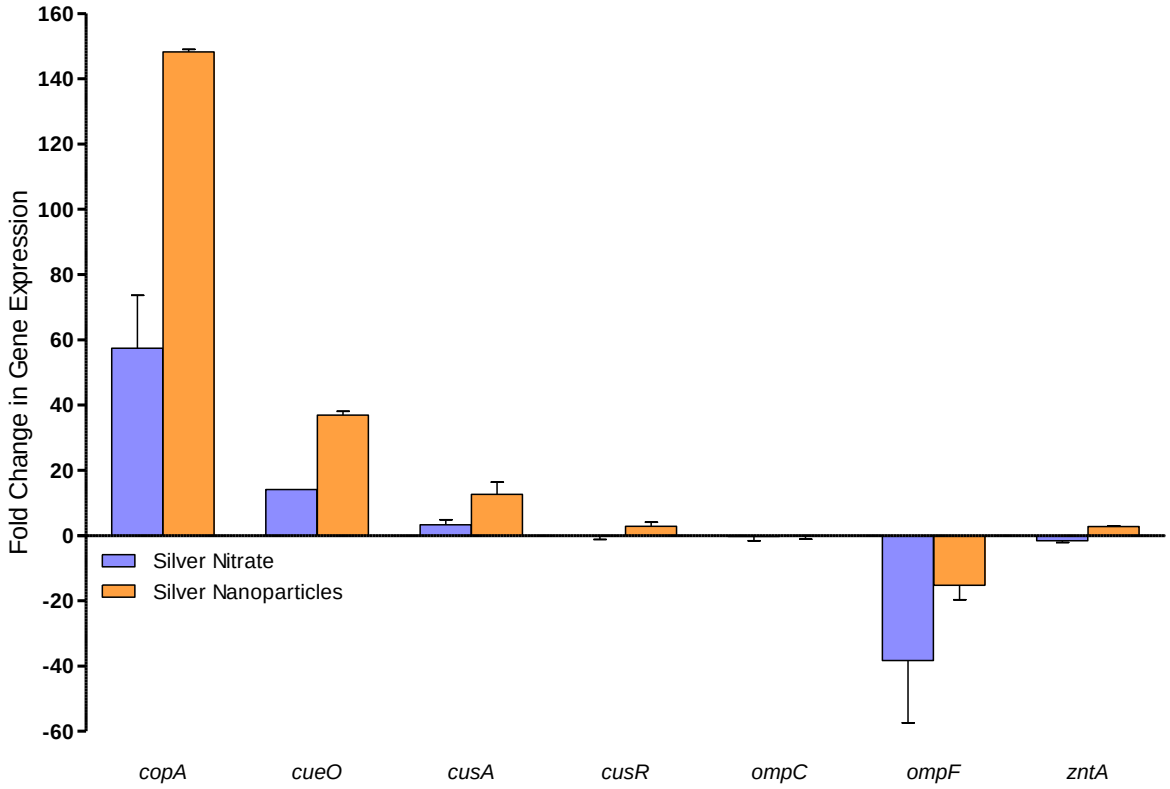


**Figure 4.8. Real-Time PCR data for transcription of the gene panel in response to silver, after exposure for 10 minutes at 37°C. Fold change in gene expression is relative to an untreated control. The silver nanoparticle concentration was 400 µg/mL, and the silver ion concentration was 280 ng/mL, which was equivalent to the predicted nanoparticle-associated silver ion concentration after 10 minutes of dissolution. Gene expression was normalized against two internal reference genes, *rrsB* and *gapA*. The error bars are the standard error of the mean (n=2)**

Three genes, *copA*, *cueO* and *cusA* were up-regulated by silver nanoparticles compared to silver ions, as a function of the measured bulk solution phase silver ion concentration. The greatest difference was for *copA*; up-regulated 2.6-fold higher for silver nanoparticles compared to silver nitrate, 148.3-fold compared to the control (no silver). The differences in gene expression occurred even though the bulk solution phase silver ion concentration was equivalent for each culture. Contrarily, the *ompF* gene was down-regulated to a greater extent by silver nitrate than by silver nanoparticles. This was a 2.5-fold difference, 38.3-fold down-regulated compared to the control. In contrast the expression level of *cusR* and *ompC* showed no response to silver. The *zntA* gene, also

showing no response, is regulated specifically by divalent metal ions ($Zn^{2+}$, $Cd^{2+}$ and $Pb^{2+}$) [46]. Therefore the expression of this gene was expected not to change. Gene expression was normalised using two independent internal reference genes: *rrsB*, encoding the 16s ribosomal RNA, and *gapA*, encoding glyceraldehyde-3-phosphate dehydrogenase, which gave consistent results. These were validated from whole genome microarray data, as in Chapter 5, where their transcription did not significantly alter in response to silver.

The genes used to measure the $Ag^{+}$ response were deleted from strain MG1655 to generate a series of deletion mutants and metal tolerances were tested in a 2-fold, serial dilution MIC assay. Although *copA* and *cueO* were up-regulated in silver treated bacteria, the mutant strains, Δ*copA* and Δ*cueO*, were not found to be sensitive to silver ions. Conversely both strains were demonstrably sensitive to copper ions. The Δ*cusA* and Δ*cusR mutants* were mildly sensitive to silver ions, but not copper ions. None of the mutant strains were found to be sensitive to zinc ions, except the *ΔzntA* mutant. All the strains grew at the same rate in modified-LB indicating that the differences were not due to a general defect in growth. The MIC values are given in Table 4.4.

**Table 4.4. MICs of $Ag^{+}$, $Cu^{+}$ and $Zn^{2+}$ for *E. coli* deletion mutants.**

| | MIC | | |
|---|---|---|---|
| **Strain** | $Ag^{+}$ | $Cu^{+}$ | $Zn^{2+}$ |
| MG1655 | 8 ug/mL | 256 ug/mL | 256 ug/mL |
| MG1655 Δ*copA* | 8 ug/mL | 128 ug/mL | 256 ug/mL |
| MG1655 Δ*cueO* | 8 ug/mL | 128 ug/mL | 256 ug/mL |
| MG1655 Δ*cusA* | 7 ug/mL | 256 ug/mL | 256 ug/mL |
| MG1655 Δ*cusR* | 7 ug/mL | 256 ug/mL | 256 ug/mL |
| MG1655 Δ*cusF* | 7 ug/mL | 256 ug/mL | 256 ug/mL |

## 4.3. Discussion

### 4.3.1. Nanoparticle Characterisation

The silver nanoparticles had an approximately spherical morphology with irregular, high energy surfaces, Figure 4.1. They were synthesised with no surface ligand and therefore had a poor colloidal stability and ill defined size and shape, as is characteristic of gas phase nanoparticle synthesis routes [50]. In contrast, silver nanoparticles synthesised by wet-chemical methods, including those described in Chapter 3, are relatively mono-disperse and have a reduced rate of agglomeration, and are stable in a colloidal suspension. However, a chemical synthesis approach yielded very small quantities of the nano-material and therefore this approach for anti-bacterial research may be limited. In comparison, the gas phase synthesis route can be tailored to produce gram amounts of nano-material, and, excluding equipment costs, is relatively inexpensive per unit mass of product [50].

Without a capping ligand the stability of the nanoparticles in various bacteriological media was an important consideration. Aggregated nanoparticles have a relatively small surface area, extending to low activity. The silver nanopowder had a BET isotherm specific surface area of 4 ± 1 $m^2$/g. However, the active surface area from which silver ions are released is dependent upon how the nanoparticles are kept disperse in the medium. For example, in a high ionic strength solution, Phosphate Buffered Saline (PBS) or a minimal salts culture medium, the silver nanoparticles were dispersed by the mechanical work that was added to the system by the sonicator. When this energy source was removed, in the absence of any stabilising surface ligand, the nanoparticles formed flocculates with no detectable anti-bacterial activity (data not shown). In contrast, in a nutrient medium the nanoparticles formed a visibly homogeneous suspension. However, flocculates of

agglomerated nanoparticles were not visible after 8 hours indicating that the nanoparticles were colloidal for this length of time.

The nanoparticle stability in modified-LB medium may be explained by the presence of various short chain polypeptides which adsorb to the silver surface and stabilise the nanoparticles by steric factors. The association of protein with nanoparticle surfaces, specifically silver, has been reported and has been described as a protein corona [51-53]. This interaction may be similar to that between the silver or gold nanoparticles and Bovine Serum Albumin protein (BSA) in Chapter 3. The BSA molecules interact with nanoparticle surfaces, judging by changes to the particle plasmon resonance, and make colloidal nanoparticles stable in physiological concentrations of sodium ions. In a minimal salts medium containing BSA the silver nanoparticles did not flocculate, but had no observed anti-bacterial activity (data not shown). This can be explained because the relatively large BSA molecules (14 x 4 x 4 nm, 66 kDa), compared to the short chain peptides in the modified-LB, may restrict the path of nanoparticle surface atoms into the bulk solution phase. Therefore, this may reduce the rate of dissolution, and dissolved silver may be sequestered as it may react with up to 35 cysteine residues on the protein [54].

### 4.3.2. Bacterial-Nanoparticle Interactions

The silver nanoparticles were allowed to interact with *E. coli* bacteria in the modified-LB medium, and then the bacteria were washed by sequential sedimentation and re-suspension in sterile medium, then PBS, and then various fixative and staining solutions. Unbound or loosely associated nanomaterial was removed from the bacteria. During the process of sample preparation for scanning electron microscopy the nanoparticles formed into agglomerates of various sizes and the images did not show the expected interaction of individual, primary nanoparticles with the bacteria, as reported in

various other studies [14, 16, 55, 56]. In contrast, thin bacterial sections, shown in TEM images, provided evidence that the primary nanoparticles made close associations with sites on the bacterial surface and large agglomerates of nanomaterial may have been removed by washing.

Unexpectedly, some of the silver nanoparticles in TEM images appeared to be integral with the cell envelope and cytosol. Internalisation of silver nanoparticles into *E. coli* has been reported [14, 16, 56], but without a clear mechanism for how they might move across the double membrane and sacculus. The hypothesis, as in Chapter 3, is that the silver nanoparticles cause considerable damage to the cell envelope through the activity of the silver ion on membrane proteins. Hence, silver nanoparticles might enter the cell by diffusion where the integrity of the cell wall is reduced. However, the cell envelope was circumferential in the TEM images and there was no evidence of electron dense 'pits', representing sites of damage in the cell wall, which have been reported for silver nanoparticle treated *E. coli* elsewhere [16]. The 2-dimensional images are limited and cannot confirm that the entire specimen was intact. The thin section of the cell wall appeared to be circumferential, but may have been damaged and discontinuous, thus allowing nanoparticles to enter by simple diffusion, at a site out of the field of view. Further, the nanoparticles may not be inside the bacterium, but above or below the section, as discussed in Chapter 3. If the very terminus of a bacterium were viewed then extracellular nanoparticles on the bacterial surface might appear to be within the cytosol. Further, the nanoparticles could have been moved by the sectioning knife, and there was evidence for this from the orientation of the nanoparticles that were seen distal to the cells, all of which were scattered in the same direction.

The bacterial-nanoparticle interactions, as observed in TEM images, leads to the hypothesis that dissolution from the attached nanoparticles yields a local concentration of

$Ag^+$, which can react directly with the bacterium at the bacterial-nanoparticle interface. Therefore, the bulk solution phase may contain a low concentration of the dissolved silver, but the anti-bacterial efficacy may be high. To test this, the bulk solution phase concentration of silver was measured, and the anti-bacterial efficacy of the silver concentration was compared with or without the presence of the nanoparticles.

### 4.3.3. Nanoparticle Dissolution

To determine the rate at which the silver nanoparticles contributed silver ions to the bulk solution phase, the total silver concentration in modified-LB medium was measured using ICP-MS after removing colloidal silver nanoparticles by ultracentrifugation. The accuracy of the ICP-MS measurements was critical, allowing a comparison between the implications of $Ag^+$ released from silver nanoparticles and the equivalent concentration of $Ag^+$, as silver nitrate, on *E. coli* K12. ICP-MS was suitable for measuring, accurately, the concentration of silver in the samples. This technique is highly specific and sensitive, able to detect elemental mass as low as parts per trillion [57]. The ICP-MS measurements were performed several times and had a low statistical error, and the dissolution rate was consistent between nanoparticle dispersions produced at different times. Additionally, ICP-MS measurements were made from solutions of known $Ag^+$ concentration. This determined if any silver would be lost during the sample preparation, for example, from silver ions adhering to the sample vessels. Loss of $Ag^+$ was less than 5%; this may have been achieved because the samples, prior to ICP-MS, were always manipulated in polypropylene tubes instead of glass, which has a negative surface charge and attracts cations.

Measuring the dissolved $Ag^+$ in the modified-LB medium involved the sedimentation of the silver nanoparticles by ultracentrifugation. However, it is unlikely that all of the silver

nanoparticles were removed by this process. ICP-MS measurements of total silver do not distinguish between ionic silver and insoluble elemental silver, therefore the reported values may be overestimates. Other methods for separating nanomaterials in solution have been used elsewhere, including ultra-filtration [58] and dialysis [59]. The centrifugation method was preferred because of the lower limit of effective pore diameter for commercially available filter membranes is approximately 100 nm; the silver nanopowder clearly contained nanoparticles smaller than this. Dialysis requires time to achieve equilibrium across the dialysis membrane. Therefore, it is unsuitable for determining silver concentration at specific time points.

The theoretical fit of the ICP-MS data assumes that the rate of dissolution is linearly related to the nanoparticle surface area, equation (1), and dissolved $Ag^+$ concentration as a function of time can be estimated using equation (2). Dissolution rate is a useful toxicology metric for determining the efficacy of silver nanoparticles, and time to dissolution ($t_{diss}$) would constitute an important parameter in assessing the lifetime of a silver nanoparticle-based product. For example, a high dissolution rate will favour anti-microbial activity but at the cost of a short $t_{diss}$, and so a short efficacy period. The frequency of changing silver nanoparticle-coated medical devices, including catheters or wound dressings, may then be tailored accordingly. Silver nanoparticles could inhibit bacterial colonisation and biofilm formation [60], but only for a limited time.

The observed size [5, 15, 56] and shape [14] dependence of silver nanoparticle toxicity can be explained by differences in dissolution rate. For example, truncated triangular shapes with a high atom density {111} facet surface dissolve faster than spherical or rod shapes with mainly {100} facet surfaces, according to the number of surface atoms that can enter the bulk solution phase over a period of time. Therefore, truncated triangles demonstrate a greater activity against *E. coli* than spheres or rods [14,

61]. The silver nanoparticles in this work had approximately spherical, irregular surfaces. Due to the gas-phase synthesis route, involving volatilization and condensation of the bulk material, the nanoparticles probably had rough surfaces, as is characteristic of this technique [50]. This would favour a high rate of dissolution. However over time the nanoparticle surface may become smooth and dissolution rate may decline. This is consistent with the asymptotic trend in the ICP-MS data.

The dissolution rate as a function of nanoparticle concentration was not investigated here. However, it is expected that, during sonication, the dissolution rate may increase proportionately with concentration where there is sufficient mechanical work to inhibit agglomeration. After sonication the dissolution rate is expected to increase with nanoparticle concentration, but the trend may not be linear because of an increased rate of aggregation where there is a greater probability of nanoparticle collisions in the system. Accordingly, the efficacy of a suspension of silver nanoparticles may become limited at higher concentrations.

### 4.3.4. Differential Activity of Silver Nanoparticles and Silver Ions

A hypothesis for silver toxicity is that the anti-bacterial activity is proportional to the rate of release of silver ions [23]. Nanoparticulate silver can interact directly with localised sites on the bacterial surface [14, 16, 56]. This, in theory, results in the release of silver ions directly onto their site of action, and produces a high local $Ag^+$ concentration at the bacterial envelope and an enhanced anti-bacterial activity. Thus the bulk solution phase silver ion concentration may be very low, but the biologically available (bio-available) silver ion concentration, i.e. the local concentration, may be higher.

The silver nanoparticles were bacteriostatic in modified-LB medium at a concentration of 100 µg/mL and an inoculum of $10^7$ colony forming units. Conversely, by

adding $Ag^+$ to an equivalent inoculum of bacteria at the measured rate of silver nanoparticle dissolution the viable cell number increased at a similar rate to the untreated control. Silver nanoparticles had greater toxicity than silver nitrate as a function of the bulk solution phase $Ag^+$ concentration, in keeping with Navarro *et al* [62], who reported an enhanced inhibitory effect of silver nanoparticles compared to silver nitrate on photosynthesis in fresh water algae. Thus, this may be a general phenomenon. These observations may be due to the bacterial-nanoparticle interactions, as observed in TEM images. This bacterial-nanoparticle interaction may produce a high-interfacial concentration of $Ag^+$, and therefore the silver ions may be immediately biologically available. In contrast, silver ions in the bulk solution phase contact the bacterium at a rate that is dependent upon various physical parameters, including the diffusion coefficient of $Ag^+$.

Further investigation into the effects of silver on *E. coli* led to the identification of a decline and recovery trend in the cultures. At a bactericidal dose of silver the colony forming units decline by several orders of magnitude and then recover after several hours, Figure 4.7. Similar trends in bacterial viable cell numbers are observed in cultures that are treated with high doses of antibiotics; a small proportion of the bacteria remains viable and may replenish the population once the antibiotic has been removed; referred to as persister cells [63]. The silver was not removed from these cultures, however over time the silver ion concentration may fall as the ions are sequestered by proteins and other molecules with which they interact. As the silver ion concentration over time was not determined this trend cannot be attributed to a persister cell population, and may reflect the presence of a resistant population instead.

The concentration of biologically available silver in the modified-LB medium was compared for silver nanoparticles and silver ions by measuring the transcriptional

response. Although silver has no known role in metabolism, $Ag^+$ is isoelectronic with $Cu^+$, which is a co-factor in numerous metalloenzymes. Therefore, *E. coli* responds to $Ag^+$ as to $Cu^+$, by up-regulating the expression of genes for the de-toxification and efflux of excess copper ions. Two regulons that control copper ion homeostasis in *E. coli*, CusRS and CueR, were up-regulated after treatment with silver nanoparticles and silver nitrate. However, the level of gene transcription was up to 2.6-fold greater (for *copA*) when the bacteria were exposed to silver nanoparticles. The transcription of *cueO* and *cusA* was also enhanced after treatment with nanoparticles, indicating that the two transcriptional regulators, CusR and CueR were hyper-activated by the nanoparticles, which may dissolve at the cell surface.

The accurate measurement of gene expression was dependant on the correct choice of reference genes in order to normalise differences in the quantity of cDNA template between the control (no silver) and silver-treated samples. Ideally, the expression of the reference genes must not vary under the experimental conditions. Thus, their expression level must not respond to silver. The two reference genes, *rrsB* and *gapA*, and their orthologues in other organisms, are commonly used as references for real-time PCR because they perform essential 'housekeeping' functions within the cell, thus their regulation is usually independent of changes to the ambient conditions. However, their expression must be determined experimentally in order to achieve reliable real-time PCR data. Accordingly, the reference genes show no significant change in expression after exposure to silver nitrate in microarray analysis, as described in Chapter 5, and elsewhere [64]. Thus, they were appropriate genes for the normalisation of real-time PCR data.

It remains unclear whether the copper de-toxification systems in *E. coli* actually confer resistance to $Ag^+$. *E. coli* Δ*copA* and Δ*cueO* were no more sensitive to silver nitrate than the parent strain, but were at least 2-fold more sensitive to copper sulfate, consistent

with Rensing *et al* [41]. Conversely, the *ΔcusA* and Δ*cusR* strains were very mildly more sensitive to silver nitrate, but not copper sulfate. Elsewhere studies indicate that the *cus* locus is important for copper homeostasis, but only under microaerophillic conditions [34], and therefore CusA, an RND family antiporter, may be a dual $Cu^{+}/Ag^{+}$ transporter in *E. coli*. Other RND driven efflux systems in *E. coli* confer multi-drug resistance, including AcrB, which forms a tripartite complex with AcrA and TolC. Similarly, CusA associates with the products of co-operonic genes, *cusB* and *cusC* [65]. A detailed model has been described for substrate transport by AcrAB-TolC; the “peristaltic pump” mechanism [66-68]. However, CusA has 20.5% amino acid identity with AcrA and a wide divergence at conserved substrate binding sites [69]. Thus, transport mechanisms may be largely different. The X-Ray crystal structure of the co-transcribed CusB has been examined [70], but similar data for CusA would be useful for elucidating the ion selection and transport properties of the system and for comparing heavy metal cation transporting RND family members with their multi-drug transporting relatives.

Finally, the outer membrane porin genes, *ompC* and *ompF,* encode mildly cation selective outer membrane diffusion pores. The predicted pore diameters are 1.08 and 1.16 nm respectively, and could easily permit movement of 0.128 nm silver cations down an electrochemical gradient. Thus, the down-regulation of the *ompF* gene in response to silver could constitute a ‘chemiosmotic defence’. The *ompF* and *ompC* genes are inversely regulated [71], thus *ompC* expression was unchanged. The presence of OmpC facilitates the exchange of solutes with the modified-LB medium, thus providing adequate cellular resources to effect a stress response. Surprisingly, silver nitrate treated *E. coli* showed greater repression of *ompF* expression than after exposure to silver nanoparticles. The reasons for this differential regulation are unknown.

### 4.3.5. Conclusions

Silver nanoparticles are a highly effective vector for delivery of silver ions to *E. coli* because they may interact directly with the bacterial surface. This nanoparticle-specific silver ion delivery and associated anti-bacterial action is a novel hypothesis, which has gross implications for the design and development of silver nanoparticle based antimicrobials.

Antimicrobial efficacy is favoured by a high rate of dissolution, but at the expense of a short lifespan. This effective lifespan, which is referred to as the time to dissolution, $t_{diss}$, can be modified to suit specific applications by changing the nanoparticle size, and therefore surface area, and the morphology of the surface.

Surface ligands that advocate a strong microbial interaction will also have a stronger antimicrobial efficacy, so long as the presence of the surface molecule does not drastically hinder the rate of dissolution.

A molecular basis for resistance to $Ag^+$, based upon ion efflux, has been identified in the CusRS regulon. However, if this system is incapacitated by deleting a central gene then the mutant has only a mild hypersensitivity to silver nitrate. This leads to the hypothesis that this system may not be central in defending the metabolism against $Ag^+$. In order to investigate this further the whole transcriptome of *E. coli* was measured in response to silver, either silver ions or silver nanoparticles. This study is presented in Chapter 5.

## 4.4. References


1. Elechiguerra, J.L., et al., *Interaction of silver nanoparticles with HIV-1.* J Nanobiotechnology, 2005. **3**: p. 6.
2. Kim, J.S., et al., *Antimicrobial effects of silver nanoparticles.* Nanomedicine, 2007. **3**(1): p. 95-101.
3. Panácek, A., et al., *Antifungal activity of silver nanoparticles against Candida spp.* Biomaterials, 2009. **30**(31): p. 6333-6340.
4. Wright, J.B., et al., *Efficacy of topical silver against fungal burn wound pathogens.* Am J Infect Control, 1999. **27**(4): p. 344-50.
5. Baker, C., et al., *Synthesis and antibacterial properties of silver nanoparticles.* J Nanosci Nanotechnol, 2005. **5**(2): p. 244-9.
6. Bryaskova, R., et al., *Antibacterial activity of poly(vinyl alcohol)-b-poly(acrylonitrile) based micelles loaded with silver nanoparticles.* J Colloid Interface Sci. **344**(2): p. 424-8.
7. Govindaraju, K., et al., *Extracellular synthesis of silver nanoparticles by a marine alga, Sargassum wightii Grevilli and their antibacterial effects.* J Nanosci Nanotechnol, 2009. **9**(9): p. 5497-501.
8. Jaiswal, S., et al., *Enhancement of the antibacterial properties of silver nanoparticles using beta-cyclodextrin as a capping agent.* Int J Antimicrob Agents, 2010. **36**(3): p. 280-283.
9. Juan, L., et al., *Deposition of silver nanoparticles on titanium surface for antibacterial effect.* Int J Nanomedicine, 2010. **5**: p. 261-7.
10. Krishnaraj, C., et al., *Synthesis of silver nanoparticles using Acalypha indica leaf extracts and its antibacterial activity against water borne pathogens.* Colloids Surf B Biointerfaces, 2010. **76**(1): p. 50-6.
11. Li, W.R., et al., *Antibacterial activity and mechanism of silver nanoparticles on Escherichia coli.* Appl Microbiol Biotechnol, 2010. **85**(4): p. 1115-22.
12. Lok, C.N., et al., *Proteomic analysis of the mode of antibacterial action of silver nanoparticles.* J Proteome Res, 2006. **5**(4): p. 916-24.
13. Lok, C.N., et al., *Silver nanoparticles: partial oxidation and antibacterial activities.* J Biol Inorg Chem, 2007. **12**(4): p. 527-34.
14. Pal, S., Y.K. Tak, and J.M. Song, *Does the antibacterial activity of silver nanoparticles depend on the shape of the nanoparticle? A study of the Gram-negative bacterium Escherichia coli.* Appl Environ Microbiol, 2007. **73**(6): p. 1712-20.

15. Panacek, A., et al., *Silver colloid nanoparticles: synthesis, characterization, and their antibacterial activity.* J Phys Chem B, 2006. **110**(33): p. 16248-53.

16. Sondi, I. and B. Salopek-Sondi, *Silver nanoparticles as antimicrobial agent: a case study on E. coli as a model for Gram-negative bacteria.* J Colloid Interface Sci, 2004. **275**(1): p. 177-82.

17. Syed, M.A., et al., *Antibacterial effects of silver nanoparticles on the bacterial strains isolated from catheterized urinary tract infection cases.* J Biomed Nanotechnol, 2009. **5**(2): p. 209-14.

18. Tripathi, A., et al., *Antibacterial applications of silver nanoparticles synthesized by aqueous extract of Azadirachta indica (Neem) leaves.* J Biomed Nanotechnol, 2009. **5**(1): p. 93-8.

19. Valodkar, M., et al., *Morphology and antibacterial activity of carbohydrate-stabilized silver nanoparticles.* Carbohydr Res, 2010. **345**(12): p. 1767-73.

20. Vaseeharan, B., P. Ramasamy, and J.C. Chen, *Antibacterial activity of silver nanoparticles (AgNps) synthesized by tea leaf extracts against pathogenic Vibrio harveyi and its protective efficacy on juvenile Feneropenaeus indicus.* Lett Appl Microbiol, 2010. **50**(4): p. 352-6.

21. Vasilev, K., et al., *Antibacterial surfaces by adsorptive binding of polyvinyl-sulphonate-stabilized silver nanoparticles.* Nanotechnology, 2010. **21**(21): p. 215102.

22. Wei, D., et al., *The synthesis of chitosan-based silver nanoparticles and their antibacterial activity.* Carbohydr Res, 2009. **344**(17): p. 2375-82.

23. Wijnhoven, S.W.P., et al., *Nano-silver: a review of available data and knowledge gaps in human and environmental risk assessment.* Nanotoxicology, 2009. **3**(2): p. 109 - 138.

24. Clement, J.L. and P.S. Jarrett, *Antibacterial silver.* Met Based Drugs, 1994. **1**(5-6): p. 467-82.

25. Lancashire, J.L., *Comprehensive Coordination Chemistry*. Vol. 5. 1987: Pergamon Press.

26. Rosenkranz, H.S. and H.S. Carr, *Silver sulfadiazine: effect on the growth and metabolism of bacteria.* Antimicrob Agents Chemother, 1972. **2**(5): p. 367-72.

27. Rosenkranz, H.S. and S. Rosenkranz, *Silver sulfadiazine: interaction with isolated deoxyribonucleic acid.* Antimicrob Agents Chemother, 1972. **2**(5): p. 373-83.

28. Singer, B. and H. Fraenkel-Conrat, *Enzyme resistance of complexes with ribonucleic acid with metals.* Biochemistry, 1962. **1**: p. 852-858.

29. Tamane, T. and N. Davidson, *On the complexing of deoxyribonucleic acid by silver (I).* Biochim. Biophy. Acta, 1962. **55**: p. 609-621.

30. Bauman, J.E. and J.C. Wang, *Imidazole Complexes of Nickel(II), Copper(II), Zinc(II), and Silver(I).* Inorganic Chemistry, 1964. **3**(3): p. 368-373.

31. Silver, S. and L. Phung, *A bacterial view of the periodic table: genes and proteins for toxic inorganic ions.* Journal of Industrial Microbiology; Biotechnology, 2005. **32**(11): p. 587-605.

32. Nies, D.H., *Efflux-mediated heavy metal resistance in prokaryotes.* FEMS Microbiol Rev, 2003. **27**(2-3): p. 313-39.

33. Munson, G.P., et al., *Identification of a Copper-Responsive Two-Component System on the Chromosome of Escherichia coli K-12.* J. Bacteriol., 2000. **182**(20): p. 5864-5871.

34. Outten, F.W., et al., *The Independent cue and cus Systems Confer Copper Tolerance during Aerobic and Anaerobic Growth in Escherichia coli.* Journal of Biological Chemistry, 2001. **276**(33): p. 30670-30677.

35. Franke, S., et al., *Molecular analysis of the copper-transporting efflux system CusCFBA of Escherichia coli.* J Bacteriol, 2003. **185**(13): p. 3804-12.

36. Franke, S., G. Grass, and D.H. Nies, *The product of the ybdE gene of the Escherichia coli chromosome is involved in detoxification of silver ions.* Microbiology, 2001. **147**(Pt 4): p. 965-72.

37. Grass, G. and C. Rensing, *Genes Involved in Copper Homeostasis in Escherichia coli.* J. Bacteriol., 2001. **183**(6): p. 2145-2147.

38. Gupta, A., et al., *Diversity of silver resistance genes in IncH incompatibility group plasmids.* Microbiology, 2001. **147**(12): p. 3393-3402.

39. Lok, C.N., et al., *Proteomic identification of the Cus system as a major determinant of constitutive Escherichia coli silver resistance of chromosomal origin.* J Proteome Res, 2008. **7**(6): p. 2351-6.

40. Stoyanov, J.V., J.L. Hobman, and N.L. Brown, *CueR (YbbI) of Escherichia coli is a MerR family regulator controlling expression of the copper exporter CopA.* Molecular Microbiology, 2001. **39**(2): p. 502-512.

41. Rensing, C., et al., *CopA: An Escherichia coli Cu(I)-translocating P-type ATPase.* Proceedings of the National Academy of Sciences of the United States of America, 2000. **97**(2): p. 652-656.

42. Grass, G. and C. Rensing, *CueO Is a Multi-copper Oxidase That Confers Copper Tolerance in Escherichia coli.* Biochemical and Biophysical Research Communications, 2001. **286**(5): p. 902-908.

43. Beinert, H., *A quarter-century Biochemistry of copper with Bill Blumberg.* BioMetals, 1990. **3**(2): p. 61-63.

44. Linder, M.C. and M. Hazegh-Azam, *Copper biochemistry and molecular biology.* The American Journal of Clinical Nutrition, 1996. **63**(5): p. 797S-811S.

45. Shannon, R.D., *Revised effective ionic radii and systematic studies of interatomic distances in halides and chalcogenides.* Acta Crystallographica Section A, 1976. **32**(5): p. 751-767.

46. Rensing, C., B. Mitra, and B.P. Rosen, *The zntA gene of Escherichia coli encodes a Zn(II)-translocating P-type ATPase.* Proceedings of the National Academy of Sciences of the United States of America, 1997. **94**(26): p. 14326-14331.

47. Yamamoto, K. and A. Ishihama, *Transcriptional Response of Escherichia coli to External Zinc.* J. Bacteriol., 2005. **187**(18): p. 6333-6340.

48. Li, X.Z., H. Nikaido, and K.E. Williams, *Silver-resistant mutants of Escherichia coli display active efflux of $Ag^+$ and are deficient in porins.* J Bacteriol, 1997. **179**(19): p. 6127-32.

49. Nikaido, H., *Microdermatology: cell surface in the interaction of microbes with the external world.* J Bacteriol, 1999. **181**(1): p. 4-8.

50. Reip, P., *Personal Communication*. 2009.

51. Casals, E., et al., *Time Evolution of the Nanoparticle Protein Corona.* ACS Nano, 2010. **4**(7): p. 3623-3632.

52. Cedervall, T., et al., *Understanding the nanoparticle protein corona using methods to quantify exchange rates and affinities of proteins for nanoparticles.* Proceedings of the National Academy of Sciences, 2007. **104**(7): p. 2050-2055.

53. Lundqvist, M., et al., *Nanoparticle size and surface properties determine the protein corona with possible implications for biological impacts.* Proceedings of the National Academy of Sciences, 2008. **105**(38): p. 14265-14270.

54. Brown, J.R., *Structural origins of mammalian albumin.* Fed Proc, 1976. **35**(10): p. 2141-4.

55. Dror-Ehre, A., et al., *Silver nanoparticle-E. coli colloidal interaction in water and effect on E. coli survival.* J Colloid Interface Sci, 2009. **339**(2): p. 521-6.

56. Jose Ruben, M. and et al., *The bactericidal effect of silver nanoparticles.* Nanotechnology, 2005. **16**(10): p. 2346.

57. Thomas, R., *Practical guide to ICP-MS*. 2004: Marcel Dekker.

58. Miao, A.J., et al., *Zinc oxide engineered nanoparticles: Dissolution and toxicity to marine phytoplankton.* Environmental Toxicology and Chemistry, 2010. **29**(12): p. 2814-2822.

59. Franklin, N.M., et al., *Comparative Toxicity of Nanoparticulate ZnO, Bulk ZnO, and ZnCl2 to a Freshwater Microalga (Pseudokirchneriella subcapitata): The Importance of Particle Solubility.* Environmental Science & Technology, 2007. **41**(24): p. 8484-8490.

60. Steven, L.P., G.B. Phillip, and D. Jayne, *Antimicrobial activity of silver-containing dressings on wound microorganisms using an in vitro biofilm model.* International Wound Journal, 2007. **4**(2): p. 186-191.

61. Hatchett, D.W. and H.S. White, *Electrochemistry of Sulfur Adlayers on the Low-Index Faces of Silver.* The Journal of Physical Chemistry, 1996. **100**(23): p. 9854-9859.

62. Navarro, E., et al., *Toxicity of Silver Nanoparticles to Chlamydomonas reinhardtii.* Environmental Science & Technology, 2008. **42**(23): p. 8959-8964.

63. Keren, I., et al., *Persister cells and tolerance to antimicrobials.* FEMS Microbiol Lett, 2004. **230**(1): p. 13-8.

64. Wu, M., Oerther, D., B., *Using Genomics to Understand Disinfection with Silver.* Proceedings of the Water Environment Federation, 2006. **2006**: p. 1285-1293.

65. Blair, J.M. and L.J. Piddock, *Structure, function and inhibition of RND efflux pumps in Gram-negative bacteria: an update.* Curr Opin Microbiol, 2009. **12**(5): p. 512-9.

66. Murakami, S., et al., *Crystal structures of a multidrug transporter reveal a functionally rotating mechanism.* Nature, 2006. **443**(7108): p. 173-179.

67. Seeger, M.A., et al., *The AcrB efflux pump: conformational cycling and peristalsis lead to multidrug resistance.* Curr Drug Targets, 2008. **9**(9): p. 729-49.

68. Seeger, M.A., et al., *Structural Asymmetry of AcrB Trimer Suggests a Peristaltic Pump Mechanism.* Science, 2006. **313**(5791): p. 1295-1298.

69. Yu, E.W., J.R. Aires, and H. Nikaido, *AcrB multidrug efflux pump of Escherichia coli: composite substrate-binding cavity of exceptional flexibility generates its extremely wide substrate specificity.* J Bacteriol, 2003. **185**(19): p. 5657-64.

70. Xu, Y., et al., *Crystallization and preliminary X-ray crystallographic analysis of Escherichia coli CusB.* Acta Crystallographica Section F, 2009. **65**(7): p. 743-745.

71. Forst, S., J. Delgado, and M. Inouye, *Phosphorylation of OmpR by the osmosensor EnvZ modulates expression of the ompF and ompC genes in Escherichia coli.* Proceedings of the National Academy of Sciences of the United States of America, 1989. **86**(16): p. 6052-6056.

# Chapter 5: The *E. coli* K12 Transcriptome Response to Silver

## 5.1 Introduction

The complete genome sequence of *E. coli* K12, strain MG1655, was first published by Frederick Blattner and co-workers in 1997 [1], 3 years before completion of the human genome [2]. The data from sequencing projects on *E. coli* strains [3-4] enables high throughput analysis of gene expression in this organism using DNA microarray technology, which was first reported by Schena and co-workers in 1995 [5]. *E. coli* lends itself to functional genomics investigations due to the plethora of bioinformatics tools available to the research community, and the high level of annotation available on the genome sequence. This facilitates the extraction of biological information from large quantities of gene expression data, and accurate interpretation of functional genomics experiments.

In Chapter 4, real-time PCR data indicated that *E. coli* produces a transcriptional response to silver that involves the expression of genes for copper homeostasis. This can be explained because the $Ag^+$ and $Cu^+$ ions are isoelectronic. Therefore $Ag^+$ may interact with $Cu^+$-sensing proteins and simulate an excess of free $Cu^+$. It was also found that $Ag^+$ led to the repression of the constitutive outer membrane porin gene, *ompF.* However, the total transcriptional response to silver is likely to be far greater than can be appreciated from the limited gene panel that was tested. The affinity of $Ag^+$ for all sulfur-containing molecules in the cell, including any protein containing cysteine residues or containing iron-sulfur (FeS) clusters, leads to the hypothesis that the toxic effects are pan-metabolism. Accordingly, the hypothetical whole transcriptome response is a large transcriptional shift that reflects the regulation of diverse biological processes for homeostasis.

The objective of the work presented in this chapter is to test the early time (10 minute) whole transcriptome response to silver in *E. coli* K12, using gene expression

microarrays. The silver was added to bacterial cultures as silver ions, from silver nitrate, or as silver nanoparticles, which release silver ions through dissolution. Presently, it is unclear whether the differential silver ion delivery mechanism from a nanoparticle will elicit a different genetic response. However, it was demonstrated in Chapter 4 that the mode of ion delivery has a considerable effect on the anti-bacterial efficacy. Qualitative differences in the transcriptome after exposure to silver nitrate or silver nanoparticles can be established by comparing the two microarray data sets.

An earlier effort to determine the whole transcriptome response to silver nitrate in *E. coli* was published in 2006 [6]. However, the data was largely inconsistent with work elsewhere. For example, the genes for copper homeostasis, which are known to respond to $Ag^+$ [7-10], were not expressed under the experimental conditions. This is acknowledged by the authors but not explained. It is likely that the experimental design did not allow the full silver transcriptional response to be captured because the gene expression was measured from *E. coli* after recovery from a bacteriostatic concentration of silver nitrate. This prevented the cultures from growing for approximately 5 hours at which point the transcriptional response may have become attenuated as the bacteria entered a phase of exponential growth. The early time response to silver ‘shock’, as measured in this study, has not been reported previously. Clearly, this constitutes an important data set for understanding disinfection with silver because the early changes to the gene expression profile may indicate which biological processes are important for defending the metabolism against $Ag^+$.

The action of $Ag^+$ on the cell through reaction with sulfur-containing proteins is likely to emulate the action of the cadmium ion, $Cd^{2+}$, which has a similar affinity for sulfur [11]. Cadmium stress leads to the regulation of genes that control sulfur metabolism for the synthesis of cysteine, and for the construction of FeS clusters [12]. This may replenish

damaged cellular stocks. Furthermore, cadmium induces the expression of genes for the disaggregation and proteolysis of unfolded proteins; probably a consequence of the action of $Cd^{2+}$ on di-sulfide bridges between adjacent cysteine residues leading to a loss of protein tertiary structure. Overall, the response to cadmium stress in *E. coli* K12 involved the regulation of at least 124 genes. The transcriptional response to silver stress may therefore be of a similar magnitude and involve the regulation of similar biological processes.

The National Centre for Biotechnology Information (NCBI) maintains a database of microarray experimental data, the Gene Expression Omnibus (GEO) [13-14], and it is an additional objective of this study to submit the data set to the GEO database in accordance with the Minimal Information about a Microarray Experiment (MIAME) regulations. To date 151 GEO accessions exist for *E. coli* K12, and 43 are specific for MG1655. However, no accessions for the bacterial response to silver shock appear in the GEO database. Somewhat similar work was a study of the whole transcriptome response of human T-cells to $Ag^{+}$ and Ag nanoparticles (GEO accession GSE20692, unpublished), and the *E. coli* whole transcriptome response to $Cu^{+}$, which is isoelectronic with $Ag^{+}$ (GEO accession GSE1780) [15].

## 5.2. Results

### 5.2.1. *E. coli* culture

*E. coli* K12 (MG1655) was cultured in a modified-LB medium (LB without sodium chloride), aerobically at 37$^{o}$C. When the bacteria were replicating at an exponential rate the cultures were mixed (1:1, vol:vol) with sterile medium, containing either silver nitrate (4 µg/mL) or silver nanoparticles (400 µg/mL). These concentrations were determined empirically to cause a reduction in growth rate, but not a cessation in growth. The cultures were harvested for gene expression analysis after 10 minutes. If the cultures were left alone, the bacteria maintained growth for approximately 1.5 hours, before entering stationary phase, Figure 5.1.

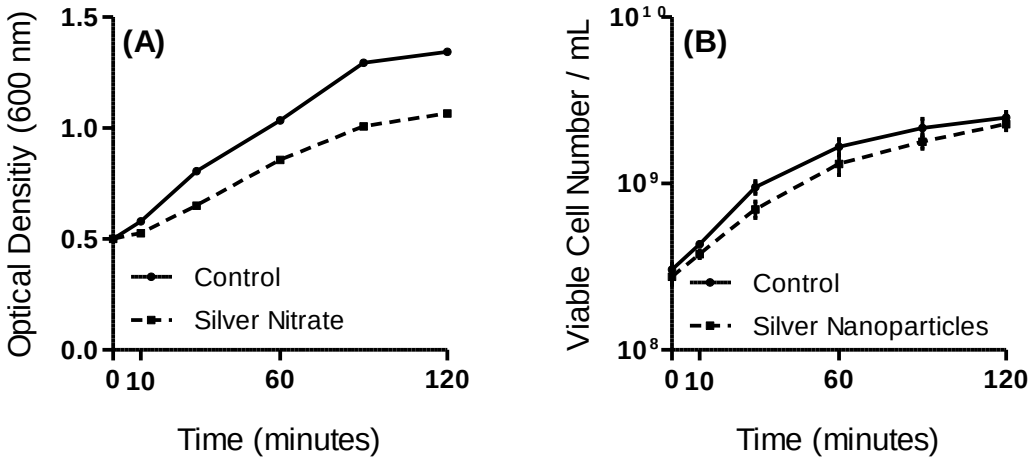


**Figure 5.1. Growth and replication of *E. coli* K12 in modified-LB medium containing silver ions (A) or silver nanoparticles (B), at 37$^{o}$C. Different methods were used to measure bacterial replication; optical density for the silver ion treated cultures for convenience, and colony forming units for the nanoparticle treated cultures as the large scattering cross sections of the nanoparticles preclude accurate optical measurements. The error bars are the standard error of the mean (n=4).**

### 5.2.2 Gene Expression Analysis

Each microarray experiment was set up in quadruplicate by comparing the intensity of Cy3 (control) and Cy5 (silver-treated) labeled RNA that hybridized with each feature on the microarray. After feature extraction, the fluorescence value for each feature was normalised using the global (within array) lowess method to adjust for dye intensity bias [16]. Features with a normalised fluorescence intensity of more than 1 standard deviation from the mean were excluded. Subsequently, each ORF was filtered according to expression ratio, removing genes whose regulation failed to alter by more than 2-fold. Gene expression ratios were subject to confidence testing using the t-test with multiple test correction [17] and ANOVA, removing genes with a p-value of more than 0.05. The filtered gene lists contained 258 genes that were regulated by more than 2-fold in response to silver nitrate; 220 were up-regulated and 38 were down-regulated. Additionally, for silver nanoparticles, 497 genes showed a significant regulation; 273 genes were up-regulated and 224 genes were down-regulated. Biological information was interpreted from the filtered gene lists by searching for gene ontology (GO) biological process terms, which were significantly enriched in the data. The results are shown in Figure 5.2, for transcription in response to silver nitrate, and Figure 5.3 for transcription in response to silver nanoparticles. Additionally, the data is presented in Table 5.1, for up-regulated biological processes, and Table 5.2 for down-regulated biological processes. The genes with corresponding annotations that were not significantly enriched in the data are included in a complete list in appendix B.

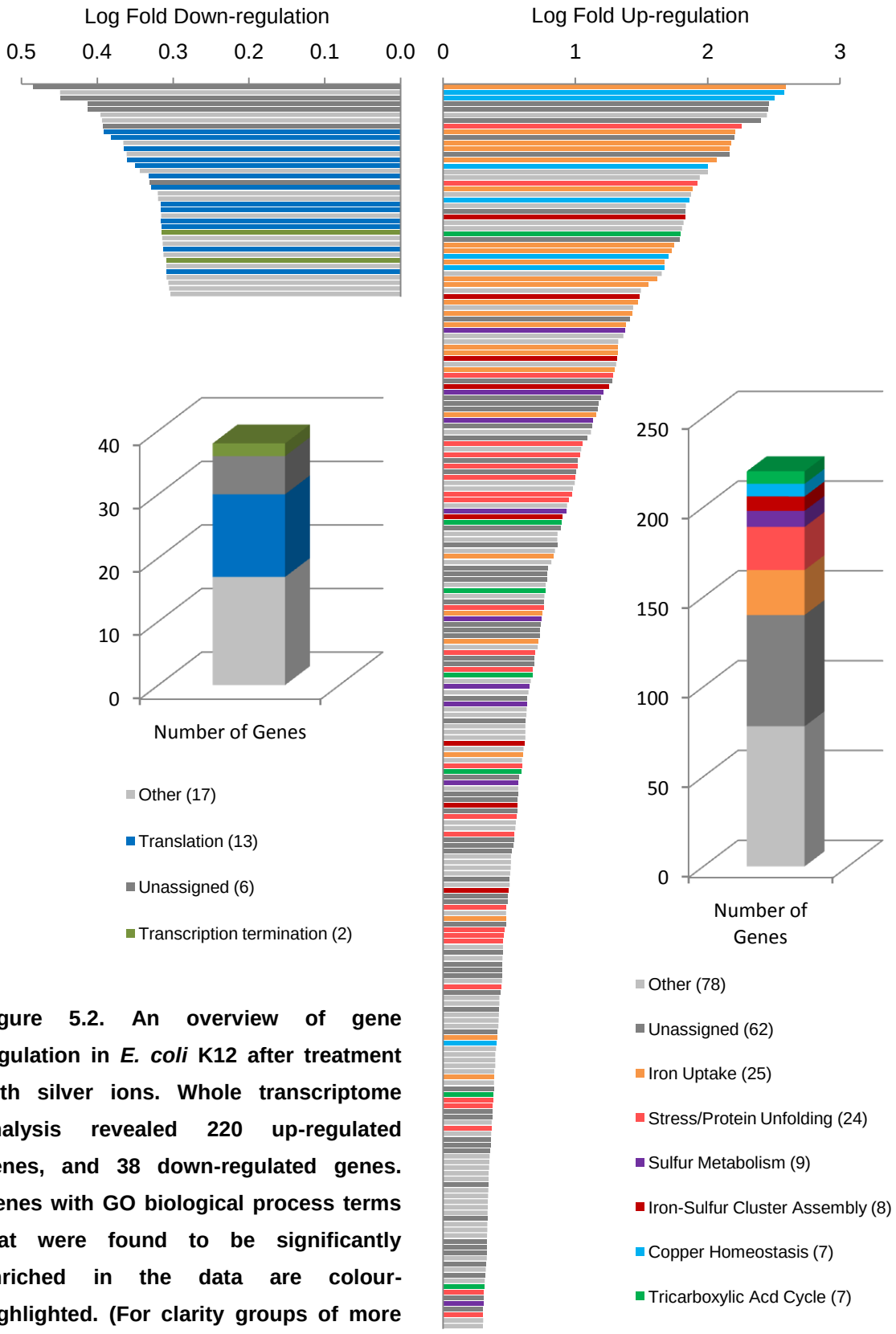


**Figure 5.2. An overview of gene regulation in *E. coli* K12 after treatment with silver ions. Whole transcriptome analysis revealed 220 up-regulated genes, and 38 down-regulated genes. Genes with GO biological process terms that were found to be significantly enriched in the data are colour-highlighted. (For clarity groups of more than 5 genes are shown).**

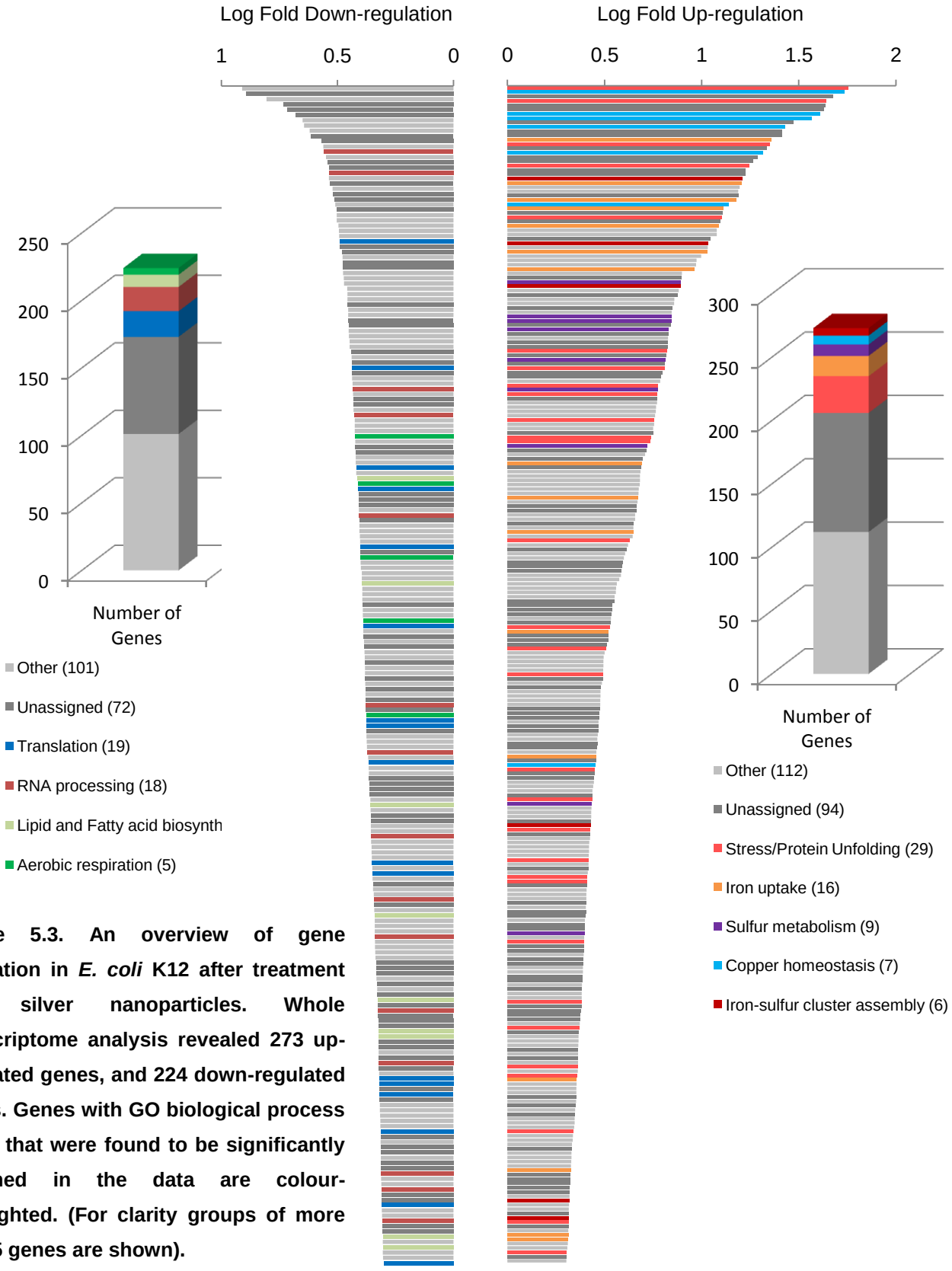


**Figure 5.3. An overview of gene regulation in *E. coli* K12 after treatment with silver nanoparticles. Whole transcriptome analysis revealed 273 up-regulated genes, and 224 down-regulated genes. Genes with GO biological process terms that were found to be significantly enriched in the data are colour-highlighted. (For clarity groups of more than 5 genes are shown).**

## Table 5.1. Up-Regulated Biological Processes

| Gene | Protein Function | Expression Ratio | |
|---|---|---|---|
| | | $AgNO_3$ | $Ag_{(NP)}$ |
| **Iron Uptake** (GO:0006826 - iron ion transport; GO:0009239 - enterobactin biosynthetic process) | | | |
| *entA* | Biosynthesis of the enterobactin siderophore [18-19]. | 146.78 | 9.19 |
| *entB* | | 116.39 | 10.65 |
| *entC* | | 161.96 | 4.91 |
| *entD* | | 6.82 | 4.69 |
| *entE* | | 77.22 | 12.95 |
| *entF* | | 53.56 | 15.07 |
| *ybdB* | | 160.24 | 7.49 |
| *Cir* | Outer Membrane $Fe^{3+}$/ligand receptors [20]. | 386.65 | 4.44 |
| *Fiu* | | 41.44 | 3.32 |
| *fepA* | Uptake of $Fe^{3+}$/enterobactin [21-22]. | 47.48 | 12.21 |
| *fepB* | | 55.40 | 2.87 |
| *fepC* | | 24.10 | - |
| *fepD* | | 20.76 | - |
| *fepG* | | 27.12 | - |
| *fecR* | Uptake of ferric citrate [23-24]. | 29.91 | 2.05 |
| *fecI* | | 35.64 | 2.27 |
| *fecA* | | 5.21 | - |
| *fecB* | | 2.99 | - |
| *fhuA* | Uptake of ferrichrome [25]. | 14.38 | - |
| *fhuC* | | 5.62 | - |
| *fhuE* | | 20.93 | 16.07 |
| *fhuF* | | 19.91 | - |
| *tonB* | Inner membrane complex; energises the outer membrane $Fe^{3+}$/ligand transporters [26-28]. | 2.43 | - |
| *exbB* | | 4.19 | - |
| *exbD* | | 4.03 | - |

| Gene | Protein Function | Expression Ratio $AgNO_3$ | Expression Ratio $Ag_{(NP)}$ |
|---|---|---|---|
| **Sulfur Metabolism** (GO:0006790 - sulfur metabolic process) | | | |
| *cysA* | Sulfate assimilation and biosynthesis of cysteine [29-31]. | 16.19 | 6.50 |
| *cysC* | | 4.29 | 5.94 |
| *cysD* | | 4.49 | 7.00 |
| *cysH* | | 13.66 | 6.97 |
| *cysI* | | 8.49 | 7.83 |
| *cysK* | | 3.70 | 2.49 |
| *cysN* | | 23.75 | 6.74 |
| *cysP* | | 2.02 | 2.72 |
| *cysW* | | 5.54 | 5.22 |
| **Iron-Sulfur Cluster Assembly** (GO:0016226 - iron-sulfur cluster assembly) | | | |
| *iscA* | Fe-S assembly complex [32-33]. | 4.11 | 2.09 |
| *iscU* | | 3.65 | 2.06 |
| *iscS* | | 3.14 | - |
| *iscR* | Regulatory protein for *iscSUA* [34]. | 7.99 | 2.68 |
| *sufA* | Fe-S assembly complex [35]. | 62.29 | 16.26 |
| *sufB* | | 30.58 | 10.82 |
| *sufC* | | 20.58 | 11.97 |
| *sufD* | | 18.06 | 7.83 |
| **Response to Protein Unfolding and Stress** (GO:0009408 - response to heat; GO:0006950 - response to stress; GO:0050821 - protein stabilization; GO:0006457 - protein folding; GO:0006508 - proteolysis) | | | |
| *ipaA* | Small heat shock proteins. May stabilise unfolded proteins [36-38]. | 180.16 | 6.44 |
| *ipaB* | | 4.76 | 17.55 |
| *clpB* | Re-solubilisation of aggregated proteins [39-40] | 83.16 | 12.66 |
| *clpP* | Proteolysis | 2.04 | 3.23 |
| *dnaK* | DnaK-DnaJ-GrpE (DJE) complex; chaperone for protein folding; protein disaggregation; regulation of the heat shock response [41-42]. | 19.32 | 6.62 |
| *dnaJ* | | 3.46 | 2.06 |
| *grpE* | | 4.96 | 4.25 |
| *groS* | GroEL complex; chaperone for protein folding; protein re-folding [43-44]. | 9.93 | 5.69 |
| *groL* | | 9.44 | 5.44 |
| *htpG* | Protein folding; homologue to mammalian HSP90 [45-46]. | 11.33 | 5.97 |
| *htpX* | Protease; degradation of unfolded proteins [47]. | 8.94 | 5.47 |

| Gene | Protein Function | Expression Ratio | |
|---|---|---|---|
| | | $AgNO_3$ | $Ag_{(NP)}$ |
| *hslJ* | Heat shock locus proteins [48-52]. | - | 5.91 |
| *hslO* | | 3.62 | 3.37 |
| *hslR* | | 2.90 | 2.62 |
| *hslU* | | 2.36 | 2.28 |
| *hslV* | | 2.33 | 2.72 |
| *lon* | DNA-binding ATP-dependent protease [53]. | 2.85 | 3.11 |
| *raiA* | Cold shock protein associated with 30S ribosomal subunit [54]. | 10.43 | 56.85 |
| *spy* | Envelope stress-induced periplasmic protein [55]. | 10.87 | 43.68 |
| *betA* | Predicted hydroxynitrile lyase; associated with stress [56]. | 5.81 | - |
| *osmC* | Peroxidase; associated with stress [57-58]. | 3.95 | 22.35 |
| *idhA* | NAD-linked fermentative lactate dehydrogensase; associated with heat stress [59]. | 3.01 | 2.48 |
| *hflK* | Putative proteases; associated with heat stress [60]. | 2.88 | 2.31 |
| *hflX* | | - | 2.41 |
| *rrmJ* | Ribosome associated methyltransferase; associated with heat stress [61]. | 2.76 | 3.12 |
| *hfq* | RNA binding protein; associated with stress [62-63]. | 2.01 | - |
| *cpxA* | CpxAR regulon; responds to protein unfolding in the periplasm; responds to $Cu^+$ [8, 64-65]. | | |
| *cpxR* | | - | 2.80 |
| *ppiA* | | - | 2.67 |
| *dsbA* | | - | 2.57 |
| *uspC* | Universal stress proteins [66-68]. | - | 2.19 |
| *uspF* | | - | 2.58 |

| Gene | Function | Expression Ratio $AgNO_3$ | Expression Ratio $Ag_{(NP)}$ |
|---|---|---|---|
| **Copper Homeostasis** (GO:0046688 - response to copper ion) | | | |
| *copA* | P-type ATPase; copper transporter [8]. | 47.09 | 13.71 |
| *cueO* | Periplasmic cuprous oxidase [69]. | 320.45 | 36.72 |
| *cusC* | RND-protein driven cation/proton exchanger; may transport $Cu^+$ and $Ag^+$ [7, 10, 70]. | 72.48 | 40.54 |
| *cusF* | | 376.39 | 54.08 |
| *cusB* | | 99.98 | 26.90 |
| *cusA* | | 50.32 | 20.72 |
| *cusR* | Two-component regulatory system; regulates *cusCFBA* [71]. | 2.53 | 5.11 |
| *cusS* | | - | 2.83 |
| **Tricarboxylic Acid Cycle** (GO:0006099 - tricarboxylic acid cycle) | | | |
| *aceA* | TCA cycle proteins [72]. | 5.97 | - |
| *aceB* | | 4.75 | - |
| *aceK* | | 3.91 | - |
| *acnA* | | 7.88 | - |
| *fumC* | | 67.82 | - |
| *icd* | | 2.41 | - |
| *sdhB* | | 2.07 | - |
| **Spermidine Transport** (GO:0015848 - spermidine transport) | | | |
| *mdtI* | Small multi-drug resistance (SMR) family proteins; spermidine export [72]. | 65.60 | 2.03 |
| *mdtJ* | | 99.91 | 2.62 |
| **Asparagine Biosynthesis** (GO:0006529 - asparagine biosynthetic process) | | | |
| *asnA* | Biosynthesis of asparagine [72]. | 4.04 | 2.64 |
| *asnB* | | 2.79 | - |
| *aldA* | | 2.01 | 6.58 |
| **Glycine Betane Biosynthesis** (GO:0019285 - glycine betaine biosynthetic process from choline) | | | |
| *betA* | Biosynthesis of betane from choline [72]. | 5.81 | - |
| *betB* | | 7.30 | - |
| *betI* | | 11.05 | - |

## Table 5.2. Down-Regulated Biological Processes

| Gene | Function | Expression Ratio $AgNO_3$ | Expression Ratio $Ag_{(NP)}$ |
|---|---|---|---|
| **Translation** (GO:0006412 - translation) | | | |
| *gltX* | Glutamyl-tRNA synthetase [73]. | - | 0.40 |
| *infA* | Translation initiation factors [74-75]. | 0.47 | 0.32 |
| *infB* | | - | 0.38 |
| *prfA* | Peptide chain release factors [76]. | - | 0.43 |
| *prfC* | | 0.39 | 0.48 |
| *rplB* | 50s ribosomal subunit proteins [72]. | - | 0.48 |
| *rplC* | | - | 0.42 |
| *rplD* | | - | 0.45 |
| *rplM* | | - | 0.48 |
| *rplP* | | 0.44 | - |
| *rplS* | | 0.48 | - |
| *rplU* | | 0.45 | 0.50 |
| *rplV* | | 0.49 | - |
| *rplW* | | - | 0.49 |
| *rplY* | | - | 0.45 |
| *rpmC* | | 0.42 | - |
| *rpsC* | 30s ribosomal subunit proteins [72]. | 0.48 | - |
| *rpsF* | | 0.41 | 0.48 |
| *rpsJ* | | - | 0.41 |
| *rpsP* | | 0.48 | 0.36 |
| *rpsR* | | 0.47 | - |
| *rpsS* | | 0.49 | 0.48 |
| *rpsT* | | 0.43 | 0.42 |

| Gene | Function | Expression Ratio $AgNO_3$ | Expression Ratio $Ag_{(NP)}$ |
|---|---|---|---|
| **RNA Processing** (GO:0006399 - tRNA metabolic process; GO:0070475 - rRNA base methylation; GO:0006396 - RNA processing) | | | |
| *cmoA* | Predicted methyltransferase enzymes [72]. | - | 0.44 |
| *cmoB* | | - | 0.48 |
| *dusB* | tRNA-dihydrouridine synthase [77]. | 0.44 | 0.28 |
| *dusC* | | - | 0.46 |
| *gidB* | Methyltransferase; methylation of 16s rRNA [78-79]. | - | 0.43 |
| *miaB* | tRNA methylthiolase [80]. | - | 0.39 |
| *mnmA* | tRNA modification [81-82]. | - | 0.49 |
| *mnmE* | | - | |
| *rlmF* | rRNA modification [83-85]. | - | 0.29 |
| *rlmG* | | - | 0.37 |
| *rlmN* | | - | 0.37 |
| *rnc* | RNase enzymes [72]. | - | 0.39 |
| *rnd* | | - | 0.47 |
| *rnt* | | - | 0.49 |
| *rrmA* | 23S rRNA methyltransferase [72]. | - | 0.45 |
| *sirA* | tRNA modification; sulfur mediator [72]. | - | 0.42 |
| **Lipid and Fatty Acid Biosynthesis** (GO:0008654 - phospholipid biosynthetic process; GO:0006633 - fatty acid biosynthetic process) | | | |
| *cfa* | Phospholipid biosynthesis [72]. | - | 0.40 |
| *fabA* | Fatty acid biosynthesis [72]. | - | 0.50 |
| *fabD* | | - | 0.50 |
| *fabF* | | - | 0.47 |
| *fabI* | | - | 0.48 |
| *lpxA* | Lipid A biosynthesis [86]. | - | 0.44 |
| *plsX* | Phospholipid biosynthesis [87]. | 0.49 | 0.38 |

| Gene | Function | Expression Ratio | |
|---|---|---|---|
| | | $AgNO_3$ | $Ag_{(NP)}$ |
| **Aerobic Respiration** (GO:0009060 - aerobic respiration; GO:0019646 - aerobic electron transport chain) | | | |
| *cyoA* | Subunits of cytochrome *bo* terminal oxidase [88]. | - | 0.42 |
| *cyoB* | | - | 0.40 |
| *cyoC* | | - | 0.41 |
| *cyoD* | | - | 0.38 |
| *cyoE* | | - | 0.40 |
| *nuoA* | Subunits of NADH:ubiquinone oxidoreductase [89]. | - | 0.35 |
| *nuoB* | | - | 0.39 |
| *nuoC* | | - | 0.41 |
| *nuoE* | | - | 0.48 |
| **Flagellum Assembly** (GO:0009296 - flagellum assembly) | | | |
| *flhD* | Part of a regulatory complex with *flhC*, which promotes expression of genes for flagella biosynthesis [90]. | 0.48 | 0.22 |
| *fliM* | Part of the *fli* operon, encoding various flagellar subunits [91]. | 0.48 | - |

### 5.2.3. Microarray Validation

The microarray data sets were validated by comparing the gene expression ratio of 4 genes, obtained from the microarray data, with those obtained using the Real-Time PCR method. The values obtained from each technique were plotted against one another with a strong positive correlation ($R^2$=0.9972, silver nitrate data set; $R^2$=0.9983, silver nanoparticle data set), as shown in Figure 5.4, indicating that the techniques gave consistent results.

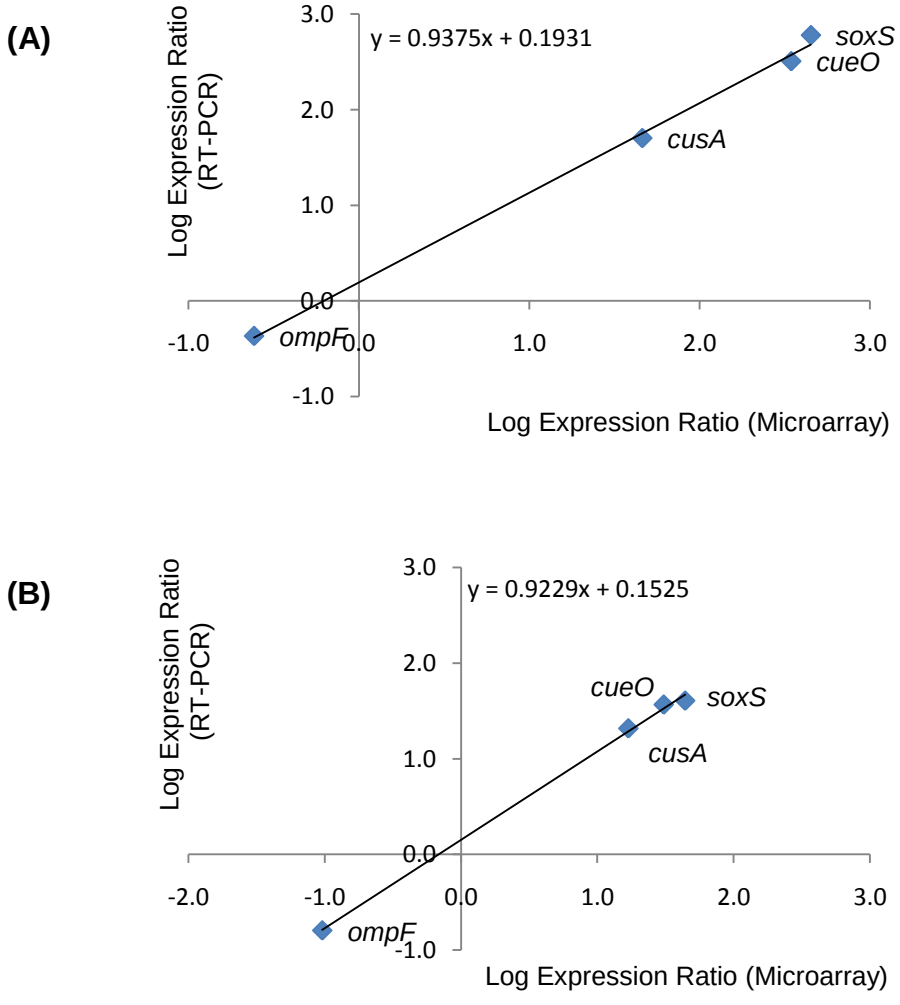


**Figure 5.4. Microarray validation by Real-Time PCR. A strong correlation indicates that both molecular techniques gave similar results after exposure to silver nitrate (A, $R^2$=0.9972) or silver nanoparticles (B, $R^2$=0.9983).**

### 5.2.4. Unknown Genes

A large proportion of the regulated genes were of unknown function; 79 after treatment with silver nitrate and 94 after treatment with silver nanoparticles. Some of these were expressed to very high levels, indicating that the corresponding proteins may be important components of the adaptive response to $Ag^+$. However, deletion of the unknown genes with very high expression ratios (greater than 50-fold up-regulation) did not change the susceptibility of the *E. coli* to silver nitrate in MIC assays, Table 5.3. Therefore these genes are not considered further.

**Table 5.3. Minimum Inhibitory Concentration of $Ag^+$ on Gene Deletion Mutants**

| Strain | $Ag^+$ MIC |
|---|---|
| *MG1655* | 8 µg/mL |
| Δ*yebE* | 8 µg/mL |
| Δ*ybdK* | 8 µg/mL |
| Δ*ybdZ* | 8 µg/mL |
| Δ*yjjZ* | 8 µg/mL |
| Δ*yncJ* | 8 µg/mL |
| Δ*ydiE* | 8 µg/mL |

### 5.2.5 Differential Gene Regulation

A novel hypothesis in this work is that different modes of silver ion delivery, either from silver nitrate in the bulk solution or from a nanoparticle dissolving proximal to the cell membrane, elicit a qualitatively different transcriptional response. The two sets of gene expression data are compared and it was found that the transcriptome response to nanoparticles, as a function of the number of genes that were regulated, was almost twice the magnitude of the response to silver nitrate. Moreover, there were a number of differentially regulated genes, Figure 5.5, indicating that the mode of silver ion delivery changes the overall transcriptional profile of the *E. coli*.

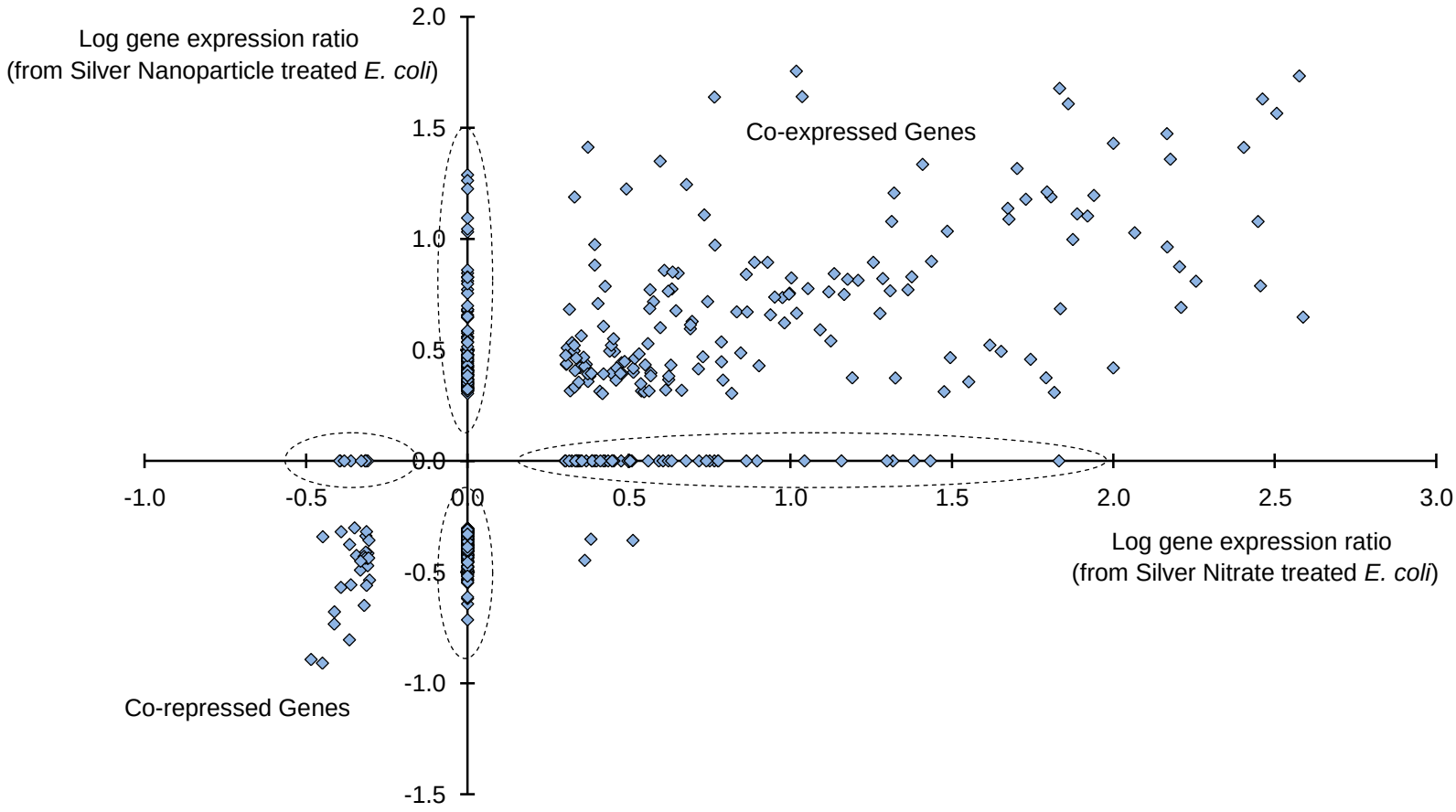


**Figure 5.5. Differential silver nitrate and silver nanoparticle induced transcription. A plot of log gene expression ratio (silver nitrate treated *E. coli*) versus log gene expression ratio (silver nanoparticle treated *E. coli*), showing co-expressed, co-repressed or differentially regulated genes (dashed ovals). Only 3 genes were found to be inversely regulated between the two data sets.**

## 5.3 Discussion

Gene expression microarray experiments were carried out to determine the early time (10 minute) transcriptional response of the model bacterium *E. coli* K12 (MG1655) to silver, either as $Ag^{+}$ or as nanoparticles, in modified-LB medium. Silver induced the regulation of 497 genes; a greater transcriptional change than that reported for the response to the $Cd^{2+}$ ion (173 genes [12]) or the $Zn^{2+}$ ion (29 genes [92]), or for the response to silver nitrate by Wu *et al* (106 genes [6]). The size of this response is subject to the accuracy of the strict statistical and expression filters that were applied to the data. Genes were excluded whose regulation failed to alter by more than 2-fold, thus excluding genes that may have been regulated at very low levels. In addition, the data was subject to confidence testing, selecting for differentially expressed genes with a corresponding *P* value of less than 0.05. The *P* value represents a trade-off between significance and completeness in the data set, thus, optimally selecting *P* values may increase or decrease the observed number of regulated genes. As shown in Figure 5.6, the *P* values for the microarray data in this study, calculated using t-test or ANOVA, do not follow a uniform distribution. The *P* value cut-off may have led to a number of false negative (type II) errors in the data sets.

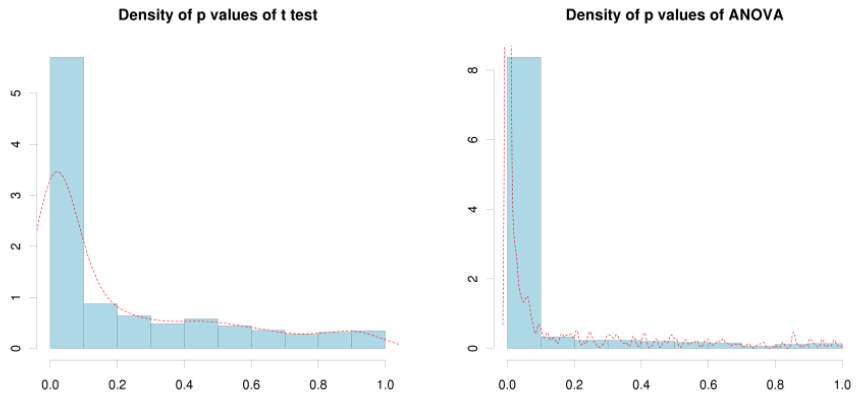


**Figure 5.6. Distribution of *P* values from the microarray data [93].**

The size of the response supports a novel 'pan-metabolism toxicity' hypothesis for the toxicity of the silver ion. The hypothesis is intrinsically reasonable because the silver ion may target proteins non-specifically via cysteine, methionine or histidine residues [94-95]. Subsequently, *E. coli* must respond by regulating a very large portion of the transcriptome to protect the metabolism, replenish damaged proteins and remove or detoxify the silver ions. This adaptive response was identified by searching the filtered gene lists in order to elucidate Gene Ontology (GO) biological process terms that were significantly enriched in the data, with reference to the *E. coli* genome, using the GeneCoDis algorithm [96-97]. These genes are highlighted against the entire list of regulated genes in Figure 5.2 and Figure 5.3, and the individual genes with their corresponding expression ratios are shown in Table 5.1 and Table 5.2. Then, in addition to these genes, there is a far larger quantity of regulated genes that may play no role in the adaptation to silver stress. These may reflect a response to the action of $Ag^+$ on cell signalling proteins and are considered to be part of a disruptive response wherein this transcriptional shift may be unnecessary, thus augment the $Ag^+$-stress with an energy cost to the cell. These genes are part of a complete list for the filtered expression data in appendix B.

### 5.3.1. Silver Induces the Up-Regulation of Genes that Encode Molecular Chaperones and Proteases that Stabilise, Re-fold or Degrade Denatured Proteins

In line with the hypothesis that $Ag^+$ denatures proteins, silver induces a transcriptional response similar to that observed during heat shock [98-99]. This is consistent with gene expression analyses carried out for the response to silver in other organisms, including the fruit fly, *D. melanogaster* [100], and soil nematode, *C. elegans* [101].

In *E. coli* this response is exemplified by the up-regulation of the genes encoding the DnaK-DnaJ-GrpE (DJE) and GroEL-GroES molecular chaperone complexes. These are the most abundant heat shock systems in *E. coli*, constituting up to 20% of total protein during heat stress at 46$^{o}$C [98]. Both systems are positively regulated by a rapid increase in the cytosolic concentration of the $\sigma^{32}$ subunit of RNA polymerase (RNAP), the product of the *rpoH* gene. This was not up-regulated by silver, probably because a regulatory element in the *rpoH* promoter prevents RNAP from binding unless a region of secondary structure is denatured by an increase in temperature [102]. Thus, for silver, the $\sigma^{32}$ levels are probably controlled by a DnaK-dependant homeostatic mechanism: DnaK binds to $\sigma^{32}$ and promotes its degradation by a protease, FtsH, unless DnaK is sequestered by unfolded protein substrates [98, 103]. Accordingly, the action of $Ag^{+}$ on proteins creates an abundance of DnaK substrates, leading to the release of $\sigma^{32}$. The DJE and GroEL-GroES systems could protect against the effects of silver on proteins by facilitating the reforming of tertiary structure.

Denatured proteins can aggregate through hydrophobic interactions between exposed core residues and undergo covalent cross linking between various reactive groups within the primary amino acid structure [104]. The microarray data indicates that, after exposure to silver, the formation of aggregates is countered by the expression of the small heat shock proteins, IbpA and IbpB (inclusion body associated proteins) [38]. These may stabilise the denatured protein fraction and aid proteolysis. Furthermore, if the denatured protein burden is sufficient to overcome these defences, and protein aggregates accumulate within the cell, then they can be disassembled by ClpB in coordination with DnaK [39]. The various heat shock proteins that are induced by silver could constitute an effective adaptive response to the pan-metabolism protein unfolding, Figure 5.7.

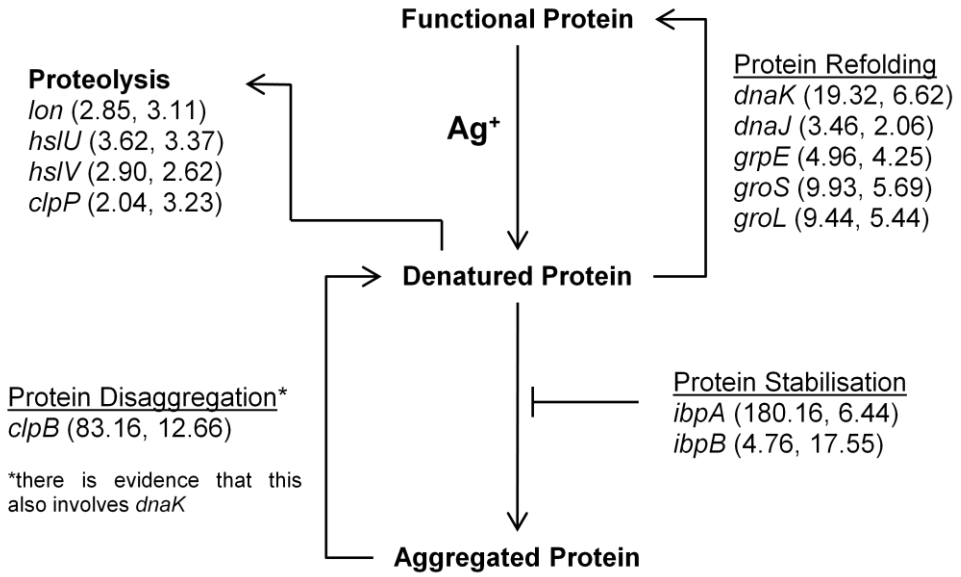


**Figure 5.7. The silver induced expression of genes for removing denatured proteins. The expression ratio for each gene is given in brackets, first for silver nitrate and second for silver nanoparticles.**

The activation of systems for removing denatured proteins is common with Cadmium stress. The $Cd^{2+}$ ion, like $Ag^{+}$, may interact with sulfur containing compounds in the cell such as the thiol group on cysteine residues, leading to protein disruption. There is also evidence that copper stress involves the accumulation of denatured proteins through the expression of genes under the control of the CpxRA regulon, which responds to unfolded proteins in the periplasm [64-65, 105-106]. However, the transcriptome response to different doses of copper [15] did not include the regulation of the array of heat shock proteins, and associated genes, as observed for the response to $Ag^{+}$ (this study) and $Cd^{2+}$ [12]. This may indicate that protein unfolding is not a primary mechanism in copper toxicity.

### 5.3.2. Silver Induces the Expression of Genes for Iron and Sulfur Metabolism, and Iron-Sulfur Cluster Assembly: Further Evidence that Silver Acts Upon Proteins

In *E. coli*, up to 80 proteins contain iron-sulfur clusters (FeS), which perform electron transfer and redox catalysis as iron alternates between the $Fe^{2+}$ (ferric) and $Fe^{3+}$ (ferrous) oxidation states. FeS proteins regulate and function within diverse metabolic

processes including respiration, gene regulation, RNA modification, DNA replication and repair, and other areas of the metabolism [32]. These processes could be inhibited as $Ag^+$ interacts with FeS, leading to pan metabolism toxic effects. For example, silver nitrate induced the expression of various genes that encode tricarboxylic acid cycle proteins; a metabolic pathway that is heavily dependent upon FeS [107-109]. The degradation of this pathway through the action of $Ag^+$ on FeS and signalling via feedback mechanisms may explain the up-regulation of the corresponding genes. Moreover, *E. coli* responded to $Ag^+$ by up-regulating genes for the FeS assembly apparatus, the *iscRSUA* and *sufABCD* operons [32], and the concomitant increase in expression of genes for iron uptake and sulfate assimilation may have enhanced the rate of acquisition of the raw materials for FeS biosynthesis.

The acquisition of iron post exposure to silver was demonstrated by the comprehensive expression of genes for the uptake of iron complexes from the environment, periplasmic chaperones for movement of iron complexes across the cell envelope, and inner membrane transport systems for moving iron into the cytosol, Figure 5.8. Notably, the enterobactin-FepA pathway was up-regulated by silver [21, 110]. Enterobactin is a tri-dentate ferric iron ligand, which is synthesised from chorismic acid in a process that involves at least 6 enzymes, encoded on the *entABCDEF* operon, Figure 5.9, all of which were up-regulated in response to silver, Table 5.1.

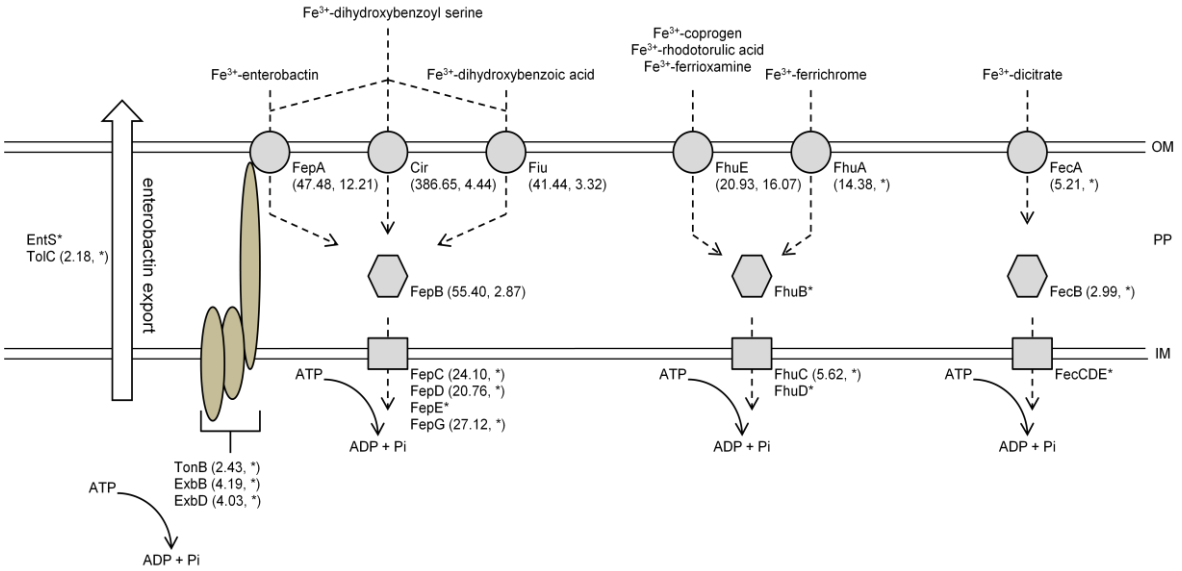


**Figure 5.8. Iron acquisition in *E. coli K12* after exposure to silver. Key: Outer membrane (OM); inner membrane (IM); outer membrane $Fe^{3+}$/ligand receptors (circles); molecular chaperones (hexagons); inner membrane transporters (squares). The arrow heads indicate the movement of $Fe^{3+}$. In addition, the TonB-ExbB-ExbD complex is shown. This is integral with the inner membrane and interacts with, and energises, all of the outer membrane $Fe^{3+}$/ligand receptor proteins. Enterobactin is synthesised in the cytosol and exported through EntS and TolC. The expression ratio for each gene is given in brackets, first for the silver nitrate data and second for silver nanoparticle data. An asterisk indicates that the gene was not found to be regulated.**

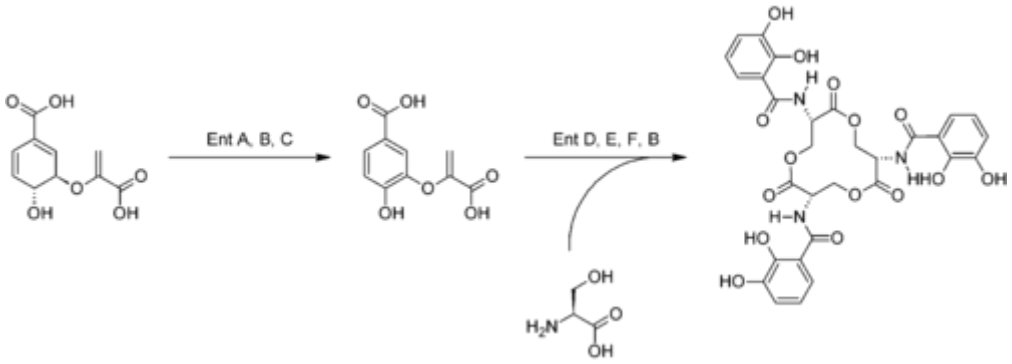


**Figure 5.9. The synthesis of enterobactin. Chorismic acid (left) is converted to 2,3-dihydroxybenzoic acid (DHB) by 3 enzymes, EntA, EntB and EntC. DHB (centre) is linked via an amide bond to L-serine and 3 molecules of DHB-serine undergo intramolecular cyclisation to form enterobactin, catalysed by 4 enzymes, EntD, EntE, EntF and EntB.**

Iron uptake in *E. coli* is regulated by the activity of a cytosolic transcriptional repressor, the Ferric iron Uptake Regulator (Fur). The Fur repressor is active when coordinated with a ferrous iron co-repressor ion, thus genes encoding iron uptake proteins are expressed when the concentration of iron in the cytosol is sub-optimal [111-115]. Therefore, the expression of these genes after exposure to $Ag^{+}$ may indicate that the iron concentration in the cytosol was reduced. This did not reflect the exhaustion of iron in the culture medium because, post exposure, the bacteria maintained exponential growth for at least 1.5 hours, Figure 5.1. However, the expression of *cueO*, encoding a cuprous oxidase, may have reduced the rate of iron uptake because the CueO enzyme may oxidise and inactivate enterobactin [69]. Kershaw *et al* found that exposure to copper, during which the CueO enzyme has a protective effect by oxidising $Cu^{+}$, also resulted in an increase in the expression of genes for iron uptake [15]. Second, the cytosolic deficiency of iron may not reflect limited iron availability, but rather an increase in the cellular demand for incorporation into new FeS clusters.

### 5.3.3. Evidence that Exposure to Silver Leads to the Formation of Reactive Chemical Species

Previous studies indicate that exposure to silver causes redox stress, a condition in which the rate of formation of reactive chemical species in the cell, specifically those containing oxygen, exceeds the rate at which they and their effects are neutralised. Silver ions and silver nanoparticles induced the expression of redox-stress related genes in human hepatoma cells [116], zebra fish hepatocytes [117] and fruit fly (*D. Melanogaster)* larvae [100]. These observations are reciprocated in this study wherein, post exposure to $Ag^{+}$, *E. coli* up-regulates the expression of genes belonging to the redox-activated *soxRS* regulon, controlled by a two gene two component signalling system.

The SoxR protein is a cytosolic homodimer of rhombic [2Fe2S] FeS-containing sub-units [118] and, upon oxidation of the FeS clusters [119-120], promotes the expression of *soxS* encoding a transcriptional regulator [121-122]. Silver ions and silver nanoparticles induced the expression of 16 genes that are regulated by SoxS. In contrast, the regulation of the *soxS* gene could not be determined because the gene did not pass the various statistical confidence filters that were applied to the data, a consequence of the sub-optimal selection of *P* values. However, real-time PCR confirmed that soxS was expressed at high levels after exposure to silver; up-regulated by 449-fold after exposure to silver nitrate, or 44-fold after exposure to silver nanoparticles.

The silver ion does not undergo redox cycling, however the degradation of iron and copper coordination sites by $Ag^{+}$ may increase the concentration of free intracellular iron and copper ions. In turn, these fuel the production of cellular oxidants including the hydroxyl radical through reaction with hydrogen peroxide [123], a by-product of oxidative metabolism. Disruption of the *soxS* gene to produce a mutant strain that was deficient for

SoxS activity did not alter the sensitivity to silver nitrate (data not shown) and redox stress may not be a primary mechanism of silver toxicity.

### 5.3.4. Exposure to Silver Leads to the Repression of Genes for Lipid Metabolism and RNA Processing, Flagella Biosynthesis and Ribosome Sub-units

These transcriptional changes may be explained by the reduction in bacterial growth and replication rate in the silver-containing medium. The regulation of these processes in response to bacterial growth rate is well known [63, 124] and may represent a saving in the ATP budget of the cell, so conserving the resources to protect other areas of the metabolism. In particular, the observed repression of genes for motility, specifically *flhD which* encodes a positive regulator of flagella biosynthesis [90], may conserve ATP and biomaterials. This observation is consistent with the response to various other environmental insults including high temperature, osmotic stress and copper ions [125-126].

The repression of genes encoding ribosome sub-units indicates that rate of translation decreased under the experimental conditions. The consequence of this is that there may have been a discrepancy between the observed transcriptome and the proteome, specifically a greater than typical lag between the up-regulation of a particular set of genes and the concurrent increase in the activity of the gene products to produce the response. The discrepancy between the transcriptome, proteome and metabolome could make microarray data misleading. A pan-omic approach, incorporating measurements of the transcriptome, proteome and metabolome by matching transcripts, proteins and metabolites into specific biological pathways or processes will provide a clear insight into the metabolic changes occurring under a given set of conditions.

### 5.3.5. The Action of $Ag^+$ on Cell Signalling May Lead to a Disruptive Transcriptional Response

The transcription of genes encoding heat shock proteins and proteins that catalyse the formation of FeS enables the bacterium to repair or replenish the damaged protein fraction, whilst the expression of genes under the control of the superoxide responding regulon protects the cell against oxidative damage; an adaptive response to $Ag^+$. Contrarily, the majority of the regulated genes had corresponding GO biological process terms that were not significantly enriched in the gene lists, appendix B. This could represent 'noise' within the data. However, the rigorous statistical testing and the practice of a minimum two-fold change in expression should have minimised this occurrence. Therefore, it is further considered that the regulation of these genes is a consequence of the pan-metabolism disruption caused by the action of $Ag^+$; specifically on *E. coli* signalling cascades. This disruptive response is a hypothetical mechanism through which the sub-inhibitory concentration of silver led to the regulation of up to 497 genes of which a minority had GO biological process terms that were found to be significantly enriched in the data.

Particular reference is given to two-component signalling because $Ag^+$ accumulates in the cell envelope [127-128] and proximal to the integral inner membrane 'sensor' component, Figure 5.10. A direct consequence of this is that the activator and repressor functions of response regulators may be inverted. *E. coli* K12 encodes at least 21 two-component signalling systems (identified using EcoCyc [72]), wherein the sensor protein may contain up to 14 cysteine residues as potential targets for $Ag^+$ activity.

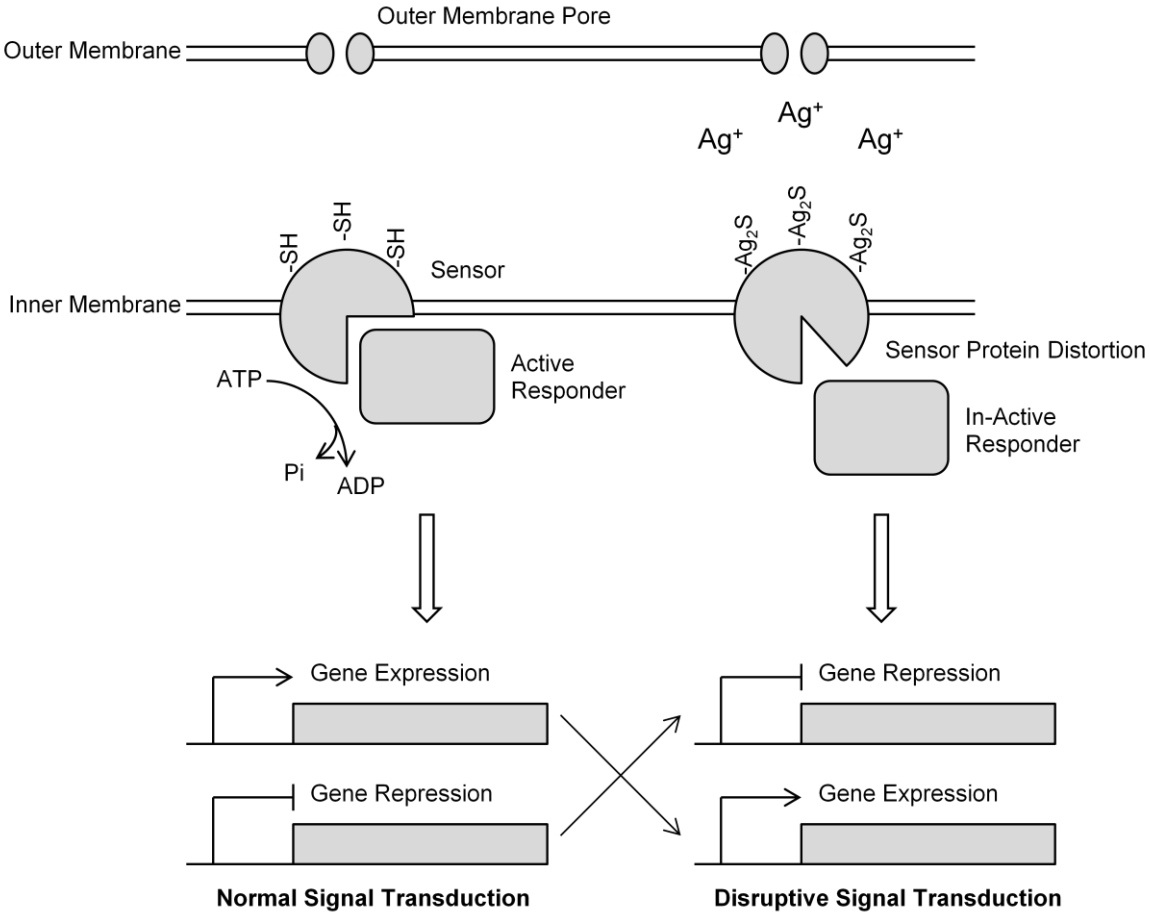


**Figure 5.10. A cartoon representation of two-component signalling in bacteria. An integral inner membrane protein (sensor) controls the activity of a cytosolic transcription factor (responder) [129-130]. The responder may activate or repress the transcription of genes. Under silver stress $Ag^+$ reacts with cysteine residues, which could denature the protein sensor and obstruct an interaction with the responder, which subsequently may not activate or repress gene expression. This could lead to inversion of gene regulation; a disruptive response.**

### 5.3.6. Exposure to Silver Induces Genes for Copper Homeostasis: an Adaptive and Disruptive Response

The gene expression data from this study demonstrates that *E. coli* responds to $Ag^+$ by up-regulating the expression of genes in the CusRS and CueR regulons, leading to a reduction in excess free $Cu^+$ [7-10, 70]. The hypothesis for this regulation is that $Cu^+$ and $Ag^+$, which are isoelectronic, have a similar coordination with the copper regulatory proteins. This response may be disruptive if the concentration of $Ag^+$ simulates an excess

of $Cu^{+}$ when the actual concentration may be optimal. Paradoxically, this response may also have a protective function if the CusCBA chemiosmotic transporter, part of the CusRS regulon, can efflux $Ag^{+}$ consistent with the $Ag^{+}$-sensitivity of a *cusA* deletion mutant (Chapter 3, [7, 9]). The response may also protect the metabolism by removing any free $Cu^{+}$ displaced from metalloproteins by the action of Ag+ on cysteine and histidine residues, which form part of the Cu-coordination complex. Free $Cu^{+}$ may augment the $Ag^{+}$ stress with oxidative damage if $Cu^{+}$ undergoes redox cycling in the periplasm to form the hydroxyl radical [123].

### 5.3.7. Silver Nitrate and Silver Nanoparticles Elicit a Differential Transcriptome Response in *E. coli* K12

An objective of this study was to identify changes in gene expression that arise owing to the $Ag^{+}$, as discussed above, and differentially owing to the nanoparticle-based delivery of $Ag^{+}$ to the outer membrane: a bacterial nanoparticle interaction which was hypothesised in Chapter 4. In light of this hypothesis it was found that the transcriptome response to nanoparticles was both quantitatively (in terms of the number of genes that were regulated) and qualitatively different indicating that the mode of silver ion delivery changes the overall transcriptional profile of the *E. coli*. However, a proportion of the differential transcriptional response may be explained by differences in the concentration of silver ions that were applied to the bacteria in either experiment. The silver concentration in all of the cultures led to a reduction in bacterial growth rate, but did not cause a cessation of growth and replication, as shown from the growth plots in Figure 5.1. Nonetheless, the exact concentration of silver ions, and therefore growth rate, in each experiment was probably different. For example, only silver nanoparticles led to the down-regulation of genes involved in the synthesis of lipids and fatty acids, genes involved in the

processing of RNAs and genes that are associated with aerobic respiration including cytochrome *bo* terminal oxidase and NADH:ubiquinone oxidoreductase; a metabolic down-shift. Conversely, only silver nitrate led to the expression of genes that encode various Tricarboxylic Acid Cycle (TCA cycle) proteins, which may represent a general metabolic up-shift. These patterns of regulation indicate that the growth of the silver nanoparticle-treated *E. coli* was inhibited to a greater degree than that of the silver nitrate-treated bacteria.

Different methods were used to measure the rate of bacterial growth and replication in the modified-LB medium, thus the growth rates cannot be compared directly. Optical density was used for silver-nitrate containing cultures because the method is relatively rapid and it is preferable when measuring replicate cultures at accurate time points. In contrast, the CFU counting method is time consuming and leads to inaccuracies in the data; i.e. by the time the sample has been diluted and spread onto solid medium the time point has passed. Nonetheless, it was necessary to use this method as the large scattering cross sections of the nanoparticles preclude accurate optical measurements.

Another source of differential transcription could have been the nitrate counter ion at a concentration of approximately 2.35 µM. Nitrate-induced gene expression is commonly observed under anaerobic conditions, however the conditions used for experiments were aerobic, and cultures were shaken continuously to aerate the medium. Further, the switch to nitrate as an electron acceptor is under hierarchical control with the oxygen sensitive Fnr protein at the top. Accordingly, in the aerated medium $NO_3^-$ did not induce the expression of downstream nitrate-responsive operons *narGHJI*, *narXL* and *narZYWV*, or associated genes *narK* and *narU* [131]. As an important component of the respiratory apparatus in *E. coli* it is likely that nitrate has some gene regulatory functions, even when under aerobic conditions. However, in the context of these experiments it was

preferable to have the nitrate discrepancy than to use sodium nitrate as a control and have the metal ion ($Na^+$) discrepancy instead.

Although the overall transcriptional response to silver nitrate and silver nanoparticles was different, the biological processes that were enriched in either data set were strikingly similar. The majority of the differentially regulated genes had functional annotations that were not significantly enriched, and may reflect a dose dependent disruption of cell signalling.

### 5.3.8. Conclusions

The microarray data provides a clear mechanism for how *E. coli* adapts to silver stress. Denatured proteins are re-folded or disaggregated and degraded whilst iron and sulfur metabolism increases so that FeS clusters can be replaced. Reactive chemical species, which may be produced from redox cycling of metal ions displaced by silver, are neutralised by the products of the SoxRS regulon.

Regulated genes with corresponding annotations that were not significantly enriched are considered to reflect the disruptive nature of $Ag^{+}$ on signalling proteins; a disruptive response.

This study yielded very different results from those obtained by Wu *et al* [6] wherein their *E. coli* made a relatively minimal (106 genes) transcriptional response to silver nitrate, probably reflecting differences in experimental design; this study capturing the response to sudden silver shock.

There is limited evidence that differential delivery of $Ag^{+}$, either free in the bulk solution or from a nanoparticle dissolving at the cell surface, leads to a differential transcriptional response. Any differences in biological process regulation can be attributed to a dose response or to the presence of the nitrate counter ion in the silver nitrate-treated *E. coli*.

So far in this thesis bacterial-nanoparticle interactions have been considered where the toxic mode of action is dependent upon nanoparticle dissolution alone. This may be a primary mechanism of nanoparticle toxicity. However, in the following Chapter the study leads onto a nanomaterial for which whole nanoparticle effects in addition to dissolution might contribute to a new mechanism of toxicity.

## 5.4. References


1. Blattner, F.R., et al., *The Complete Genome Sequence of Escherichia coli K-12.* Science, 1997. **277**(5331): p. 1453-1462.
2. Venter, J.C., et al., *The Sequence of the Human Genome.* Science, 2001. **291**(5507): p. 1304-1351.
3. Durfee, T., et al., *The complete genome sequence of Escherichia coli DH10B: insights into the biology of a laboratory workhorse.* J Bacteriol, 2008. **190**(7): p. 2597-606.
4. Hayashi, K., et al., *Highly accurate genome sequences of Escherichia coli K-12 strains MG1655 and W3110.* Mol Syst Biol, 2006. **2**: p. 2006 0007.
5. Schena, M., et al., *Quantitative Monitoring of Gene Expression Patterns with a Complementary DNA Microarray.* Science, 1995. **270**(5235): p. 467-470.
6. Wu, M., Oerther, D., B., *Using Genomics to Understand Disinfection with Silver.* Proceedings of the Water Environment Federation, 2006. **2006**: p. 1285-1293.
7. Franke, S., G. Grass, and D.H. Nies, *The product of the ybdE gene of the Escherichia coli chromosome is involved in detoxification of silver ions.* Microbiology, 2001. **147**(Pt 4): p. 965-72.
8. Grass, G. and C. Rensing, *Genes Involved in Copper Homeostasis in Escherichia coli.* J. Bacteriol., 2001. **183**(6): p. 2145-2147.
9. Gupta, A., et al., *Diversity of silver resistance genes in IncH incompatibility group plasmids.* Microbiology, 2001. **147**(12): p. 3393-3402.
10. Franke, S., et al., *Molecular analysis of the copper-transporting efflux system CusCFBA of Escherichia coli.* J Bacteriol, 2003. **185**(13): p. 3804-12.
11. Nies, D. and S. Silver, *Bacterial Transition Metal Homeostasis*, in *Molecular Microbiology of Heavy Metals*. 2007, Springer Berlin / Heidelberg. p. 117-142.
12. Helbig, K., C. Grosse, and D.H. Nies, *Cadmium Toxicity in Glutathione Mutants of Escherichia coli.* J. Bacteriol., 2008. **190**(15): p. 5439-5454.
13. Barrett, T., et al., *NCBI GEO: archive for high-throughput functional genomic data.* Nucl. Acids Res., 2009. **37**(suppl_1): p. D885-890.
14. Edgar, R., M. Domrachev, and A.E. Lash, *Gene Expression Omnibus: NCBI gene expression and hybridization array data repository.* Nucleic Acids Res, 2002. **30**(1): p. 207-10.
15. Kershaw, C.J., et al., *The expression profile of Escherichia coli K-12 in response to minimal, optimal and excess copper concentrations.* Microbiology, 2005. **151**(4): p. 1187-1198.

16. Berger, J., et al., *Optimized LOWESS normalization parameter selection for DNA microarray data.* BMC Bioinformatics, 2004. **5**(1): p. 194.

17. Benjamini, Y. and Y. Hochberg, *Controlling the False Discovery Rate: A Practical and Powerful Approach to Multiple Testing.* Journal of the Royal Statistical Society. Series B (Methodological), 1995. **57**(1): p. 289-300.

18. O'Brien, I.G. and F. Gibson, *The structure of enterochelin and related 2,3-dihydroxy-N-benzoylserine conjugates from Escherichia coli.* Biochim Biophys Acta, 1970. **215**(2): p. 393-402.

19. Pollack, J.R. and J.B. Neilands, *Enterobactin, an iron transport compound from.* Biochemical and Biophysical Research Communications, 1970. **38**(5): p. 989-992.

20. Andrews, S.C., A.K. Robinson, and F. Rodriguez-Quinones, *Bacterial iron homeostasis.* FEMS Microbiol Rev, 2003. **27**(2-3): p. 215-37.

21. Buchanan, S.K., et al., *Crystal structure of the outer membrane active transporter FepA from Escherichia coli.* Nat Struct Biol, 1999. **6**(1): p. 56-63.

22. Usher, K.C., et al., *The plug domain of FepA, a TonB-dependent transport protein from Escherichia coli, binds its siderophore in the absence of the transmembrane barrel domain.* Proc Natl Acad Sci U S A, 2001. **98**(19): p. 10676-81.

23. Angerer, A., et al., *Transcriptional regulation of ferric citrate transport in Escherichia coli K-12. FecI belongs to a new subfamily of sigma 70-type factors that respond to extracytoplasmic stimuli.* Mol Microbiol, 1995. **18**(1): p. 163-74.

24. Ferguson, A.D., et al., *Structural basis of gating by the outer membrane transporter FecA.* Science, 2002. **295**(5560): p. 1715-9.

25. Ferguson, A.D., et al., *Siderophore-mediated iron transport: crystal structure of FhuA with bound lipopolysaccharide.* Science, 1998. **282**(5397): p. 2215-20.

26. Higgs, P.I., P.S. Myers, and K. Postle, *Interactions in the TonB-dependent energy transduction complex: ExbB and ExbD form homomultimers.* J Bacteriol, 1998. **180**(22): p. 6031-8.

27. Postle, K., *TonB protein and energy transduction between membranes.* J Bioenerg Biomembr, 1993. **25**(6): p. 591-601.

28. Skare, J.T., et al., *Energy transduction between membranes. TonB, a cytoplasmic membrane protein, can be chemically cross-linked in vivo to the outer membrane receptor FepA.* J Biol Chem, 1993. **268**(22): p. 16302-8.

29. Hesse, H., et al., *Molecular analysis and control of cysteine biosynthesis: integration of nitrogen and sulphur metabolism.* Journal of Experimental Botany, 2004. **55**(401): p. 1283-1292.

30. Kredich, N.M. and G.M. Tomkins, *The Enzymic Synthesis of l-Cysteine in Escherichia coli and Salmonella typhimurium.* Journal of Biological Chemistry, 1966. **241**(21): p. 4955-4965.

31. Sekowska, A., H.F. Kung, and A. Danchin, *Sulfur metabolism in Escherichia coli and related bacteria: facts and fiction.* J Mol Microbiol Biotechnol, 2000. **2**(2): p. 145-77.

32. Py, B. and F. Barras, *Building Fe-S proteins: bacterial strategies.* Nat Rev Microbiol, 2010. **8**(6): p. 436-46.

33. Zheng, L., et al., *Assembly of iron-sulfur clusters. Identification of an iscSUA-hscBA-fdx gene cluster from Azotobacter vinelandii.* J Biol Chem, 1998. **273**(21): p. 13264-72.

34. Schwartz, C.J., et al., *IscR, an Fe-S cluster-containing transcription factor, represses expression of Escherichia coli genes encoding Fe-S cluster assembly proteins.* Proc Natl Acad Sci U S A, 2001. **98**(26): p. 14895-900.

35. Takahashi, Y. and U. Tokumoto, *A third bacterial system for the assembly of iron-sulfur clusters with homologs in archaea and plastids.* J Biol Chem, 2002. **277**(32): p. 28380-3.

36. Allen, S.P., et al., *Two novel heat shock genes encoding proteins produced in response to heterologous protein expression in Escherichia coli.* J. Bacteriol., 1992. **174**(21): p. 6938-6947.

37. Kitagawa, M., et al., *Escherichia coli small heat shock proteins, IbpA and IbpB, protect enzymes from inactivation by heat and oxidants.* European Journal of Biochemistry, 2002. **269**(12): p. 2907-2917.

38. Kuczynska-Wisnik, D., et al., *The Escherichia coli small heat-shock proteins IbpA and IbpB prevent the aggregation of endogenous proteins denatured in vivo during extreme heat shock.* Microbiology, 2002. **148**(6): p. 1757-1765.

39. Doyle, S.M. and S. Wickner, *Hsp104 and ClpB: protein disaggregating machines.* Trends in Biochemical Sciences, 2009. **34**(1): p. 40-48.

40. Squires, C.L., et al., *ClpB is the Escherichia coli heat shock protein F84.1.* J. Bacteriol., 1991. **173**(14): p. 4254-4262.

41. Genevaux, P., C. Georgopoulos, and W.L. Kelley, *The Hsp70 chaperone machines of Escherichia coli: a paradigm for the repartition of chaperone functions.* Molecular Microbiology, 2007. **66**(4): p. 840-857.

42. Skowyra, D., C. Georgopoulos, and M. Zylicz, *The E. coli dnaK gene product, the hsp70 homolog, can reactivate heat-inactivated RNA polymerase in an ATP hydrolysis-dependent manner.* Cell, 1990. **62**(5): p. 939-44.

43. Chaudhuri, T.K., V.K. Verma, and A. Maheshwari, *GroEL assisted folding of large polypeptide substrates in Escherichia coli: Present scenario and assignments for the future.* Progress in Biophysics and Molecular Biology, 2009. **99**(1): p. 42-50.

44. Fayet, O., T. Ziegelhoffer, and C. Georgopoulos, *The groES and groEL heat shock gene products of Escherichia coli are essential for bacterial growth at all temperatures.* J. Bacteriol., 1989. **171**(3): p. 1379-1385.

45. Bardwell, J.C. and E.A. Craig, *Eukaryotic Mr 83,000 heat shock protein has a homologue in Escherichia coli.* Proceedings of the National Academy of Sciences of the United States of America, 1987. **84**(15): p. 5177-5181.

46. Thomas, J.G. and F. Baneyx, *ClpB and HtpG facilitate de novo protein folding in stressed Escherichia coli cells.* Molecular Microbiology, 2000. **36**(6): p. 1360-1370.

47. Kornitzer, D., et al., *Isolation, characterization, and sequence of an Escherichia coli heat shock gene, htpX.* J. Bacteriol., 1991. **173**(9): p. 2944-2953.

48. Jakob, U., et al., *Chaperone Activity with a Redox Switch.* Cell, 1999. **96**(3): p. 341-352.

49. Korber, P., et al., *A New Heat Shock Protein That Binds Nucleic Acids.* Journal of Biological Chemistry, 1999. **274**(1): p. 249-256.

50. Lilic, M., et al., *Identification of the CysB-regulated gene, hslJ, related to the Escherichia coli novobiocin resistance phenotype.* FEMS Microbiol Lett, 2003. **224**(2): p. 239-46.

51. Rohrwild, M., et al., *HslV-HslU: A novel ATP-dependent protease complex in Escherichia coli related to the eukaryotic proteasome.* Proceedings of the National Academy of Sciences of the United States of America, 1996. **93**(12): p. 5808-5813.

52. Vijayalakshmi, J., et al., *The 2.2 Å Crystal Structure of Hsp33: A Heat Shock Protein with Redox-Regulated Chaperone Activity.* Structure (London, England : 1993), 2001. **9**(5): p. 367-375.

53. Chung, C.H. and A.L. Goldberg, *The product of the lon (capR) gene in Escherichia coli is the ATP-dependent protease, protease La.* Proc Natl Acad Sci U S A, 1981. **78**(8): p. 4931-5.

54. Agafonov, D.E., et al., *A protein residing at the subunit interface of the bacterial ribosome.* Proceedings of the National Academy of Sciences of the United States of America, 1999. **96**(22): p. 12345-12349.

55. Hagenmaier, S., Y.D. Stierhof, and U. Henning, *A new periplasmic protein of Escherichia coli which is synthesized in spheroplasts but not in intact cells.* J. Bacteriol., 1997. **179**(6): p. 2073-2076.

56. Lamark, T., et al., *The complex bet promoters of Escherichia coli: regulation by oxygen (ArcA), choline (BetI), and osmotic stress.* J. Bacteriol., 1996. **178**(6): p. 1655-1662.

57. Gutierrez, C. and J.C. Devedjian, *Osmotic induction of gene osmC expression in Escherichia coli K12.* Journal of Molecular Biology, 1991. **220**(4): p. 959-973.

58. Rehse, P.H., et al., *Crystallographic Structure and Biochemical Analysis of the Thermus thermophilus Osmotically Inducible Protein C.* Journal of Molecular Biology, 2004. **338**(5): p. 959-968.

59. Bunch, P.K., et al., *The IdhA Gene Encoding the Fermentative Lactate Dehydrogenase of Escherichia Coli.* Microbiology, 1997. **143**(1): p. 187-195.

60. Banuett, F. and I. Herskowitz, *Identification of polypeptides encoded by an Escherichia coli locus (hflA) that governs the lysis-lysogeny decision of bacteriophage lambda.* J. Bacteriol., 1987. **169**(9): p. 4076-4085.

61. Caldas, T., et al., *The FtsJ/RrmJ Heat Shock Protein of Escherichia coli Is a 23 S Ribosomal RNA Methyltransferase.* Journal of Biological Chemistry, 2000. **275**(22): p. 16414-16419.

62. Møller, T., et al., *Hfq: A Bacterial Sm-like Protein that Mediates RNA-RNA Interaction.* Molecular cell, 2002. **9**(1): p. 23-30.

63. Zhang, A., et al., *The Sm-like Hfq Protein Increases OxyS RNA Interaction with Target mRNAs.* Molecular cell, 2002. **9**(1): p. 11-22.

64. Danese, P.N., et al., *The Cpx two-component signal transduction pathway of Escherichia coli regulates transcription of the gene specifying the stress-inducible periplasmic protease, DegP.* Genes & Development, 1995. **9**(4): p. 387-398.

65. De Wulf, P., O. Kwon, and E.C.C. Lin, *The CpxRA Signal Transduction System of Escherichia coli: Growth-Related Autoactivation and Control of Unanticipated Target Operons.* J. Bacteriol., 1999. **181**(21): p. 6772-6778.

66. Gustavsson, N., A. Diez, and T. Nyström, *The universal stress protein paralogues of Escherichia coli are co-ordinately regulated and co-operate in the defence against DNA damage.* Molecular Microbiology, 2002. **43**(1): p. 107-117.

67. Nachin, L., U. Nannmark, and T. Nystrom, *Differential Roles of the Universal Stress Proteins of Escherichia coli in Oxidative Stress Resistance, Adhesion, and Motility.* J. Bacteriol., 2005. **187**(18): p. 6265-6272.

68. Saveanu, C., et al., *Structural and nucleotide-binding properties of YajQ and YnaF, two Escherichia coli proteins of unknown function.* Protein Science, 2002. **11**(11): p. 2551-2560.

69. Grass, G., et al., *Linkage between catecholate siderophores and the multicopper oxidase CueO in Escherichia coli.* J Bacteriol, 2004. **186**(17): p. 5826-33.

70. Kittleson, J.T., et al., *Periplasmic metal-resistance protein CusF exhibits high affinity and specificity for both CuI and AgI.* Biochemistry, 2006. **45**(37): p. 11096-102.

71. Munson, G.P., et al., *Identification of a Copper-Responsive Two-Component System on the Chromosome of Escherichia coli K-12.* J. Bacteriol., 2000. **182**(20): p. 5864-5871.

72. Keseler, I.M., et al., *EcoCyc: a comprehensive view of Escherichia coli biology.* Nucleic Acids Res, 2009. **37**(Database issue): p. D464-70.

73. Eriani, G., et al., *Partition of tRNA synthetases into two classes based on mutually exclusive sets of sequence motifs.* Nature, 1990. **347**(6289): p. 203-206.

74. Cummings, H.S. and J.W. Hershey, *Translation initiation factor IF1 is essential for cell viability in Escherichia coli.* J. Bacteriol., 1994. **176**(1): p. 198-205.

75. Dubnoff, J.S. and U. Maitra, *Characterization of the Ribosome-dependent Guanosine Triphosphatase Activity of Polypeptide Chain Initiation Factor IF 2.* Journal of Biological Chemistry, 1972. **247**(9): p. 2876-2883.

76. Capecchi, M.R. and H.A. Klein, *Release factors mediating termination of complete proteins.* Nature, 1970. **226**(5250): p. 1029-33.

77. Bishop, A.C., et al., *Identification of the tRNA-Dihydrouridine Synthase Family.* Journal of Biological Chemistry, 2002. **277**(28): p. 25090-25095.

78. Okamoto, S., et al., *Loss of a conserved 7-methylguanosine modification in 16S rRNA confers low-level streptomycin resistance in bacteria.* Molecular Microbiology, 2007. **63**(4): p. 1096-1106.

79. Romanowski, M.J., J.B. Bonanno, and S.K. Burley, *Crystal structure of the Escherichia coli glucose-inhibited division protein B (GidB) reveals a methyltransferase fold.* Proteins: Structure, Function, and Bioinformatics, 2002. **47**(4): p. 563-567.

80. Esberg, B., et al., *Identification of the miaB Gene, Involved in Methylthiolation of Isopentenylated A37 Derivatives in the tRNA of Salmonella typhimurium and Escherichia coli.* J. Bacteriol., 1999. **181**(23): p. 7256-7265.

81. Elseviers, D., L.A. Petrullo, and P.J. Gallagher, *Novel E. coli mutants deficient in blosynthesis of 5-methylamlnomethyl-2-thiouridine.* Nucleic Acids Research, 1984. **12**(8): p. 3521-3534.

82. Kambampati, R. and C.T. Lauhon, *MnmA and IscS Are Required for in Vitro 2-Thiouridine Biosynthesis in Escherichia coli.* Biochemistry, 2003. **42**(4): p. 1109-1117.

83. Sergiev, P.V., et al., *Identification of Escherichia coli m2G methyltransferases: II. The ygjO Gene Encodes a Methyltransferase Specific for G1835 of the 23 S rRNA.* Journal of Molecular Biology, 2006. **364**(1): p. 26-31.

84. Sergiev, P.V., et al., *The ybiN Gene of Escherichia coli Encodes Adenine-N6 Methyltransferase Specific for Modification of A1618 of 23 S Ribosomal RNA, a Methylated Residue Located Close to the Ribosomal Exit Tunnel.* Journal of Molecular Biology, 2008. **375**(1): p. 291-300.

85. Toh, S.M., et al., *The methyltransferase YfgB/RlmN is responsible for modification of adenosine 2503 in 23S rRNA.* RNA, 2008. **14**(1): p. 98-106.

86. Anderson, M.S., C.E. Bulawa, and C.R. Raetz, *The biosynthesis of gram-negative endotoxin. Formation of lipid A precursors from UDP-GlcNAc in extracts of Escherichia coli.* Journal of Biological Chemistry, 1985. **260**(29): p. 15536-15541.

87. Yoshimura, M., T. Oshima, and N. Ogasawara, *Involvement of the YneS/YgiH and PlsX proteins in phospholipid biosynthesis in both Bacillus subtilis and Escherichia coli.* BMC Microbiology, 2007. **7**(1): p. 69.

88. Kita, K., K. Konishi, and Y. Anraku, *Terminal oxidases of Escherichia coli aerobic respiratory chain. I. Purification and properties of cytochrome b562-o complex from cells in the early exponential phase of aerobic growth.* Journal of Biological Chemistry, 1984. **259**(5): p. 3368-3374.

89. Matsushita, K., T. Ohnishi, and H.R. Kaback, *NADH-ubiquinone oxidoreductases of the Escherichia coli aerobic respiratory chain.* Biochemistry, 1987. **26**(24): p. 7732-7.

90. Liu, X. and P. Matsumura, *The FlhD/FlhC complex, a transcriptional activator of the Escherichia coli flagellar class II operons.* J. Bacteriol., 1994. **176**(23): p. 7345-7351.

91. Kuo, S.C. and D.E. Koshland, Jr., *Sequence of the flaA (cheC) locus of Escherichia coli and discovery of a new gene.* J. Bacteriol., 1986. **166**(3): p. 1007-1012.

92. Yamamoto, K. and A. Ishihama, *Transcriptional Response of Escherichia coli to External Zinc.* J. Bacteriol., 2005. **187**(18): p. 6333-6340.

93. Yang, R., *Personnal Communication*. 2010.

94. Vickery, H.B. and C.S. Leavenworth, *THE BEHAVIOR OF CYSTINE WITH SILVER SALTS.* Journal of Biological Chemistry, 1930. **86**(1): p. 129-143.

95. Sundberg, R.J. and R.B. Martin, *Interactions of histidine and other imidazole derivatives with transition metal ions in chemical and biological systems.* Chemical Reviews, 1974. **74**(4): p. 471-517.

96. Carmona-Saez, P., et al., *GENECODIS: a web-based tool for finding significant concurrent annotations in gene lists.* Genome Biol, 2007. **8**(1): p. R3.

97. Nogales-Cadenas, R., et al., *GeneCodis: interpreting gene lists through enrichment analysis and integration of diverse biological information.* Nucleic Acids Res, 2009. **37**(Web Server issue): p. W317-22.

98. Arsene, F., T. Tomoyasu, and B. Bukau, *The heat shock response of Escherichia coli.* Int J Food Microbiol, 2000. **55**(1-3): p. 3-9.

99. Hightower, L.E., *A brief perspective on the heat-shock response and stress proteins.* Marine Environmental Research, 1993. **35**(1-2): p. IN1-IN2, 79-83.

100. Ahamed, M., et al., *Silver nanoparticles induced heat shock protein 70, oxidative stress and apoptosis in Drosophila melanogaster.* Toxicology and Applied Pharmacology, 2009. **242**(3): p. 263-269.

101. Roh, J.-y., et al., *Ecotoxicity of Silver Nanoparticles on the Soil Nematode Caenorhabditis elegans Using Functional Ecotoxicogenomics.* Environmental Science & Technology, 2009. **43**(10): p. 3933-3940.

102. Morita, M., et al., *Heat-Induced Synthesis of sigma 32 in Escherichia coli: Structural and Functional Dissection of rpoH mRNA Secondary Structure.* J. Bacteriol., 1999. **181**(2): p. 401-410.

103. Bukau, B., *Regulation of the Escherichia coli heat-shock response.* Molecular Microbiology, 1993. **9**(4): p. 671-680.

104. Tyedmers, J., A. Mogk, and B. Bukau, *Cellular strategies for controlling protein aggregation.* Nat Rev Mol Cell Biol, 2010. **11**(11): p. 777-788.

105. Batchelor, E., et al., *The Escherichia coli CpxA-CpxR Envelope Stress Response System Regulates Expression of the Porins OmpF and OmpC.* J. Bacteriol., 2005. **187**(16): p. 5723-5731.

106. Yamamoto, K. and A. Ishihama, *Characterization of copper-inducible promoters regulated by CpxA/CpxR in Escherichia coli.* Biosci Biotechnol Biochem, 2006. **70**(7): p. 1688-95.

107. Cecchini, G., et al., *Variation in proton donor/acceptor pathways in succinate:quinone oxidoreductases.* FEBS Letters, 2003. **545**(1): p. 31-38.

108. Jordan, P.A., et al., *Biochemical and spectroscopic characterization of Escherichia coli aconitases (AcnA and AcnB).* Biochem. J., 1999. **344**(3): p. 739-746.

109. Varghese, S., Y. Tang, and J.A. Imlay, *Contrasting Sensitivities of Escherichia coli Aconitases A and B to Oxidation and Iron Depletion.* J. Bacteriol., 2003. **185**(1): p. 221-230.

110. Raymond, K.N., E.A. Dertz, and S.S. Kim, *Enterobactin: An archetype for microbial iron transport.* Proceedings of the National Academy of Sciences of the United States of America, 2003. **100**(7): p. 3584-3588.

111. Althaus, E.W., et al., *The ferric uptake regulation (Fur) repressor is a zinc metalloprotein.* Biochemistry, 1999. **38**(20): p. 6559-69.

112. Bagg, A. and J.B. Neilands, *Ferric uptake regulation protein acts as a repressor, employing iron (II) as a cofactor to bind the operator of an iron transport operon in Escherichia coli.* Biochemistry, 1987. **26**(17): p. 5471-7.

113. Escolar, L., J. Perez-Martin, and V. de Lorenzo, *Opening the iron box: transcriptional metalloregulation by the Fur protein.* J Bacteriol, 1999. **181**(20): p. 6223-9.

114. Hantke, K., *Regulation of ferric iron transport in Escherichia coli K12: isolation of a constitutive mutant.* Mol Gen Genet, 1981. **182**(2): p. 288-92.

115. Stojiljkovic, I. and K. Hantke, *Functional domains of the Escherichia coli ferric uptake regulator protein (Fur).* Mol Gen Genet, 1995. **247**(2): p. 199-205.

116. Kim, S., et al., *Oxidative stress-dependent toxicity of silver nanoparticles in human hepatoma cells.* Toxicology in Vitro, 2009. **23**(6): p. 1076-1084.

117. Choi, J.E., et al., *Induction of oxidative stress and apoptosis by silver nanoparticles in the liver of adult zebrafish.* Aquatic Toxicology, 2010. **100**(2): p. 151-159.

118. Pomposiello, P.J. and B. Demple, *Redox-operated genetic switches: the SoxR and OxyR transcription factors.* Trends in Biotechnology, 2001. **19**(3): p. 109-114.

119. Gaudu, P., N. Moon, and B. Weiss, *Regulation of the soxRS Oxidative Stress Regulon.* Journal of Biological Chemistry, 1997. **272**(8): p. 5082-5086.

120. Hidalgo, E., H. Ding, and B. Demple, *Redox Signal Transduction: Mutations Shifting [2Fe-2S] Centers of the SoxR Sensor-Regulator to the Oxidized Form.* Cell, 1997. **88**(1): p. 121-129.

121. Martin, R.G., et al., *Analysis of Microarray Data for the marA, soxS, and rob Regulons of Escherichia coli*, in *Methods in Enzymology*. 2003, Academic Press. p. 278-280.

122. Nunoshiba, T., et al., *Two-stage control of an oxidative stress regulon: the Escherichia coli SoxR protein triggers redox-inducible expression of the soxS regulatory gene.* J. Bacteriol., 1992. **174**(19): p. 6054-6060.

123. Haber, F., Weiss, J., *On the catalysis of hydroperoxide.* Naturwissenschaften, 1932. **20**: p. 948-950.

124. Srivastava, A.K. and D. Schlessinger, *Mechanism and Regulation of Bacterial Ribosomal RNA Processing.* Annual Review of Microbiology, 1990. **44**(1): p. 105-129.

125. Li, C., et al., *Adverse conditions which cause lack of flagella in Escherichia coli.* Journal of bacteriology, 1993. **175**(8): p. 2229-35.

126. Shi, W., et al., *Mechanism of adverse conditions causing lack of flagella in Escherichia coli.* J. Bacteriol., 1993. **175**(8): p. 2236-2240.

127. Rosenkranz, H.S. and H.S. Carr, *Silver sulfadiazine: effect on the growth and metabolism of bacteria.* Antimicrob Agents Chemother, 1972. **2**(5): p. 367-72.

128. Sondi, I. and B. Salopek-Sondi, *Silver nanoparticles as antimicrobial agent: a case study on E. coli as a model for Gram-negative bacteria.* J Colloid Interface Sci, 2004. **275**(1): p. 177-82.

129. Buckler, D.R., G.S. Anand, and A.M. Stock, *Response-regulator phosphorylation and activation: a two-way street?* Trends Microbiol, 2000. **8**(4): p. 153-6.

130. Stock, A.M., V.L. Robinson, and P.N. Goudreau, *Two-component signal transduction.* Annu Rev Biochem, 2000. **69**: p. 183-215.

131. Bonnefoy, V. and J.A. Demoss, *Nitrate reductases in Escherichia coli.* Antonie Van Leeuwenhoek, 1994. **66**(1-3): p. 47-56.

# Chapter 6: The Antibacterial Effects of ZnO Nanoparticles

## 6.1. Introduction

Zinc oxide is produced in high tonnage, approximately $10^5$ tonnes annually [1], including zinc oxide nanoparticles that have an anti-bacterial efficacy against Gram positive and Gram negative bacteria [2-8] and are used for the production of anti-bacterial fabrics [9] and orthopaedic cements [10-12].

As reported in the two previous chapters, dissolution is one mode of nanoparticle toxicity; however the ZnO nanoparticle, in addition to $Zn^{2+}$ toxicity resulting from dissolution [2-8], has a nanoparticle-specific photo-electron generation mechanism. This is postulated to induce redox toxicity in the metabolism of *E. coli*, thus augment the metal ion toxic effects.

Zinc ions are essential for metabolism in *E. coli*, present in approximately 3% of the proteins as a structural co-factor, including members of all 6 functional classes of enzymes [13-19]. Paradoxically, excess free $Zn^{2+}$ is toxic; it may compete for divalent metal ion coordination sites on proteins, thus impeding cellular processes. Additionally, the material has a direct band gap of 3.37 electron Volts (eV) corresponding to 375 nm within the UV portion of the electromagnetic spectrum, Figure 6.1. Therefore, conduction band electrons may be available in UV light to redox-active species in the medium and may lead to the formation of free radicals.

In this study, the anti-bacterial effects of an industrial grade ZnO nanopowder were tested against *E. coli* K12. First, the anti-bacterial efficacy of the zinc oxide nanopowder was tested in the dark, where the primary mode of toxicity is expected to be from the release of zinc ions.

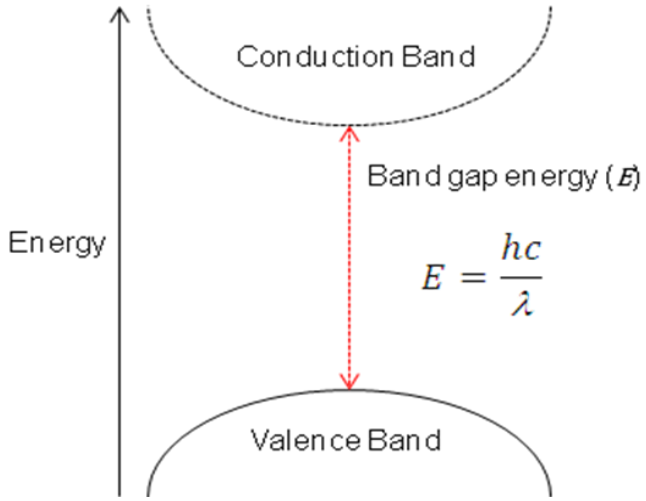


**Figure 6.1. Band gap energy for ZnO. The minimum energy required to excite an electron in the valence band to the conduction band for ZnO is 3.37 eV. This is equivalent to electromagnetic radiation with a wavelength of 375 nm. Where *E* is the band gap energy, *h* is Planck's constant, *c* is the speed of light in a vacuum and $\lambda$ is the wavelength of light.**

The rate of dissolution was characterised using ICP-MS, and the efficacy of the nanoparticles was compared with zinc ions, at the concentration that was determined to have been released from the nanoparticles. Additionally, the transcriptional response to $Zn^{2+}$ was measured quantitatively using real-time PCR. This determined the regulation of genes that encode specific transport proteins for moving zinc ions, and other di-valent metal ions including $Cd^{2+}$ and $Pb^{2+}$, across the plasma membrane. Zinc ions are moved across the cell envelope in both directions, enabling the cell to maintain an optimal concentration in the cytosol. The primary $Zn^{2+}$ importer is an ABC (ATP-binding cassette) family member [20], ZnuABC [21, 22], which is regulated through the activity of the Zinc Uptake Regulator (Zur), a Fur family member transcription factor [23, 24]. The primary $Zn^{2+}$ exporter is a P-Type ATPase, ZntA [25-28] which is regulated through the activity of ZntR, a MerR family member [29-31]. These genes are inversely regulated in response to femtomolar changes in the free $Zn^{2+}$ concentration in the cytosol [23].

Second, the photo-redox toxicity of the nanoparticles was tested under ultra violet light where photo-electron production is postulated to result in the formation of free radicals, inducing redox stress within the metabolism. The presence of reactive species of oxygen, specifically the superoxide radical and hydrogen peroxide was determined by measuring the expression of genes within the OxyR and SoxRS regulons, which control the cellular level response [32]. The OxyR and SoxR proteins are redox-dependant protein switches that regulate the expression of genes to counteract oxidative stress in response to hydrogen peroxide or superoxide radicals respectively. The OxyR protein is synthesised constitutively in the cytosol and forms an inactive tetramer. In response to $H_2O_2$ the complex undergoes structural re-arrangement through inter-molecular di-sulphide bond formation between redox active cysteine residues [33, 34]. The active complex may regulate the expression of at least 32 genes including *katG*; a homo-tetrameric enzyme that catalyses the reaction $2H_2O_2 \rightarrow O_2 + 2H_2O$ ($K_M$ = 4.2 mM at pH 7) [35]. SoxR is activated by superoxide after oxidation of redox-sensitive Fe-S clusters. Active SoxR promotes transcription of a second transcription factor, SoxS, which may regulate the expression of up to 47 genes, including anti-oxidant systems such as the superoxide dismutases, which catalyse the dismutation of the superoxide radical [32].

The two toxicity-mechanism hypotheses are tested by monitoring the anti-bacterial effects and the regulation of genes by real-time PCR in an investigation analogous to the study of silver nanoparticles in Chapter 4. These findings may benefit the understanding of how zinc oxide nanomaterials can be used as anti-bacterial agents, and the potential ecotoxicological effects from release of the material into the environment.

## 6.2. Results

### 6.2.1. Nanoparticle Characterisation

Z-COTE® is an industrial grade zinc oxide nanopowder, hereinafter referred to as 'zinc oxide nanopowder'. After suspension in water the nanopowder was observed under a transmission electron microscope (TEM), indicating that the nanoparticles had a polyhedral, irregular morphology and a wide size distribution, Figure 6.2. The nanoparticles were between 10 and 350 nm across. This was inconsistent with the manufacturers' specifications, which indicated that the nanoparticles were less than 200 nm.

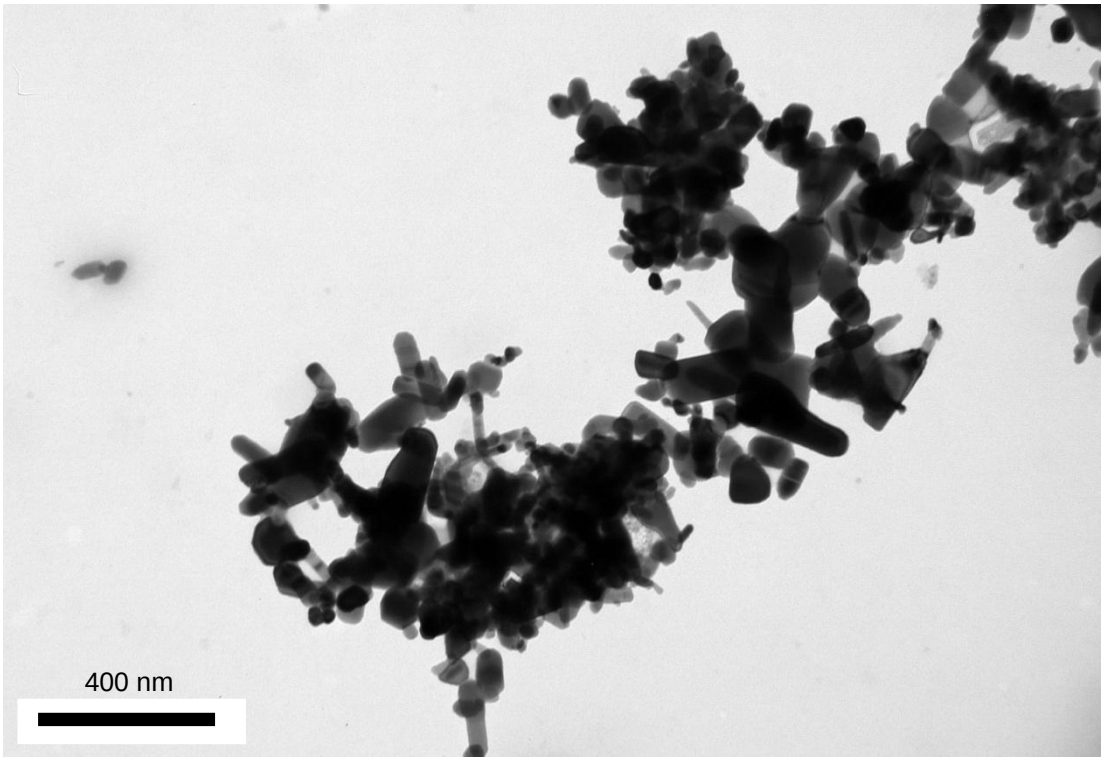


**Figure 6.2. TEM image of the zinc oxide nanoparticles. The nanoparticles had an irregular, polyhedral morphology and a large size distribution (10-350 nm across).**

The elemental composition of the nanopowder was determined using a scanning electron microscope (SEM) coupled with an energy dispersive X-ray analyser. The nanopowder was composed of zinc and oxygen with no other elements detected.

The nanoparticles formed a white, semi-opaque suspension, which had a characteristic UV-Visible absorbance spectrum with $\lambda_{max}$ at 375 nm, representing the material band gap. The absorption of UV light was proportional to the concentration of nanoparticles suspended in the medium, Figure 6.3. The $\lambda_{max}$ did not change over 24 hours, indicating that the suspension was colloidal for this period of time, Figure 6.4.

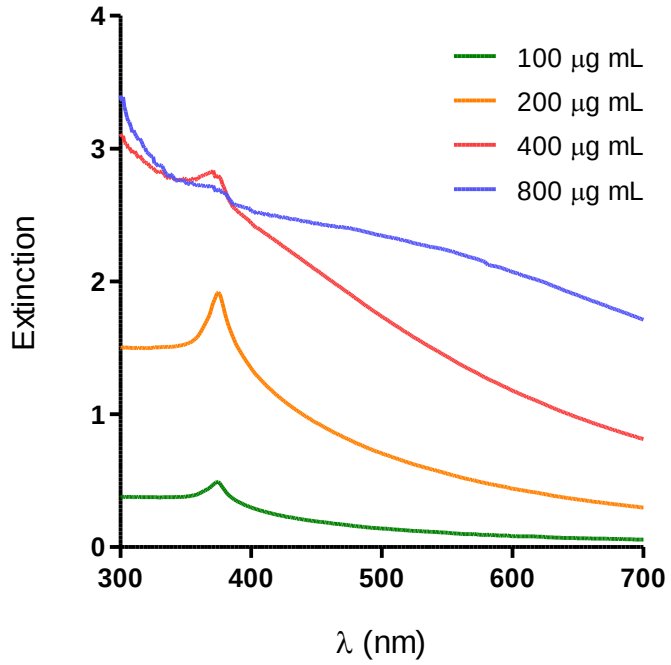


**Figure 6.3. UV-visible extinction spectra for the zinc oxide nanoparticles suspended in the minimal salts medium. The nanoparticle suspensions absorb ultraviolet and blue visible light. The dispersions had a $\lambda_{max}$ at 375 nm, which corresponds to the band gap energy of the material.**

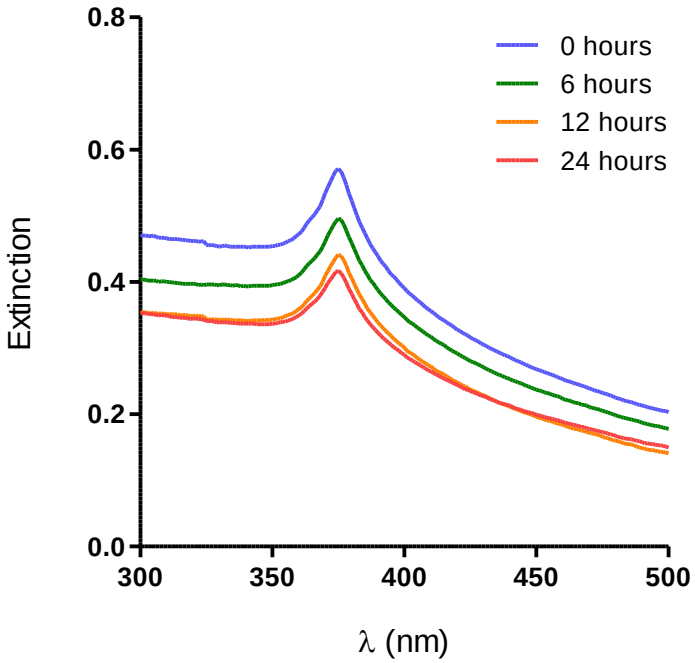


**Figure 6.4. The extinction spectrum of a colloidal suspension of the zinc oxide nanoparticles at a concentration of 100 µg/mL over 24 hours.**

### 6.2.2. Dissolution in Minimal Salts Medium

ICP-MS was carried out in standard mode with external calibration using Zn standard solutions and Rh as an internal standard. The results obtained using any of the Zn isotopes were in good agreement, thus only the data obtained by measuring the most abundant isotope, $^{64}$Zn, is presented in Figure 6.5. Each sample was measured 5 times and the reported values are the mean of 2 independent experiments, which were consistent. The relative standard deviation (RSD) was between 0.26 % and 2.22 % at each time point.

The background concentration of Zn in the minimal salts medium was 0.227 µg/mL. The bulk solution phase Zn concentration was 46.86 ± 0.74 µg/mL after suspension of the nanoparticles. Therefore, approximately 58 % of the zinc mass was detected in the bulk solution phase during the suspension protocol. Subsequently, concentration of zinc in the medium increased to 50.24 ± 0.34 µg/mL over 4 hours. The amount of Zn lost during

sample processing (for example where Zn cations electrostatically adhere to the charged surfaces on glassware) was determined by measuring solutions of zinc chloride that underwent the same procedure. Recovery from 2 independent controls was approximately 100 %.

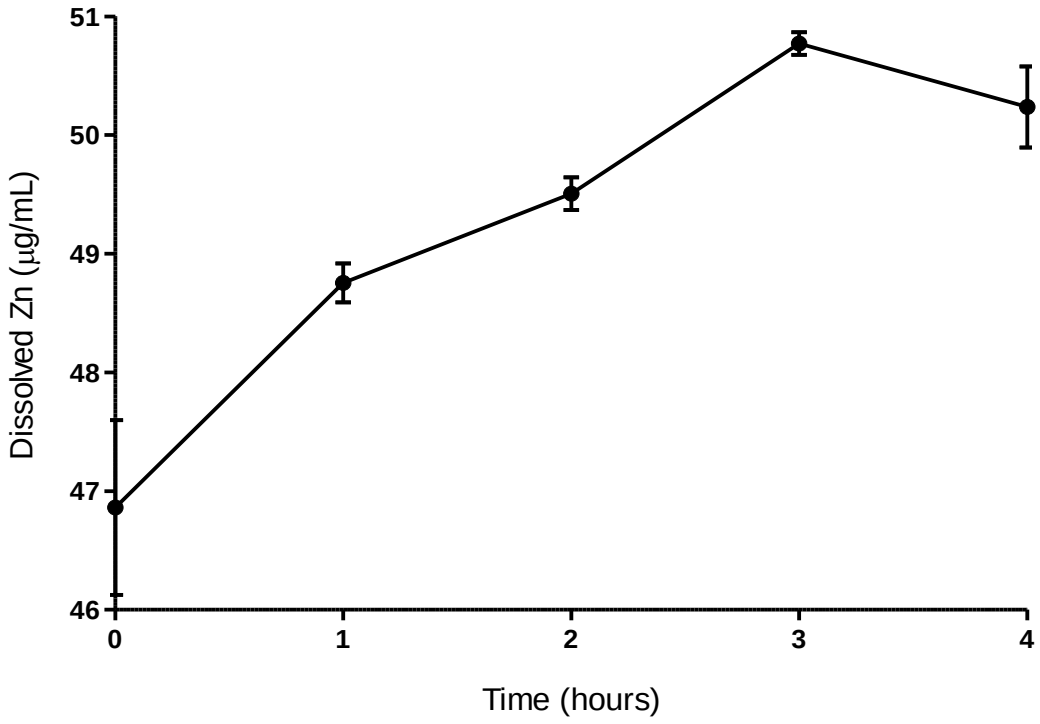


**Figure 6.5 The estimated rate of dissolution of the zinc oxide nanoparticles in minimal salts medium. Zinc oxide nanoparticles were suspended in the medium at a concentration of 100 µg/mL, increasing the concentration of the bulk solution phase Zn to a maximum of 50.77 ± 0.10 µg/mL after 3 hours. The error bars are the standard error of the mean (n=2).**

### 6.2.3. Anti-Bacterial Efficacy of Zinc Oxide Nanoparticles in the Dark

The physical *E. coli*-ZnO nanoparticle interactions were imaged using TEM. Cells were collected by gentle centrifugation from a suspension of the bacteria and nanoparticles in the minimal salts medium. Subsequently the cells were washed very gently so as to avoid displacing any associated nanoparticles by placing the specimen grids onto a droplet of glutaraldehyde fixative and then onto sequential drops of water. This minimal preparative procedure was adopted because TEM images prepared from bacterial sections, following the same procedure as described in Chapters 3 and 4, were absent any nanoparticles (not shown). The cells prepared using the minimal preparation appeared as shown in Figure 6.6.

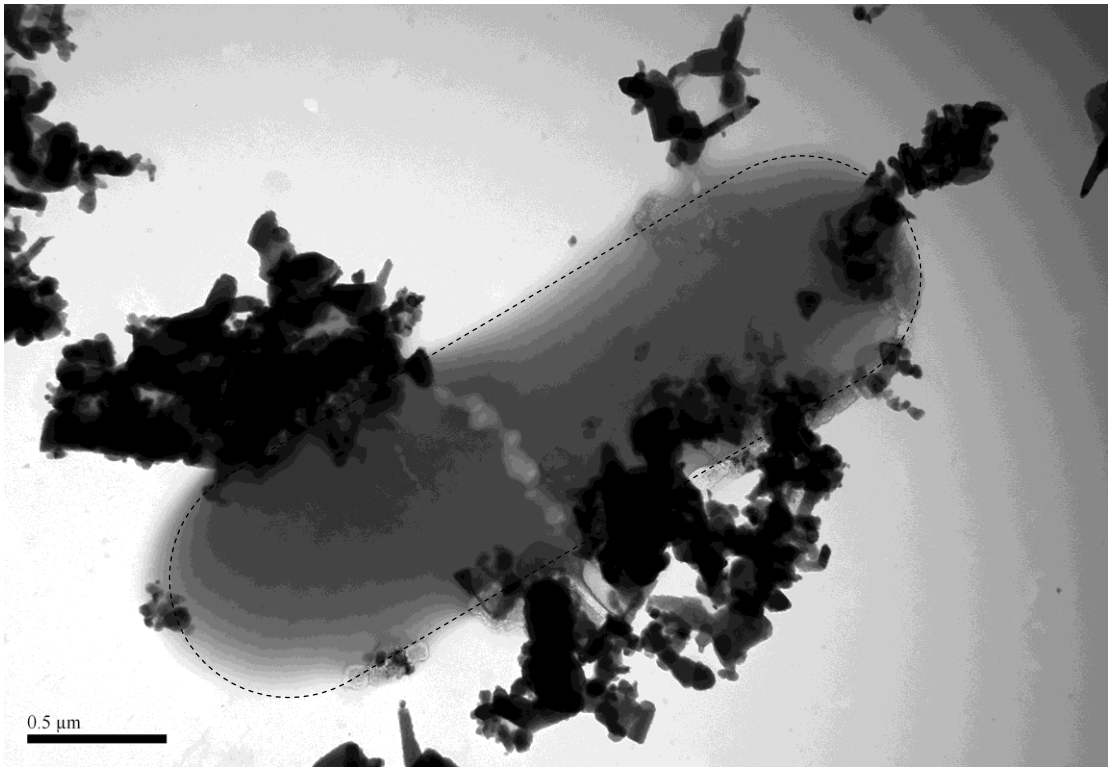


**Figure 6.6. TEM image of *E. coli* (dotted outline) after exposure to ZnO nanoparticles following minimal, non-disruptive specimen preparation.**

For toxicity testing the *E. coli* bacteria were cultured in a minimal salts medium until the mid-exponential phase of the growth curve, which had been determined beforehand (data not shown). Subsequently, the culture was mixed (1:1, vol:vol) with a suspension of zinc oxide nanoparticles, in sterile medium, or the culture was mixed with sterile medium to which $Zn^{2+}$ was added at a pre-determined rate to mimic the rate of nanoparticle dissolution. Bacterial growth and replication was measured by colony forming units, Figure 6.7.

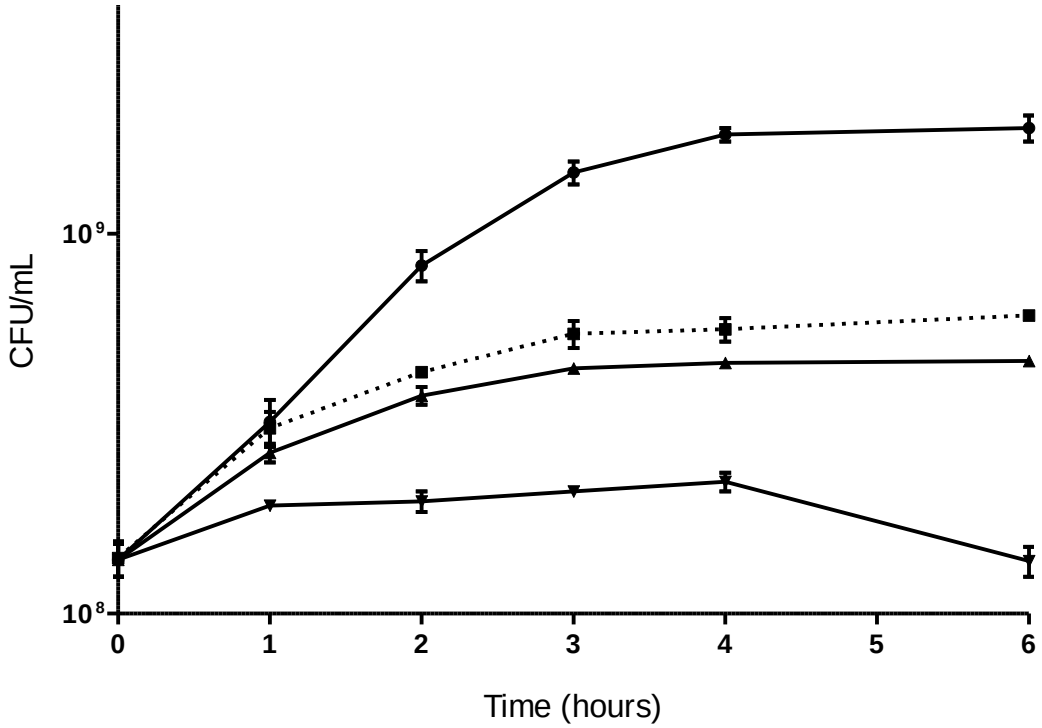


**Figure 6.7. Growth and replication of *E. coli* in the minimal salts medium containing zinc oxide nanoparticles or zinc ions. Exponentially replicating cultures were mixed (1:1, vol:vol) with sterile medium (●), sterile medium containing a suspension of zinc oxide nanoparticles (100 µg/mL: ▲ or 200 µg/mL: ▼), or sterile medium that was augmented with $Zn^{2+}$ at the estimated rate of dissolution for 100 µg/mL of the nanoparticles (■). The error bars are the standard error of the mean (n=3).**

The zinc oxide nanoparticles reduced the rate of bacterial replication in comparison to the control. If the cultures were augmented with $Zn^{2+}$ at the estimated rate of nanoparticle dissolution, the effect on colony forming units was slightly less in comparison to adding the nanoparticles. This is consistent with the data from silver nanoparticles in Chapter 4, *i.e.* the nanoparticles have a greater inhibitory effect on the bacteria than the ion as a function of the bulk solution phase ion concentration.

A zinc-sensitive mutant, *ΔzntA*, was constructed from *E. coli* K12 strain MG1655. This confirmed that the observed inhibitory effects of the zinc oxide nanoparticles involved the release of $Zn^{2+}$. The mutant did not possess a gene that encodes a P-Type ATPase, ZntA, which exports excess $Zn^{2+}$ from the cytosol. Accordingly, it was found that the mutant was more sensitive to $Zn^{2+}$ as the chloride, compared to the parent strain. The mutant was also more sensitive to the zinc oxide nanoparticles, compared to the parent strain, indicating that they release $Zn^{2+}$ into the medium, Figure 6.8.

The $Zn^{2+}$ dependant toxic effects of the zinc oxide nanopowder were investigated further by measuring the transcript levels of $Zn^{2+}$-responding genes during exposure to the zinc oxide nanoparticles, or zinc ions, in comparison to a control (bacteria in minimal salts medium without additional zinc). These genes were chosen based upon published work where their expression has been shown to change with increasing levels of $Zn^{2+}$ [21, 24, 28-30]. The bacteria were mixed with a dispersion of the nanopowder to a final concentration of 100 µg/mL, or with zinc ions at a concentration that was determined to have been released from the nanoparticles. After 10 minutes the cultures were harvested and gene expression was measured quantitatively using real-time PCR, Figure 6.9. The transcriptional response was found to be pronounced during exposure to the zinc oxide nanoparticles compared to the equivalent concentration of bulk solution phase $Zn^{2+}$.

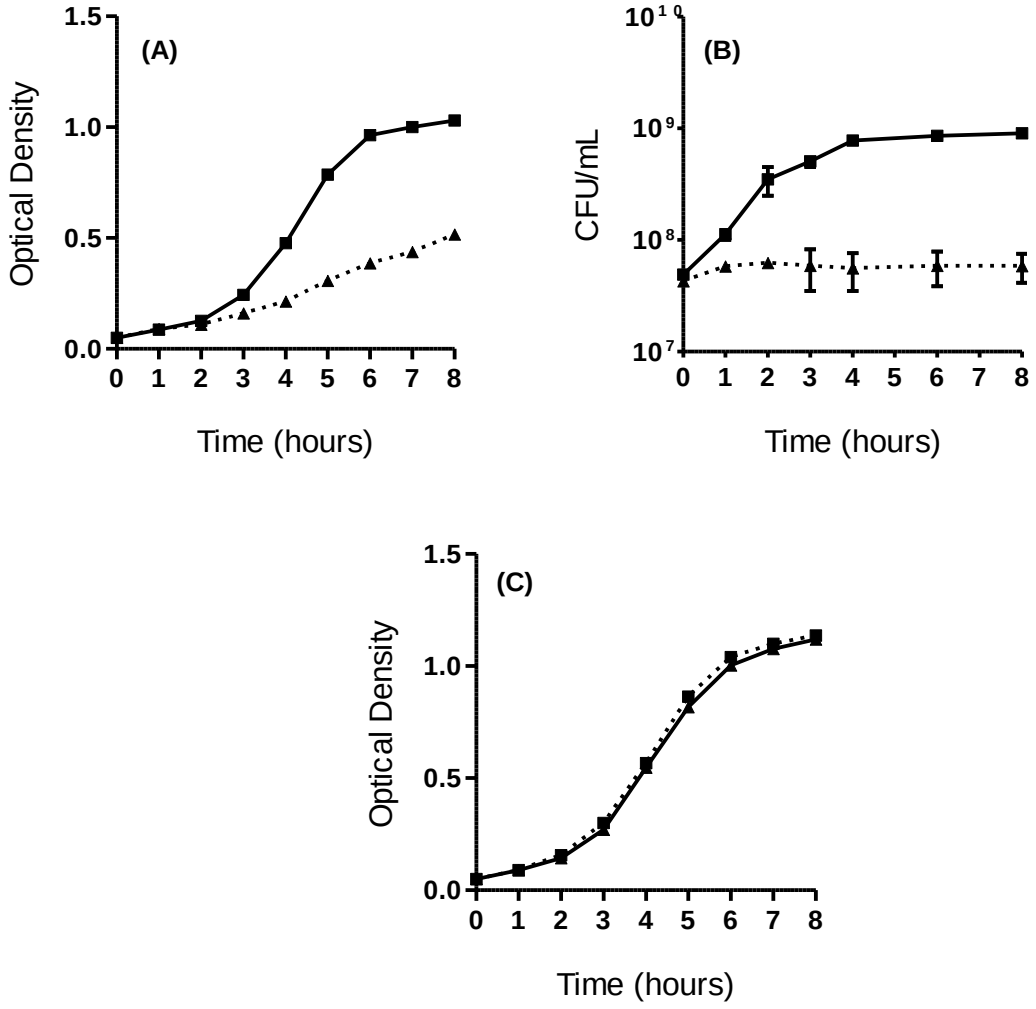


**Figure 6.8. Growth curves for *E. coli* strain MG1655 (■) and MG1655*ΔzntA* (▲) in the minimal salts medium, with 10 µg/mL of $Zn^{2+}$ (A) or 100 µg/mL of the zinc oxide nanoparticles (B). The strains grew and replicated at the same rate in the minimal salts medium without additional Zn (C). The error bars, where visible, are the standard error of the mean (n=3).**

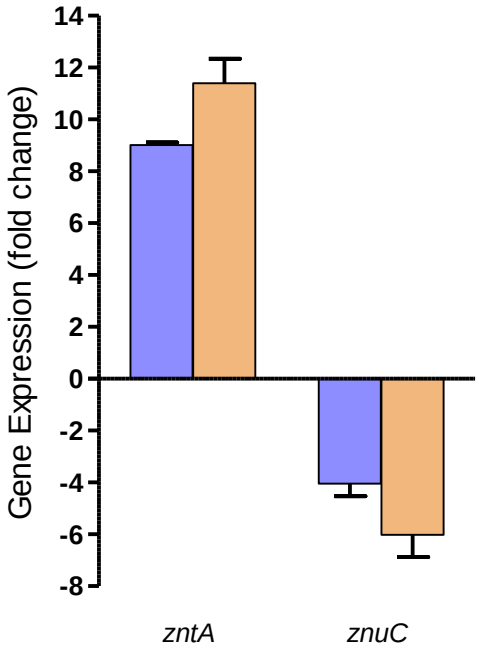


**Figure 6.9. Transcript abundance zinc ion transporter genes in *E. coli* K12 during exposure to zinc chloride, or zinc oxide nanoparticles, at 37°C, aerobically in minimal salts medium. Transcript levels are compared to a control, without additional Zn, and the data is normalised using *rrsB* as an internal reference. The error bars are the standard error of the mean (n=3).**

### 6.2.4. Anti-Bacterial Efficacy of Zinc Oxide Nanoparticles in Ultra Violet light

DCPIP is a redox-sensitive dye which forms a dark blue solution. When reduced by 2 electrons it forms a colourless solution, Figure 6.10.

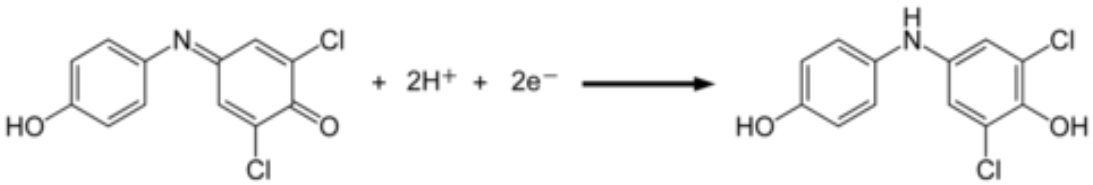


**Figure 6.10. The redox sensitive dye, 2,6-dichlorophenolindolphenol (DCPIP) in the oxidised state forms a blue solution. The molecule may be reduced by photo-electrons produced from the ZnO nanoparticles with a well defined stoichiometry: one molecule requiring 2 electrons, turning the solution colourless.**

The redox state of DCPIP in a suspension of zinc oxide nanoparticles in water was investigated in the dark and in ultra violet light (375 nm), corresponding to the band gap energy of zinc oxide. The suspension of nanoparticles shows the blue colour of the DCPIP, which is not reduced by the ZnO nanoparticles without photo-exposure. The suspension became colourless in UV light, but not in the dark, indicating that the DCPIP was being reduced. A UV only control (no ZnO) did not cause a colour change indicating that no detectable photo-bleaching of the DCPIP took place, and the reaction was revesible; the nanoparticle suspensions eventually becoming blue after the UV source was removed. The colour of the solution was measured as a function of the optical density at 595 nm over 220 minutes, Figure 6.11. The rate of reduction was dependent upon the medium in which the nanoparticles were suspended. In the minimal salts medium the DCPIP was not observed to be reduced. Conversely, in 0.1 % (w/v) glucose solution, the rate of DCPIP reduction was observed to be more rapid than in water, Figure 6.12.

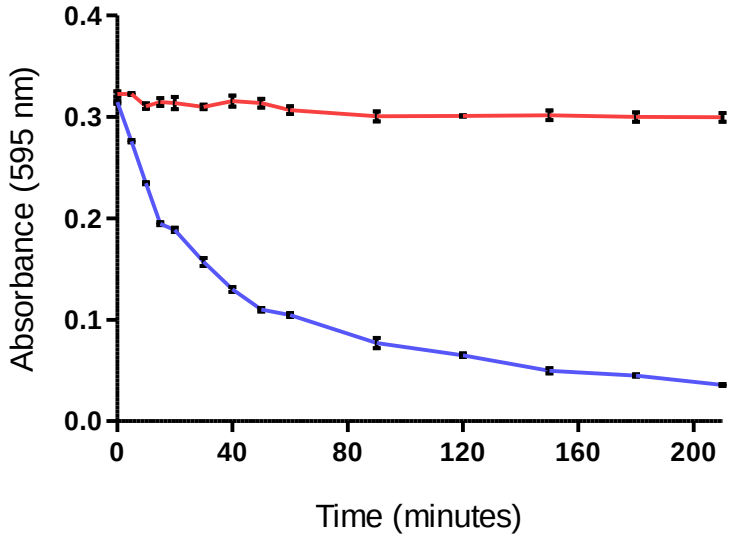


**Figure 6.11 The reduction of the redox-sensitive dye, DCPIP, by zinc oxide nanoparticles under UV light. The absorbance of the suspension at 595 nm was measured in the dark (red) and in UV (375 nm) light (blue). The absorbance is related to the oxidation state of the DCPIP, which becomes colourless when reduced by 2 electrons (inset). The error bars are the standard error of the mean (n=3).**

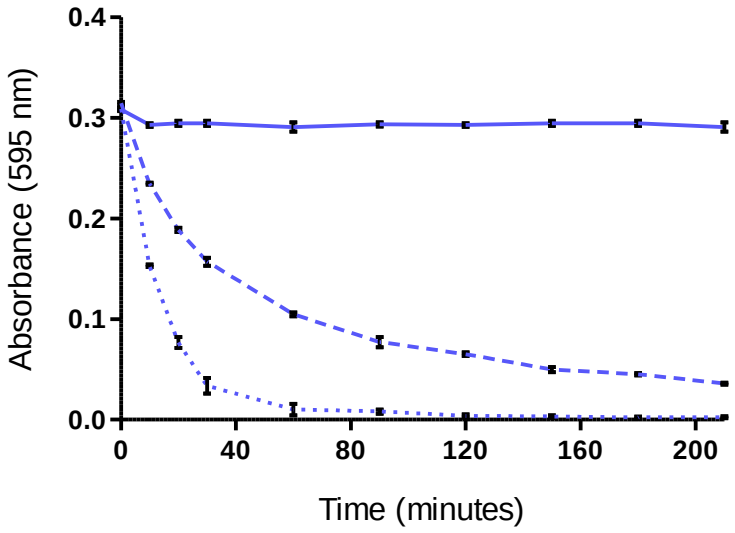


**Figure 6.12. DCPIP was added to a suspension of zinc oxide nanoparticles in water (dashed line), in minimal salts medium (solid line) or in 0.1 % (w/v) glucose solution (dotted line). The absorbance of the suspension at 595 nm was measured over 220 minutes in UV (375 nm) light. The error bars are the standard error of the mean (n=3).**

The survival of *E. coli* K12 in a suspension of the nanoparticles, in water, was determined by measuring colony forming units over time. This was performed in the dark, and in UV light (375 nm), Figure 6.13. Suspension of the bacteria in water, with or without UV, did not change the number of colony forming units detected over 2 hours. However, suspension with the ZnO nanoparticles reduced the bacterial survival to approximately 5% after an hour and to less than 1% by the end of the experiment. This loss in viability was enhanced in UV light where the bacterial survival was approximately 2% after an hour and less than 0.2 % after 2 hours.

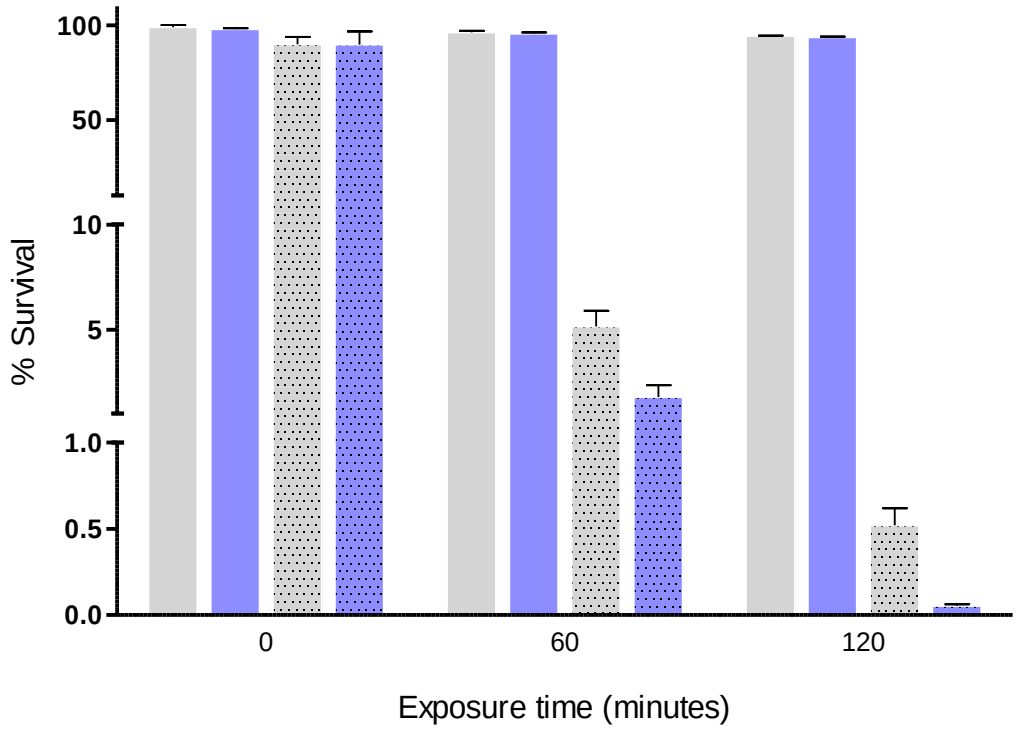


**Figure 6.13. *E. coli* were added to water in the dark (grey bars), or with 375 nm UV light (blue bars). The shaded bars indicate the presence of zinc oxide nanoparticles. Survival was measured by colony forming units and is given as a percentage of the starting inoculum. The error bars are the standard error of the mean (n=3).**

Finally, exponentially replicating *E. coli* from a culture in the minimal salts medium were mixed with a suspension of the ZnO nanoparticles, also in the minimal salts medium, at a final concentration of 100 µg/mL. The cultures were either kept in the dark or under UV light (375 nm). Alternatively, for controls, *E. coli* were mixed with minimal salts medium without the nanoparticles, with or without UV light. The bacteria were harvested after 10 minutes of exposure. Gene expression was measured quantitatively using real-time PCR to determine the transcript abundance of genes that are known to respond to superoxide or hydrogen peroxide, Figure 6.14. Two genes, *soxS* and *katG* were expressed at higher levels in the *E. coli* that had been treated with the ZnO nanoparticles in UV light than in those that were treated with the nanoparticles in the dark. Two superoxide dismutase

encoding genes, *sodA* and *sodC* did not show a differential expression over the conditions tested.

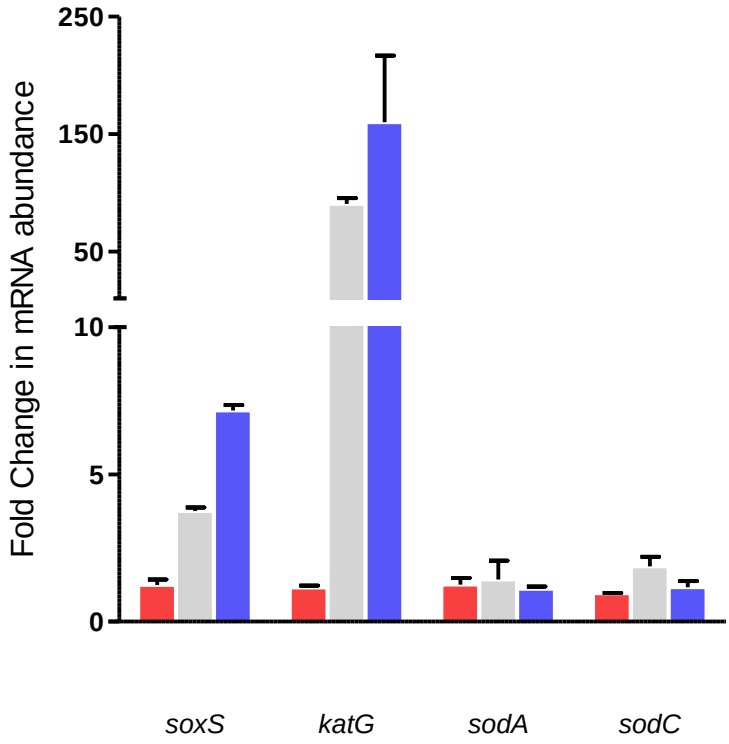


**Figure 6.14. Transcript abundance of superoxide-responsive genes (*soxS*, *sodA* and *sodC*) and a hydrogen peroxide-responsive gene (*katG*) in *E. coli* K12 during exposure to zinc oxide nanoparticles. The cells were exposed to UV light (375 nm) (red bars) or a suspension of zinc oxide nanoparticles (100 µg/mL), with (blue bars) or without (grey bars) UV light. The transcript abundance is compared to *E. coli* that were suspended in plain medium, in the dark, and the data was normalised to the transcript abundance of the *rrsB* gene (the internal reference). The error bars are the standard error of the mean (n=3).**

## 6.3. Discussion

In this study, the anti-bacterial efficacy of an industrial grade zinc oxide nanopowder was tested against *E. coli* K12, in the dark and under UV light. So far in this thesis, the anti-bacterial effects of nanoparticles have been considered based upon nanoparticle dissolution and the release of toxic $Ag^+$. Herein these observations are reciprocated for an entirely different nanoparticle composed of ZnO, with additional consideration given to a 'whole nanoparticle' toxicity mechanism from the interaction of the material with UV light.

### 6.3.1. Nanoparticle Physical Characteristics

SEM/EDAX and TEM images showed that the experimental nanomaterial was polydisperse, with nanoparticle sizes ranging from 10-350 nm, Figure 6.1. The synthesis route had not been disclosed by the manufacturer. However, the irregular morphology and the polydispersity of the material were characteristic of a vapour phase synthesis. In other studies, zinc oxide nanoparticles have been produced using wet-chemical techniques wherein the nanoparticles have been comparatively monodisperse with a defined morphology, for example 20 ± 10 nm spheres [36]. As a consequence, the nanoparticles used for different studies may have very different characteristics, thus factors such as the dissolution rate may be very different. For example, a polydisperse preparation of may dissolve with a high initial rate, reflecting dissolution of the smallest fraction, followed by a slower uniform rate representing the dissolution of the larger nanoparticles. Further, irregular high energy surfaces, as are characteristic of vapour-phase synthesis, will dissolve quickly and subsequently the surfaces may become smooth and dissolve more slowly. The Z-COTE ZnO nanoparticles were chosen for this study because it is an active ingredient in many commercially available products. Therefore what is discovered from study of this material may be applied directly. In contrast, characterisation of the properties

of various ZnO preparations that may never become utilised for actual applications may be wasteful, given that their specific properties may be different from those that are relevant to industry. Dissolution is also dependent upon the agglomeration of the nanoparticles. The ZnO nanoparticles were stable in the minimal salts medium owing to the negative charge of the ZnO nanoparticle surfaces at the pH of 7.2 [37]. In contrast, the silver nanoparticles that were investigated in Chapter 4 of this study were unstable in the minimal salts medium but were comparatively stable in the modified-LB medium. The range of proteins and small peptide fragments in the modified-LB may have stabilised the silver nanoparticles as they adsorb to their surfaces. This may occur through steric factors and where the proteins produce a charged surface dominated by their isoelectic point the medium pH. The zinc oxide nanoparticles were stable in both media, however the minimal salts medium was chosen in line with many studies using *E. coli* [38, 39] as it is a chemically defined medium.

### 6.3.2. Zinc Oxide Nanoparticle Anti-Bacterial Activity in the Dark

The predicted mode of zinc oxide nanoparticle toxicity in the dark was from dissolution and release of toxic zinc ions, $Zn^{2+}$. The rate of dissolution of zinc oxide nanoparticles was measured in minimal salts medium using ICP-MS, which had been used previously to measure the rate of silver nanoparticle dissolution in a modified-LB medium, Chapter 4. $ZnCl_2$ solutions underwent the sample processing procedure and it was found that 100% of the Zn was recovered. This demonstrated that the solution phase Zn was not removed by the unltracentrifugation procedure to sediment the undissolved nanoparticles. In contrast, in Chapter 4, approximately 5 % of the silver concentration was lost during the sample processing. The $Ag^{+}$ and $Zn^{2+}$ cations may both adhere to the surface of a glass vessel according to an electrostatic interaction. However, the concentration of silver in the

medium in Chapter 4 was in the range of ng/mL, compared to µg/mL of Zn in this study. Therefore, a small amount of loss to the sides of the sample vessels in this study was less significant.

There was a very high initial rate of dissolution consistent with the large particle size distribution: smaller nanoparticles possibly resulting from the gas-phase synthesis are expected to dissolve rapidly. Similarly, very small nanoparticles are less likely to be removed from solution by the ultracentrifugation process and hence the initial rapid increase in bulk solution phase $Zn^{2+}$ may be attributed to rapid dissolution of small nanoparticles and poor recovery of small nanoparticles by ultracentrifugation. Subtracting the starting concentration of Zn (time 0) from the dissolution data, the observed rate of dissolution is still rapid in comparison to that observed for silver nanoparticles in Chapter 4. The Zn concentration in the medium increased by approximately 3 µg/mL over the 4 hour time course. In comparison the same concentration of silver nanoparticles increased the Ag concentration in the bulk solution phase by 500 ng/mL over 24 hours.

The ICP-MS data was used to test a differential toxicity hypothesis. This states that the dissolution of a nanoparticle at the bacterial membrane may enhance the anti-bacterial efficacy whereby the ions that are released from the nanoparticles are immediately available to the bacterial envelope, thus they are more biologically available than those in the bulk solution. Although the dissolution rate may have been overestimated, there was still a differential effect on *E. coli* growth between the nanoparticles and the measured concentration of $Zn^{2+}$ that they released into the bulk solution, Figure 6.5. This is consistent with the observations made for silver nanoparticles in Chapter 4 and therefore is additional support for the conclusions made in that study.

The physical bacterial-nanoparticle interactions for the Z-COTE were not determined using the thin section TEM procedure because the nanoparticles were not

observed in TEM images after mixing with the *E. coli*. This may reflect a low energy of association between the ZnO nanoparticles and the bacteria; therefore they are removed when the specimens are sedimented and re-suspended several times as the samples are fixed, stained and washed ready for imaging. Alternatively the nanoparticles may dissolve to completion, or to a size that is too small to resolve at the TEM operating potential of 100 keV. However, this appears unlikely as the nanoparticles were clearly visible in TEM images without the bacteria. Moreover, the hypothesis for the enhanced activity of the nanoparticles compared to the bulk solution phase $Zn^{2+}$ claims a membrane interaction. Therefore, to confirm that the nanoparticles made at least some interaction with the bacteria, crude TEM images were prepared from whole *E. coli* that had been exposed to the nanoparticle suspensions, but precluding any disruptive sample preparation. The images that were obtained were of a very poor quality, as expected due to the absence of any rigorous specimen preparation procedure. However, they did indicate that the bacteria associated with the nanoparticles, Figure 6.6.

This minimalistic TEM specimen preparation was used by Droh-Ehre *et al.* who via an unknown factor manage to present much clearer images of whole *E. coli* with associated gold nanoparticles using this minimal preparative technique. It is a useful way of imaging bacterial-nanoparticle interactions with a low energy of association. However, the lack of various fixation and staining stages, and specimen embedding and sectioning generates a very poor quality image.

In addition to demonstrating nanoparticle dissolution by ICP-MS measurements, a $Zn^{2+}$-sensitive mutant, *ΔzntA*, was constructed and demonstrated a hypersensitivity to the nanoparticles and to zinc chloride. The *zntA* gene is clearly an important regulator of cellular $Zn^{2+}$ because the observed difference in sensitivity compared to the parent strain was considerable. In a concentration of zinc chloride that did not inhibit the parent strain

compared to the control, the mutant culture grew to only approximately half the optical density. In a suspension of the nanoparticles the mutant did not grow at all but the parent strain increased in colony forming units by approximately 10 fold. The biological function of ZntA is well characterised and this is good confirmatory evidence that the nanoparticles are toxic through the release of $Zn^{2+}$. In Chapter 4 a silver sensitive mutant was prepared by disrupting another metal ion transporter, encoded by the *cusA* gene. However the effect of this gene deletion of silver sensitivity was minimal in comparison. The ZntA protein is an ATP dependant active transporter, whereas the CusA protein is a chemiosmotic, proton motive force driven system. Thus, these pumps may operate with different efficiencies. Moreover, evidence suggests that $Zn^{2+}$ is the major substrate for ZntA, whereas the usual substrate for CusA may be $Cu^{+}$, but $Ag^{+}$ may also be transported because it has the same $d^{10}$ electronic configuration.

The final experiment to investigate the nanoparticle effects in the dark was to examine a transcriptional profile of the *E. coli* in response to the $Zn^{2+}$ concentration with or without the nanoparticles present. The *E. coli* were cultured with the nanoparticles or $Zn^{2+}$ at a concentration that was determined to have been released by the nanoparticles. As for the differential growth data, an overestimation of the nanoparticle dissolution rate may have reduced any observed differences. Nonetheless there was a clear differential expression; the nanoparticles induced a stronger transcriptional response than the bulk solution phase ions. The bacteria up-regulated the expression of the *zntA* gene (encoding the di-valent metal ion efflux protein), and down-regulated the expression of a gene encoding a di-valent metal ion import protein, Figure 6.9. This is consistent with the expected change in the flux of the $Zn^{2+}$ ions across the cell envelope under a state of $Zn^{2+}$ stress; an up-regulation of efflux and a down-regulation of import leading to a net movement of ions out of the cell. This response was greater, *i.e.* a greater regulation either

up or down was observed if the *E. coli* were exposed to the nanoparticles rather than just the predicted nanoparticle associated $Zn^{2+}$ concentration. If the intensity of the transcriptional response is proportional to the biologically available concentration of the $Zn^{2+}$, (wherein the ions induce the response when they interact with the Zur and ZntR gene regulatory proteins), this data indicates that the nanoparticles have their enhanced activity by increasing the biologically available concentration of $Zn^{2+}$. This may occur as the nanoparticles dissolve at the bacterial envelope according to the hypothesis that was considered for silver nanoparticle toxicity in Chapter 4.

### 6.3.3. Zinc Oxide Nanoparticle Anti-Bacterial Activity in UV light

A suspension of the zinc oxide nanoparticles in water (data not shown) or in minimal salts medium, Figure 6.3, had a characteristic UV-Visible extinction spectrum. The nanoparticle suspensions absorbed UV light including the harmful UVA and UVB radiation [36, 40, 41] which is why they are included in sunscreen formulations. Furthermore, as can be inferred from the UV-Visible spectrum of extinction the nanoparticle suspensions absorb weakly at visible wavelengths producing colourless or white sunscreens which are cosmetically more desirable. The band gap UV absorption properties of this nanomaterial lead to the hypothesis that under UV light the conduction band electrons may be available to redox active species in the medium producing free radicals as an alternative mechanism of nanoparticle toxicity. This principle has become a key concern for the manufacture of topical formulations containing ZnO (and $TiO_2$ which has similar photo-chemical properties) [41].

The formation of free radicals was investigated using DCPIP as a redox sensor. The nanoparticles were suspended in water and photo-electrons produced directly by the band gap transition may have passed to the surrounding DCPIP molecules, effecting their

reduction. This causes the DCPIP molecules to change their optical characteristics, changing the solution from blue to colourless, Figure 6.11. Alternatively the DCPIP may accept electrons in-directly from radical species that are formed from oxygen ($O_2^-$) and water molecules ($OH^-$) in the suspension. A DCPIP colour change was not observed if the nanoparticles were suspended in the minimal salts medium, indicating that the rate of reduction was very slow, or inhibited. This may reflect the presence of various molecules in the medium that compete for the photo-electrons, for example $Fe^{2+}$. In a 0.1% glucose solution the DCPIP was reduced at a faster rate. The chemical mechanism for this may involve the splitting of the carbon ring structure and the availability of the COOH (carboxylic acid) group, which may propagate the radical formation.

In an *E. coli* culture to which the nanoparticles were added, the radicals formed by the photo-electrons may be distributed throughout the medium and, for a nanoparticle associated with the outer membrane of the bacteria, can be delivered directly to the metabolism. This direct delivery is important as radicals clearly have a limited lifetime in solution and once inside the cytoplasm the redox environment will then control the lifetime and propagate new radicals such as $O_2^{2-}$ and the production of $H_2O_2$, and lipid peroxides. These are dangerous species for the cell. The radicals may propagate within the cell, particularly through redox cycling of free metal cations including $Cu^+$ and $Fe^{2+}$. The predicted intracellular concentration of these free metal ions is higher in the nanoparticle treated *E. coli* whereby the dissolution and concentration of free $Zn^{2+}$ may displace these ions from their coordination sites with proteins. The free radical damage to membrane lipids, proteins and DNA contribute to the loss of cell viability as observed in Figure 6.13. Their concentration within the bacterium will be combated by the redox stress response [32], which was determined from the transcription of redox-stress associated genes, Figure 6.14.

Two genes, *katG* and *soxS*, which are up-regulated following the activation of the *soxRS* and *oxyR* (redox stress-responding) regulons showed a response to the presence of the nanoparticles in 375 nm light. However, the *E. coli* also made this transcriptional response at a reduced level in the dark. This UV-independent response may represent the disruption of metal ion coordination sites by the excess $Zn^{2+}$, thus leading to an increase in free copper and iron, which may form radicals through redox cycling; for example hydroxyl radicals through a reaction with hydrogen peroxide [42, 43]. *E. coli* also make a transcriptional response to redox stress after exposure to silver nanoparticles, as discussed in Chapter 5. This may occur through a similar mechanism; silver ions disrupt protein metal ion coordination sites, leading to an increase in free ion concentration and the formation of radicals through redox cycling. The superoxide dismutase encoding genes, *sodA* and *sodC* did not show any regulation following exposure to the nanoparticles, either in the dark or under UV light. The *sodA* gene is positively regulated by *soxS*, however another level of regulation for this gene could exist such that it was not transcribed even though *soxS* was expressed at high levels.. In contrast the *sodC* gene is regulated by the *rpoS* sigma, associated with stationary phase. The transcriptional response was measured for exponentially replicating bacteria that were suddenly exposed to the anti-bacterial effects. This may not have driven the bacteria into a stationary phase within the 10 minutes that they were exposed prior to harvest for RNA isolation. Nonetheless, the regulation of *soxS* and *katG* is good evidence that the observed light-dependent augmentation of the nanoparticle toxic effects occurs through redox stress in the *E. coli* metabolism, consistent with the formation of photo-electrons and free radicals.

### 6.3.4. Conclusions

Three pieces of data confirm that the zinc oxide nanoparticles are toxic due to the release of zinc ions; the observed dissolution profile, the hypersensitivity of a zinc ion efflux mutant and the expression of $Zn^{2+}$-responding genes.

The toxic effects on *E. coli* replication in the minimal salts medium and the transcriptional response to excess $Zn^{2+}$ was enhanced for the nanoparticle. This indicates that the biologically available concentration of $Zn^{2+}$ was greater than if the medium was augmented with $Zn^{2+}$ at the predicted rate of nanoparticle dissolution, which is explained by a physical interaction on the nanoparticles with the bacterial envelope. This evidence supports the same hypothesis which was made for silver nanoparticles in Chapter 4, and demonstrates another novel bacterial-nanoparticle interaction.

The formation of photo-electrons and free radicals from the nanoparticles in UV light is considered to contribute to cellular damage and augment the dissolution based toxic mechanism.

Topical application studies [44] demonstrate how these nanomaterials may not cross the outermost layer of skin, the stratum corneum, thus the underlying epidermis may be protected from their effects. However, the skin surface is covered with an immunologically important normal skin flora [45] which will be subject to both nanotoxicity mechanisms; dissolution and photo-electron effects. Application of ZnO-containing formulations to the skin surface may have a considerable impact these organisms. This, in turn, may leave the host open to the carriage of pathogenic species where these organisms restrict colonisation by occupying each environmental niche on the skin surface (colonisation resistance) [46].

## 6.4. References


1. Klingshirn, C., *ZnO: material, physics and applications.* Chemphyschem, 2007. **8**(6): p. 782-803.
2. Brayner, R., et al., *Toxicological Impact Studies Based on Escherichia coli Bacteria in Ultrafine ZnO Nanoparticles Colloidal Medium.* Nano Letters, 2006. **6**(4): p. 866-870.
3. Hu, X., et al., *In vitro evaluation of cytotoxicity of engineered metal oxide nanoparticles.* Science of The Total Environment, 2009. **407**(8): p. 3070-3072.
4. Huang, Z., et al., *Toxicological Effect of ZnO Nanoparticles Based on Bacteria.* Langmuir, 2008. **24**(8): p. 4140-4144.
5. Jiang, W., H. Mashayekhi, and B. Xing, *Bacterial toxicity comparison between nano- and micro-scaled oxide particles.* Environmental Pollution, 2009. **157**(5): p. 1619-1625.
6. Li, X., et al., *Antimicrobial activities of ZnO powder-coated PVC film to inactivate food pathogens.* International Journal of Food Science & Technology, 2009. **44**(11): p. 2161-2168.
7. Reddy, K.M., et al., *Selective toxicity of zinc oxide nanoparticles to prokaryotic and eukaryotic systems.* Appl Phys Lett, 2007. **90**(213902): p. 2139021-2139023.
8. Zhang, L., et al., *Investigation into the antibacterial behaviour of suspensions of ZnO nanoparticles (ZnO nanofluids).* Journal of Nanoparticle Research, 2007. **9**(3): p. 479-489.
9. Nadanathangam, V. and et al., *Functional finishing of cotton fabrics using zinc oxideâ€“soluble starch nanocomposites.* Nanotechnology, 2006. **17**(20): p. 5087.
10. Aydin Sevinç, B. and L. Hanley, *Antibacterial activity of dental composites containing zinc oxide nanoparticles.* Journal of Biomedical Materials Research Part B: Applied Biomaterials, 2010. **94B**(1): p. 22-31.
11. Boyd, D., et al., *The antibacterial effects of zinc ion migration from zinc-based glass polyalkenoate cements.* Journal of Materials Science: Materials in Medicine, 2006. **17**(6): p. 489-494.
12. Moorer, W.R. and J.M. Genet, *Evidence for antibacterial activity of endodontic gutta-percha cones.* Oral Surgery, Oral Medicine, Oral Pathology, 1982. **53**(5): p. 503-507.
13. Auld, D.S., *Zinc coordination sphere in biochemical zinc sites.* BioMetals, 2001. **14**(3): p. 271-313.
14. Vallee, B.L. and D.S. Auld, *Active zinc binding sites of zinc metalloenzymes.* Matrix Suppl, 1992. **1**: p. 5-19.
15. Vallee, B.L. and D.S. Auld, *Functional zinc-binding motifs in enzymes and DNA-binding proteins.* Faraday Discuss, 1992(93): p. 47-65.

16. Christianson, D.W., *Structural biology of zinc.* Adv Protein Chem, 1991. **42**: p. 281-355.

17. Vallee, B.L. and D.S. Auld, *Zinc coordination, function, and structure of zinc enzymes and other proteins.* Biochemistry, 1990. **29**(24): p. 5647-59.

18. Coleman, J.E., *Zinc proteins: enzymes, storage proteins, transcription factors, and replication proteins.* Annu Rev Biochem, 1992. **61**: p. 897-946.

19. Katayama, A., et al., *Systematic search for zinc-binding proteins in Escherichia coli.* European Journal of Biochemistry, 2002. **269**(9): p. 2403-2413.

20. Davidson, A.L., et al., *Structure, Function, and Evolution of Bacterial ATP-Binding Cassette Systems.* Microbiol. Mol. Biol. Rev., 2008. **72**(2): p. 317-364.

21. Patzer, S.I. and K. Hantke, *The ZnuABC high-affinity zinc uptake system and its regulator Zur in Escherichia coli.* Molecular Microbiology, 1998. **28**(6): p. 1199-1210.

22. Grass, G., et al., *ZupT Is a Zn(II) Uptake System in Escherichia coli.* J. Bacteriol., 2002. **184**(3): p. 864-866.

23. Outten, C.E. and T.V. O'Halloran, *Femtomolar sensitivity of metalloregulatory proteins controlling zinc homeostasis.* Science, 2001. **292**(5526): p. 2488-92.

24. Patzer, S.I. and K. Hantke, *The zinc-responsive regulator Zur and its control of the znu gene cluster encoding the ZnuABC zinc uptake system in Escherichia coli.* J Biol Chem, 2000. **275**(32): p. 24321-32.

25. Grass, G., et al., *ZitB (YbgR), a Member of the Cation Diffusion Facilitator Family, Is an Additional Zinc Transporter in Escherichia coli.* J. Bacteriol., 2001. **183**(15): p. 4664-4667.

26. Rensing, C., B. Mitra, and B.P. Rosen, *The zntA gene of Escherichia coli encodes a Zn(II)-translocating P-type ATPase.* Proc Natl Acad Sci U S A, 1997. **94**(26): p. 14326-31.

27. Beard, S.J., et al., *Zinc(II) tolerance in Escherichia coli K-12: evidence that the zntA gene (o732) encodes a cation transport ATPase.* Mol Microbiol, 1997. **25**(5): p. 883-91.

28. Blencowe, D.K. and A.P. Morby, *Zn(II) metabolism in prokaryotes.* FEMS Microbiology Reviews, 2003. **27**(2-3): p. 291-311.

29. Binet, M.R. and R.K. Poole, *Cd(II), Pb(II) and Zn(II) ions regulate expression of the metal-transporting P-type ATPase ZntA in Escherichia coli.* FEBS Lett, 2000. **473**(1): p. 67-70.

30. Brocklehurst, K.R., et al., *ZntR is a Zn(II)-responsive MerR-like transcriptional regulator of zntA in Escherichia coli.* Mol Microbiol, 1999. **31**(3): p. 893-902.

31. Outten, C.E., F.W. Outten, and T.V. O'Halloran, *DNA distortion mechanism for transcriptional activation by ZntR, a Zn(II)-responsive MerR homologue in Escherichia coli.* J Biol Chem, 1999. **274**(53): p. 37517-24.

32. Demple, B., *Radical ideas: genetic responses to oxidative stress.* Clin Exp Pharmacol Physiol, 1999. **26**(1): p. 64-8.

33. Choi, H., et al., *Structural basis of the redox switch in the OxyR transcription factor.* Cell, 2001. **105**(1): p. 103-13.

34. Zheng, M., F. Aslund, and G. Storz, *Activation of the OxyR transcription factor by reversible disulfide bond formation.* Science, 1998. **279**(5357): p. 1718-21.

35. Singh, R., et al., *Comparative study of catalase-peroxidases (KatGs).* Archives of Biochemistry and Biophysics, 2008. **471**(2): p. 207-214.

36. Becheri, A., et al., *Synthesis and characterization of zinc oxide nanoparticles: application to textiles as UV-absorbers.* Journal of Nanoparticle Research, 2008. **10**(4): p. 679-689.

37. Walker, N., *Personal Communication*. 2010.

38. Blattner, F.R., et al., *The Complete Genome Sequence of Escherichia coli K-12.* Science, 1997. **277**(5331): p. 1453-1462.

39. Neidhardt, F.C., P.L. Bloch, and D.F. Smith, *Culture medium for enterobacteria.* J Bacteriol, 1974. **119**(3): p. 736-47.

40. Marissa, D.N., S. Mira, and I.E. Jeffrey, *The safety of nanosized particles in titanium dioxideâ€“ and zinc oxideâ€“based sunscreens.* Journal of the American Academy of Dermatology, 2009. **61**(4): p. 685-692.

41. Nohynek, G.J., et al., *Grey Goo on the Skin? Nanotechnology, Cosmetic and Sunscreen Safety.* Critical Reviews in Toxicology, 2007. **37**(3): p. 251-277.

42. Fenton, H.J.H., *Oxidation of tartaric acid in presence of iron.* Journal of the Chemical Society, 1894. **65**(899-911).

43. Haber, F., Weiss, J., *On the catalysis of hydroperoxide.* Naturwissenschaften, 1932. **20**: p. 948-950.

44. Gamer, A.O., E. Leibold, and B. van Ravenzwaay, *The in vitro absorption of microfine zinc oxide and titanium dioxide through porcine skin.* Toxicology in Vitro, 2006. **20**(3): p. 301-307.

45. Gao, Z., et al., *Molecular analysis of human forearm superficial skin bacterial biota.* Proceedings of the National Academy of Sciences, 2007. **104**(8): p. 2927-2932.

46. Noble, W.C., *The Skin Microflora and Microbial Skin Disease*. 1993: Cambridge University Press.

# Chapter 7: General Conclusions and Future Work

Bionanotechnology is an expansive field in which there is a considerable potential for the development of new technologies and new industries within all areas of the life sciences. Prototypical applications for ‘nanomaterials’ have been widely reported in the literature; from antimicrobials to medical diagnostics and biosensing. However, there was a considerable paucity of data pertaining to the detailed underlying biological interactions. Accordingly, the objective of this study was to identify bacterial-nanoparticle interactions, taking the model organism approach to study.

The direct observation of bacteria-nanoparticle interactions is a significant challenge. There may be a considerable uncertainty present in TEM images, which is the imaging technique of choice to observe the sub-micron detail of biological specimens and nanomaterials. In TEM the interaction was observed retrospectively; *i.e.* one assumes that the observed specimen appears as it was prior to the various fixation and staining procedures, and that the image does not include any artefacts from this process. Moreover, the image has no resolution in the *z*-axis. For these reasons the very promising observation of gold nanoparticles inside the bacteria shown in Chapter 3 must be discounted as an imaging anomaly. The imaging uncertainty questions whether any of the reported entry of nanoparticles into bacteria are credible and whether there is any evidence for a bacterial uptake mechanism. However, uptake may be induced by localised nanoparticle damage to the membrane or encapsulation say during the division process. However, it was found that non-toxic nanoparticles are excluded from the bacterium by the barrier properties of the cell wall. The only caveat would be for very small nanoparticles of order 1-4 nm that may pass directly through membrane pores.

Another observation that was identified from TEM investigation was that silver nanoparticles, which were clearly visible in TEM images after synthesis, were not visible in association with the *E. coli*. From this observation the silver nanoparticles were considered to have dissolved. Silver' is left surrounding the cell, visible as a 'haze'. This led to a novel hypothesis of this thesis: that the dissolution of nanoparticles at the cell membrane is a unique nanoparticle-based toxic mechanism that favours antimicrobial activity. The nanoparticle produces a high local concentration of the solute, which can interact immediately with the metabolism of the bacterium (an interfacial dissolution effect). In contrast, the solute is dispersed in the bulk solution phase and the concentration may be comparatively minimal. This has been demonstrated for two industrial grade nanopowders; a silver nanopowder that may be incorporated into wound dressings and the surfaces of medical devices, and a zinc oxide nanopowder that is an active UV-blocker in sunscreens and cosmetics. The concentration of toxic metal cations, $Ag^{+}$ or $Zn^{2+}$, that suspensions of these nanopowders contribute to the bulk solution phase as they dissolve does not account for their observed toxic effects. This was determined by measuring the bulk solution phase concentration of metal ions directly, then comparing the effects of that concentration with or without the presence of the nanoparticles. Moreover, the increased biological availability of the ions that are released from a nanoparticle at the membrane was hypothesised from an enhanced transcriptional response to the ion.

This differential nanoparticle and ion toxicity has massive implications for nanoparticle antimicrobial products. For example, the effect is dependent upon a direct, physical interaction between the nanomaterial and the target organism. Thus, incorporation of nanomaterials into hollow fibres or polymer matrices wherein they are not available to associate with a membrane may be ineffective, *i.e.* their toxic effects depend solely on their dissolution in close proximity to their target. A far greater efficacy could be

achieved from a colloidal suspension of nanomaterials, or where nanomaterials are exposed at a surface and can therefore make direct contact with a cell membrane.

Understanding the rate of nanoparticle dissolution is an important nanotoxicological metric, for which a novel time to dissolution ($t_{diss}$) parameter is proposed in this thesis. The $t_{diss}$ represents the time taken for a nanoparticle to dissolve to completion in a given medium, which will influence the efficacy and lifetime of a nano-enabled antimicrobial. It is considered that a metric based upon $t_{diss}$, specifically ½($t_{diss}$) representing the nanoparticle effective half-life, could be used to assess the frequency with which a nanoparticle coated antimicrobial catheter or wound dressing is changed, or the dose regimens where antimicrobial nanoparticles could be used for wastewater treatment. In Chapter 4 the $t_{diss}$ for 142 nm silver nanoparticles was determined to be approximately 24 hours for a 100 µg/mL suspension. Thus, one might consider renewing the dose within this time in order to maintain antimicrobial activity.

For a nanoparticle impregnated material such as an antimicrobial surface the activity could be renewed simply by removing the top layer. For example, as preliminary further work for this study a high density polyethylene medical grade plastic was impregnated with silver nanoparticles. The nanoparticles exposed at the surface may dissolve rapidly, thus releasing silver ions that could inhibit the colonisation of opportunist pathogens. In a preliminary experiment it was found that *E. coli* and *P. aeruginosa* that adhered to this material were non-viable in a live/dead stain compared to a control material. Once the nanoparticles have dissolved one might simply use an abrasive to remove the top most layer of the material, revealing the underlying nanoparticles, thus revitalising its activity. Alternatively one could incorporate the nanoparticles into a polymer that slowly dissolves to renew the active surface over time.

In Chapter 5 of this study, the interaction of these silver nanoparticles with the metabolism of *E. coli* was investigated by measuring the transcriptome. This interaction was very similar to that observed for the silver ion, indicating that the dissolution based toxic mechanism predominates. However, the presence of a nanostructure may have had an effect on the transcriptome wherein differential gene expression was also observed. The high dose at the membrane from a nanoparticle dissolving induces a distinct response.

The response of the *E. coli* transcriptome to silver was considerable, representing the more than 2-fold regulation of up to 497 genes. The response was considered as both an adaptive response, that enables the bacterium to counter the effects of the silver ions on proteins, and a disruptive response, which was a consequence of the activity of the silver ions on the proteins. Any protein with an available cysteine, methionine or histidine residue can be denatured and this may lead to pan-metabolism disintegration including the perturbation of gene regulatory signalling networks. This results in a very effective antibacterial, which is now becoming increasingly prevalent in society.

The potential of silver to damage any pathway within the metabolism leads to the novel hypothesis that the organism may respond to replenish the entire metabolome through transcription, translation and metabolite synthesis. This could point towards those components of the cell that are essential, and active under a given set of conditions (*i.e.* are replaced), and those that are unused or quiescent (*i.e.* are not replaced). To achieve this requires an integrative ‘pan-omic’ approach, measuring the transcriptome, metabolome and proteome and successfully identifying metabolic pathways that are regulated. We already have acquired preliminary data for the $Ag^{+}$-metabolome, from which we have found several interesting patterns from self organising map (SOM) analysis, pointing towards silver-regulated metabolite pathways. *E. coli* were exposed to silver

nitrate over a time course of 60 minutes, wherein at several time points metabolites were analysed using Quadrupole Time of Flight Mass Spectrometry (QToF-MS). The SOM is a two-dimensional array such as the hexagonal array shown in Figure 6.1, where the map is composed of 20 ×20 cells based on 5555 metabolites across 6 time points. The metabolites mapped to the same cell are believed to have the same level of response to silver nitrate stress. Cells which are close to each other mean that the metabolites mapped to these cells share similar biological activities. In the map, small dots are the non-significant metabolites mapped to the cells while the large dots represent the significant metabolites.

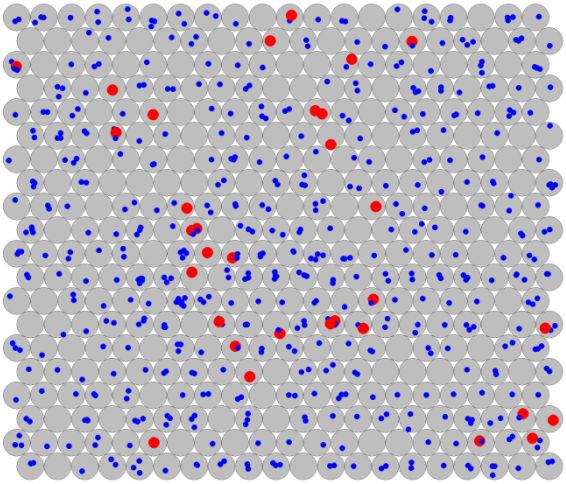

**Figure 7.1. SOM analysis showing *E. coli* metabolite clustering post exposure to silver nitrate**

This approach to investigating the silver stress provides a complementary analysis to the transcriptome approach producing different insights into the systems biology of *E. coli* in response to Ag stress. The data analysis requires a multi-disciplinary approach, utilising the advanced data analysis and interpretation methodology available within the bioinformatics community. This circumvents some of the issues with false discovery from microarray data, wherein a typical data analysis approach is to base the identification of pathways on co-regulated genes, selected from *P* values. However, as described in

chapter 5, using a standard *P* value cut off of 0.05 may lead to false discovery wherein the regulated gene sets do not have a uniform *P* value distribution.

From this study, several areas of further investigation have been identified. Firstly, the pan-metabolism response to silver requires massive attention, especially considering how silver nanoparticles (and $Ag^{+}$ in other forms) are becoming increasingly prevalent in society. Silver could potentially become a very useful ion for investigating the integrated aspects of functional genomics, metabolomics and proteomics.

Secondly, the physical bacterial-nanoparticle interaction is clearly important for the toxic effects, thus, it is necessary to study the parameters that define this interaction. Nanoparticle size and shape may determine dissolution rate, but the bacterial-membrane interaction will ultimately be determined by the surface functionalisation of the nanoparticle. For this, antibodies and antimicrobial peptides may be particularly interesting. These offer the potential to produce nanoparticles with a high, specific affinity for a bacterium. However, it is also necessary to determine the effects of various nanoparticle surface ligands on their dissolution rate. If the presence of these molecules inhibits the rate of dissolution then the benefit of the physical interaction may be lost.

The study of nanoparticle dissolution may also be extended beyond the scope of medical applications towards understanding their ecotoxicological effects. Metal ions are generally highly toxic to aquatic organisms whereas elemental nanoparticles may be relatively inert. Thus the rate of dissolution of nanoparticles, for example from industrial effluents, may determine their impact on the environment. If nanoparticles do not dissolve in the environment then the impact of whole nanoparticle ingestion on higher organisms will need to be determined. Specifically, what is the fate of a nanoparticle within a vertebrate organism; where do they accumulate within an organism and what is their ultimate fate?

Further work should be undertaken to assess the potential of nanoparticle entry into cells across viable membranes. This may not occur spontaneously; however, a mechanism for inducing this phenomenon would have potential applications for the delivery of nanoparticle conjugated drug molecules or for the introduction of DNA sequences into cells. Specifically, it would be useful to determine whether a nanoparticle that is covered with hydrophobic peptides can integrate with the cell envelope, or surmount it completely. In order to achieve this, methods for accurately determining the location of a nanoparticle with respect to a bacterium must be developed. Moreover it is necessary to observe viable specimens in 3-dimensions and with sub-200 nm resolution. For this, the scanning ion conductance microscope (SICM) is a technique that could be used to image the surface of a viable specimen with sufficient resolution in the *z*-axis of a membrane to image surface associated nanoparticles. Simultaneously, the ion flux across the membrane can be determined, thus provide information as to the membrane integrity around the site of nanoparticle binding.

Finally, this study has been conducted entirely on the model organism *E. coli* K12. The model organism approach was preferred because the data already available on this species facilitates the interpretation of experimental data. However, the experiments reported here could be reciprocated for a Gram positive bacterium. The bacterial-nanoparticle interactions therein may be strikingly different. The Gram positive cell wall is structurally distinct for that of *E. coli*, thus indicating a different physical interaction and the organism will have a distinct metabolism. Therefore, the biochemical response may also be very different. In particular, it is necessary to extend the observation of the differential nanoparticle and ion toxic effects for other organisms in order to exemplify its importance for the design and development of nanoparticle-based antimicrobials.

## Appendix A: A Method for Preparing Neidhardts' Minimal Salts Medium

The medium is prepared by mixing 100 mL of 10x MOPS mixture (see below) with 10 mL of 0.132 M $K_2HPO_4$ and 890 mL of deionised water. Prior to use add 1 g of glucose and filter sterilise.

### 10X MOPS Mixture

1. Dissolve 83.72 g of MOPS and 7.17 g of Tricine in 300 mL of deionised water.
2. Add 10 M KOH to a final pH of 7.4.
3. Bring total volume to 440 ml
4. Add 10 mL of 10 mM FeSO4, 50 mL of 1.9 M $NH_4Cl$, 10 mL of 0.276 M $K_2SO_4$, 0.25 mL of 0.02 M $CaCl_2$, 2.1 mL of 2.5 M $MgCl_2$, 100 mL of 5 M NaCl and 0.2 mL of a micronutrient stock solution (see below)
5. Make up to 1 L, and store at -20$^{o}$C.

### Micronutrient Stock Solution

Add the following to 50 mL of deionised water: 0.009 g of $(NH_4)_6Mo_7O_{24}$, 0.062 g of $H_3BO_3$, 0.018 g of $CoCl_2$, 0.006 g of $CuSO_4$, 0.040 g of $MnCl_2$ and 0.007 g of $ZnSO_4$.

# Appendix B: Gene Expression Microarray Data

**Silver nanoparticle up-regulated genes**

| Gene | Locus Tag | Ratio | t-test *P* value | Description |
|---|---|---|---|---|
| *raiA* | b2597 | 56.85 | 0.03516 | cold shock protein associated with 30S ribosomal subunit |
| *cusF* | b0573 | 54.08 | 0.01396 | periplasmic copper-binding protein |
| *yncJ* | b1436 | 47.57 | 0.00814 | predicted protein |
| *spy* | b1743 | 43.68 | 0.01362 | envelope stress induced periplasmic protein |
| *ypeC* | b2390 | 43.46 | 0.03084 | conserved protein |
| *yebE* | b1846 | 42.61 | 0.02197 | conserved protein |
| *cusC* | b0572 | 40.54 | 0.01238 | copper/silver efflux system, outer membrane component |
| *cueO* | b0123 | 36.72 | 0.03428 | multicopper oxidase (laccase) |
| *yjjZ* | b4567 | 29.74 | 0.01874 | predicted protein |
| *cusB* | b0574 | 26.90 | 0.01107 | copper/silver efflux system, membrane fusion protein |
| *ygaC* | b2671 | 25.84 | 0.03018 | predicted protein |
| *ybdZ* | b4511 | 25.78 | 0.02639 | conserved protein |
| *fes* | b0585 | 22.82 | 0.02558 | enterobactin/ferric enterobactin esterase |
| *osmC* | b1482 | 22.35 | 0.02956 | osmotically inducible, stress-inducible membrane protein |
| *ycfS* | b1113 | 21.63 | 0.01093 | conserved protein |
| *cusA* | b0575 | 20.72 | 0.00653 | copper/silver efflux system, membrane component |
| *ydhA* | b1639 | 19.41 | 0.01588 | predicted lipoprotein |
| *yjdP* | b4487 | 18.29 | 0.03115 | conserved protein |
| *ibpB* | b3686 | 17.55 | 0.00463 | heat shock chaperone |

| | | | | |
|---|---|---|---|---|
| *ymgD* | b1171 | 16.79 | 0.03376 | predicted protein |
| *yaiY* | b0379 | 16.77 | 0.02340 | predicted inner membrane protein |
| *sufA* | b1684 | 16.26 | 0.01909 | Fe-S cluster assembly protein |
| *fhuE* | b1102 | 16.07 | 0.00242 | ferric-rhodotorulic acid outer membrane transporter |
| *nrdH* | b2673 | 15.68 | 0.02849 | glutaredoxin-like protein |
| *alx* | b3088 | 15.44 | 0.03139 | predicted inner membrane protein, part of terminus |
| *ypfG* | b2466 | 15.42 | 0.01554 | predicted protein |
| *entF* | b0586 | 15.07 | 0.01028 | enterobactin synthase multienzyme complex component,  ATP-dependent |
| *copA* | b0484 | 13.71 | 0.00411 | copper transporter |
| *entE* | b0594 | 12.95 | 0.02342 | 2,3-dihydroxybenzoate-AMP ligase component of enterobactin synthase multienzyme complex |
| *ydeH* | b1535 | 12.81 | 0.00392 | conserved protein |
| *clpB* | b2592 | 12.66 | 0.01672 | protein disaggregation chaperone |
| *ymgG* | b1172 | 12.42 | 0.01120 | predicted protein |
| *fepA* | b0584 | 12.26 | 0.01583 | iron-enterobactin outer membrane transporter |
| *sufC* | b1682 | 11.97 | 0.00895 | component of SufBCD complex, ATP-binding component of ABC superfamily |
| *fpr* | b3924 | 11.96 | 0.01398 | ferredoxin-NADP reductase |
| *yceB* | b1063 | 11.07 | 0.01092 | predicted lipoprotein |
| *sufB* | b1683 | 10.82 | 0.01076 | component of SufBCD complex |
| *tnaC* | b3707 | 10.74 | 0.00000 | tryptophanase leader peptide |
| *entB* | b0595 | 10.65 | 0.01949 | isochorismatase |
| *nrdI* | b2674 | 9.93 | 0.01205 | protein that stimulates ribonucleotide reduction |
| *ivy* | b0220 | 9.42 | 0.00733 | inhibitor of vertebrate C-lysozyme |

| | | | | |
|---|---|---|---|---|
| *tqsA* | b1601 | 9.37 | 0.01053 | predicted inner membrane protein |
| *entA* | b0596 | 9.19 | 0.01314 | 2,3-dihydro-2,3-dihydroxybenzoate dehydrogenase |
| *nhoA* | b1463 | 7.91 | 0.00274 | N-hydroxyarylamine O-acetyltransferase |
| *ycgK* | b1178 | 7.84 | 0.00102 | predicted protein |
| *cysI* | b2763 | 7.83 | 0.00124 | sulfite reductase, beta subunit, NAD(P)-binding, heme-binding |
| *sufD* | b1681 | 7.83 | 0.00423 | component of SufBCD complex |
| *eco* | b2209 | 7.62 | 0.00152 | ecotin, a serine protease inhibitor |
| *ybdB* | b0597 | 7.49 | 0.00548 | conserved protein |
| *sra* | b1480 | 7.23 | 0.00245 | 30S ribosomal subunit protein S22 |
| *tnaA* | b3708 | 7.21 | 0.00002 | tryptophanase/L-cysteine desulfhydrase, PLP-dependent |
| *ycfJ* | b1110 | 7.08 | 0.00397 | predicted protein |
| *mtlA* | b3599 | 7.01 | 0.00452 | fused mannitol-specific PTS enzymes: IIA components/IIB components/IIC components |
| *cysD* | b2752 | 7.00 | 0.00373 | sulfate adenylyltransferase, subunit 2 |
| *cysH* | b2762 | 6.97 | 0.00338 | 3'-phosphoadenosine 5'-phosphosulfate reductase |
| *ybgS* | b0753 | 6.91 | 0.00011 | conserved protein |
| *cysN* | b2751 | 6.74 | 0.00045 | sulfate adenylyltransferase, subunit 1 |
| *ybjP* | b0865 | 6.73 | 0.00168 | predicted lipoprotein |
| *mtlD* | b3600 | 6.72 | 0.00410 | mannitol-1-phosphate dehydrogenase, NAD(P)-binding |
| *ysaB* | b4553 | 6.70 | 0.00148 | predicted protein |
| *ycjX* | b1321 | 6.67 | 0.00156 | conserved protein with nucleoside triphosphate hydrolase domain |
| *dnaK* | b0014 | 6.62 | 0.00005 | chaperone Hsp70, co-chaperone with DnaJ |
| *ybaJ* | b0461 | 6.57 | 0.00286 | predicted protein |

| | | | | |
|---|---|---|---|---|
| *cysA* | b2422 | 6.50 | 0.00181 | sulfate/thiosulfate transporter subunit |
| *yajI* | b0412 | 6.46 | 0.00127 | predicted lipoprotein |
| *ibpA* | b3687 | 6.44 | 0.00188 | heat shock chaperone |
| *yjjI* | b4380 | 6.27 | 0.00020 | conserved protein |
| *ydbK* | b1378 | 6.14 | 0.00170 | fused predicted pyruvate-flavodoxin oxidoreductase: conserved protein/conserved protein/FeS binding protein |
| *dacC* | b0839 | 6.11 | 0.00017 | D-alanyl-D-alanine carboxypeptidase (penicillin-binding protein 6a) |
| *htpG* | b0473 | 5.97 | 0.00107 | molecular chaperone HSP90 family |
| *cysC* | b2750 | 5.94 | 0.00000 | adenosine 5'-phosphosulfate kinase |
| *hslJ* | b1379 | 5.91 | 0.00108 | heat-inducible protein |
| *yccA* | b0970 | 5.90 | 0.00104 | inner membrane protein |
| *nhaA* | b0019 | 5.90 | 0.00226 | sodium-proton antiporter |
| *nrdF* | b2676 | 5.83 | 0.00122 | ribonucleoside-diphosphate reductase 2, beta subunit, ferritin-like protein |
| *prlC* | b3498 | 5.81 | 0.00103 | oligopeptidase A |
| *osmY* | b4376 | 5.77 | 0.00033 | periplasmic protein |
| *groS* | b4142 | 5.69 | 0.00006 | Cpn10 chaperonin GroES, small subunit of GroESL |
| *pstS* | b3728 | 5.69 | 0.00140 | phosphate transporter subunit |
| *miaA* | b4171 | 5.63 | 0.00127 | delta(2)-isopentenylpyrophosphate tRNA-adenosine transferase |
| *ycjF* | b1322 | 5.62 | 0.00045 | conserved inner membrane protein |
| *htpX* | b1829 | 5.47 | 0.00170 | predicted endopeptidase |
| *groL* | b4143 | 5.44 | 0.00087 | Cpn60 chaperonin GroEL, large subunit of GroESL |
| *cysW* | b2423 | 5.22 | 0.00046 | sulfate/thiosulfate transporter subunit |
| *yaaX* | b0005 | 5.21 | 0.00065 | predicted protein |

| | | | | |
|---|---|---|---|---|
| *cusR* | b0571 | 5.11 | 0.00035 | DNA-binding response regulator in two-component regulatory system with CusS |
| *yjfN* | b4188 | 4.99 | 0.00097 | predicted protein |
| *entC* | b0593 | 4.91 | 0.00164 | isochorismate synthase 1 |
| *ynfD* | b1586 | 4.85 | 0.00056 | predicted protein |
| *nrdE* | b2675 | 4.84 | 0.00078 | ribonucleoside-diphosphate reductase 2, alpha subunit |
| *htrG* | b3055 | 4.81 | 0.00045 | predicted signal transduction protein (SH3 domain) |
| *gatD* | b2091 | 4.81 | 0.00001 | galactitol-1-phosphate dehydrogenase, Zn-dependent and NAD(P)-binding |
| *glnA* | b3870 | 4.80 | 0.00034 | glutamine synthetase |
| *acrA* | b0463 | 4.74 | 0.00096 | multidrug efflux system |
| *gatB* | b2093 | 4.73 | 0.00072 | galactitol-specific enzyme IIB component of PTS |
| *entD* | b0583 | 4.69 | 0.00006 | phosphopantetheinyltransferase component of enterobactin synthase multienzyme complex |
| *frvX* | b3898 | 4.68 | 0.00011 | predicted endo-1,4-beta-glucanase |
| *yqaE* | b2666 | 4.62 | 0.00033 | predicted membrane protein |
| *yeeD* | b2012 | 4.61 | 0.00064 | conserved protein |
| *fxsA* | b4140 | 4.55 | 0.00070 | inner membrane protein |
| *treB* | b4240 | 4.54 | 0.00027 | fused trehalose(maltose)-specific PTS enzyme:  IIB component/IIC component |
| *yggG* | b2936 | 4.47 | 0.00034 | predicted peptidase |
| *aspA* | b4139 | 4.46 | 0.00026 | aspartate ammonia-lyase |
| *cirA* | b2155 | 4.44 | 0.00034 | ferric iron-catecholate outer membrane transporter |
| *glnP* | b0810 | 4.42 | 0.00003 | glutamine transporter subunit |
| *grpE* | b2614 | 4.25 | 0.00000 | heat shock protein |
| *chaA* | b1216 | 4.18 | 0.00000 | calcium/sodium:proton antiporter |

| | | | | |
|---|---|---|---|---|
| *ybbN* | b0492 | 4.10 | 0.00009 | predicted thioredoxin domain-containing protein |
| *asnA* | b3744 | 4.04 | 0.00016 | asparagine synthetase A |
| *slt* | b4392 | 3.98 | 0.00011 | lytic murein transglycosylase, soluble |
| *ybbA* | b0495 | 3.93 | 0.00053 | predicted transporter subunit: ATP-binding component of ABC superfamily |
| *ybiX* | b0804 | 3.89 | 0.00043 | conserved protein |
| *ybdK* | b0581 | 3.85 | 0.00000 | gamma-glutamyl:cysteine ligase |
| *gatA* | b2094 | 3.84 | 0.00081 | galactitol-specific enzyme IIA component of PTS |
| *glnQ* | b0809 | 3.76 | 0.00034 | glutamine transporter subunit |
| *zntR* | b3292 | 3.66 | 0.00019 | DNA-binding transcriptional activator in response to Zn(II) |
| *osmE* | b1739 | 3.62 | 0.00013 | DNA-binding transcriptional activator |
| *phoB* | b0399 | 3.62 | 0.00000 | DNA-binding response regulator in two-component regulatory system with PhoR (or CreC) |
| *rplL* | b3986 | 3.56 | 0.00049 | 50S ribosomal subunit protein L7/L12 |
| *yqfA* | b2899 | 3.55 | 0.00021 | predicted oxidoreductase, inner membrane subunit |
| *yqjH* | b3070 | 3.47 | 0.00002 | predicted siderophore interacting protein |
| *yhdN* | b3293 | 3.44 | 0.00009 | conserved protein |
| *ybjC* | b0850 | 3.43 | 0.00005 | predicted inner membrane protein |
| *znuA* | b1857 | 3.42 | 0.00060 | zinc transporter subunit: periplasmic-binding component of ABC superfamily |
| *ybhG* | b0795 | 3.41 | 0.00020 | predicted membrane fusion protein (MFP) component of efflux pump, membrane anchor |
| *hslU* | b3931 | 3.37 | 0.00001 | molecular chaperone and ATPase component of HslUV protease |
| *fiu* | b0805 | 3.32 | 0.00055 | predicted iron outer membrane transporter |
| *ygdI* | b2809 | 3.32 | 0.00054 | predicted protein |
| *ydeI* | b1536 | 3.31 | 0.00038 | conserved protein |

| | | | | |
|---|---|---|---|---|
| *yggE* | b2922 | 3.26 | 0.00021 | conserved protein |
| *clpP* | b0437 | 3.23 | 0.00078 | proteolytic subunit of ClpA-ClpP and ClpX-ClpP ATP-dependent serine proteases |
| *manX* | b1817 | 3.17 | 0.00016 | fused mannose-specific PTS enzymes: IIA component/IIB component |
| *dkgA* | b3012 | 3.13 | 0.00068 | 2,5-diketo-D-gluconate reductase A |
| *rrmJ* | b3179 | 3.12 | 0.00030 | 23S rRNA methyltransferase |
| *udp* | b3831 | 3.12 | 0.00057 | uridine phosphorylase |
| *poxB* | b0871 | 3.11 | 0.00000 | pyruvate dehydrogenase (pyruvate oxidase), thiamin-dependent, FAD-binding |
| *lon* | b0439 | 3.11 | 0.00022 | DNA-binding ATP-dependent protease La |
| *ygaM* | b2672 | 3.10 | 0.00034 | predicted protein |
| *nfsA* | b0851 | 3.06 | 0.00024 | nitroreductase A, NADPH-dependent, FMN-dependent |
| *ygaU* | b2665 | 3.03 | 0.00001 | predicted protein |
| *treC* | b4239 | 3.02 | 0.00008 | trehalose-6-P hydrolase |
| *treR* | b4241 | 3.02 | 0.00006 | DNA-binding transcriptional repressor |
| *dgsA* | b1594 | 3.01 | 0.00133 | DNA-binding transcriptional repressor |
| *marA* | b1531 | 3.01 | 0.00074 | DNA-binding transcriptional dual activator of multiple antibiotic resistance |
| *yceI* | b1056 | 2.99 | 0.00121 | predicted protein |
| *ykgM* | b0296 | 2.98 | 0.00156 | rpmJ (L36) paralog |
| *ykgO* | b4506 | 2.98 | 0.00025 | rpmJ (L36) paralog |
| *eptB* | b3546 | 2.95 | 0.00034 | predicted metal dependent hydrolase |
| *ybiI* | b0803 | 2.94 | 0.00001 | conserved protein |
| *yneM* | b4599 | 2.93 | 0.00009 | hypothetical protein |
| *bfd* | b3337 | 2.92 | 0.00000 | bacterioferritin-associated ferredoxin |

| | | | | |
|---|---|---|---|---|
| *araC* | b0064 | 2.91 | 0.00035 | DNA-binding transcriptional dual regulator |
| *yobH* | b4536 | 2.90 | 0.00008 | predicted protein |
| *ybbP* | b0496 | 2.90 | 0.00205 | predicted inner membrane protein |
| *tesB* | b0452 | 2.87 | 0.00032 | acyl-CoA thioesterase II |
| *fepB* | b0592 | 2.87 | 0.00094 | iron-enterobactin transporter subunit |
| *ybeD* | b0631 | 2.86 | 0.00003 | conserved protein |
| *cusS* | b0570 | 2.83 | 0.00062 | sensory histidine kinase in two-component regulatory system with CusR, senses copper ions |
| *cpxR* | b3912 | 2.80 | 0.00068 | DNA-binding response regulator in two-component regulatory system with CpxA |
| *yrbL* | b3207 | 2.80 | 0.00035 | predicted protein |
| *yggX* | b2962 | 2.79 | 0.00000 | protein that protects iron-sulfur proteins against oxidative damage |
| *asnB* | b0674 | 2.79 | 0.00047 | asparagine synthetase B |
| *bssS* | b1060 | 2.77 | 0.00016 | predicted protein |
| *rdoA* | b3859 | 2.74 | 0.00018 | Thr/Ser kinase implicated in Cpx stress response |
| *yafD* | b0209 | 2.74 | 0.00141 | conserved protein |
| *hslR* | b3400 | 2.72 | 0.00000 | ribosome-associated heat shock protein Hsp15 |
| *cysP* | b2425 | 2.72 | 0.00013 | thiosulfate transporter subunit |
| *mutM* | b3635 | 2.71 | 0.00000 | formamidopyrimidine/5-formyluracil/ 5-hydroxymethyluracil DNA glycosylase |
| *hha* | b0460 | 2.70 | 0.00000 | modulator of gene expression, with H-NS |
| *rbsB* | b3751 | 2.70 | 0.00035 | D-ribose transporter subunit |
| *yiaD* | b3552 | 2.70 | 0.00100 | predicted outer membrane lipoprotein |
| *iscR* | b2531 | 2.68 | 0.00004 | DNA-binding transcriptional repressor |
| *ppiA* | b3363 | 2.67 | 0.00033 | peptidyl-prolyl cis-trans isomerase A (rotamase A) |

| | | | | |
|---|---|---|---|---|
| *ybeL* | b0643 | 2.67 | 0.00022 | conserved protein |
| *lolA* | b0891 | 2.66 | 0.00000 | chaperone for lipoproteins |
| *nudK* | b2467 | 2.64 | 0.00175 | predicted NUDIX hydrolase |
| *manY* | b1818 | 2.63 | 0.00000 | mannose-specific enzyme IIC component of PTS |
| *mfd* | b1114 | 2.63 | 0.00101 | transcription-repair coupling factor |
| *mdtJ* | b1600 | 2.62 | 0.00421 | multidrug efflux system transporter |
| *hslV* | b3932 | 2.62 | 0.00004 | peptidase component of the HslUV protease |
| *inaA* | b2237 | 2.62 | 0.00008 | conserved protein |
| *yohN* | b2107 | 2.61 | 0.00004 | predicted protein |
| *nfo* | b2159 | 2.60 | 0.00176 | endonuclease IV with intrinsic 3'-5' exonuclease activity |
| *uspF* | b1376 | 2.58 | 0.00026 | stress-induced protein, ATP-binding protein |
| *dsbA* | b3860 | 2.57 | 0.00113 | periplasmic protein disulfide isomerase I |
| *ygbE* | b2749 | 2.56 | 0.00153 | conserved inner membrane protein |
| *cydA* | b0733 | 2.55 | 0.00005 | cytochrome d terminal oxidase, subunit I |
| *sfsA* | b0146 | 2.55 | 0.00239 | predicted DNA-binding transcriptional regulator |
| *nhaR* | b0020 | 2.55 | 0.00320 | DNA-binding transcriptional activator |
| *yobB* | b1843 | 2.55 | 0.00192 | conserved protein |
| *ucpA* | b2426 | 2.54 | 0.00036 | predicted oxidoredutase, sulfate metabolism protein |
| *yhhA* | b3448 | 2.53 | 0.00071 | conserved protein |
| *yrdA* | b3279 | 2.53 | 0.00014 | conserved protein |
| *acrB* | b0462 | 2.51 | 0.00001 | multidrug efflux system protein |
| *yeaO* | b1792 | 2.50 | 0.00323 | conserved protein |

| | | | | |
|---|---|---|---|---|
| *yaeR* | b0187 | 2.50 | 0.00004 | predicted lyase |
| *cysK* | b2414 | 2.49 | 0.00000 | cysteine synthase A, O-acetylserine sulfhydrolase A subunit |
| *acpP* | b1094 | 2.48 | 0.00044 | acyl carrier protein (ACP) |
| *ldhA* | b1380 | 2.48 | 0.00007 | fermentative D-lactate dehydrogenase, NAD-dependent |
| *yrfG* | b3399 | 2.48 | 0.00061 | predicted hydrolase |
| *yhbW* | b3160 | 2.48 | 0.00079 | predicted enzyme |
| *phoR* | b0400 | 2.47 | 0.00049 | sensory histidine kinase in two-component regulatory system with PhoB |
| *ygiB* | b3037 | 2.46 | 0.00000 | conserved outer membrane protein |
| *yibT* | b4554 | 2.46 | 0.00000 | predicted protein |
| *gcvH* | b2904 | 2.45 | 0.00339 | glycine cleavage complex lipoylprotein |
| *nanT* | b3224 | 2.45 | 0.00000 | sialic acid transporter |
| *ybiH* | b0796 | 2.44 | 0.00288 | predicted DNA-binding transcriptional regulator |
| *ybaY* | b0453 | 2.44 | 0.00105 | predicted outer membrane lipoprotein |
| *zwf* | b1852 | 2.42 | 0.00227 | glucose-6-phosphate dehydrogenase |
| *yqjA* | b3095 | 2.42 | 0.00409 | conserved inner membrane protein |
| *idi* | b2889 | 2.42 | 0.00186 | isopentenyl diphosphate isomerase |
| *rseA* | b2572 | 2.41 | 0.00001 | anti-sigma factor |
| *hflX* | b4173 | 2.41 | 0.00048 | predicted GTPase |
| *ygfZ* | b2898 | 2.41 | 0.00002 | predicted folate-dependent regulatory protein |
| *ybhF* | b0794 | 2.40 | 0.00438 | fused predicted transporter subunits of ABC superfamily: ATP-binding components |
| *yncE* | b1452 | 2.37 | 0.00000 | conserved protein |
| *ydiE* | b1705 | 2.37 | 0.00008 | conserved protein |

| | | | | |
|---|---|---|---|---|
| *sodA* | b3908 | 2.36 | 0.00000 | superoxide dismutase, Mn |
| *dps* | b0812 | 2.35 | 0.00091 | Fe-binding and storage protein |
| *ygiC* | b3038 | 2.33 | 0.00211 | predicted enzyme |
| *degQ* | b3234 | 2.32 | 0.00203 | serine endoprotease, periplasmic |
| *mltC* | b2963 | 2.32 | 0.00053 | membrane-bound lytic murein transglycosylase C |
| *adhE* | b1241 | 2.32 | 0.00000 | fused acetaldehyde-CoA dehydrogenase/iron-dependent alcohol dehydrogenase/pyruvate-formate lyase deactivase |
| *yhdU* | b3263 | 2.31 | 0.00207 | predicted membrane protein |
| *glnG* | b3868 | 2.31 | 0.00411 | fused DNA-binding response regulator in two-component regulatory system with GlnL: response regulator/sigma54 interaction protein |
| *ybaL* | b0478 | 2.31 | 0.00001 | predicted transporter with NAD(P)-binding Rossmann-fold domain |
| *uxaC* | b3092 | 2.31 | 0.00008 | uronate isomerase |
| *hflK* | b4174 | 2.31 | 0.00000 | modulator for HflB protease specific for phage lambda cII repressor |
| *treF* | b3519 | 2.31 | 0.00006 | cytoplasmic trehalase |
| *hslO* | b3401 | 2.28 | 0.00000 | heat shock protein Hsp33 |
| *fecI* | b4293 | 2.27 | 0.00085 | KpLE2 phage-like element; RNA polymerase, sigma 19 factor |
| *appB* | b0979 | 2.27 | 0.00021 | cytochrome bd-II oxidase, subunit II |
| *dcrB* | b3472 | 2.26 | 0.00000 | periplasmic protein |
| *pps* | b1702 | 2.26 | 0.00044 | phosphoenolpyruvate synthase |
| *ytjA* | b4568 | 2.26 | 0.00031 | predicted protein |
| *manA* | b1613 | 2.26 | 0.00454 | mannose-6-phosphate isomerase |
| *ygjH* | b3074 | 2.24 | 0.00221 | conserved protein |
| *mdoD* | b1424 | 2.23 | 0.00082 | glucan biosynthesis protein, periplasmic |
| *yeiI* | b2160 | 2.23 | 0.00108 | predicted kinase |

| | | | | |
|---|---|---|---|---|
| *pstC* | b3727 | 2.22 | 0.00022 | phosphate transporter subunit |
| *mtlR* | b3601 | 2.22 | 0.00245 | DNA-binding repressor |
| *rbsC* | b3750 | 2.21 | 0.00258 | D-ribose transporter subunit |
| *uspC* | b1895 | 2.19 | 0.00040 | universal stress protein |
| *glgB* | b3432 | 2.17 | 0.00373 | 1,4-alpha-glucan branching enzyme |
| *nanA* | b3225 | 2.17 | 0.00084 | N-acetylneuraminate lyase |
| *rbsA* | b3749 | 2.15 | 0.00298 | fused D-ribose transporter subunits of ABC superfamily: ATP-binding components |
| *ybeZ* | b0660 | 2.15 | 0.00147 | predicted protein with nucleoside triphosphate hydrolase domain |
| *rbsD* | b3748 | 2.14 | 0.00006 | predicted cytoplasmic sugar-binding protein |
| *gsiA* | b0829 | 2.14 | 0.00544 | fused predicted peptide transport subunits of ABC superfamily: ATP-binding components |
| *fliK* | b1943 | 2.13 | 0.00002 | flagellar hook-length control protein |
| *cpxA* | b3911 | 2.13 | 0.00003 | sensory histidine kinase in two-component regulatory system with CpxR |
| *feoA* | b3408 | 2.13 | 0.00063 | ferrous iron transporter, protein A |
| *yhjC* | b3521 | 2.11 | 0.00054 | predicted DNA-binding transcriptional regulator |
| *yaiW* | b0378 | 2.11 | 0.00242 | predicted DNA-binding transcriptional regulator |
| *yncL* | b4598 | 2.10 | 0.00131 | hypothetical protein |
| *yfgC* | b2494 | 2.10 | 0.00238 | predicted peptidase |
| *yciI* | b1251 | 2.09 | 0.00056 | predicted enzyme |
| *chaC* | b1218 | 2.09 | 0.00391 | regulatory protein for cation transport |
| *iscA* | b2528 | 2.09 | 0.00000 | FeS cluster assembly protein |
| *pspA* | b1304 | 2.08 | 0.00000 | regulatory protein for phage-shock-protein operon |
| *dgt* | b0160 | 2.07 | 0.00148 | deoxyguanosine triphosphate triphosphohydrolase |

| | | | | |
|---|---|---|---|---|
| *ybeY* | b0659 | 2.07 | 0.00188 | conserved protein |
| *iscU* | b2529 | 2.06 | 0.00007 | scaffold protein |
| *dnaJ* | b0015 | 2.06 | 0.00015 | chaperone Hsp40, co-chaperone with DnaK |
| *yheL* | b3343 | 2.06 | 0.00000 | predicted intracellular sulfur oxidation protein |
| *acrD* | b2470 | 2.06 | 0.00006 | aminoglycoside/multidrug efflux system |
| *ftnB* | b1902 | 2.06 | 0.00574 | predicted ferritin-like protein |
| *fecR* | b4292 | 2.05 | 0.00156 | KpLE2 phage-like element; transmembrane signal transducer for ferric citrate transport |
| *fldA* | b0684 | 2.05 | 0.00000 | flavodoxin 1 |
| *mdtI* | b1599 | 2.03 | 0.00727 | multidrug efflux system transporter |
| *aldA* | b1415 | 2.01 | 0.00619 | aldehyde dehydrogenase A, NAD-linked |
| *yaeH* | b0163 | 2.01 | 0.00019 | conserved protein |
| *qor* | b4051 | 2.01 | 0.00004 | quinone oxidoreductase, NADPH-dependent |

**Silver nanoparticle down-regulated genes**

| Gene | Locus Tag | Ratio | t-test *P* value | Description |
|---|---|---|---|---|
| *rplU* | b3186 | 0.50 | 0.00208 | 50S ribosomal subunit protein L21 |
| *prmA* | b3259 | 0.50 | 0.00324 | methylase for 50S ribosomal subunit protein L11 |
| *rnhB* | b0183 | 0.50 | 0.00726 | ribonuclease HII, degrades RNA of DNA-RNA hybrids |
| *fabA* | b0954 | 0.50 | 0.00039 | beta-hydroxydecanoyl thioester dehydrase |
| *pal* | b0741 | 0.50 | 0.00481 | peptidoglycan-associated outer membrane lipoprotein |
| *fabD* | b1092 | 0.50 | 0.00135 | malonyl-CoA-[acyl-carrier-protein] transacylase |
| *yejK* | b2186 | 0.49 | 0.00899 | nucleotide associated protein |
| *yeaL* | b1789 | 0.49 | 0.00325 | conserved inner membrane protein |
| *mnmA* | b1133 | 0.49 | 0.00141 | tRNA (5-methylaminomethyl-2-thiouridylate)-methyltransferase |
| *nudB* | b1865 | 0.49 | 0.00323 | dATP pyrophosphohydrolase |
| *folC* | b2315 | 0.49 | 0.00814 | bifunctional folylpolyglutamate synthase/ dihydrofolate synthase |
| *rplW* | b3318 | 0.49 | 0.00000 | 50S ribosomal subunit protein L23 |
| *yfeA* | b2395 | 0.49 | 0.00614 | predicted diguanylate cyclase |
| *yqgB* | b2939 | 0.49 | 0.00707 | predicted protein |
| *rnc* | b2567 | 0.49 | 0.00483 | RNase III |
| *menD* | b2264 | 0.49 | 0.00558 | bifunctional 2-oxoglutarate decarboxylase/ SHCHC synthase |
| *rnb* | b1286 | 0.49 | 0.00925 | ribonuclease II |
| *rnt* | b1652 | 0.49 | 0.00829 | ribonuclease T (RNase T) |
| *ybeA* | b0636 | 0.49 | 0.00337 | conserved protein |
| *yccS* | b0960 | 0.49 | 0.01078 | predicted inner membrane protein |

| | | | | |
|---|---|---|---|---|
| *mipA* | b1782 | 0.49 | 0.00309 | scaffolding protein for murein synthesizing machinery |
| *ybgF* | b0742 | 0.49 | 0.00107 | predicted protein |
| *yfaE* | b2236 | 0.49 | 0.00348 | predicted 2Fe-2S cluster-containing protein |
| *proY* | b0402 | 0.49 | 0.00908 | predicted cryptic proline transporter |
| *ybiR* | b0818 | 0.49 | 0.00927 | predicted transporter |
| *rplM* | b3231 | 0.48 | 0.00087 | 50S ribosomal subunit protein L13 |
| *proQ* | b1831 | 0.48 | 0.00176 | predicted structural transport element |
| *rph* | b3643 | 0.48 | 0.00628 | defective ribonuclease PH |
| *pyrH* | b0171 | 0.48 | 0.00394 | uridylate kinase |
| *rsxE* | b1632 | 0.48 | 0.00857 | predicted inner membrane NADH-quinone reductase |
| *mnmG* | b3741 | 0.48 | 0.00540 | glucose-inhibited cell-division protein |
| *yjcD* | b4064 | 0.48 | 0.00141 | predicted permease |
| *rpsS* | b3316 | 0.48 | 0.00026 | 30S ribosomal subunit protein S19 |
| *yijP* | b3955 | 0.48 | 0.00740 | conserved inner membrane protein |
| *rpsF* | b4200 | 0.48 | 0.00000 | 30S ribosomal subunit protein S6 |
| *rplB* | b3317 | 0.48 | 0.00000 | 50S ribosomal subunit protein L2 |
| *nuoE* | b2285 | 0.48 | 0.00952 | NADH:ubiquinone oxidoreductase, chain E |
| *yidC* | b3705 | 0.48 | 0.00214 | cytoplasmic insertase into membrane protein, Sec system |
| *cmoB* | b1871 | 0.48 | 0.00750 | predicted S-adenosyl-L-methionine-dependent methyltransferase |
| *ybeB* | b0637 | 0.48 | 0.00519 | predicted protein |
| *purE* | b0523 | 0.48 | 0.01538 | N5-carboxyaminoimidazole ribonucleotide mutase |
| *yfdG* | b2350 | 0.48 | 0.00461 | CPS-53 (KpLE1) prophage; bactoprenol-linked glucose translocase (flippase) |

| | | | | |
|---|---|---|---|---|
| *ychF* | b1203 | 0.48 | 0.00353 | predicted GTP-binding protein |
| *fabI* | b1288 | 0.48 | 0.00074 | enoyl-[acyl-carrier-protein] reductase, NADH-dependent |
| *mnmE* | b3706 | 0.47 | 0.00363 | GTPase |
| *yebC* | b1864 | 0.47 | 0.00163 | conserved protein |
| *ydgK* | b1626 | 0.47 | 0.00914 | conserved inner membrane protein |
| *ygdQ* | b2832 | 0.47 | 0.01005 | predicted inner membrane protein |
| *rnd* | b1804 | 0.47 | 0.01022 | ribonuclease D |
| *yahM* | b0327 | 0.47 | 0.01651 | predicted protein |
| *fabF* | b1095 | 0.47 | 0.00135 | 3-oxoacyl-[acyl-carrier-protein] synthase II |
| *yedJ* | b1962 | 0.47 | 0.01110 | predicted phosphohydrolase |
| *tyrP* | b1907 | 0.47 | 0.00915 | tyrosine transporter |
| *ytfL* | b4218 | 0.47 | 0.01262 | predicted inner membrane protein |
| *crcB* | b0624 | 0.47 | 0.01253 | predicted inner membrane protein associated with chromosome condensation |
| *yadB* | b0144 | 0.47 | 0.01064 | glutamyl-Q tRNA(Asp) synthetase |
| *ycbJ* | b0919 | 0.46 | 0.00981 | conserved protein |
| *yihI* | b3866 | 0.46 | 0.00380 | conserved protein |
| *speA* | b2938 | 0.46 | 0.01035 | biosynthetic arginine decarboxylase, PLP-binding |
| *mrdA* | b0635 | 0.46 | 0.00765 | transpeptidase involved in peptidoglycan synthesis (penicillin-binding protein 2) |
| *rho* | b3783 | 0.46 | 0.00335 | transcription termination factor |
| *proP* | b4111 | 0.46 | 0.00902 | proline/glycine betaine transporter |
| *dusC* | b2140 | 0.46 | 0.00951 | tRNA-dihydrouridine synthase C |
| *nth* | b1633 | 0.46 | 0.01019 | DNA glycosylase and apyrimidinic (AP) lyase (endonuclease III) |

| | | | | |
|---|---|---|---|---|
| *srmB* | b2576 | 0.46 | 0.00212 | ATP-dependent RNA helicase |
| *trmD* | b2607 | 0.46 | 0.00004 | tRNA (guanine-1-)-methyltransferase |
| *sodB* | b1656 | 0.46 | 0.00319 | superoxide dismutase, Fe |
| *era* | b2566 | 0.46 | 0.00451 | membrane-associated, 16S rRNA-binding GTPase |
| *yfiD* | b2579 | 0.46 | 0.00654 | pyruvate formate lyase subunit |
| *rrmA* | b1822 | 0.45 | 0.01098 | 23S rRNA m1G745 methyltransferase |
| *purK* | b0522 | 0.45 | 0.00752 | N5-carboxyaminoimidazole ribonucleotide synthase |
| *rsxD* | b1630 | 0.45 | 0.01070 | predicted inner membrane oxidoreductase |
| *yhdT* | b3257 | 0.45 | 0.01134 | conserved inner membrane protein |
| *secE* | b3981 | 0.45 | 0.00354 | preprotein translocase membrane subunit |
| *rplY* | b2185 | 0.45 | 0.00089 | 50S ribosomal subunit protein L25 |
| *der* | b2511 | 0.45 | 0.01398 | predicted GTP-binding protein |
| *rplD* | b3319 | 0.45 | 0.00024 | 50S ribosomal subunit protein L4 |
| *icd* | b1136 | 0.44 | 0.00198 | e14 prophage; isocitrate dehydrogenase, specific for NADP+ |
| *mdtK* | b1663 | 0.44 | 0.00700 | multidrug efflux system transporter |
| *rluC* | b1086 | 0.44 | 0.00265 | 23S rRNA pseudouridylate synthase |
| *aroE* | b3281 | 0.44 | 0.00634 | dehydroshikimate reductase, NAD(P)-binding |
| *cmoA* | b1870 | 0.44 | 0.00993 | predicted methyltransferase |
| *lpxH* | b0524 | 0.44 | 0.00294 | UDP-2,3-diacylglucosamine pyrophosphatase |
| *panF* | b3258 | 0.44 | 0.00735 | pantothenate:sodium symporter |
| *ygdD* | b2807 | 0.44 | 0.00766 | conserved inner membrane protein |
| *ygdL* | b2812 | 0.44 | 0.00585 | conserved protein |

| | | | | |
|---|---|---|---|---|
| *thiI* | b0423 | 0.44 | 0.00711 | sulfurtransferase required for thiamine and 4-thiouridine biosynthesis |
| *lpxA* | b0181 | 0.44 | 0.00291 | UDP-N-acetylglucosamine acetyltransferase |
| *ecnA* | b4410 | 0.44 | 0.00195 | entericidin A membrane lipoprotein, antidote entericidin B |
| *yfdH* | b2351 | 0.43 | 0.00930 | CPS-53 (KpLE1) prophage; bactoprenol glucosyl transferase |
| *yfbB* | b2263 | 0.43 | 0.00948 | predicted peptidase |
| *yhhQ* | b3471 | 0.43 | 0.01265 | conserved inner membrane protein |
| *yccW* | b0967 | 0.43 | 0.01213 | predicted methyltransferase |
| *prs* | b1207 | 0.43 | 0.00297 | phosphoribosylpyrophosphate synthase |
| *rsxC* | b1629 | 0.43 | 0.00834 | fused predicted 4Fe-4S ferredoxin-type protein/conserved protein |
| *prfA* | b1211 | 0.43 | 0.01161 | peptide chain release factor RF-1 |
| *sscR* | b2765 | 0.43 | 0.00600 | 6-pyruvoyl tetrahydrobiopterin synthase (PTPS) |
| *gidB* | b3740 | 0.43 | 0.01191 | methyltransferase, SAM-dependent methyltransferase, glucose-inhibited cell-division protein |
| *prmC* | b1212 | 0.42 | 0.01573 | N5-glutamine methyltransferase, modifies release factors RF-1 and RF-2 |
| *aroK* | b3390 | 0.42 | 0.00114 | shikimate kinase I |
| *rsxA* | b1627 | 0.42 | 0.00257 | predicted inner membrane subunit |
| *ydhO* | b1655 | 0.42 | 0.01685 | predicted lipoprotein |
| *rplC* | b3320 | 0.42 | 0.00000 | 50S ribosomal subunit protein L3 |
| *rpsT* | b0023 | 0.42 | 0.00081 | 30S ribosomal subunit protein S20 |
| *cyoA* | b0432 | 0.42 | 0.00332 | cytochrome o ubiquinol oxidase subunit II |
| *ycaD* | b0898 | 0.42 | 0.01516 | predicted transporter |
| *sirA* | b3470 | 0.42 | 0.00922 | conserved protein required for cell growth |
| *yejG* | b2181 | 0.42 | 0.00850 | predicted protein |

| | | | | |
|---|---|---|---|---|
| *queA* | b0405 | 0.42 | 0.01835 | S-adenosylmethionine:tRNA ribosyltransferase-isomerase |
| *ydcP* | b1435 | 0.42 | 0.01013 | predicted peptidase |
| *pdhR* | b0113 | 0.42 | 0.00517 | DNA-binding transcriptional dual regulator |
| *yfgJ* | b2510 | 0.42 | 0.00859 | predicted protein |
| *rsxB* | b1628 | 0.42 | 0.01460 | predicted iron-sulfur protein |
| *leuE* | b1798 | 0.42 | 0.00796 | neutral amino-acid efflux system |
| *yecF* | b1915 | 0.41 | 0.00896 | predicted protein |
| *rfbB* | b2041 | 0.41 | 0.01395 | dTDP-glucose 4,6 dehydratase, NAD(P)-binding |
| *trmA* | b3965 | 0.41 | 0.01446 | tRNA (uracil-5-)-methyltransferase |
| *ygdE* | b2806 | 0.41 | 0.00911 | predicted methyltransferase |
| *adk* | b0474 | 0.41 | 0.00386 | adenylate kinase |
| *yrdB* | b3280 | 0.41 | 0.01571 | conserved protein |
| *rfaH* | b3842 | 0.41 | 0.01547 | DNA-binding transcriptional antiterminator |
| *rpsJ* | b3321 | 0.41 | 0.00026 | 30S ribosomal subunit protein S10 |
| *cyoC* | b0430 | 0.41 | 0.00526 | cytochrome o ubiquinol oxidase subunit III |
| *lpxK* | b0915 | 0.41 | 0.00850 | lipid A 4'kinase |
| *nuoC* | b2286 | 0.41 | 0.01012 | NADH:ubiquinone oxidoreductase, chain C,D |
| *ybfE* | b0685 | 0.41 | 0.01260 | lexA-regulated predicted protein |
| *recO* | b2565 | 0.40 | 0.01173 | gap repair protein |
| *rimM* | b2608 | 0.40 | 0.00002 | 16S rRNA processing protein |
| *pyrG* | b2780 | 0.40 | 0.01051 | CTP synthetase |
| *cfa* | b1661 | 0.40 | 0.01643 | cyclopropane fatty acyl phospholipid synthase (unsaturated-phospholipid methyltransferase) |

| | | | | |
|---|---|---|---|---|
| *aroB* | b3389 | 0.40 | 0.00309 | 3-dehydroquinate synthase |
| *rsxG* | b1631 | 0.40 | 0.01030 | predicted oxidoreductase |
| *potC* | b1124 | 0.40 | 0.01631 | polyamine transporter subunit |
| *metK* | b2942 | 0.40 | 0.00556 | methionine adenosyltransferase 1 |
| *cyoB* | b0431 | 0.40 | 0.00576 | cytochrome o ubiquinol oxidase subunit I |
| *ylaC* | b0458 | 0.40 | 0.00420 | predicted inner membrane protein |
| *gltX* | b2400 | 0.40 | 0.00343 | glutamyl-tRNA synthetase |
| *cyoE* | b0428 | 0.40 | 0.00532 | protoheme IX farnesyltransferase |
| *fadD* | b1805 | 0.39 | 0.01616 | acyl-CoA synthetase (long-chain-fatty-acid--CoA ligase) |
| *menE* | b2260 | 0.39 | 0.01135 | o-succinylbenzoate-CoA ligase |
| *nhaB* | b1186 | 0.39 | 0.01677 | sodium:proton antiporter |
| *yceA* | b1055 | 0.39 | 0.00615 | conserved protein |
| *miaB* | b0661 | 0.39 | 0.01097 | isopentenyl-adenosine A37 tRNA methylthiolase |
| *speE* | b0121 | 0.39 | 0.01808 | spermidine synthase (putrescine aminopropyltransferase) |
| *yciY* | b4595 | 0.39 | 0.01838 | hypothetical protein |
| *yieG* | b3714 | 0.39 | 0.01540 | predicted inner membrane protein |
| *yfiF* | b2581 | 0.39 | 0.00420 | predicted methyltransferase |
| *prfC* | b4375 | 0.39 | 0.00272 | peptide chain release factor RF-3 |
| *nuoB* | b2287 | 0.39 | 0.00475 | NADH:ubiquinone oxidoreductase, chain B |
| *plsX* | b1090 | 0.38 | 0.01112 | fatty acid/phospholipid synthesis protein |
| *purR* | b1658 | 0.38 | 0.00907 | DNA-binding transcriptional repressor, hypoxanthine-binding |
| *infB* | b3168 | 0.38 | 0.00979 | fused protein chain initiation factor 2, IF2: membrane protein/conserved protein |

| | | | | |
|---|---|---|---|---|
| *ruvC* | b1863 | 0.38 | 0.00390 | component of RuvABC resolvasome, endonuclease |
| *stpA* | b2669 | 0.38 | 0.01913 | DNA binding protein, nucleoid-associated |
| *ybiT* | b0820 | 0.38 | 0.01862 | fused predicted transporter subunits of ABC superfamily: ATP-binding components |
| *ydfZ* | b1541 | 0.38 | 0.02832 | conserved protein |
| *upp* | b2498 | 0.38 | 0.00506 | uracil phosphoribosyltransferase |
| *cyoD* | b0429 | 0.38 | 0.01005 | cytochrome o ubiquinol oxidase subunit IV |
| *speD* | b0120 | 0.38 | 0.01127 | S-adenosylmethionine decarboxylase |
| *ecnB* | b4411 | 0.38 | 0.00810 | entericidin B membrane lipoprotein |
| *fis* | b3261 | 0.38 | 0.00271 | global DNA-binding transcriptional dual regulator |
| *rlmN* | b2517 | 0.37 | 0.01631 | predicted enzyme |
| *putA* | b1014 | 0.37 | 0.01733 | fused DNA-binding transcriptional regulator/proline dehydrogenase/pyrroline-5-carboxylate dehydrogenase |
| *ychM* | b1206 | 0.37 | 0.01997 | predicted transporter |
| *yecJ* | b4537 | 0.37 | 0.00827 | predicted protein |
| *pyrF* | b1281 | 0.37 | 0.01642 | orotidine-5'-phosphate decarboxylase |
| *rlmG* | b3084 | 0.37 | 0.01909 | predicted methyltransferase small domain |
| *rarD* | b3819 | 0.37 | 0.01896 | predicted chloramphenical resistance permease |
| *udk* | b2066 | 0.37 | 0.01538 | uridine/cytidine kinase |
| *ycaO* | b0905 | 0.37 | 0.01292 | conserved protein |
| *rpsP* | b2609 | 0.36 | 0.00178 | 30S ribosomal subunit protein S16 |
| *ybaK* | b0481 | 0.36 | 0.01614 | conserved protein |
| *pyrD* | b0945 | 0.36 | 0.01744 | dihydro-orotate oxidase, FMN-linked |
| *ydgI* | b1605 | 0.36 | 0.01825 | predicted arginine/ornithine antiporter transporter |

| | | | | |
|---|---|---|---|---|
| *nusA* | b3169 | 0.36 | 0.00758 | transcription termination/antitermination L factor |
| *lldP* | b3603 | 0.36 | 0.00595 | L-lactate permease |
| *rluA* | b0058 | 0.35 | 0.01890 | pseudouridine synthase for 23S rRNA (position 746) and tRNAphe(position 32) |
| *potA* | b1126 | 0.35 | 0.01598 | polyamine transporter subunit |
| *yfaZ* | b2250 | 0.35 | 0.00649 | predicted outer membrane porin protein |
| *yciH* | b1282 | 0.35 | 0.02051 | conserved protein |
| *apt* | b0469 | 0.35 | 0.00021 | adenine phosphoribosyltransferase |
| *nuoA* | b2288 | 0.35 | 0.00818 | NADH:ubiquinone oxidoreductase, membrane subunit A |
| *yigI* | b3820 | 0.35 | 0.01874 | conserved protein |
| *tadA* | b2559 | 0.35 | 0.01094 | tRNA-specific adenosine deaminase |
| *potB* | b1125 | 0.35 | 0.01470 | polyamine transporter subunit |
| *lysP* | b2156 | 0.35 | 0.02242 | lysine transporter |
| *nusG* | b3982 | 0.34 | 0.00051 | transcription termination factor |
| *gpt* | b0238 | 0.34 | 0.00430 | guanine-hypoxanthine phosphoribosyltransferase |
| *gsk* | b0477 | 0.33 | 0.01817 | inosine/guanosine kinase |
| *yhiN* | b3492 | 0.33 | 0.01574 | predicted oxidoreductase with FAD/NAD(P)-binding domain |
| *ybiP* | b0815 | 0.33 | 0.02930 | predicted hydrolase, inner membrane |
| *obgE* | b3183 | 0.33 | 0.01073 | GTPase involved in cell partioning and DNA repair |
| *ygiQ* | b4469 | 0.33 | 0.02402 | conserved protein |
| *yegQ* | b2081 | 0.32 | 0.01819 | predicted peptidase |
| *infA* | b0884 | 0.32 | 0.01141 | translation initiation factor IF-1 |
| *cspA* | b3556 | 0.32 | 0.00287 | major cold shock protein |

| | | | | |
|---|---|---|---|---|
| *hepA* | b0059 | 0.32 | 0.02514 | RNA polymerase-associated helicase protein (ATPase and RNA polymerase recycling factor) |
| *puuP* | b1296 | 0.32 | 0.03273 | putrescine importer |
| *uraA* | b2497 | 0.31 | 0.02722 | uracil transporter |
| *tpr* | b1229 | 0.31 | 0.02685 | predicted protamine-like protein |
| *ydcI* | b1422 | 0.31 | 0.02664 | predicted DNA-binding transcriptional regulator |
| *rhlE* | b0797 | 0.31 | 0.02649 | RNA helicase |
| *yhbC* | b3170 | 0.31 | 0.01628 | conserved protein |
| *yliG* | b0835 | 0.30 | 0.02249 | predicted SAM-dependent methyltransferase |
| *rluB* | b1269 | 0.30 | 0.00720 | 23S rRNA pseudouridylate synthase |
| *yciX* | b4523 | 0.29 | 0.03343 | hypothetical protein |
| *emrD* | b3673 | 0.29 | 0.03030 | multidrug efflux system protein |
| *rlmF* | b0807 | 0.29 | 0.02582 | predicted SAM-dependent methyltransferase |
| *yfhL* | b2562 | 0.29 | 0.02757 | predicted 4Fe-4S cluster-containing protein |
| *yidD* | b4557 | 0.29 | 0.00725 | predicted protein |
| *kgtP* | b2587 | 0.28 | 0.01071 | alpha-ketoglutarate transporter |
| *dusB* | b3260 | 0.28 | 0.00331 | tRNA-dihydrouridine synthase B |
| *fadL* | b2344 | 0.28 | 0.02018 | long-chain fatty acid outer membrane transporter |
| *yhbY* | b3180 | 0.27 | 0.00941 | predicted RNA-binding protein |
| *yhaM* | b4470 | 0.24 | 0.03475 | conserved protein |
| *fnr* | b1334 | 0.24 | 0.01165 | DNA-binding transcriptional dual regulator, global regulator of anaerobic growth |
| *deaD* | b3162 | 0.23 | 0.02286 | ATP-dependent RNA helicase |
| *flhD* | b1892 | 0.22 | 0.02184 | DNA-binding transcriptional dual regulator with FlhC |

| | | | | |
|---|---|---|---|---|
| *yhbE* | b3184 | 0.21 | 0.01302 | conserved inner membrane protein |
| *yafK* | b0224 | 0.19 | 0.02334 | conserved protein |
| *yeeF* | b2014 | 0.18 | 0.01517 | predicted amino-acid transporter |
| *ompF* | b0929 | 0.16 | 0.00723 | outer membrane porin 1a (Ia;b;F) |
| *ydiY* | b1722 | 0.13 | 0.01855 | conserved protein |
| *suhB* | b2533 | 0.12 | 0.02375 | inositol monophosphatase |

**Silver nitrate up-regulated genes**

| Gene | Locus Tag | Ratio | t-test *P* value | Description |
|---|---|---|---|---|
| *cirA* | b2155 | 386.65 | 0.00000 | ferric iron-catecholate outer membrane transporter |
| *cusF* | b0573 | 376.39 | 0.00000 | periplasmic copper-binding protein |
| *cueO* | b0123 | 320.45 | 0.00000 | multicopper oxidase (laccase) |
| *yebE* | b1846 | 289.49 | 0.00000 | conserved protein |
| *ydbK* | b1378 | 285.35 | 0.00000 | fused predicted pyruvate-flavodoxin oxidoreductase: conserved protein/conserved protein/FeS binding protein |
| *fpr* | b3924 | 280.40 | 0.00000 | ferredoxin-NADP reductase |
| *ybdZ* | b4511 | 253.34 | 0.00000 | conserved protein |
| *ibpA* | b3687 | 180.16 | 0.00000 | heat shock chaperone |
| *entC* | b0593 | 161.96 | 0.00000 | isochorismate synthase 1 |
| *ybdB* | b0597 | 160.24 | 0.00000 | conserved protein |
| *fes* | b0585 | 150.10 | 0.00000 | enterobactin/ferric enterobactin esterase |
| *entA* | b0596 | 146.78 | 0.00000 | 2,3-dihydro-2,3-dihydroxybenzoate dehydrogenase |
| *yjjZ* | b4567 | 146.46 | 0.00001 | predicted protein |
| *entB* | b0595 | 116.39 | 0.00000 | isochorismatase |
| *cusB* | b0574 | 99.98 | 0.00000 | copper/silver efflux system, membrane fusion protein |
| *mdtJ* | b1600 | 99.91 | 0.00000 | multidrug efflux system transporter |
| *nrdH* | b2673 | 87.02 | 0.00000 | glutaredoxin-like protein |
| *clpB* | b2592 | 83.16 | 0.00334 | protein disaggregation chaperone |
| *entE* | b0594 | 77.22 | 0.00001 | 2,3-dihydroxybenzoate-AMP ligase component of enterobactin synthase multienzyme complex |
| *nrdI* | b2674 | 74.90 | 0.00000 | protein that stimulates ribonucleotide reduction |

| | | | | |
|---|---|---|---|---|
| *cusC* | b0572 | 72.48 | 0.00000 | copper/silver efflux system, outer membrane component |
| *nrdE* | b2675 | 68.50 | 0.00000 | ribonucleoside-diphosphate reductase 2, alpha subunit |
| *yncJ* | b1436 | 68.13 | 0.00001 | predicted protein |
| *fumC* | b1611 | 67.82 | 0.00000 | fumarate hydratase (fumarase C),aerobic Class II |
| *mdtI* | b1599 | 65.60 | 0.00090 | multidrug efflux system transporter |
| *alx* | b3088 | 64.08 | 0.00000 | predicted inner membrane protein, part of terminus |
| *sufA* | b1684 | 62.29 | 0.00000 | Fe-S cluster assembly protein |
| *ydiE* | b1705 | 61.85 | 0.00000 | conserved protein |
| *fepB* | b0592 | 55.40 | 0.00101 | iron-enterobactin transporter subunit |
| *entF* | b0586 | 53.56 | 0.00000 | enterobactin synthase multienzyme complex component,  ATP-dependent |
| *cusA* | b0575 | 50.32 | 0.00000 | copper/silver efflux system, membrane component |
| *fepA* | b0584 | 47.48 | 0.00000 | iron-enterobactin outer membrane transporter |
| *copA* | b0484 | 47.09 | 0.00005 | copper transporter |
| *poxB* | b0871 | 44.91 | 0.00000 | pyruvate dehydrogenase (pyruvate oxidase), thiamin-dependent, FAD-binding |
| *fiu* | b0805 | 41.44 | 0.00000 | |
| *fecI* | b4293 | 35.64 | 0.00110 | KpLE2 phage-like element; RNA polymerase, sigma 19 factor |
| *bfd* | b3337 | 31.25 | 0.00045 | bacterioferritin-associated ferredoxin |
| *sufB* | b1683 | 30.58 | 0.00001 | component of SufBCD complex |
| *fecR* | b4292 | 29.91 | 0.00043 | KpLE2 phage-like element; transmembrane signal transducer for ferric citrate transport |
| *nhoA* | b1463 | 27.33 | 0.00000 | N-hydroxyarylamine O-acetyltransferase |
| *fepG* | b0589 | 27.12 | 0.00081 | iron-enterobactin transporter subunit |
| *ycfS* | b1113 | 25.65 | 0.00516 | conserved protein |

| | | | | |
|---|---|---|---|---|
| *fepC* | b0588 | 24.10 | 0.00109 | iron-enterobactin transporter subunit |
| *cysN* | b2751 | 23.75 | 0.00027 | sulfate adenylyltransferase, subunit 1 |
| *nhaA* | b0019 | 23.11 | 0.00023 | sodium-proton antiporter |
| *sodA* | b3908 | 21.13 | 0.00006 | superoxide dismutase, Mn |
| *fhuE* | b1102 | 20.93 | 0.00001 | ferric-rhodotorulic acid outer membrane transporter |
| *fepD* | b0590 | 20.76 | 0.00000 | iron-enterobactin transporter subunit |
| *sufC* | b1682 | 20.58 | 0.00000 | component of SufBCD complex, ATP-binding component of ABC superfamily |
| *nrdF* | b2676 | 20.36 | 0.00000 | ribonucleoside-diphosphate reductase 2, beta subunit, ferritin-like protein |
| *fhuF* | b4367 | 19.90 | 0.00004 | ferric iron reductase involved in ferric hydroximate transport |
| *dnaK* | b0014 | 19.32 | 0.00000 | chaperone Hsp70, co-chaperone with DnaJ |
| *yeeD* | b2012 | 18.93 | 0.00108 | conserved protein |
| *sufD* | b1681 | 18.06 | 0.00000 | component of SufBCD complex |
| *cysA* | b2422 | 16.19 | 0.00000 | sulfate/thiosulfate transporter subunit |
| *yncE* | b1452 | 15.54 | 0.00074 | conserved protein |
| *ybaJ* | b0461 | 15.03 | 0.00012 | predicted protein |
| *ycjF* | b1322 | 14.66 | 0.00264 | conserved inner membrane protein |
| *fhuA* | b0150 | 14.38 | 0.00010 | ferrichrome outer membrane transporter |
| *cysH* | b2762 | 13.66 | 0.00000 | 3'-phosphoadenosine 5'-phosphosulfate reductase |
| *yqjH* | b3070 | 13.33 | 0.00028 | predicted siderophore interacting protein |
| *osmY* | b4376 | 13.15 | 0.00066 | periplasmic protein |
| *ybiX* | b0804 | 12.35 | 0.00000 | conserved protein |
| *htpG* | b0473 | 11.33 | 0.00005 | molecular chaperone HSP90 family |

| | | | | |
|---|---|---|---|---|
| *betI* | b0313 | 11.05 | 0.00028 | DNA-binding transcriptional repressor |
| *spy* | b1743 | 10.87 | 0.00177 | envelope stress induced periplasmic protein |
| *yqaE* | b2666 | 10.45 | 0.00004 | predicted membrane protein |
| *raiA* | b2597 | 10.43 | 0.00000 | cold shock protein associated with 30S ribosomal subunit |
| *ycjX* | b1321 | 10.07 | 0.00012 | conserved protein with nucleoside triphosphate hydrolase domain |
| *groS* | b4142 | 9.93 | 0.00000 | Cpn10 chaperonin GroES, small subunit of GroESL |
| *miaA* | b4171 | 9.90 | 0.00000 | delta(2)-isopentenylpyrophosphate tRNA-adenosine transferase |
| *chaA* | b1216 | 9.58 | 0.00003 | calcium/sodium:proton antiporter |
| *groL* | b4143 | 9.44 | 0.00000 | Cpn60 chaperonin GroEL, large subunit of GroESL |
| *htpX* | b1829 | 8.94 | 0.00000 | predicted endopeptidase |
| *fxsA* | b4140 | 8.67 | 0.00069 | inner membrane protein |
| *cysI* | b2763 | 8.49 | 0.00000 | sulfite reductase, beta subunit, NAD(P)-binding, heme-binding |
| *iscR* | b2531 | 7.99 | 0.00004 | DNA-binding transcriptional repressor |
| *acnA* | b1276 | 7.88 | 0.00001 | aconitate hydratase 1 |
| *ycgK* | b1178 | 7.74 | 0.00000 | predicted protein |
| *frvX* | b3898 | 7.34 | 0.00002 | predicted endo-1,4-beta-glucanase |
| *betB* | b0312 | 7.30 | 0.00170 | betaine aldehyde dehydrogenase, NAD-dependent |
| *ybgS* | b0753 | 7.30 | 0.00030 | conserved protein |
| *nfsA* | b0851 | 7.01 | 0.00000 | nitroreductase A, NADPH-dependent, FMN-dependent |
| *entD* | b0583 | 6.82 | 0.00000 | phosphopantetheinyltransferase component of enterobactin synthase multienzyme complex |
| *aldA* | b1415 | 6.58 | 0.00000 | aldehyde dehydrogenase A, NAD-linked |
| *ybaL* | b0478 | 6.18 | 0.00001 | predicted transporter with NAD(P)-binding Rossmann-fold domain |

| | | | | |
|---|---|---|---|---|
| *yggX* | b2962 | 6.11 | 0.00000 | protein that protects iron-sulfur proteins against oxidative damage |
| *ybjC* | b0850 | 6.11 | 0.00000 | predicted inner membrane protein |
| *mntH* | b2392 | 5.97 | 0.00000 | manganese/divalent cation transporter |
| *aceA* | b4015 | 5.97 | 0.00000 | isocitrate lyase |
| *tqsA* | b1601 | 5.84 | 0.00000 | predicted inner membrane protein |
| *ypeC* | b2390 | 5.82 | 0.00001 | conserved protein |
| *betA* | b0311 | 5.81 | 0.00140 | choline dehydrogenase, a flavoprotein |
| *fhuC* | b0151 | 5.62 | 0.00106 | iron-hydroxamate transporter subunit |
| *cysW* | b2423 | 5.54 | 0.00001 | sulfate/thiosulfate transporter subunit |
| *yqjI* | b3071 | 5.49 | 0.00000 | predicted transcriptional regulator |
| *ydeH* | b1535 | 5.41 | 0.00000 | conserved protein |
| *ybiI* | b0803 | 5.36 | 0.00000 | conserved protein |
| *fecA* | b4291 | 5.21 | 0.00000 | KpLE2 phage-like element; ferric citrate outer membrane transporter |
| *nfo* | b2159 | 5.19 | 0.00009 | endonuclease IV with intrinsic 3'-5' exonuclease activity |
| *grpE* | b2614 | 4.96 | 0.00000 | heat shock protein |
| *ybbN* | b0492 | 4.90 | 0.00000 | predicted thioredoxin domain-containing protein |
| *ybbA* | b0495 | 4.90 | 0.00049 | predicted transporter subunit: ATP-binding component of ABC superfamily |
| *ibpB* | b3686 | 4.76 | 0.00001 | heat shock chaperone |
| *aceB* | b4014 | 4.75 | 0.00000 | malate synthase A |
| *pspA* | b1304 | 4.60 | 0.00000 | regulatory protein for phage-shock-protein operon |
| *cysD* | b2752 | 4.49 | 0.00000 | sulfate adenylyltransferase, subunit 2 |
| *acrA* | b0463 | 4.42 | 0.00000 | multidrug efflux system |

| | | | | |
|---|---|---|---|---|
| *ycfJ* | b1110 | 4.32 | 0.00021 | predicted protein |
| *cysC* | b2750 | 4.29 | 0.00081 | adenosine 5'-phosphosulfate kinase |
| *rimK* | b0852 | 4.29 | 0.00003 | ribosomal protein S6 modification protein |
| *hha* | b0460 | 4.26 | 0.00000 | modulator of gene expression, with H-NS |
| *ygfZ* | b2898 | 4.20 | 0.00003 | predicted folate-dependent regulatory protein |
| *mltC* | b2963 | 4.20 | 0.00097 | membrane-bound lytic murein transglycosylase C |
| *exbD* | b3005 | 4.19 | 0.00003 | membrane spanning protein in TonB-ExbB-ExbD complex |
| *prlC* | b3498 | 4.18 | 0.00001 | oligopeptidase A |
| *iscA* | b2528 | 4.11 | 0.00014 | FeS cluster assembly protein |
| *tnaA* | b3708 | 4.07 | 0.00000 | tryptophanase/L-cysteine desulfhydrase, PLP-dependent |
| *exbB* | b3006 | 4.03 | 0.00000 | membrane spanning protein in TonB-ExbB-ExbD complex |
| *slt* | b4392 | 3.95 | 0.00030 | lytic murein transglycosylase, soluble |
| *osmC* | b1482 | 3.95 | 0.00000 | osmotically inducible, stress-inducible membrane protein |
| *aceK* | b4016 | 3.91 | 0.00000 | isocitrate dehydrogenase kinase/phosphatase |
| *yaaX* | b0005 | 3.77 | 0.00000 | predicted protein |
| *cysK* | b2414 | 3.70 | 0.00001 | cysteine synthase A, O-acetylserine sulfhydrolase A subunit |
| *idi* | b2889 | 3.69 | 0.00000 | isopentenyl diphosphate isomerase |
| *yccA* | b0970 | 3.67 | 0.00000 | inner membrane protein |
| *ynfD* | b1586 | 3.67 | 0.00057 | predicted protein |
| *iscU* | b2529 | 3.65 | 0.00024 | scaffold protein |
| *yaiA* | b0389 | 3.63 | 0.00000 | predicted protein |
| *hslU* | b3931 | 3.62 | 0.00000 | molecular chaperone and ATPase component of HslUV protease |

| | | | | |
|---|---|---|---|---|
| *mutM* | b3635 | 3.55 | 0.00000 | formamidopyrimidine/5-formyluracil/ 5-hydroxymethyluracil DNA glycosylase |
| *fldA* | b0684 | 3.52 | 0.00000 | flavodoxin 1 |
| *dnaJ* | b0015 | 3.46 | 0.00013 | chaperone Hsp40, co-chaperone with DnaK |
| *yeiI* | b2160 | 3.44 | 0.00069 | predicted kinase |
| *ygaU* | b2665 | 3.40 | 0.00031 | predicted protein |
| *ybbP* | b0496 | 3.30 | 0.00091 | predicted inner membrane protein |
| *acrB* | b0462 | 3.26 | 0.00009 | multidrug efflux system protein |
| *inaA* | b2237 | 3.26 | 0.00000 | conserved protein |
| *lpp* | b1677 | 3.25 | 0.00006 | murein lipoprotein |
| *glcC* | b2980 | 3.22 | 0.00003 | DNA-binding transcriptional dual regulator, glycolate-binding |
| *yhcN* | b3238 | 3.19 | 0.00000 | conserved protein |
| *mhpR* | b0346 | 3.19 | 0.00041 | DNA-binding transcriptional activator, 3HPP-binding |
| *iscS* | b2530 | 3.14 | 0.00019 | cysteine desulfurase (tRNA sulfurtransferase), PLP-dependent |
| *yaiY* | b0379 | 3.10 | 0.00016 | predicted inner membrane protein |
| *yrbL* | b3207 | 3.06 | 0.00000 | predicted protein |
| *ldhA* | b1380 | 3.01 | 0.00000 | fermentative D-lactate dehydrogenase, NAD-dependent |
| *bssS* | b1060 | 3.00 | 0.00000 | predicted protein |
| *fecB* | b4290 | 2.99 | 0.00000 | KpLE2 phage-like element; iron-dicitrate transporter subunit |
| *yhbW* | b3160 | 2.98 | 0.00004 | predicted enzyme |
| *hslV* | b3932 | 2.90 | 0.00009 | peptidase component of the HslUV protease |
| *hflK* | b4174 | 2.88 | 0.00000 | modulator for HflB protease specific for phage lambda cII repressor |
| *lon* | b0439 | 2.85 | 0.00000 | DNA-binding ATP-dependent protease La |

| | | | | |
|---|---|---|---|---|
| *rsd* | b3995 | 2.84 | 0.00000 | stationary phase protein, binds sigma 70 RNA polymerase subunit |
| *yqfA* | b2899 | 2.83 | 0.00000 | predicted oxidoreductase, inner membrane subunit |
| *lldD* | b3605 | 2.81 | 0.00001 | L-lactate dehydrogenase, FMN-linked |
| *yoaE* | b1816 | 2.80 | 0.00001 | fused predicted membrane protein/conserved protein |
| *yhiI* | b3487 | 2.80 | 0.00001 | predicted HlyD family secretion protein |
| *ygdI* | b2809 | 2.79 | 0.00000 | predicted protein |
| *acpP* | b1094 | 2.79 | 0.00000 | acyl carrier protein (ACP) |
| *rrmJ* | b3179 | 2.76 | 0.00000 | 23S rRNA methyltransferase |
| *ybaO* | b0447 | 2.72 | 0.00000 | predicted DNA-binding transcriptional regulator |
| *dacC* | b0839 | 2.67 | 0.00000 | D-alanyl-D-alanine carboxypeptidase (penicillin-binding protein 6a) |
| *glpK* | b3926 | 2.66 | 0.00000 | glycerol kinase |
| *yibT* | b4554 | 2.64 | 0.00000 | predicted protein |
| *asnA* | b3744 | 2.64 | 0.00000 | asparagine synthetase A |
| *rbbA* | b3486 | 2.63 | 0.00011 | fused ribosome-associated ATPase: ATP-binding protein/ATP-binding protein/predicted membrane protein |
| *qor* | b4051 | 2.62 | 0.00013 | quinone oxidoreductase, NADPH-dependent |
| *yjbJ* | b4045 | 2.58 | 0.00000 | predicted stress response protein |
| *ftnB* | b1902 | 2.57 | 0.00033 | predicted ferritin-like protein |
| *cusR* | b0571 | 2.53 | 0.00000 | DNA-binding response regulator in two-component regulatory system with CusS |
| *talB* | b0008 | 2.51 | 0.00000 | transaldolase B |
| *metQ* | b0197 | 2.48 | 0.00000 | DL-methionine transporter subunit |
| *eco* | b2209 | 2.48 | 0.00000 | ecotin, a serine protease inhibitor |
| *ivy* | b0220 | 2.48 | 0.00000 | inhibitor of vertebrate C-lysozyme |

| | | | | |
|---|---|---|---|---|
| *pheP* | b0576 | 2.43 | 0.00000 | phenylalanine transporter |
| *tonB* | b1252 | 2.43 | 0.00000 | membrane spanning protein in TonB-ExbB-ExbD complex |
| *mdlB* | b0449 | 2.43 | 0.00000 | fused predicted multidrug transporter subunits of ABC superfamily: ATP-binding components |
| *yrfG* | b3399 | 2.42 | 0.00000 | predicted hydrolase |
| *icd* | b1136 | 2.41 | 0.00000 | e14 prophage; isocitrate dehydrogenase, specific for NADP+ |
| *hflX* | b4173 | 2.39 | 0.00000 | predicted GTPase |
| *hslO* | b3401 | 2.36 | 0.00000 | heat shock protein Hsp33 |
| *ygaC* | b2671 | 2.36 | 0.00000 | predicted protein |
| *ygiB* | b3037 | 2.36 | 0.00012 | conserved outer membrane protein |
| *argT* | b2310 | 2.33 | 0.00064 | lysine/arginine/ornithine transporter subunit |
| *hslR* | b3400 | 2.33 | 0.00017 | ribosome-associated heat shock protein Hsp15 |
| *lldP* | b3603 | 2.31 | 0.00000 | L-lactate permease |
| *ybeL* | b0643 | 2.31 | 0.00000 | conserved protein |
| *yneM* | b4599 | 2.29 | 0.00000 | hypothetical protein |
| *yhhJ* | b3485 | 2.26 | 0.00000 | predicted transporter subunit: membrane component of ABC superfamily |
| *zntR* | b3292 | 2.25 | 0.00002 | DNA-binding transcriptional activator in response to Zn(II) |
| *gpmA* | b0755 | 2.24 | 0.00000 | phosphoglyceromutase 1 |
| *mfd* | b1114 | 2.23 | 0.00008 | transcription-repair coupling factor |
| *metC* | b3008 | 2.21 | 0.00000 | cystathionine beta-lyase, PLP-dependent |
| *hflB* | b3178 | 2.21 | 0.00000 | protease, ATP-dependent zinc-metallo |
| *ytjA* | b4568 | 2.21 | 0.00000 | predicted protein |
| *grxB* | b1064 | 2.20 | 0.00000 | glutaredoxin 2 (Grx2) |

| | | | | |
|---|---|---|---|---|
| *lpxC* | b0096 | 2.19 | 0.00000 | UDP-3-O-acyl N-acetylglucosamine deacetylase |
| *tolC* | b3035 | 2.18 | 0.00000 | transport channel |
| *dppA* | b3544 | 2.18 | 0.00000 | dipeptide transporter |
| *glpD* | b3426 | 2.17 | 0.00000 | sn-glycerol-3-phosphate dehydrogenase, aerobic, FAD/NAD(P)-binding |
| *yobH* | b4536 | 2.17 | 0.00000 | predicted protein |
| *uof* | b4637 | 2.16 | 0.00003 | ryhB-regulated fur leader peptide |
| *dadA* | b1189 | 2.16 | 0.00000 | D-amino acid dehydrogenase |
| *nhaR* | b0020 | 2.15 | 0.00000 | DNA-binding transcriptional activator |
| *ypfG* | b2466 | 2.14 | 0.00000 | predicted protein |
| *ybeZ* | b0660 | 2.14 | 0.00000 | predicted protein with nucleoside triphosphate hydrolase domain |
| *ydeI* | b1536 | 2.14 | 0.00002 | conserved protein |
| *dkgA* | b3012 | 2.14 | 0.00000 | 2,5-diketo-D-gluconate reductase A |
| *ybhG* | b0795 | 2.11 | 0.00005 | predicted membrane fusion protein (MFP) component of efflux pump, membrane anchor |
| *pepQ* | b3847 | 2.10 | 0.00001 | proline dipeptidase |
| *ybeY* | b0659 | 2.08 | 0.00000 | conserved protein |
| *htrG* | b3055 | 2.07 | 0.00000 | predicted signal transduction protein (SH3 domain) |
| *sdhB* | b0724 | 2.07 | 0.00031 | succinate dehydrogenase, FeS subunit |
| *clpP* | b0437 | 2.04 | 0.00000 | proteolytic subunit of ClpA-ClpP and ClpX-ClpP ATP-dependent serine proteases |
| *yafD* | b0209 | 2.03 | 0.00000 | conserved protein |
| *cysP* | b2425 | 2.02 | 0.00001 | thiosulfate transporter subunit |
| *yceI* | b1056 | 2.01 | 0.00000 | predicted protein |
| *hfq* | b4172 | 2.01 | 0.00000 | HF-I, host factor for RNA phage Q beta replication |

| | | | | |
|---|---|---|---|---|
| *mdlA* | b0448 | 2.01 | 0.00000 | fused predicted multidrug transporter subunits of ABC superfamily: ATP-binding components |
| *glgA* | b3429 | 2.00 | 0.00000 | glycogen synthase |

**Silver nitrate down-regulated genes**

| Gene | Locus Tag | Ratio | t-test *P* value | Description |
|---|---|---|---|---|
| *emrD* | b3673 | 0.50 | 0.00100 | multidrug efflux system protein |
| *thiI* | b0423 | 0.50 | 0.00000 | sulfurtransferase required for thiamine and 4-thiouridine biosynthesis |
| *ycaO* | b0905 | 0.49 | 0.00002 | conserved protein |
| *plsX* | b1090 | 0.49 | 0.00000 | fatty acid/phospholipid synthesis protein |
| *rplV* | b3315 | 0.49 | 0.00000 | 50S ribosomal subunit protein L22 |
| *pyrD* | b0945 | 0.49 | 0.00024 | dihydro-orotate oxidase, FMN-linked |
| *nusG* | b3982 | 0.49 | 0.00000 | transcription termination factor |
| *fadL* | b2344 | 0.49 | 0.00000 | long-chain fatty acid outer membrane transporter |
| *rpsS* | b3316 | 0.49 | 0.00000 | 30S ribosomal subunit protein S19 |
| *folA* | b0048 | 0.49 | 0.00000 | dihydrofolate reductase |
| *rnk* | b0610 | 0.48 | 0.00001 | regulator of nucleoside diphosphate kinase |
| *rho* | b3783 | 0.48 | 0.00000 | transcription termination factor |
| *prfC* | b4375 | 0.48 | 0.00000 | peptide chain release factor RF-3 |
| *rpsC* | b3314 | 0.48 | 0.00000 | 30S ribosomal subunit protein S3 |
| *fliM* | b1945 | 0.48 | 0.00000 | flagellar motor switching and energizing component |
| *rplS* | b2606 | 0.48 | 0.00000 | 50S ribosomal subunit protein L19 |
| *rpsP* | b2609 | 0.48 | 0.00000 | 30S ribosomal subunit protein S16 |
| *flhD* | b1892 | 0.48 | 0.00268 | DNA-binding transcriptional dual regulator with FlhC |
| *putA* | b1014 | 0.48 | 0.00000 | fused DNA-binding transcriptional regulator/proline dehydrogenase/pyrroline-5-carboxylate dehydrogenase |
| *rpsR* | b4202 | 0.47 | 0.00000 | 30S ribosomal subunit protein S18 |

| | | | | |
|---|---|---|---|---|
| *yfaZ* | b2250 | 0.47 | 0.00000 | predicted outer membrane porin protein |
| *infA* | b0884 | 0.47 | 0.00000 | translation initiation factor IF-1 |
| *fis* | b3261 | 0.45 | 0.00000 | global DNA-binding transcriptional dual regulator |
| *rplU* | b3186 | 0.45 | 0.00000 | 50S ribosomal subunit protein L21 |
| *rplP* | b3313 | 0.44 | 0.00000 | 50S ribosomal subunit protein L16 |
| *dusB* | b3260 | 0.44 | 0.00000 | tRNA-dihydrouridine synthase B |
| *rpsT* | b0023 | 0.43 | 0.00000 | 30S ribosomal subunit protein S20 |
| *ompF* | b0929 | 0.43 | 0.00000 | outer membrane porin 1a (Ia;b;F) |
| *rpmC* | b3312 | 0.42 | 0.00000 | 50S ribosomal subunit protein L29 |
| *rpsF* | b4200 | 0.41 | 0.00000 | 30S ribosomal subunit protein S6 |
| *yhbY* | b3180 | 0.41 | 0.00000 | predicted RNA-binding protein |
| *cspE* | b0623 | 0.40 | 0.00066 | DNA-binding transcriptional repressor |
| *priB* | b4201 | 0.40 | 0.00000 | primosomal protein N |
| *yhbE* | b3184 | 0.39 | 0.00000 | conserved inner membrane protein |
| *yeeF* | b2014 | 0.39 | 0.00004 | predicted amino-acid transporter |
| *yfiD* | b2579 | 0.36 | 0.00000 | pyruvate formate lyase subunit |
| *suhB* | b2533 | 0.36 | 0.00000 | inositol monophosphatase |
| *ydiY* | b1722 | 0.33 | 0.00000 | conserved protein |